



MEDICAL UNIVERSITY
OF VIENNA

**Going with the flow – development of a plate-scale
perfusion culture system and its effects on
pancreatic islet cell lines**

Doctoral thesis at the Medical University of Vienna
for obtaining the academic degree

Doctor of Philosophy

Submitted by

Robert Pazdzior

Supervisor

Dr. Stefan Kubicek

CeMM Research Center for Molecular Medicine
of the Austrian Academy of Sciences
Lazarettgasse 14, AKH BT 25.3, 1090 Vienna, Austria

Vienna, 11/2021

DECLARATION

The work presented in this thesis was carried out by the author, Robert Pazdzior, in the laboratory of Dr. Stefan Kubicek at the Research Center for Molecular Medicine (CeMM) of the Austrian Academy of Sciences in Austria. Individual contributions as they pertain to Results sections 2.1 and 2.2 are detailed below.

The results presented in Section 2.1 were previously reported in the following publication:

Pazdzior R, Kubicek S (2021). PlateFlo – A software-controllable plate-scale perfusion system for culture of adherent cells. *Hardware X*.
<https://doi.org/10.1016/j.ohx.2021.e00222>

It is reprinted in its entirety under the Creative Commons Attribution, Non-Commercial, No Derivates 4.0 (CC BY-NC-ND 4.0) license: <http://creativecommons.org/licenses/by-nc-nd/4.0/>

Robert Pazdzior and Stefan Kubicek conceived of and oversaw the project. **Robert Pazdzior** designed and built the PlateFlo culture system and FETbox electronics and wrote the accompanying documentation. **Robert Pazdzior** wrote the software and accompanying documentation. **Robert Pazdzior** performed the experiments and analyzed the resulting data. **Robert Pazdzior** and Stefan Kubicek wrote the manuscript.

Section 2.2:

Robert Pazdzior and Stefan Kubicek conceived of and oversaw the study; **Robert Pazdzior** performed all experiments and analyzed all resulting data unless otherwise noted; Next-Generation Sequencing and analysis of the raw data was performed by the Biomedical Sequencing Facility (BSF) at CeMM; mass spectrometry was carried out in the proteomics facility at CeMM; and **Robert Pazdzior** wrote the section with input from Stefan Kubicek.

This doctoral thesis was written by the author, Robert Pazdzior, with input from Stefan Kubicek.

TABLE OF CONTENTS

Declaration	ii
Table of Contents.....	iii
List of Figures.....	v
List of Tables	v
Abstract	vi
Zusammenfassung	viii
Publications Arising from this Thesis.....	x
Abbreviations	xi
Acknowledgments	xiv
1. Introduction	1
1.1 The Road to Static Mammalian Cell Culture	1
1.1.1 <i>The Advent of Tissue Culture</i>	1
1.1.2 <i>Defining Tissue Culture Media</i>	5
1.1.3 <i>The First Cell Lines</i>	7
1.1.4 <i>Emergence of Basal Media</i>	7
1.2 Static Mammalian Cell Culture.....	11
1.2.1 <i>In Vitro Culture Systems</i>	11
1.2.2 <i>Primary Cultures</i>	12
1.2.3 <i>Cell Lines</i>	12
1.2.4 <i>General Methodology</i>	13
1.3 Pancreatic Islet Culture	16
1.3.1 <i>Primary Islets</i>	17
1.3.2 <i>Islet Cell Lines</i>	19
1.3.3 <i>Hormone Secretion Assay</i>	20
1.4 Dynamic Culture.....	20
1.5 Aims.....	23
2. Results.....	24
2.1 PlateFlo – A software-controllable plate-scale perfusion system for culture of adherent cells	24
2.1.1 <i>Prologue</i>	24
2.1.2 <i>Publication PDF</i>	24
2.2 Continuous perfusion alters selenoprotein expression and lipid metabolism in islet cell lines..	127
2.2.1 <i>Continuous perfusion causes cell type-dependent growth effects</i>	127

TABLE OF CONTENTS

2.2.2	<i>Selenoprotein expression is upregulated by continuous perfusion culture</i>	129
2.2.3	<i>Continuous perfusion culture alters the expression of genes involved in lipid metabolism</i>	131
2.2.4	<i>Selenoprotein upregulation does not correspond with oxidative stress signatures</i>	133
2.2.5	<i>Fatty acid & lipid composition are altered in αTC1-LT</i>	133
2.2.6	<i>Supplementary Data</i>	135
3.	Discussion	144
3.1	General Discussion	144
3.2	Conclusions and Outlook.....	150
4.	Materials & Methods	151
4.1	Cell Culture.....	151
4.2	Continuous Perfusion Cell Culture	152
4.3	Automated Cell Imaging and Area Analysis	153
4.4	Western Blotting	153
4.5	RT-qPCR.....	153
4.6	Proteomics	154
4.6.1	<i>Sample Preparation</i>	154
4.6.2	<i>Offline Fractionation via RP-HPLC at High pH</i>	155
4.6.3	<i>2D-RP/RP Liquid Chromatography Mass Spectrometry</i>	155
4.6.4	<i>Data Analysis</i>	156
4.7	RNA-Sequencing.....	157
4.7.1	<i>NGS Library Preparation</i>	157
4.7.2	<i>Next-Generation Sequencing and Raw Data Acquisition</i>	157
4.7.3	<i>Data Analysis</i>	157
4.8	Free Fatty Acid Quantification	158
4.9	Semi-Quantitative Untargeted Lipidomics.....	159
4.9.1	<i>Sample Preparation</i>	159
4.9.2	<i>LC-MS</i>	159
4.9.3	<i>Data Analysis</i>	160
5.	References	161
6.	Curriculum Vitae	177

LIST OF FIGURES

Figure 1: Ross Harrison's hanging drop method for tissue culture.	2
Figure 2: Assorted Carrel flasks.	4
Figure 3: In vitro systems and their relationships	11
Figure 4: Workflow overview and growth characterization	128
Figure 5: Quantitative global proteomics reveals perfusion culture upregulates numerous selenoproteins in both α TC1-LT and β TC3.....	130
Figure 6: RNA-sequencing reveals differential expression of numerous metabolic enzymes, especially those associated with lipid and cholesterol metabolism.....	132
Figure 7: Perfusion culture alters fatty acid and lipid composition of α TC1-LT cells in perfusion culture, particularly oleic acid (C18:1) and oleic-acid derived phospholipids.....	134
Figure 8: Overview of the effects of perfusion culture on lipid metabolic pathways.	147
Figure S1: Whole membrane Ponceau and GPX1 immunostaining time-course..	141
Figure S2: Bulk RNA-seq \log_2 fold-changes (perfused/static) of curated oxidative stress marker genes	142
Figure S3: RNA-sequencing STAR Aligner mapped read counts for each sample sequenced.....	143

LIST OF TABLES

Table 1: Composition of common basal media.	9
Table 2: Significantly up- and down-regulated proteins in perfused vs. static culture of α TC1-LT.....	136
Table 3: Significantly up- and down-regulated proteins in perfused vs. static culture of β TC3.....	137
Table 4: Top 25 differentially expressed protein-coding transcripts following in perfused vs. static culture of α TC1-LT	138
Table 5: Top 25 differentially expressed protein-coding transcripts following in perfused vs. static culture of β TC3	139
Table 6: Mouse primer sequences used in RT-qPCR analyses.....	140

ABSTRACT

Despite advances in cell culture technology and the rapid development of new culture models, routine cell culture is still most commonly carried out using the near century old technique of static culture. This technique is cost and labor efficient, however is of limited physiological relevance. In static culture, cells are cultured under a pool of nutrient-rich medium which is exchanged for fresh medium every few days or as cells are passaged. In the interim, nutrient concentrations decline, and waste products and secreted factors accumulate in the culture medium, then are abruptly reset upon media exchange or subculture. This is in stark contrast to the physiological conditions experienced by cells in the tissues of animals, where the circulatory system generally continuously perfuses tissues, bringing a steady supply of oxygen and nutrients and removing waste and secreted factors. A wide variety of ingenious bioreactor designs have been developed that address this issue, particularly for spheroids and 3D cultures. Continuous circulation improves cell feeding, oxygen diffusion, and can add physiological shear forces beneficial to some systems. Widespread adoption of these more sophisticated solutions for routine cell culture has been rather limited, however, likely due in part to the added cost, complexity, and in some cases, expertise required to implement them. Limited compatibility with existing culture models used in molecular biology laboratories may also be a factor. Inexpensive perfusion culture systems directly compatible with the culture of adherent cell lines in the familiar plate format are lacking but could help bridge the gap between traditional static culture and more physiological dynamic culture systems and afford new experimental opportunities.

In the first part of this thesis, I aimed to develop such a perfusion system – especially one that could be built using common tools and very little fabrication expertise. The resulting fully open-source system, which I called PlateFlo, can be used directly with the adherent cell lines typically cultured under static conditions. It requires only the modification of the lids of commercially available tissue culture plates (e.g., one-well rectangular plates or standard petri dishes), to build the culture chamber, as such it bypasses the complications associated with fabricating a sterile treated culture substrate. To make the PlateFlo system as accessible as possible, I provided detailed documentation on its build and usage. Along with the perfusion plate, I designed a hardware controller, the FETbox, with a well-documented Python control library that enables a researcher to program dynamic perfusion experiments utilizing sensors, valves, and other electronic components. It can be used to simply recirculate media in a single plate, or for example, perfuse a co-culture of several plates in series if needed.

In the second part of this thesis, I thoroughly characterized the effects of perfusion on cell lines in culture using my perfusion system. Dynamic culture systems are generally assessed using

functional readouts such as viability, growth rate, selected gene expression, or response to stimulus (e.g. hormone secretion). To the best of my knowledge, however, a detailed systematic investigation of the effects of continuous perfusion on cells in culture using global proteomics, RNA-sequencing, and metabolomics has not been carried out before. I selected pancreatic islet α and β cell lines, α TC1 and β TC3, on which to characterize the effects of continuous perfusion culture. These cells of the endocrine pancreas integrate sensing of glucose and other molecular signals in order to maintain blood glucose homeostasis through a concerted effort. They are therefore inherently sensitive to microenvironmental composition and could in particular benefit from better control of the media composition afforded in this system.

Compared to traditional static culture, α TC1 and β TC3 under continuous perfusion exhibited altered metabolic pathway expression, especially those linked to lipid metabolism. Perfusion culture significantly reduced the expression of genes linked to cholesterol biosynthesis, resulting in altered lipid composition. It also resulted in broad selenoprotein upregulation. My findings primarily suggest improved nutrient availability under perfusion culture and may hint at significant nutritional deficits in static culture conditions.

Overall, I have established a novel perfusion culture system and shown that it can have profound biological effects when used with cell lines routinely grown in static culture. It is my hope that this work contributes to the adoption of more physiological culture practices in molecular biology laboratories around the world.

ZUSAMMENFASSUNG

Trotz technologischer Fortschritte und der Entwicklung immer komplexerer Zellsysteme wird Zellkultur meist noch immer unter vor fast hundert Jahren erstmals etablierten statischen Kulturbedingungen durchgeführt. Diese sind kosten- und arbeitseffizient, jedoch nur von begrenzter physiologischer Relevanz. Bei der statischen Kultur werden Zellen in einem nährstoffreichen Medium kultiviert, das alle paar Tage gegen frisches Medium ausgetauscht wird. In im Laufe dieser Kultivierungsperiode verbrauchen die Zellen Nährstoffe aus dem Medium, welches sich gleichzeitig mit Stoffwechselprodukten und sekretierten Faktoren anreichert. Erst beim Medienaustausch oder der Subkultivierung werden diese Kulturbedingungen dann abrupt zurückgesetzt. Dies steht im krassen Gegensatz zu den physiologischen Bedingungen, denen Zellen in Geweben von Tieren ausgesetzt sind. Dabei wird das Gewebe im Allgemeinen durch das Kreislaufsystem kontinuierlich durchströmt, wodurch stete Versorgung mit Sauerstoff und Nährstoffen sowie die Entfernung von Stoffwechselprodukten und sekretierten Faktoren sichergestellt wird. Um solche Perfusionsbedingungen auch in der Zellkultur zu ermöglichen, sind mehrere ausgeklügelte Bioreaktordesigns entwickelt worden, insbesondere für Sphäroide und 3D-Kulturen. Dabei wurde beobachtet, dass die kontinuierliche Medienzirkulation Auswirkungen auf den zellulären Stoffwechsel und die Sauerstoffdiffusion hat, sowie die einige Systeme vorteilhaften physiologische Scherkräfte nachahmt. Diese anspruchsvolleren Lösungen sind für die routinemäßige Zellkultur bis jetzt aber wenig verbreitet, was wahrscheinlich zum Teil auf die zusätzlichen Kosten, die Komplexität und das für die Implementierung nötige Fachwissen zurückzuführen ist. Eingeschränkte Kompatibilität mit bestehenden Zellkulturmodellen und die Verfügbarkeit dieser Systeme typischerweise als industrielle Bioreaktoren oder als mikrofluidische Apparate, nicht aber im typischen Labormaßstab, kann ebenfalls ein Faktor sein. Kostengünstige Perfusionskultursysteme, die direkt mit der Kultur adhärenter Zelllinien im bekannten Plattenformat kompatibel sind, könnten dazu beitragen, die Lücke zwischen traditioneller statischer Kultur und physiologischeren dynamischen Kultursystemen zu schließen und damit neue experimentelle Möglichkeiten eröffnen.

Im ersten Teil dieser Arbeit hatte ich das Ziel, ein Perfusionssystem zu entwickeln, das mit relativ einfachen Werkzeugen und begrenzter technisch-konstruktiver Erfahrung gebaut werden kann. Das resultierende vollständig Open-Source-System, das ich PlateFlo nannte, kann direkt mit allen adhärenen Zelllinien verwendet werden, die normalerweise unter statischen Bedingungen kultiviert werden. Die Konstruktion der Kulturkammer erfordert ausschließlich die Modifikation der Deckel handelsüblicher Zellkulturplatten oder Standard-Petrischalen, und vermeidet damit Komplikationen, die mit der Herstellung eines sterilen und oberflächenbehandelten Kultursubstrats einhergehen. Um größtmögliche Zugänglichkeit

sicherzustellen, habe ich eine detaillierte Dokumentation zum Aufbau und zur Verwendung des PlateFlo-Systems bereitgestellt. Zur Steuerung des Systems entwarf ich einen Hardware-Controller, die FETbox, mit einer gut dokumentierten Python-Steuerungsbibliothek, die es einem Forscher ermöglicht, dynamische Perfusionsexperimente unter Verwendung von Sensoren, Ventilen und anderen elektronischen Komponenten zu programmieren. Damit ermöglicht das System komplexe Anwendungen, wie die Rezirkulation von Medien oder die Co-Perfusion mehrerer Zellkulturplatten hintereinander.

Im zweiten Teil dieser Arbeit habe ich die Auswirkungen der Perfusion von Zelllinien im oben entwickelten PlateFlo System verglichen mit statischen Kulturbedingungen charakterisiert. Dynamische Kultursysteme wurden bis jetzt vorwiegend unter Verwendung funktioneller Messwerte wie Viabilität, Wachstumsrate, Expression ausgewählter Gene oder Reaktion auf Reize (z. B. Hormonsekretion) bewertet. Eine detaillierte systematische Untersuchung der Auswirkungen kontinuierlicher Perfusion mittels globaler Proteomik, RNA-Sequenzierung und Metabolomik wurde meines Wissens bisher jedoch nicht durchgeführt. Ich wählte die Zelllinien α TC1 und β TC3, die von pankreatischen α - und β - Langerhans-Inselzellen abgeleitet wurden, um die Auswirkungen einer kontinuierlichen Perfusionskultur zu charakterisieren. Diese endokrinen Zellen der Bauchspeicheldrüse integrieren die externe Glukosekonzentration und weitere Faktoren, um die Blutglukosehomöostase durch eine konzertierte Ausschüttung ihrer Hormone Glukagon und Insulin aufrechtzuerhalten. Sie sind daher von Natur aus empfindlich für metabolische Veränderungen und könnten insbesondere von einer besseren Kontrolle der Medienzusammensetzung in Perfusionssystemen profitieren.

Im Vergleich zu traditioneller statischer Kultur zeigten α TC1 und β TC3 unter kontinuierlicher Perfusion eine veränderte Expression von Stoffwechselwegen, insbesondere solche, die mit dem Lipidstoffwechsel verbunden sind. Die Perfusionskultur reduzierte die Expression von Genen, die mit der Cholesterinbiosynthese verbunden sind, was zu einer veränderten Lipidzusammensetzung führte. Im Weiteren beobachtete ich Hochregulierung von Selenoproteinen. Meine Ergebnisse deuten in erster Linie darauf hin, dass eine verbesserte Nährstoffverfügbarkeit unter Perfusionskultur zu Veränderungen der zellulären Zusammensetzung führt. Im Umkehrschluss bedeuten diese Erkenntnisse, dass potentielle signifikante Nährstoffdefizite unter statischen Kulturbedingungen die Funktion pankreatischer Zellen beeinträchtigen könnte.

PUBLICATIONS ARISING FROM THIS THESIS

Section 2.1.2 of this thesis was published in the journal HardwareX in 2021.

Impact Factor 2020 = 3.24

PlateFlo – A software-controllable plate-scale perfusion system for culture of adherent cells

Pazdzior R, Kubicek S

HardwareX 2021

Volume 10

E00222

DOI: <https://doi.org/10.1016/j.ohx.2021.e00222>

Submitted: 6 May 2021

Accepted: 5 August 2021

Published: 29 September 2021

Reprinted under the Creative Commons Attribution, Non-Commercial, No Derivates 4.0 (CC BY-NC-ND 4.0) license: <http://creativecommons.org/licenses/by-nc-nd/4.0/>

ABBREVIATIONS

2D	two-dimensional
3D	three-dimensional
AGC	automatic gain control
ATCC	American Type Culture Collection
bFGF	basic fibroblast growth factor
BME	basal medium Eagle
CE	cholesteryl ester
CHO	Chinese hamster ovary
CMRL	Connaught Medical Research Laboratories
CRISPR-Cas9	Clustered regularly interspaced palindromic repeats/CRISPR-associated protein 9
DMEM	Dulbecco's modified minimal essential medium
DTT	dithiothreitol
ECACC	European Collection of Authenticated Cell Cultures
ECM	extracellular matrix
EGF	epidermal growth factor
ELISA	enzyme-linked immunosorbent assay
ER	endoplasmic reticulum
EtOH	ethanol
FAD	fatty acid desaturase
FBS	fetal bovine serum
Fdps	farnesyl diphosphate synthase
FDR	false discovery rate
FFA	free fatty acid
FTH	ferritin heavy chain
FTL	ferritin light chain
GPX1	glutathione peroxidase 1
GPX4	glutathione peroxidase 4
GSIS	glucose-stimulated insulin secretion
HCD	Higher energy collision induced dissociation
HIF-1α	hypoxia inducible factor 1 α
Hmgsc1	3-hydroxy-3-methylglutaryl-CoA synthase 1
IEQ	islet equivalents
IGF-1	insulin-like growth factor-1
INSIG	insulin-induced gene
IRE	iron response element

ABBREVIATIONS

KRB	Krebs-Ringer Buffer
LC-MS	liquid chromatography mass spectrometry
LDL	low-density lipoprotein
LDLR	low-density lipoprotein receptor
LOQ	limit of quantification
Lss	lanosterol synthase
MDS	multi-dimensional scaling
MEM	minimal essential medium
mRNA	messenger ribonucleic acid
MS	mass spectrometry
Msmo1	methylsterol monooxygenase 1
Mt1	metallothionein
MUFA	mono-unsaturated fatty acid
Mvd	mevalonate pyrophosphate decarboxylase
NCE	normalized collision energy
Ndufb4	NADH:Ubiquinone Oxidoreductase Subunit B4
NGS	next-generation sequencing
Nsdhl	NAD(P)-dependant steroid dehydrogenase-like
PC	phosphatidylcholine
PCA	principal component analysis
PCSK9	proprotein convertase subtilisin/kexin type 9
PDMS	polydimethylsiloxane
PEG	poly(ethylene glycol)
PEG	phosphatidylethanolamine
PM	plasma membrane
PUFA	poly-unsaturated fatty acid
RNA	ribonucleic acid
RNA-seq	ribonucleic acid sequencing
RP-HPLC	reversed phase high performance liquid chromatography
RPMI	Roswell Park Medical Institute
RT-qPCR	real time quantitative polymerase chain reaction
S/N	signal-to-noise ratio
SCAP	SREBP-cleavage activating protein
Scd	stearoyl CoA desaturase
SDS	sodium dodecyl sulphate
Sec	Selenocysteine

ABBREVIATIONS

SECIS	selenocysteine insert sequence
SP3	single-pot solid-phase-enhanced sample preparation
SPE	solid phase extraction
SREBP	sterol response element binding protein
SV40	simian vacuolating virus 40
TEAB	triethylammonium bicarbonate
TMT	tandem mass tag
UHPLC	ultra-high performance liquid chromatography

ACKNOWLEDGMENTS

It has been six years since a younger version of me landed in Vienna on only his second venture beyond the comfort and safety of the Canadian borders. Six amazing years. *Hey!* I know what you're thinking! But we all move at our own pace – and I am not ashamed to have taken a few detours and enjoyed the view along the way. All the while I've had the great privilege to be surrounded by the smartest, coolest, and most supportive people that I have ever met. These really have been some of the best years of life, due in no small part to these fantastic folks. As such I'd like to seize this opportunity and thank as many of them as possible.

When I first joined CeMM in Keiryn Bennett's lab, I was welcomed in with open arms and open beers – or red wine, in Keiryn's case. Thank you, Juli and Dijana, for looking out for me and showing me the ropes. Katja, for your wisdom and patience. And of course, Keiryn, for seeing potential in me and doing your absolute best, applying boot to ass, to bring some semblance of order to my chaos. I truly wish things had worked out differently for you at CeMM. Cheers to you all.

When things didn't work out, however, Stefan was the first to step up and take me in. And since then, you've been nothing but absolutely supportive every step of the way. You were always there to help in any way you could, but you also gave me the freedom to explore, and to discover on my own, to become my own kind of scientist. For this I will always be grateful.

The Kubicek lab, members past and present: thanks for being awesome. Thanks for all the laughs, and for all the snacks. There isn't a better bunch of people that I could have shared the fourth floor with. In particular, thank you to the β cell gang – Brenda, Lennart, and Tamara – for enduring all the questions, and especially enduring *all* the puns, and for the delicious Sichuan, which was almost as tasty as my jokes.

Thank you to the members of my thesis committee, Anne-Claude Gingras, and Jörg Menche. Your encouragement, feedback, and thoughtful discussions were of great help.

Thank you to the Austrian Academy of Science for supporting me financially throughout my project with the DOC fellowship.

Thank you to the friends I've made along the way. To my best buddy, Jan, for always having my back – and for literally fueling my research. To Lindsay and Alex for picking me back up in the moshpit, and for your appreciation of a nice crisp, refreshing, lager. To Mischa for all the Schnipo Schranke and banter (and a bit of climbing, I guess). To the crew of 2015 who made this strange new place a whole lot less scary and a whole lot more fun. To Tamara, the best partner that a guy like me could ask for, and for whom words could never fully express my gratitude. You showed me the world and invited me into your family when mine was out of

reach. You were always there to hold me up when I was at my lowest. Whether on our bikes, in the park, at the bar, or simply on the sofa - thank you for sharing these past few years with me, I will cherish them.

Thank you to my family, whose love I felt even from afar. To my sister Ewa and to Noel, for your wisdom and level heads (and of course, storing all my junk while I'm over here). To Norbby and Kristina for always checking in. And thank you mom and dad, for getting me here in the first place, believing in me, and always making sure that I have everything I need. I love you all. I know, I should probably call a bit more often...

Lastly, thank you to CeMM, for paving the road to this whole journey. For all the assistance over the years, going above and beyond, cushioning the crushing blows of Austrian bureaucracy. It was truly a privilege be surrounded by such passionate, polite, professional, and persistent people.

“So long and thanks for all the fish.”

*If the achievements of humankind punctuate the history of our species,
then the tools we craft are the words in between.*

1. INTRODUCTION

1.1 The Road to Static Mammalian Cell Culture

A biologist today can grow somatic animal cells in a dish, expanding and manipulating them at will. The researchers can then communicate their findings to colleagues on the other side of the world who can grow nearly identical cells using nearly identical culture medium and techniques to validate or advance that work. All of this without once having to perform a specific dissection of e.g., a mouse or rat to extract just the right specimen, meanwhile the clock ticks away on its viability and physiologically relevant characteristics. The plethora of readily available immortal cell lines and growth media has empowered generations of scientists now to push human understanding of fundamental processes using relatively well-defined systems. While often taken for granted, this did not simply come to be overnight. In this section the major historical milestones that brought about the tissue culture revolution of the 20th century are outlined chronologically.

1.1.1 The Advent of Tissue Culture

The tools and techniques used in modern cell culture are the descendants of pioneering works from the late 19th and early 20th centuries. Though they were instrumental in setting off a cascade of development that would later permit the culture of mammalian cells, these techniques and tools at first weren't developed while working with human, even or mouse material. Rather, frogs bore the great misfortune of being the model organism of choice in many of the physiological experiments of the era (Holmes, 1993).

In a pair of publications from 1882-1883, the British clinician and physiologist Sydney Ringer described a balanced salt solution approximating the concentrations of key ions in blood (Ringer, 1882, 1883). This allowed him to keep a dissected frog's heart beating in solution for several hours following removal from the body. Thus, this considered the first extended *in vitro* experiment, the great grandfather of cell culture. This relatively simple solution of inorganic salts known as Ringer's solution – NaCl, KCl, CaCl₂, and sodium bicarbonate (HNaCO₃) – is still in use today and paved the way for the development of numerous balanced salt solutions throughout the following decades.

The mistaken use of tap water in the preparation of Ringer's initial formulation by his lab assistant proved rather serendipitous. They subsequently observed that the same solution prepared with distilled water, as originally intended, required the addition of sodium

bicarbonate in order to maintain heart contractility (Ringer, 1883). This sparked further inquisition into which constituents of tap water made it a more physiological solution (Locke, 1895). As the prospect of *in vitro* tissue experimentation spread, numerous additives and substances would be tested in order to extend the survival of tissues outside of the host organism. Specimens could be maintained in salt solutions with nutrient supplements such as glucose for several days but did not survive indefinitely and lacked observable signs of proliferation (Loeb, 1897).

In 1907, Ross Harrison proved that tissues could be grown outside of the body in what is generally regarded as the first published method for successful animal tissue culture. He extracted small pieces (~3 mm) of frog embryonic tissue which were then known to differentiate into nerve fibers, placed them on a cover slip, and mounted it in freshly extracted lymph fluid from an adult frog. The lymph would coagulate quickly, and the slide could be inverted onto a glass slide with a spherical depression, sealing the edges with paraffin wax as in **Figure 1**. This allowed him to observe the tissue as it differentiated and grew into nerve fibres over a week, and in some cases almost a month (Harrison *et al*, 1907). The hanging drop provided a valuable tool for the study of developmental biology and physiology as a specimen could be observed directly under the microscope as it developed. Following his success, Harrison was joined by Montrose T. Burrows in 1909, a fellow in the lab of Alexis Carrel. Burrows learned the hanging drop method during his short stay in Harrison's lab – a formative visit that would lead Burrows and Carrel to make great strides in the burgeoning field of tissue culture.

Frog lymph fluid was far from an ideal culture medium. It did not coagulate uniformly, it was not available year-round, it could not be obtained in large quantities from a single animal, and

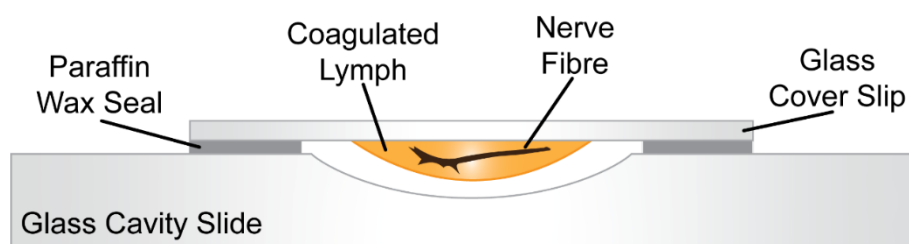


Figure 1: Ross Harrison's hanging drop method for tissue culture.

most importantly it did not support the growth of warm-blooded animal tissues. Burrows discovered that plasma from chicken blood, which was available in large quantities throughout the year, could be used in place of frog lymph to cultivate chick embryonic cells (Burrows, 1910) and sarcomas (Carrel & Burrows, 1910).

Carrel and Burrows solidified their methods in a publication in 1911 which laid out several concepts would be critical for the advancement of tissue culture and that are still in use today.

First, they make the distinction between the *survival* of cells *in vitro*, which had been demonstrated many times over the past decades, and *cultivation*, the *growth* of cells *in vitro* – thus coining the term “tissue culture”. They emphasize the importance of careful handling and aseptic technique, which at the time was non-trivial. They introduce and discuss the technique of serial culture – transferring a subset of the culture into new a new medium to grow in the absence of many growth inhibiting factors – and large scale cultivation directly on glass plates set in larger dishes, rather than in a hanging drop (Carrel & Burrows, 1911a).

Using these techniques, Robert Lambert and Frederic Hanes shortly thereafter describe the growth of rat tissues in plasma taken from various different species, or “heterogenic” plasma (Lambert & Hanes, 1911). Referencing this work, Carrel and Burrows briefly discuss success in mixing heterogenic natural media with artificial medium (Locke’s solution) in an addendum to their landmark publication later that year (Carrel & Burrows, 1911b). The use of heterogenic medium diluted with a defined artificial medium is not unlike the modern-day use of fetal bovine serum as a supplement in basal medium in modern tissue culture. The use of plasma – the liquid, non-clotting component of blood plasma – was a key step forward, as it would lead Carrel to design what is considered the prototype for the modern tissue culture flask, the D-type Carrel flask, in 1923 (**Figure 2**) (Carrel, 1923). These were the first tissue culture flasks to be made from Corning Pyrex rather than soda-lime glass. The high temperature resistance of this type of glass permits sterilization with high temperature steam in an autoclave and would become the *de facto* material of choice for tissue culture glassware, greatly improving tissue culture sterility.

At this point, tissues in culture would only grow for up to two weeks before exhibiting signs of senescence, or “senility” as Carrel referred to it; growth rate declined, and cells became smaller in appearance. Over the next years, Carrel would work towards extending the lifetime

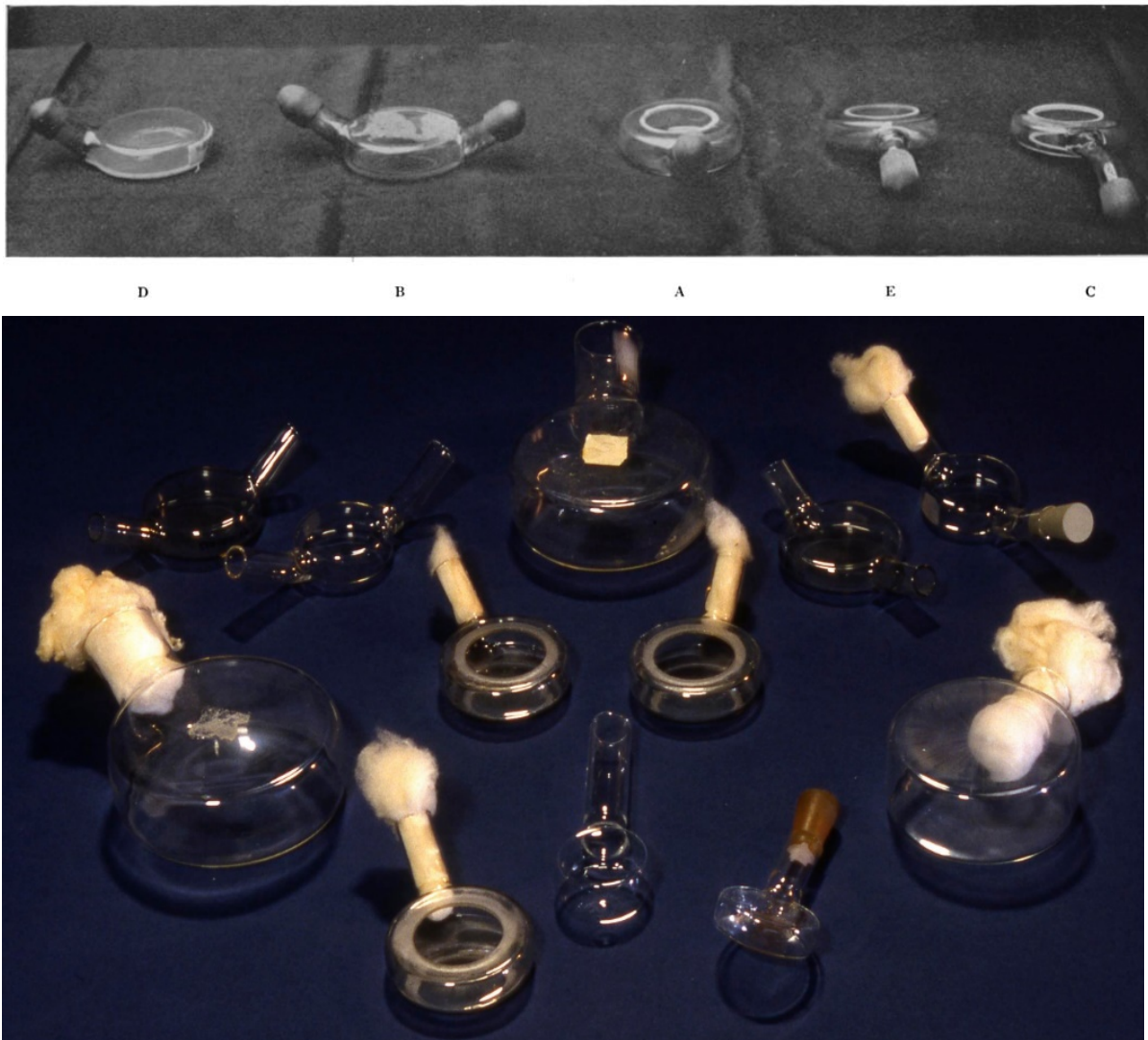


Figure 2: Assorted Carrel flasks, named for their inventor, Alexis Carrel. D-type (top, leftmost) Carrel flasks were the precursor to modern tissue culture flasks.

Top reproduced with permission from Carrel, 1923.

*Bottom reproduced under “fair use” terms from The Smithsonian:
https://americanhistory.si.edu/collections/search/object/nmah_1111991*

of tissues in culture indefinitely (Carrel, 1912, 1913a, 1913b) and even claim to have succeeded (Ebeling, 1922). For decades thereafter, until 1946, the fibroblasts extracted from embryonic chicken hearts would supposedly be continuously sub-cultured in his lab at Rockefeller. Carrel’s “immortal” culture was written about widely and celebrated as a testament to the technical prowess of Carrel and his lab.

Only decades later would the intrinsic replication limit of cells in culture be determined, overturning the dogma of the era: that all cells are immortal and will grow indefinitely if handled correctly. It is generally accepted now that Carrel’s “immortal strain” was not all that he claimed it to be. Carrel was inextricably attached to the idea of cellular immortality, and he staked much of his fame on the maintenance of his showpiece cell line. His general absence from the lab

was also well known. The combination of pressure from Carrel with lack of his direct oversight likely led those in his lab to occasionally “refresh” the strain with young embryonic fibroblasts before the culture could fail. An unnamed technician from Carrel’s lab is quoted as having said as much in 1930: “Well, Dr. Carrel would be so upset if we lost the strain, we just add a few embryo cells now and then... We make new strains for new experiments.” (Witkowski, 1980).

Carrel’s devotion to the concept of cellular immortality was likely a key factor in sustaining the cellular immortality dogma – cells are intrinsically immortal and only through our ignorance of the correct growth medium or perhaps a lack of skill in their handling did they die in culture (Hayflick, 1998). Though dogma may have hindered the scientific study of cellular mortality as a whole, it also likely served as a motivating factor in the exploration and improvement of the tissue culture field; there were no excuses: if the cells died, it was the investigator’s fault. In the mid-1920s a number of books and reviews were published in an attempt to corral knowledge of the technique of tissue culture that had poured out over the previous years; most notably *Technique of tissue culture in vitro*, a laboratory manual by Strangeways (1924) with detailed instructions on many of the procedures and even how to setup a tissue culture laboratory. This was important for wider adoption and utilization of tissue culture, as Carrel famously over-emphasized the difficulty of the technique, leaning heavily on his expertise as a surgeon, while also being somewhat sparse on specifics in several publications (Witkowski, 1979). Though, he too published a practical description of tissue culture techniques in 1923 while introducing the prototypical culture flasks described previously (Carrel, 1923).

With a number of the same principles and tools used in contemporary tissue culture in hand – culture flasks, aseptic technique, serial culture, liquid media, and media exchange – it seemed as though the field of tissue culture was well on its way. Culture medium still relied heavily on natural products of unknown composition such as peptone (a soluble, partially digested protein mixture), and the decades following would see great efforts made toward understanding the components therein that enabled cells to grow in culture.

1.1.2 Defining Tissue Culture Media

Margaret Reed Lewis and Warren Lewis were some of the early pioneers in the defining the necessary chemical constituents of tissue culture medium, examining growth systematically in well-defined salt solutions (Lewis & Lewis, 1911). In addition to testing various salts and concentrations, they also briefly mention the beneficial effect of amino acid and polypeptide supplementation, but do not provide further details (Lewis & Lewis, 1912). Glucose was one of the first specific molecules to be deemed essential in growth medium, particularly in simple balanced salt solutions (Lewis, 1922).

Embryonic extract was a key natural product used by Carrel to promote growth in his (in)famous fibroblast cell line (Carrel, 1913a; Ebeling, 1922). The protein fraction of the embryonic extract was found to have proliferation-inducing effects on chick embryo fibroblasts when used to supplement the growth medium (Baker & Carrel, 1926b; Baker, 1929; Baker & Carrel, 1926a). Exactly which molecules in the protein fraction were responsible for this effect would not become clearer for several decades still. The essentially of insulin, present in serum, was however soon discovered through the study of glucose supplementation – without insulin, the full benefit of glucose supplementation was not realized (Vogelaar & Erlichman, 1933). Improving upon Vogelaar’s “feeding solution” for fibroblasts, Lillian Baker found vitamins A, B₁, B₂ as well as antioxidant ascorbic acid and glutathione to aid in fibroblast growth (Baker, 1936). These “artificial” media as they were referred to, however, still contained natural products such as peptone and/or sera/plasma, thus convoluted the investigation of individual media components. For example, the use of natural products in earlier investigations led several prominent researchers to falsely conclude that amino acids are not necessary for growth nor accelerate it (Baker & Carrel, 1926a, 1928; Carrel & Ebeling, 1924).

Philip R White, renowned for his work on plant tissue culture, reported a fully synthetic medium capable of sustaining fibroblasts and cardiomyocytes for months in culture (White, 1946). It was an extension of Baker’s medium in several ways: based on Tyrode’s solution (essentially Ringer’s solution with bicarbonate buffer, magnesium, and sugar) (Tyrode, 1910), containing vitamin A and a mixture of B vitamins, and antioxidants ascorbic acid and glutathione. He omitted natural products, however, supplementing with a mixture of 11 amino acids as well as carotene. White cultured tissues using a roller-tube apparatus, however, which afforded a very high tissue-to-medium ratio as was the case in Lewis & Lewis’ liquid hanging drop method. Thus, it’s impossible to rule out that natural products derived from the tissue preparation could have been present in the media throughout the course of both experiments (Jensen, 1948; Jacoby & Darke, 1948). Jensen proposed using Carrel flasks and a larger volume of media along with more frequent media exchange when performing culture medium experiments.

At the same time Albert Fischer was conducting pioneering work studying the essentiality of amino acids in growth media while avoiding some of the methodological pitfalls of his predecessors. He first demonstrated that the low-molecular-weight fraction of embryonic extract and plasma was in fact essential for growth once the contributions from natural media were removed by dialysis (Fischer, 1941). He then evaluated the essentiality of cystine, methionine, lysine, glutamic acid, aspartic acid, tryptophan, arginine, and glutathione individually (Fischer, 1948). Chief among his findings was the essentiality of cystine and glutamine as well as cell-dependant importance of the other amino acids.

1.1.3 The First Cell Lines

Until this point, work on defining the critical components of culture medium was largely conducted in primary cell cultures. Many of the basal media in use today were formulated following the development of the first cell lines. This would finally give researchers around the world access to cells of the same genetic background, capable of growing indefinitely in culture, and free them of the complexity, burden, and variability introduced by having to harvest tissues from animals prior to each experiment.

Even under ideal conditions normal animal cells will not grow and divide indefinitely, they're subject to age-related senescence, i.e. the Hayflick Limit (Hayflick & Moorhead, 1961; Hayflick, 1998). However, tumor cells largely escape this limit and acquire apparent immortality through e.g. telomere maintenance (Hanahan & Weinberg, 2000, 2011). The first cell line capable of continuous propagation *in vitro* was generated by carcinogenesis in mouse (Earle, 1943). Fibroblasts from the induced tumors were able to replicate indefinitely thus the mouse "L cell" cell line was born (Sanford *et al*, 1948). The first human cell line was derived from an exceptionally aggressive uterine cervical cancer tumor in 1951 (Gey *et al*, 1952). The "HeLa" cell line, named for the woman from whom they were taken – patient consent was not the norm at the time and Henrietta Lacks had not given permission to use her cells before succumbing to her cancer (Masters, 2002). Nevertheless, HeLa and the cell lines that would follow as a result of its success would greatly accelerate the progress of biology.

1.1.4 Emergence of Basal Media

The most common basal media used in modern tissue, that is media requiring supplementation with additional components, were originally developed throughout the 1950s and 60s. The first of these, Medium 199 (M199) from Connaught Medical Research Laboratories (CMRL) in 1950, was formulated for the culture of chick embryonic cells (Morgan *et al*, 1950). It contained a wide variety of components including amino acids, fat-soluble vitamins, nucleic acids precursors, cholesterol in addition to the components of White's medium, upon which it was based (M199, **Table 1**). M199 was intended as a basal medium for the study of individual components in serum, as such contain protein; therefore, as with White's medium, serum supplementation is necessary to promote growth.

Harry Eagle developed basal media for L and HeLa cell lines using an approach inspired by Fischer's method to determine the essentiality and minimum concentrations of low-molecular-weight compounds required for growth. He concluded that when supplemented with 10% serum, there was no need to supplement with additional purines, pyrimidines, fat-soluble vitamins, or tissue extracts. Rather, both cell lines could grow readily in a basal medium containing only amino acids, a mixture of B vitamins, balanced salts, and glucose. This

formulation has remained relatively unchanged except for the omission of *p*-aminobenzoic acid and addition of *D*-inositol (formerly considered a B-vitamin), and is sold today as Basal Medium Eagle (BME, **Table 1**). (Eagle, 1955b, 1955a). Examining the requirement of a wider variety of cell lines, he later developed Minimum Essential Medium which contains roughly twice the concentration of most amino acids found in BME (MEM, Table 1) (Eagle, 1959). BME was also modified by Dulbecco and Freeman to contain four-fold the amino acid concentration of BME for use in the study of plaque formation in polyoma virus in mouse embryonic cells (Dulbecco & Freeman, 1959).

In 1966/1966 Roswell Park Medical Institute (RPMI) researcher Moore *et al.* published the use of RPMI-1640 (Moore *et al.*, 1966, 1967). It is essentially a low calcium/magnesium adaptation of McCoy's 5A medium (McCoy *et al.*, 1959). McCoy had previously identified pyruvate as a key low-molecular-weight component for carcinosarcoma cells using Fischer's dialyzed serum method (Neuman & McCoy, 1958). Unlike 5A, however, RPMI-1640 does not contain animal protein digest (RPMI 1640, **Table 1**).

Basal media has seen continuous development since this then, with numerous modifications arising as the needs of specific applications are tailored to over the years. For example, high-glucose DMEM containing 4.5 g/L *D*-glucose containing more than four-fold the original concentration of glucose in the original formulation, is more common in modern tissue culture than the original. Together BME, DMEM, MEM, and RPMI-1640 are used in ~90% of published *in vitro* works containing the term "culture medium" (McKee & Komarova, 2017).

Table 1: Composition of common basal media.

	Amino Acids [mM]					Vitamins [mg/L]				
	M199 ¹	BME ²	MEM ³	DMEM ⁴	RPMI 1640 ⁵	M199 ¹	BME ²	MEM ³	DMEM ⁴	RPMI 1640 ⁵
Glycine	0.67	-	-	0.40	0.13	Ascorbic Acid	0.05	-	-	-
L-Alanine	0.28	-	-	-	-	Biotin	0.01	1	-	0.2
L-Arginine	0.33	0.01	0.60	0.40	1.15	Choline chloride	0.5	1	1	4
L-Asparagine	-	-	-	-	0.38	D-Calcium pantothenate	0.01	1	1	4
L-Aspartic acid	0.23	-	-	-	0.15	Folic Acid	0.01	1	1	4
L-Cystine	0.10	0.05	0.10	0.20	0.21	Menadione (Vitamin K₃)	0.01	-	-	-
L-Glutamic Acid	0.51	-	-	-	0.14	Niacinamide	0.025	1	1	4
L-Glutamine	0.68	-	2.00	4.00	2.05	p-Aminobenzoic Acid	0.05	-	-	1
L-Histidine	0.10	0.05	0.20	0.20	0.10	Pyridoxal hydrochloride	0.025	1	1	-
L-Hydroxyproline	0.08	-	-	-	0.15	Pyridoxine hydrochloride	0.025	-	-	4
L-Isoleucine	0.31	0.20	0.40	0.80	0.38	Riboflavin	0.01	0.1	0.1	0.4
L-Leucine	0.46	0.20	0.40	0.80	0.38	Thiamine hydrochloride	0.01	1	1	4
L-Lysine	0.38	0.20	0.40	0.80	0.22	Vitamin A	0.10	-	-	-
L-Methionine	0.10	0.05	0.10	0.20	0.10	Vitamin B₁₂	-	-	-	0.005
L-Phenylalanine	0.15	0.10	0.20	0.40	0.09	Vitamin D₂	0.1	-	-	-
L-Proline	0.35	-	-	-	0.17	alpha Tocopherol	0.01	-	-	-
L-Serine	0.24	-	-	0.40	0.29	i-Inositol	0.05	2	2	7.2
L-Threonine	0.25	0.20	0.40	0.80	0.17					
L-Tryptophan	0.05	0.02	0.05	0.08	0.02					
L-Tyrosine	0.22	0.10	0.20	0.40	0.11					
L-Valine	0.21	0.20	0.40	0.80	0.17					

(continued)

Inorganic Salts [mg/L]						Other Components [mg/L]					
	M199 ¹	BME ²	MEM ³	DMEM ⁴	RPMI 1640 ⁵		M199 ¹	BME ²	MEM ³	DMEM ⁴	RPMI 1640 ⁵
Calcium Chloride (CaCl ₂ •2H ₂ O)	200	200	264	200		2-deoxy-D-ribose	0.50	-	-	-	-
Calcium nitrate (Ca(NO ₃) ₂ •4H ₂ O)	-	-	-	-	100	Adenine sulfate	10.00	-	-	-	-
Ferric Nitrate (Fe(NO ₃) ₃ •9H ₂ O)	0.7	-	-	0.1	-	Adenosine 5'-phosphate	0.20	-	-	-	-
Magnesium Sulfate (MgSO ₄)	97.7	97.7	200	97.7	48.84	Adenosine 5'-triphosphate	1.00	-	-	-	-
Potassium Chloride (KCl)	400	400	400	400	400	Cholesterol	0.20	-	-	-	-
Sodium Bicarbonate (NaHCO ₃)	2200	2200	2200	3700	2000	D-Glucose (Dextrose)	1000	1000	1000	4000	2000
Sodium Chloride (NaCl)	6800	6800	6800	6400	6000	Glutathione (reduced)	0.05	-	-	-	1
Sodium Phosphate monobasic (NaH ₂ PO ₄ •2H ₂ O)	140	140	158	125		Guanine hydrochloride	0.30	-	-	-	-
Sodium Phosphate dibasic (Na ₂ HPO ₄)	-	-	-	-	800	Hypoxanthine	0.40	-	-	15	5
						Phenol Red	20.00	10	10	-	-
						Ribose	0.50	-	-	-	-
						Sodium Acetate	50.00	-	-	-	-
						Thymine	0.30	-	-	-	-
						Tween 80®	20.00	-	-	-	-
						Uracil	0.30	-	-	-	-
						Xanthine-Na	0.34	-	-	-	-

¹ (Morgan *et al*, 1950) – ThermoFischer Scientific media formulation #11150, Medium 199 (ThermoFischer Scientific)² (Eagle, 1955a) - ThermoFischer Scientific media formulation #21010, Basal Medium Eagle (BME) (ThermoFischer Scientific)³ (Eagle, 1959) - ThermoFischer Scientific media formulation #31095, MEM (ThermoFischer Scientific)⁴ (Dulbecco & Freeman, 1959) - ThermoFischer Scientific media formulation #11965, DMEM, high glucose (ThermoFischer Scientific)⁵ (Moore *et al*, 1967) - ThermoFischer Scientific media formulation #11875, RPMI 1640 (ThermoFischer Scientific)

1.2 Static Mammalian Cell Culture

In this section the techniques and tools most commonly employed in routine mammalian cell culture are outlined.

1.2.1 *In Vitro* Culture Systems

In vitro systems can be divided into three broad categories: isolated tissues/organs, primary and early passage cultures, and cell lines (Coecke *et al*, 2005). Figure 3 outlines the interrelation of these categories.

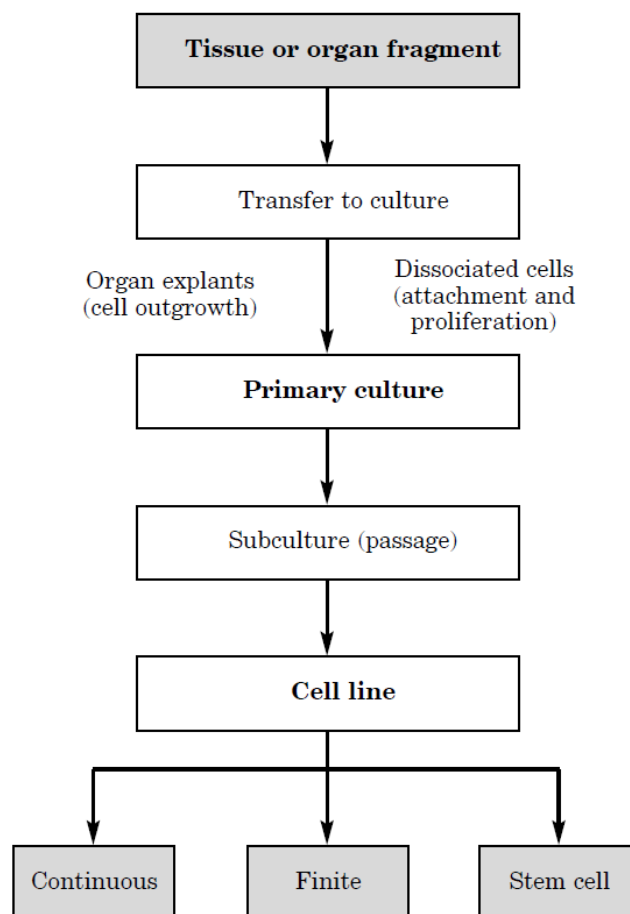


Figure 3: *In vitro* systems and their relationships. Reused with permission from Coecke *et al* (2005).

Culture begins once isolated tissues or organ fragments are transferred into culture. Organ culture typically involves uses perfusion with physiological buffers, as was first pioneered in the 1930s using a first of its kind fully autoclavable glassware pump (Carrel & Lindbergh, 1935). Organ culture techniques are of course highly specific to the sample under study, however. It is not uncommon to subdivide organs and tissues into sections in order to apply different perturbations and collect multiple replicates.

Once an organ or tissue sample is *in vitro* it is considered a primary culture. Primary cultures often retain key *in vivo* characteristics making them particularly valuable for e.g. basic research and pre-clinical drugs studies. Samples can be transferred into *in vitro* culture intact or, for example, dispersed in order to purify sub-populations of cells. Primary cultures are commonly carried out in suspension (Sauvageau *et al*, 2004) or as a monolayer on glass or plastic substrates (Paw & Zon, 1998).

1.2.2 Primary Cultures

It is possible to sub-culture some primary cultures into “early passage cultures”, however most primary cultures have a limited lifespan. This is generally caused by an inability to replicate *in vivo* conditions *in vitro*. Primary pancreatic islets, for example, suffer from core necrosis – cell death in the center of the islet spheroids – due to the loss of functional vascularization following isolation (Williams *et al*, 2012). Primary cells can also lose their *in vivo* differentiation state following culture *in vitro* for a wide variety of reasons: lack of differentiation factor signalling in the culture medium, presence of dedifferentiating factors in serum supplements, loss of extracellular matrix contact, and loss of cell-cell interactions, to name a few (Fraczek *et al*, 2013). Innovative culture strategies and technologies to address limitations in primary culture are constantly evolving.

1.2.3 Cell Lines

Cell lines collectively make up the most commonly utilized *in vitro* culture system. This is likely due in no small part to their general ease of handling, low cost, and genetic tractability (Pellegrino & Gutierrez, 2021). Upon first passage/subculture, a cell line is referred to as a cell culture (Schaffer, 1990). Although “cell culture” and “tissue culture” are colloquially used interchangeably (as well as in this work), they technically have distinct definitions; in “cell culture” the growing cells no longer maintain their original tissue organization (Schaffer, 1990). Cell lines can be further sub-divided into three categories: continuous (immortal), finite (limited lifespan), and stem cell lines (a special case of continuous/immortal cell lines). Continuous cell lines may be propagated (serially cultured) indefinitely, however long-term propagation (e.g., > 3 months) is should be avoided in order to avoid genotypic changes (Masters & Stacey, 2007). Finite cell lines, such as human diploid fibroblasts, eventually senesce after ~50 generations, i.e. the Hayflick Limit (Hayflick & Moorhead, 1961; Hayflick, 1998). Most continuous cell lines in routine cell culture originate from cancers (Masters & Stacey, 2007). Stem cells are also continuous cell lines, but are derived from embryonic or germ cell lines and retain their characteristics – chiefly pluripotency and proliferative capacity (Coecke *et al*, 2005). Stem cell lines, which are able to differentiate into many different cell types, require

extra care at all stages of handling compared to most continuous cell lines in order to maintain their pluripotency.

Immortalized cell lines can be generated through several methods. Exposing otherwise normal cells to mutagens (e.g. radiation or chemical mutagens) in order to induce immortality through mutagenesis is one method. This is, for example, is how the first mouse cell line was created (Sanford *et al*, 1948). Certain viruses can also induce immortality in certain infected cultures, such as Epstein-Barr virus in B cells, or Human T-Cell Leukemia Virus (HTLV-1) and Herpesvirus Saimiri in human lymphocytes (Katakura *et al*). Transfection with viral oncogenes is also a common method for immortalizing cells in culture, especially the SV40-large T antigen and human papilloma virus E6/E7 genes (Wu *et al*, 2020). Rodent cells are also known to spontaneously immortalize, thus they can be isolated from regular culture; this is estimated to occur at a rate of approximately 1 in 10^6 , approximately 10^6 -fold higher than that in human cells (Katakura *et al*).

If each lab must generate immortal cell lines for its own use, or obtain them for colleagues, however, the common reference point advantage of distributed cell lines is diminished, and validation of cell line identity and quality control becomes problematic. As was the case for years following the discovery of HeLa cells. Excitement about the potential of human cell lines led to numerous reports of new cell lines – most of which were found to simply have been contaminated by HeLa cell in the end (Masters, 2002; Gartler, 1968). As such cells banks arose out of the need for a common reference point for 'authentic' cell cultures, such as the American Type Culture Collection (ATCC), first set up in 1962. Other cell banks, or bioresources, include the Japanese Collection of Research Bioresources and the European Collection of Authenticated Cell Cultures (ECACC). Nearly 1000 cell lines are available from ATCC and ECACC.

The longer a cell line is in handled in a given research setting, the greater the risk of genetic drift induced by high passage number or other phenotypic changes induced by microbial or even cell line cross contamination. This can be a confounding factor in research and even lead to failure in validation of findings. It is therefore important to closely monitor cell lines in routine use, validate by genotyping, and even regularly refreshing stocks from known good references such as cell banks (Reid, 2011).

1.2.4 General Methodology

Routine mammalian cell culture is typically carried out using two-dimensional static culture methods. Essentially, cells are cultured in plastic flasks, petri dishes, or multi-well plates in or under a pool of culture medium in a humidified, CO₂-controlled, 37°C incubator. This medium is exchanged regularly, and cells are passaged serially with or without dilution as needed. Due

to the relative simplicity, ease of manipulation, compatibility with imaging, and above all low cost, this approach is commonly utilized when culturing cell lines and even primary cells and tissues.

Culture Substrate

With a few exceptions, most cells derived from mammalian tissues are anchorage-dependant (adherent), which means they must anchor to a solid surface or substrate in order to remain viable (Discher, 2005). In physiological tissues, cells attach via plasma membrane proteins such as integrin to extracellular matrix (ECM) proteins containing arginine-glycine-aspartic acid (RGD) recognition sites (e.g. fibronectin, collagens) (Ruoslahti & Pierschbacher, 1987). The ECM acts as both a mechanical support for cells as well as a bioactive reservoir for complex signalling interactions (Cheng *et al*, 2020). The plastic culture vessels used in routine static culture lack such ECM attachment sites and are typically made from hydrophobic/non-polar plastics such as polystyrene. This can be addressed several ways depending on the system under study but most commonly by chemical modification of the culture surface (Turkoglu Sasmazel *et al*, 2021) or coating of the surface with ECM-like substrate or ECM proteins. Commercially available atmospheric plasma treated culture ware are often marketed under tradenames such as Nunclon® Δ , for example. Rather than binding to proteins, cells attach to the polar surface of treated vessels via protein adsorption (Turkoglu Sasmazel *et al*, 2021). Despite being less physiological than an ECM-mimetic coating, treated culture vessels are commonly used in routine static cell line culture due to the lower cost and labor associated with preparation and handling.

Culture Medium

As touched upon in previous sections, the composition of the culture medium is of critical importance in tissue culture. There are many distinct formulations of culture medium and modifications thereof, which is indicative of the cell/tissue-specific nature of culture media. When using common cell lines and culture systems, literature or supplier recommendations are therefore a good starting point for media selection, as well as those from cell banks (see Cell Lines). For example, α -MEM, DMEM, and Ham's F-12 are common recommendations for adherent cultures, and RPMI 1640 for suspension cultures (Yao & Asayama, 2017). Basal medium, such as DMEM, contains amino acids, inorganic salts, vitamins, a pH buffering system and indicator, and an energy source such as glucose (see Table 1). The exact components and concentrations in each formulation vary by intended application, but the most commonly used basal media in routine culture cannot sustain growth without additional supplementation. The classic Eagle's series of minimal media – BME, MEM, DMEM, and derivatives – were originally formulated with dialyzed serum for example (Eagle, 1955a).

Serum

Serum is the liquid fraction of blood that has been allowed to coagulate/clot, it is devoid of clotting factors and blood cells. It is an exceptionally complex mixture that is commonly used to supplement classical basal media. Fetal bovine serum (FBS) is the most widely used supplement to basal medium in routine culture (Yao & Asayama, 2017), first used in 1958 (Puck *et al*, 1958), and is typically added at a concentration of 5-20% v/v. It contains many of the components necessary for growth, maintenance and proliferation including hormones, vitamins, various transport proteins, trace elements, growth factors, and factors important for cell attachment and spreading (Valk *et al*, 2018).

FBS in particular contains a rich assortment of peptide, small protein, and hormonal growth factors that stimulate growth in culture while simultaneously containing low gamma-globulin levels that can negatively affect growth, making it a nearly universal supplement for cell line culture (Yao & Asayama, 2017). These growth factors include insulin, insulin-like growth factor-1 (IGF-1), epidermal growth factor (EGF), basic fibroblast growth factor (bFGF), and albumin, for example, and can be particularly important for clonal growth and culture at low cell densities (Lim *et al*, 2013).

Serum is also a source of lipids for cells in culture. Chief among which are polyunsaturated fatty acids (PUFA), for which mammalian cells lack the necessary biosynthetic enzymes – $\Delta 12$ and $\Delta 15$ fatty acids desaturase (FAD12 and FAD15). Two fatty acids in particular are essential for omega-3 and omega-6 series of fatty acids, linoleic acid and α -linoleic acid (Holman, 1998). Compared to human serum, however, FBS has markedly lower concentrations of PUFAs (Delplanque & Jacotot, 1987). Some cell lines are capable of adapting to in serum-free conditions without lipid supplementation, such as the Chinese hamster ovarian (CHO) cell lines typically used in antibody production (Ritacco *et al*, 2018), however, this is an exception rather than the norm (Yao & Asayama, 2017). Serum is also a source of cholesterol, an important component of cellular membranes and precursor to a number of sterol hormones. Cholesterol in serum is packaged as cholesterol esters (cholesterol covalently linked to a fatty acid) in particles of low-density lipoprotein, which greatly enhance the solubility of cholesterol in aqueous solution and aid in uptake via membrane receptors (Hayavi & Halbert, 2005). Serum is also a source of numerous other lipid species including monounsaturated fatty acids, choline, ethanolamine, various steroids, and others.

Serum also contains trace elements that are absent in most basal media formulations, such as copper, iron, zinc, manganese molybdenum, selenium, vanadium and cobalt (Ritacco *et al*, 2018).

The complexity of serum makes it a good general source for many components required for cell growth, however this complexity can also be problematic. As a biological product the exact composition of serum such as FBS is unknown and varies from batch-to-batch (Price & Gregory, 1982), by geographical origin, and even with the seasons (Nelson *et al*, 2016). This can lead to reproducibility challenges in research as biologically active substances change composition (van der Valk *et al*, 2010) or even unknowingly interact with small molecules such as drugs. The widespread use of FBS is also ethically problematic, as the blood of upwards of 2 million bovine fetuses are harvested yearly (Brindley *et al*, 2012) and potentially experience pain or discomfort during the process (Jochems *et al*, 2002). The availability of FBS is closely tied to the beef and cattle industry, therefore subject to complex external factors (Brindley *et al*, 2012), a consideration that is particularly relevant in era of COVID-19 disrupted global supply chains. As such, efforts towards serum-free culture have been ongoing for decades, particularly in the manufacture of biologics (Ritacco *et al*, 2018), but have yet to replace FBS in routine cell culture.

Atmosphere

Purpose-built incubators are typically utilized for growing mammalian cells in culture. They are primarily purpose is to maintain: 1) constant temperature of 37°C, 2) saturated water-vapor atmosphere (high humidity), 3) a defined CO₂ gas concentration. Mammalian cells are well-adapted for growth at 37°C, and so are many of the cells and cell lines derived therefrom. The gas permeability of plastic culture vessel is extremely poor, therefore a monolayer of cells growing on a plastic substrate must exchange gases such as CO₂ and O₂ primarily through the culture medium. For this reason, common culture-ware permits physical gas exchange through e.g., a filtered screw cap, or a gapped lid. A humidified atmosphere greatly slows the evaporation of culture medium through these features. Modern basal media generally contain a bicarbonate buffer, therefore require a 5% v/v CO₂ atmosphere in order for dissolved CO₂ in the form of carbonic acid to complete the buffer system and maintain a physiological pH of ~7.2-7.4 (Yao & Asayama, 2017). Phenol red is used to visually monitor the pH of culture medium by colour: (pH < 6.5, yellow) < (pH 7.0, orange) < (pH 7.4, red) < (pH 7.6, pink) < (pH > 8.0, purple) (Masters & Stacey, 2007).

1.3 Pancreatic Islet Culture

Pancreatic islets (of Langerhans) are the functional unit of the endocrine pancreas and are collectively responsible for maintaining blood glucose homeostasis (Campbell & Newgard, 2021). Islets are small clusters of cells distributed throughout the pancreas with a slight concentration towards the tail region (Wittingen & Frey, 1974; Saito *et al*, 1978). Islets range in size from a few dozen cells to several thousand, with size and number varying widely

between individuals, more so in human compared to rodent (In't Veld & Marichal, 2010). The main endocrine cell types in the islet are insulin-secreting β cells, glucagon-secreting α cells, and somatostatin-secreting δ cells (Brissova *et al*, 2005). Other minor populations include pancreatic polypeptide-expressing PP cells (Kimmel *et al*, 1975) and ghrelin-expressing ϵ cells (Wierup *et al*, 2002).

1.3.1 Primary Islets

Islets isolated from human donors and animal models are often used *in vitro* to study islet biology and disease (Marquina-Sanchez *et al*, 2020). Isolated islets are quantified in terms of islet equivalents (IEQ), a metric equal to the tissue volume of a 150 μm sphere meant to approximate a “typical” islet (Ricordi *et al*, 1990). Though the assumption that islets are perfectly spherical and even the very concept of a “typical” islet is problematic, it is a common reference adopted internationally by islet isolation facilities (Ramachandran *et al*, 2015).

Islets are heavily vascularised, three dimensional structures (In't Veld & Marichal, 2010). Isolation inherently leads to the destruction of functional circulation, severely limiting nutrient and small-molecule access to the islet core to passive diffusion, which is entirely inadequate in larger islets (Bertram & Pernarowski, 1998; Williams *et al*, 2012). This is problematic not only because it leads to cell death in the islet core (Giuliani *et al*, 2005), but also limits the researcher's ability to effectively drug or genetically manipulate intact islets in culture to the outer layers of cells (Friedlander *et al*, 2021). The wide variability in islet size (Brissova *et al*, 2005) further exacerbates heterogeneity with respect to these factors, potentially further convoluting islet culture experiments. Additionally, stress from the isolation procedure (Bottino *et al*, 2004), loss of molecular cues from extracellular matrix contact, and loss of growth factors can lead to death in isolated islet culture (Paraskevas *et al*, 2000). Intact islets therefore show marked degradation in physiological function and morphology in culture within two weeks (Schmied *et al*, 2000).

To address these limitations several methods have been developed in order to reaggregate primary islets into smaller, uniform islet spheroids, sometimes referred to as neo-islets or pseudo-islets – though the term pseudo-islet is also used for cell line-based spheroids. These methods capitalize on the innate ability of dispersed islet cells to spontaneously coalesce and form ordered three dimensional structures resembling that of native islets (Halban *et al*, 1987). Common methods include spontaneous aggregation in wells or hanging drops, and specially designed micro-wells (Friedlander *et al*, 2021).

Spontaneous aggregation is the most straight-forward approach and is widely used and validated in transduction experiments (Zaldumbide *et al*, 2013; Arda *et al*, 2016). Dispersed islet cells are seeded at a defined density into low-attachment culture vessels, such as

untreated 35 mm petri dishes (Wassmer *et al*, 2020) or 96-well plates (Bevacqua *et al*, 2021), and incubated to form islet spheroids over a defined period of time, generally several days. Sometimes an initial centrifugation step is used to initiate aggregation, and can narrow the size distribution of islet spheroids (Liu *et al*, 2019). The main advantage of spontaneous aggregation when compared to other methods is its relative simplicity and accessibility due to the use of general-purpose culture ware. Specialized commercial solutions are also available such as Akura™ (inSphero, Switzerland) plates, which reduce aggregation volume and optimize well geometry to improve aggregation efficiency and consistency and BIOFLOAT™ (faCellitate, Germany) plates which have a proprietary non-adherent coating to reduce cell-plate adhesion.

Hanging drop methods take advantage of the shape of inverted media droplets, generally placed on culture ware lids. The smooth, bowl-like shape that forms in the droplets work with gravity to concentrate dispersed islet cells together near the bottom of each hanging drop. The drops are suspended above a dish filled with e.g., PBS (Wassmer *et al*, 2020), in order to avoid drying the small droplets. This approach derives from applications long used in, for example, embryo culture (Potter & Morris, 1985). The hanging drop method produces spheroids of better-defined size than spontaneous aggregation without requiring specialized equipment. It is more laborious, but can be adapted for use with liquid-handling automation (Walker *et al*, 2020).

Micro-wells for islet spheroid generation are diverse in the specifics of their design and fabrication but are based on the same underlying principle as the hanging drop method – cells are guided together by the geometry of the well via gravity or centrifugation to produce spherical aggregates (Mohr *et al*, 2006). One islet spheroid is produced in each micro-well, and their diameter can be tuned by adjusting the size of the micro-wells and seeding density (Ichihara *et al*, 2016; Shinohara *et al*, 2014). A large number of micro-wells can be arrayed into standard culture ware wells allowing for much higher throughput than spontaneous aggregation or hanging drop techniques, for example, generating tens of thousands of spheroids in a single 12-well plate (Hilderink *et al*, 2015). Laboratory fabrication of micro-wells is primarily carried out using soft lithography, molding biocompatible materials such as agarose gel, polydimethylsiloxane (PDMS), or poly(ethylene glycol) (PEG) hydrogel over rigid mold negatives (Choi *et al*, 2010; Lin & Anseth, 2011; Bernard *et al*, 2012; Hilderink *et al*, 2015; Ichihara *et al*, 2016; Shinohara *et al*, 2014; Hwang *et al*, 2011; Wassmer *et al*, 2020; Lee *et al*, 2020; Myasnikova *et al*, 2019). These techniques require specialized equipment and expertise to utilize, however, several commercial solutions are also available such as AggreWell™ (STEMCELL Technologies, Germany) and Sphericalplate5D™ (Kugelmeiers, Switzerland). The primary advantage of using micro-well arrays is the ability to

generate islet spheroids at much higher throughput, with the trade-off being primarily the cost related to fabrication (expertise and equipment) or purchasing of commercial plates.

1.3.2 Islet Cell Lines

Numerous continuous cell lines have been generated for the study of islet biology and disease. Much of islet research focuses on diabetes and therapeutics, as such the cell line toolbox is heavily biased towards β cell models. There is only one commercially available α cell line, murine α TC1 (Powers *et al*, 1990b) available from ATCC (CRL-2934), while a number of β cell lines are commonly used: RIN (Rajkov *et al*, 2018), HIT (Santerre *et al*, 1981), β TC (Efrat *et al*, 1988), MIN-6 (Miyazaki *et al*, 1990), NIT-1 (Hamaguchi *et al*, 1991), INS-1 (Asfari *et al*, 1992), and β HC-9 (Noda *et al*, 1996) rodent cell lines as well as the human cell lines EndoC- β H (Ravassard *et al*, 2011) and 1.1B4 (McCluskey *et al*, 2011). As is typically the case, however, each cell line has its own strengths, limitations, and divergences from its parent cells; Green *et al*. have curated a comprehensive overview of the various rodent and human β cell lines, including pros, cons, and individual quirks (Green *et al*, 2018). The majority of *in vitro* β cell line work is carried out on cells derived from rodent insulinomas, Min6 and INS-1 in particular (Bakhti *et al*, 2019), which are generated using SV40 large-T antigen expression tied to the insulin gene promoter in transgenic animals (Skelin, 2010).

The proliferative capacity of cell line models is vital in enabling large-scale experiments, for example high-content screening (Li *et al*, 2017a), and other drug screens (Tsonkova *et al*, 2018). Unfortunately, the process by which islet cells are generated can lead to non-physiological phenotypes such as abnormal insulin secretion responsiveness (Efrat, 2004), low overall insulin content, abnormal co-expression of genes (Poitout *et al*, 1996), and immunological differences (Radvanyi *et al*, 1993). High passage of islet cell lines can also lead to, for example, the loss of insulin secretion and altered metabolism in Min6 cells (Cheng *et al*, 2012).

The murine pancreatic alpha cell line, α TC1, and beta cell lines, β TC, were derived from insulinoma and glucagonoma tumour cells in transgenic mice expressing the SV-40 large-T antigen oncogene under rat insulin and preproglucagon promoter control, respectively (Powers *et al*, 1990a; Efrat *et al*, 1988). Subclones and variations of each have since been developed with improved characteristics. The α TC1 parental cell line, for example, produced insulin as well as glucagon and was quickly replaced by α TC1 clone 6, a more differentiated clone expressing no detectable levels of insulin protein (Hamaguchi & Leiter, 1990). Several distinct β TC cell lines and subclones have arisen including β TC3 and β TC6, and that exhibit stabler differentiation than the original β TC and show more physiological insulin secretion with respect to glucose concentration (Efrat *et al*, 1991; Poitout *et al*, 1995). These cell lines have

been used extensively since and have recently been characterized on the transcript and epigenetic levels and compare favorably to their primary islet counterparts (Lawlor *et al*, 2017). They are routinely cultured in monolayers under static culture conditions in DMEM basal medium, low-glucose (1 g/L), supplemented with 10% FBS (Li *et al*, 2017a, 2009).

1.3.3 Hormone Secretion Assay

The primary function of islets in the body is to secrete insulin and glucagon in order to regulate blood glucose concentrations. As such, the primary readout used to assess islet function in culture experiments is to measure hormone secretion in response to glucose stimulation, with a general focus on insulin secretion, i.e. glucose-stimulated insulin secretion (GSIS) (Zuellig *et al*, 2017; Schmied *et al*, 2000; Yu *et al*, 2018; Ribeiro *et al*, 2018). Cell lines, dissociated islets, or intact islets are first pre-incubated in a low-glucose (~1-3 mM) solution for one to two hours, typically Krebs-Ringer Buffer (KRB) or a low-glucose modified culture medium, to remove residual insulin (Pagliuca *et al*, 2014; Davis *et al*, 2020). If assaying glucagon secretion in parallel, the supernatant can be sampled from this incubation step for quantification by e.g., ELISA (Fomina-Yadlin *et al*, 2010). Insulin secretion is then stimulated by incubation in a high-glucose (16.7 mM) solution with a low-glucose (unstimulated) control in parallel for another 30-60 min, after which both supernatants are assayed for insulin content and normalized to islet cluster or cell number (Fomina-Yadlin *et al*, 2010). It is also common to perform these two measurements on the same samples, rather than two in parallel, by incubating first in the low-glucose, then high-glucose solution (Ichihara *et al*, 2016; Hwang *et al*, 2011). The ratio of insulin secreted in high- vs. low-glucose stimulated conditions is sometimes reported as the stimulation index or as fraction of the total insulin as quantified following lysis (Yu *et al*, 2018; Wassmer *et al*, 2020). GSIS stimulation index values vary greatly but are generally within one order of magnitude of basal secretion (Yu *et al*, 2018).

1.4 Dynamic Culture

Dynamic culture systems offer a number of advantages over conventional static culture. In 2D static culture systems in particular, the impermeable polystyrene culture surface typically used provides neither a means for nutrients nor dissolved gases to access the cells in culture (Halldorsson *et al*, 2015). Cells in such a system must rely purely on passive diffusion to meet their metabolic needs, which can be limiting in many scenarios (Place *et al*, 2017), a fundamental limitation that has been known for decades (McLimans *et al*, 1968). This same diffusive limitation applies to secreted signalling factors in culture, which can be of particular importance in some systems (Bou-Ghannam *et al*, 2021).

In suspension cell culture, such as with 3D spheroids or non-adherent cells, this can be addressed by continuously agitating the culture medium using, for example, spinner flasks (Newland *et al*, 2020) or rocker (Singh, 2002; Tsai *et al*, 2017) dynamic culture platforms. Culture medium still needs to be replenished regularly, however nutrients and dissolved gasses are more uniformly distributed throughout the culture, maximizing their availability to each cell. Comparatively simple and affordable dynamic culture systems for anchorage-dependant cell culture are generally lacking, however. Microfluidics systems often require specialized equipment and expertise to fabricate, and do not typically yield the large amount of biological material required for genome-wide perturbations and proteomics experiments. While the hollow-fiber bioreactors typically utilized in large-scale production of biologics such as mono-clonal antibodies (Jayaprakash, 2021) are not compatible with microscopy and generally cost prohibitive for routine culture. See “Hardware in Context”, Section 2.1.2 for further discussion of bioreactor design categories.

Continuous flow of culture medium through the vessel can also improve diffusion by maximizing the concentration gradient of nutrients, waste, and secreted factors (Sankar *et al*, 2011). The application of dynamic culture with 3D tissue models such as spheroids has been shown to be beneficial in a number of ways. A variety of fluidic devices have been developed for the culture of islets and pseudo islets under flow (Li *et al*, 2017b; Jun *et al*, 2019; Sokolowska *et al*, 2021), the quantification of hormone secretion (Erickson *et al*, 2021; Eaton & Roper, 2021; Shaikh Mohammed *et al*, 2009; Schulze *et al*, 2017, 2021; Gliberman *et al*, 2019), and the differentiation of stem cells into islet cell types (Tao *et al*, 2019; Barati *et al*, 2019), for example. In particular reaggregated islets cultured under flow showed improved viability, morphology, glucose responsiveness, and maintained differentiation better under long term culture than those cultured under static conditions (Jun *et al*, 2019).

Systematic studies on the differences caused by static vs. perfused conditions on cellular transcriptomes, proteomes, metabolomes, lipidomes or secretomes are rare. Hepatocyte spheroids grow faster and presented more physiological morphology under perfusion than in static culture (Kim *et al*, 2021). Colon explants cultured on a rocker plate showed improved gene marker profiles associated with differentiation, polarization, and apoptosis (Drew *et al*, 2015). Mouse embryonic stem cells also differentiated more effectively in dynamic culture (Gerlach *et al*, 2010). The effects of these culture systems on their cell models are generally assessed through functional readouts (e.g., insulin- and/or glucagon secretion assays), specific marker genes/protein staining (Manfredonia *et al*, 2019), morphology (Jun *et al*, 2019), and cell viability/number (Essaouiba *et al*, 2021).

While the benefits of dynamic culture in these systems is apparent, the application of dynamic culture to more routine 2D culture formats is less well studied (Hughes *et al*, 2021). 3D culture systems generally offer more physiologically relevant models, however, their lack of widespread adoption in routine culture work is a testament to the challenges they can bring with them. The application of flow to a 2D monoculture has shown some potential with several cell lines in a microfluidic devices, improving viability and introducing physiological properties such as shear force and increased mass transfer (Lee *et al*, 2006). But the potential benefits of applying dynamic culture to adherent monolayer culture have yet to be thoroughly assessed.

1.5 Aims

Here, I hypothesize that exact culture conditions will be of particular importance for the cellular composition and function of pancreatic islet cell types. These cells are optimized to sense glucose and other nutrients and integrate these signals for a coordinated response with hormones secretion to the blood stream. Standard static culture conditions are inappropriate in multiple ways: media composition does not reflect the normal nutrient status these cells are exposed to in an organism; batch culture causes a slow depletion of nutrient and glucose over days as opposed to the periodic postprandial changes in vivo; and finally, secreted factors including hormones are not transported away but rather accumulate in the culture dish. I therefore predict that perfusion culture will lead to profound changes to islet cell physiology. Therefore, I aim to first build a system for the large-scale cultivation of islet cells and then comprehensively analyze cellular changes relative to static culture.

The first aim of this project is to develop a perfusion culture system that is directly compatible with routine cell culture - anchorage dependant cell lines in particular – in order to bridge the gap between static culture and more advance dynamic 3D culture systems. Thus, it is critical that this system be inexpensive, accessible, and not introduce any undue handling complications. As a culture tool, it also needs to be flexible enough for use in a range of dynamic experimental setups.

Once established, the second aim of the project is to characterize the effects of continuous perfusion using this system on cell lines routinely utilized in the lab. By virtue of their function as regulators of blood glucose, islets endocrine cells are exquisitely sensitive to the composition of their microenvironment. We therefore hypothesize that perfusion culture is likely have an effect on islet cell lines in culture, potentially bringing them towards a more physiological state. To the best of our knowledge a systems-level investigation utilizing tools such as proteomics, RNA-sequencing, and metabolomics, to determine the effects of continuous perfusion has not been carried out to date.

2. RESULTS

2.1 PlateFlo – A software-controllable plate-scale perfusion system for culture of adherent cells

2.1.1 Prologue

Static 2D monolayer culture remains the de facto method for mammalian cell culture primarily by virtue of its cost-effectiveness and ease of handling. Available dynamic culture solutions are geared towards advanced 3D culture models such as spheroids or organoids and often make use of custom fabricated culture chambers that require expertise and equipment. The greatly improved physiological condition of these culture systems therefore comes at a cost both literally and metaphorically, with increased expense and handling effort, for example. Few solutions exist for the millilitre-scale perfusion of cell lines in a format that is familiar and accessible for routine culture. Here we present an open-source culture system, PlateFlo, that allows cell lines and other adherent cells to be cultured under perfusion directly in a typical culture plate. Along with detailed build instructions for the culture plate lid, we provide a toolbox that allows for the integration of valves and other 12V devices into a more sophisticated and dynamic culture experiment utilizing software control.

This article was published in:

Pazdzior R & Kubicek S. PlateFlo – A software-controllable plate-scale perfusion system for culture of adherent cells. *HardwareX* **10** (2021). <https://doi.org/10.1016/j.ohx.2021.e00222>

2.1.2 Publication PDF

This section includes a reproduction of the published work. This publication relies heavily on online resources detailing the construction of the PlateFlo lid and FETbox module, setup and operation of the perfusion system, and usage manual for *plateflo* Python package to supplement the main text. A live version of these resources is available at <https://plateflo.readthedocs.io> and an archived version for offline viewing (in HTML format) is available from the publication repository at <https://osf.io/hev2z/> (unzip the folder, then open “index.html” with your preferred browser).

A PDF export of the ReadTheDocs resource is appended for completeness following the main text of the publication below, however, for optimal viewing the reader is highly encouraged to visit one of the links provided above.



PlateFlo – A software-controllable plate-scale perfusion system for culture of adherent cells



Robert Pazdzior, Stefan Kubicek*

CeMM Research Center for Molecular Medicine of the Austrian Academy of Sciences, Vienna, Austria

ARTICLE INFO

Article history:

Received 6 May 2021

Received in revised form 23 July 2021

Accepted 5 August 2021

Keywords:

Adherent

Perfusion

Millifluidic

Microplate

Cell culture

Automation

ABSTRACT

Here we present a versatile system for milliliter-scale perfusion culture of adherent cells that can be built using basic tools, based on a readily available one-well culture plate (84 cm² culture area). Media composition and flow paths can be programmatically controlled via USB serial interface using the FETbox hardware controller and associated PlateFlo Python package. The FETbox can control up to five high current 12 V devices such as common pinch valves, solenoids, and DC motor peristaltic pumps. It was designed to be easily customized with built-in accommodation for additional electronic components (e.g. analog sensors and input), use of the ubiquitous Arduino Nano platform, and easily expanded serial communication protocol. Multiple FETboxes can be used in parallel for additional devices. Applications of the PlateFlo system include perfusion culture of laboratory experiments requiring large cell numbers including genome-scale genetic screens and proteomics, as well as novel perfusion schemes including dynamic media conditions and sequential cell culture.

© 2021 The Authors. Published by Elsevier Ltd. This is an open access article under the CC BY-NC-ND license (<http://creativecommons.org/licenses/by-nc-nd/4.0/>).

Specifications table

Hardware name	<i>PlateFlo plate-scale perfusion system</i>
Subject area	<ul style="list-style-type: none"> • Biological Sciences (e.g. Microbiology and Biochemistry) • Biological sample handling and preparation
Hardware type	<i>Software - GNU General Public License (GPL) v3;</i>
Open Source License	<i>Hardware - CERN Open Hardware License, Weakly Reciprocal (OHL-W) v1.2</i>
Cost of Hardware	<i>Hardware: 350 EUR*</i>
Source File Repository	<i>Consumables: < 10 EUR/plate</i> OSF - https://doi.org/10.17605/OSF.IO/PYJCH

*Minimum of two additional individually controllable peristaltic pumps, and associated tubing/fittings are required.

Abbreviations: BOM, bill of materials; CFD, computational fluid dynamics; DMEM, Dulbecco's modified Eagle's medium; EUR, Euro; FDM, fused deposition modelling; hIPSC, human induced pluripotent stem cell; MCU, microcontroller unit; MOSFET, metal oxide semiconductor field effect transistor; PBS, phosphate-buffered saline; PCB, printed circuit board; PWM, pulse width modulation.

* Corresponding author.

E-mail address: SKubicek@cemm.oeaw.ac.at (S. Kubicek).

<https://doi.org/10.1016/j.ohx.2021.e00222>

2468-0672/© 2021 The Authors. Published by Elsevier Ltd.

This is an open access article under the CC BY-NC-ND license (<http://creativecommons.org/licenses/by-nc-nd/4.0/>).

Hardware in context

Most *in vitro* tissue culture models used in biological research, be it immortalized cell lines or primary tissue, are cultured in traditional petri dishes or multi-well plates under a static pool of nutrient medium. Cells in static culture are subjected to unphysiological buildup of secreted factors and waste products while simultaneously depleting glucose, amino acids, and other nutrients from the medium. This gradual decline/accumulation is punctuated by a sharp reversal in concentration trends when the nutrient medium is periodically renewed in bulk during regular cell maintenance [1]. This creates unintended temporal heterogeneity in the extracellular environment that could be a confounding factor in some biological systems. Static culture also lacks the mechanical stimulation provided by fluid shear forces along vesicles and within the interstitial *in vivo*, a key factor in the differentiation of endothelial cells [2] and osteoclasts [3], for example. One way to overcome these shortcomings is to continuously perfuse fresh or partially recirculated nutrient medium through the culture vessel [4,5]. Different technical solutions for perfusion cell culture have been implemented (Table 1).

Stirred-tank bioreactors are commonly employed in perfusion culture, particularly in industry [6]. These are culture vessels in which cells are kept in suspension by an impeller and medium is supplied and drawn from the tank to maintain nutrient concentration, pH, and other process factors. This style of perfusion device is effective at maintaining high cell density and is thus favored in production, particularly of recombinant proteins such as antibodies. Commercial laboratory-scale solutions also exist, for example disposable spinner flasks that are available in different sizes with sidearms for inlet/outlet connection. Many cell types are anchorage-dependent (adherent), however, and are not viable in suspension [7] on their own. In order to culture these cells in suspension, suspended particles are utilized to provide a suitable surface for attachment and growth [8]. These so-called microcarriers have proven effective in stirred reactors, particularly for example, with mesenchymal stem cells, and can be tuned in numerous ways including size, shape, and porosity.

Hollow fiber bioreactors are well-suited to adherent cell culture [9]. They consist of many semi-porous capillaries through which nutrient media is circulated and a surrounding compartment in which cells are seeded and grow [10], often in the form of a single-use cartridges in commercial solutions (e.g. FiberCell Systems Inc., Cellab GmbH, and Terumo BCT Inc.). Small molecules and dissolved gas perfuse through the porous tubing in both directions, providing nutrients to- and removing waste from cells adhering to the tubing within the outer compartment. Hundreds, even thousands, of capillary tubes can fit in a single cartridge, thus, an extremely large growth area is possible in a relatively small footprint. Cells grow to very high confluency and secreted protein products and extracellular vesicles can be continuously collected downstream and concentrated, thus making hollow fiber bioreactors highly effective in production applications. The main downside, as with most commercial solutions, is the upfront cost for ready-built systems as well as the recurring price of consumable single-use bioreactor cartridges. Cells must be harvested, e.g. trypsinized, in order to perform microscopy thus strongly perturbing the system. Because of the compartmentalized nature of the nutrient media flow path, cells are isolated from shear stress – which may be desirable in some applications but is less physiological than direct perfusion.

Microfluidic devices offer near infinite diversity in design, limited only by the imagination and fabrication skill of the creator, and can be tailored to fit the application or biological question at hand [11]. Microfluidic devices can be fabricated by a wide variety of methods, most of which require specialized equipment and skills such as photolithography [12], CNC milling [13], or laser micromachining [14]. The alternative, commercial solutions, whether it be custom or off-the-shelf can be cost-prohibitive, depending on complexity and specialization. The small scale of microfluidic chips permits precise real-time control of flow parameters and composition while avoiding dilution of secreted factors important for e.g. hormone secretion assays. With this small scale comes some limitations, however; pumping and directing flow at nanoliter flow rates, often with pneumatic systems, can be more complex to setup/control. Biological material generation can also be a limiting factor for downstream readouts such as proteomics and genome-scale genetic screening.

In the broad class of bioreactors termed here ‘perfused scaffold chamber’ reactors, cells or tissue models are embedded within a permeable matrix that allows media to flow directly through the entire construct. The oscillating chamber bioreactor, patented by Moretti [15,16], utilizes a similar concept but takes a unique approach in implementing it. Instead of mechanically pumping media through the chamber with e.g. a peristaltic pump, gas-permeable semi-circular reservoir tubing containing nutrient medium on either side of the chamber alternately perfuses the interstitial space by gravity; this is achieved by rotating the entire chamber back and forth along the axis perpendicular to the plane of the tubing path [17]. In these systems the chamber can be constructed with a transparent window for optical readout and sensors and electrodes integrated for monitoring or stimulation. Interstitial perfusion allows for thorough exchange with the perfusion medium and full compatibility with three-dimensional tissue models. The obligatory support matrix, while often beneficial for 3D tissue models, adds complexity to both setup and harvest. Common matrix supports, such as Matrigel, can also complicate downstream proteomic preparation [18] or negatively impact proteomic results if not considered.

Perfused well bioreactors are also a diverse class of devices, but many assume a roughly microplate footprint with several culture chambers therein. Some examples are given in Table 1 that range in scale from 96- to 12-well formats. These are constructed using a variety of techniques including (micro)machining, silicon wafer etching, and PDMS casting. These smaller wells are well suited to experiments requiring multiple treatments or conditions, especially Domansky et al’s multi-well plate where each well has an independent reservoir and medium is pumped through the 14.9 mm culture scaffolds using pneumatic diaphragm micropumps [19]. Pasini et al, in contrast, use serially perfused chambers in a 12-well format machined from PMMA (acrylic) in combination with glass coverslip culture surfaces for more traditional 2D cell culture [20].

Table 1

A general overview of comparable perfusion culture approaches.

Bioreactor Type	Description	Examples	Comments		
Perfused Plate	Modified commercial rectangular culture plates or petri dishes with treated culture surface over which media flows	This work		Cost	\$
				Scale	+++ 84 cm ² culture area 10–25 mL
				Flow Rate	0.1–10 mL/min
				Complexity	++
				Availability	Open-source
				Adherent/ Suspension	Adherent
				2D/3D	2D
Perfused Well	Diverse custom fabricated multi-well constructions. Some incorporating pumping directly in each well or utilizing hydrostatic (gravity) feeding.	[40–42], e.g. Corning MicroDEN	Complexity is primarily driven by (micro)fabrication requirements.	Cost	\$\$
				Scale	+
				Flow Rate	µL/min
				Complexity	+++
				Availability	Publication, Commercial
				Adherent/ Suspension	Adherent or matrix embedded
				2D/3D	2D
Perfused Scaffold Chamber	Cells or tissue contained in a perfusable cartridge-like scaffold/matrix	[43–46]	Diverse class of devices. Scaffold size, composition, and topology are highly tunable.	Cost	\$\$
				Scale	++
				Flow Rate	Diverse. µL/min - mL/min
				Complexity	+++
				Availability	Publication
				Adherent/ Suspension	Adherent/embedded
				2D/3D	3D
Hollow-Fiber Bioreactor	Waste/nutrient exchange via semi-porous capillary tubing and cells grown in extra-capillary space. The massive number of capillaries that can be contained inside a culture chamber enables extremely high culture density.	[8,10,47]	Diverse commercial solutions due to use in part to widespread use in the production of biologicals. Lab-scale solutions also available. Capillary fouling is must be considered. See text for examples. See [48] for a summary of production technologies including hollow-fiber bioreactors.	Cost	\$\$\$-\$\$\$\$
				Scale	++ - ++++
				Flow Rate	Up to 200 cm ² /mL Diverse
				Complexity	++
				Availability	Commercial
				Adherent/ Suspension	Both
				2D/3D	2D
Oscillating Chamber Bioreactor	Sensor-equipped, optically transparent construct chamber perfused by oscillating motion of medium through connected semi-circular gas permeable tubing.	[38,39]	All-in-one device allows electrical stimulation, electrical sensor integration, and optical readouts.	Cost	\$\$\$
				Scale	++
				Flow Rate	ø 12 mm × h 3 mm, 10 mL medium, per chamber. 100 µm/s linear equivalent
				Complexity	++++
				Availability	Publication, Commercialized
				Adherent/ Suspension	Both
				2D/3D	3D

(continued on next page)

Table 1 (continued)

Bioreactor Type	Description	Examples	Comments	Cost	Scale	Flow Rate	Complexity	Availability	Adherent/ Suspension
Stirred Tank Bioreactor	An impellor agitates the culture medium, preventing cells from sedimenting while maximizing waste removal and nutrient delivery by homogenizing the medium.	[48,49], e.g. Corning Spinner Flasks	Basic in principle, but endlessly customizable and extremely scalable. Sensors can be easily integrated, impellor design optimized, and diverse microcarriers utilized. Continuous perfusion is complicated by the need for filtration or other solutions to prevent aspiration of suspended cells. Fed-batch is a simplified alternative to continuous feeding/perfusion.	\$ - \$\$\$\$	+ - +++++ mL – kL	$\mu\text{L}/\text{min}$ – L/s	Diverse	Diverse	Suspension, adherent on micro-carriers, adherent as spheroids
									2D/3D 3D

The “PlateFlo” system presented here is a flexible, low cost, solution for laboratory-scale perfusion of adherent cells. It can be built using only basic tools and the modular nature of the design allows for substitution of main components to better suit specific applications if need be. The perfusion plate design utilizes a modified off-the-shelf culture plate rather than a custom-fabricated culture chamber. This lidded, one-well, rectangular microplate can be loaded with cells, pre-treated, imaged, etc., as a typical culture plate independently of the fluidic components of the system. This improves sterile handling, allows for microscopy-based readouts, and is compatible with diverse cell harvesting methods – e.g. cell scraping, trypsinization, or in-plate lysis. Biological material can be generated in sufficient quantity from a single plate for unbiased multi-omics analysis including proteomics and various sequencing technologies. The electronic components of the system are intended to interface via USB with a control computer where dynamic perfusion programs can be created using the plateflo Python library, or any serial interface capable software such as LabVIEW.

The most comparable commercial alternative to the PlateFlo system is the Corning MicroDEN perfusion platform. Similar to the device presented here, media is pumped across a tissue culture surface continuously using peristaltic pumps. A key difference is the closed nature of the perfusion chamber, and closed loop recirculating flow approach which uses a single pump for each chamber. Each recirculating flow path has a 13 mL volume and advertised yield of six million cells each and is marketed for production of dendritic cells. At the time of writing, this system was listed for \$18,430, and the single-use perfusion chamber/reservoir combo unit was listed at \$1930 per pair. The MicroDEN platform is purpose-built for a specific application, however, thus lacks the versatility and flexibility of the PlateFlo system; with the system described here media can be recirculated (closed loop) or continuously exchanged (open loop), selected from multiple reservoirs using one or more valves, the pumps controlled dynamically, and more. With the PlateFlo system we provide as many tools as possible to adapt it to suite a wide range of experimental setups.

Hardware description

The PlateFlo system consists of three main components: (1) the perfusion plate and associated fluidics for cell culture, (2) the FETbox hardware controller for high-current device control (e.g. valves, DC pumps), and (3) the plateflo Python package for programmatic control over (1) and (2). These components are presented as a toolbox with which it is possible to build plate-scale perfusion systems ranging in complexity from a single plate, single reservoir, constant flow rate setup to e.g. a sequential culture system chaining multiple cell lines in series, dosing glucose, drugs, or different nutrient medium on a predefined schedule.

Perfusion plate

The perfusion culture chamber is a modified Nunc OmniTray one-well plate (Fig. 1). The culture area of a Nunc OmniTray plate is 84 cm², for reference, this is approximately 50% greater than that of a typical 10 cm petri dish (55 cm²). Nutrient medium is pumped in one side and out the other, flowing nearly uniformly across the culture surface. Only modifications to the lid are necessary, therefore it can be built, sterilized, and otherwise handled independently of the base. This permits hot swapping of the plate base for e.g. microscopy, additional biological replicates, etc., without having to disassemble and re-sterilize the associated fluidics. Standard 200 μ L (P200) pipette tips are repurposed for the nozzles and are inserted through drilled holes in the plate lid with tubing press fit into the tapered section of the pipette tip. A modified lid can be reused several times with replacement of the nozzles as necessary to avoid cross-contamination.

Two independently controllable peristaltic pumps are required to pump fresh media into the plate and remove the effluent simultaneously - one for the inlet nozzle and one for the pair of outlet nozzles. Multi-channel peristaltic pumps can be used to run multiple plates in parallel. The need for two peristaltic pumps introduces a technical challenge, however; if the inlet and outlet flow rates are not absolutely identical there will be a net movement of media into or out of the perfusion plate, potentially overflowing or running dry; for example, at a flow rate of 120 μ L/min, just a 1% difference between the inlet and outlet flow rates will result in a plate volume change of greater than 5 mL over the course of 72 h (~50% of the OmniTray working volume used here). To avoid the added cost and complexity of closed-loop sub-milliliter flow metering, or constant pump recalibration and validation, for example, a ‘skimming’ system was implemented for plate volume regulation.

An additional independent outlet nozzle, the skimmer nozzle, is set at the desired fluid height using a 3D printed clamping mechanism and height blocks. The main outlet pump is run marginally slower than the inlet to ensure a small net positive influx of media. The exact flow rate delta should be a safe margin, determined by characterizing the flow rate accuracy of the specific pumps and cassette tubing chosen. An inexpensive peristaltic pump or aspirator is used to remove the small excess media as it reaches the skimmer. This eliminates the need for expensive, complex, and potentially difficult to clean microflow meters and closed-loop pump control.

FETbox hardware controller

The FETbox hardware controller enables USB serial controlled switching of up to five high-current 12 V devices such as pinch valves, solenoids, and DC motor peristaltic pumps (Fig. 2A). Some of these outputs are intended to drive inexpensive skimmer pumps or aspirator solenoid valves. The remaining outputs or additional FETboxes can be used for fluid path control in the system via pinch valves – e.g. switching between media reservoirs, recirculating media, or redirecting effluent to a sampling system.

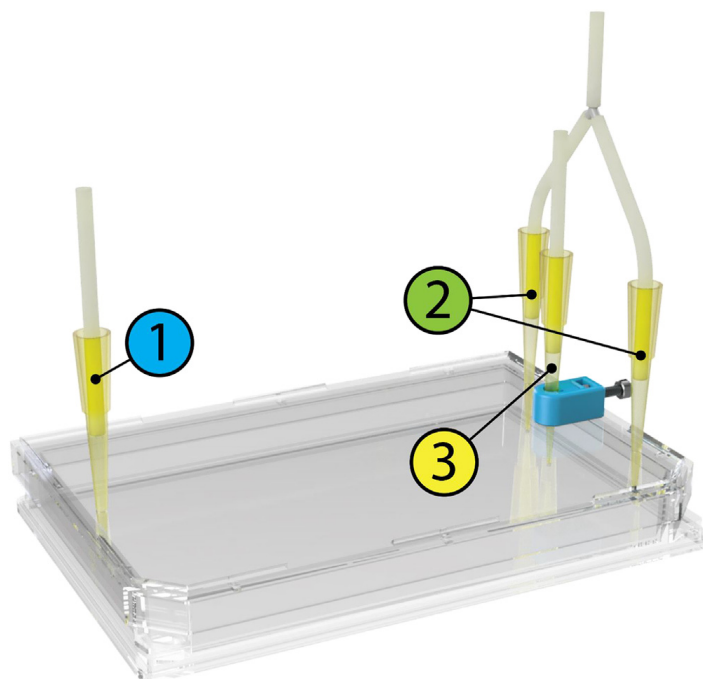


Fig. 1. PlateFlo Perfusion Plate. A Nunc OmniTray base with lid modified with 1) one inlet nozzle, 2) two outlet nozzles, and 3) a height-adjustable skimmer nozzle with 3D printed clamping mechanism.

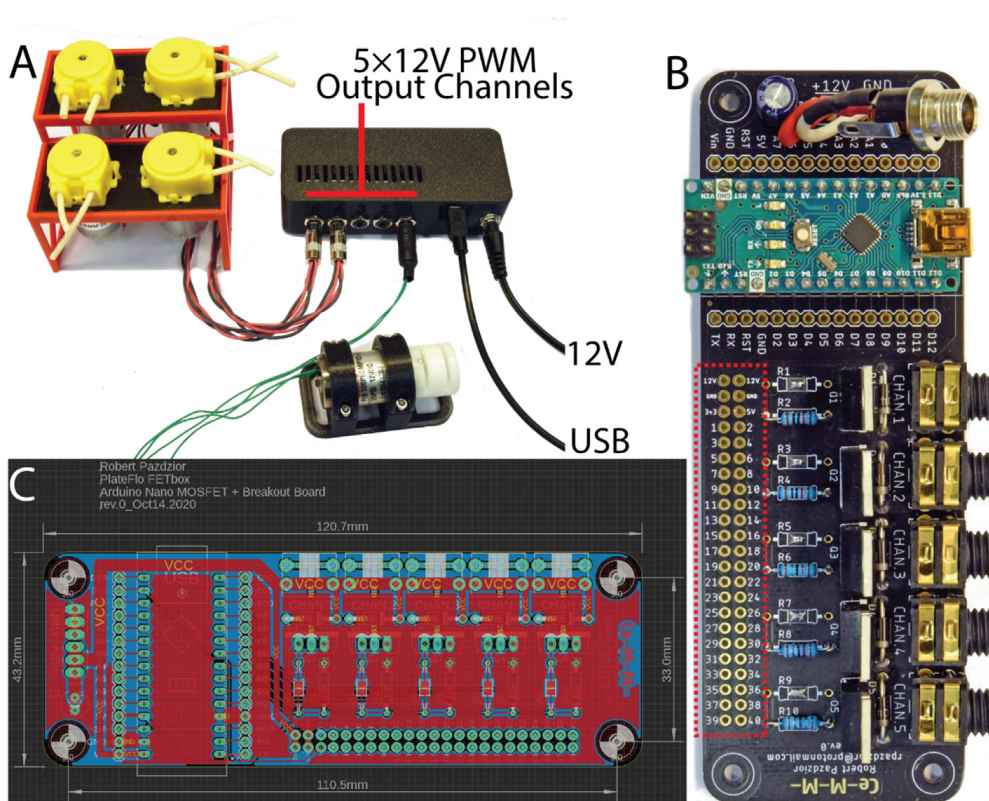


Fig. 2. FETbox Hardware Controller. A) Example application of the FETbox, controlling a bank of inexpensive 12 V peristaltic pumps for four skimmer channels and a solenoid pinch valve. B) Assembled FETbox PCB. Dotted red box indicates unconnected solder pads for user customizability and expansion. C) FETbox board overview in EAGLE CAD software, red denotes top copper layer, blue the bottom copper layer as viewed through the top. (For interpretation of the references to colour in this figure legend, the reader is referred to the web version of this article.)

Through-hole devices were used exclusively, avoiding surface mount devices (SMDs), in the design of the FETbox circuit board to make board assembly accessible to soldering novices. It is built around the ubiquitous open-source Arduino Nano development board and ATmega 328P micro controller unit (MCU), with all board pins broken out onto the PCB for user customizability (Fig. 2B, C). There is also a 2.54 mm (0.1") 2×20 grid of unconnected through-holes along with +12/+5/+3.3 V and GND connections for mounting of additional connectors and components (Fig. 2B, red box). To further simplify customization of the board, the plateflo Python package's fetbox module includes methods to read and set all analog/digital pins on the Arduino Nano via USB serial. Custom serial commands can be added easily to the Arduino firmware for e.g. querying digital sensors or additional functionality (see "Firmware Modification" in the online documentation). At the default baud rate of 115,200 bits/sec, approximately 50–60 commands/queries can be sent per second for e.g. data logging purposes.

Each FETbox can supply +12 V up to a total of 4.5 A through the five PWM-capable MOSFET-switched outputs, with each individual device drawing no more than 3 A. In order to minimize the BOM component count, +5 V is supplied from the Arduino's onboard regulator and limited to ~350 mA for peripherals. Likewise, +3.3 V is supplied by the Arduino's FTIC chip and is limited to ~150 mA.

PlateFlo Python Package

The plateflo Python package, available from the Python Package Index (PyPI), includes several main modules: (1) fetbox, (2) scheduler, and a sub-package, (3) ismatec with modules for the Reglo Digital and Reglo ICC peristaltic pumps. Detailed API and usage documentation can be found at the project ReadTheDocs.

The fetbox module enables programmatic serial control of the FETbox hardware controller through a number of convenience functions. Each of the numbered MOSFET outputs can be switched on/off, output at a specific a PWM duty cycle, or use a type of switching optimized for solenoid valves called "hit-and-hold". The latter takes advantage of the fact that solenoid valves require far less power to maintain in the "on" position than they do during the initial switching operation. Full output power is supplied momentarily before reducing to a user specified PWM duty cycle. Using the hit-and-hold functionality reduces power draw and consequently heat generated by the solenoid coil. All of the Arduino's digital and analog input pins can also be read or written to via serial. Arbitrary strings can also be sent with either pass/fail or string responses for expanded functionality.

As the name implies, the scheduler module provides a means of creating tasks to be executed in the future. They can be set to execute at regular intervals, specific times, and scheduled tasks can be cancelled/removed from the scheduler at any time. Although intended as a companion to the fetbox module and ismatec sub-package, any callable Python object can be added to the scheduler with both keyword and positional arguments.

The ismatec sub-package has three modules: ismatec_scanner, ismatec_dig, and ismatec_icc. The ismatec_scanner is a utility for scanning system serial ports for attached Ismatec Reglo Digital and Reglo ICC peristaltic pumps. The ismatec_dig and ismatec_icc modules provide convenience functions for serial control of said pumps. These include starting/stopping, setting flowrate and direction, as well as querying current pump status, and printing messages on the pump's display. In the case of the Reglo ICC, individual pump channels can also be controlled.

Design files

All STL files are pre-oriented for FDM 3D printing. F3D and F3Z CAD files were created by Autodesk Fusion 360. PCB design source files, SCH & BRD, were created using Autodesk EAGLE [21]. Free education and hobbyist licenses are available for both Fusion 360 and EAGLE at the time of writing.

Design file name	File type	Open source license	Location
skimmer_clamp_M3	STL; CAD (F3Z); CAD (STEP)	CERN-OHL-W	https://doi.org/10.17605/OSF.IO/PYJCH
skimmer_height_block_<height > mm.stl	STL	CERN-OHL-W	https://doi.org/10.17605/OSF.IO/PYJCH
perfusion_lid_drill_jig	STL; CAD (STEP)	CERN-OHL-W	https://doi.org/10.17605/OSF.IO/PYJCH
petri_drill_jig_<size>_<inlet/outlet>	STL; CAD (STEP)	CERN-OHL-W	https://doi.org/10.17605/OSF.IO/PYJCH
valve_clip_base	STL; CAD (STEP)	CERN-OHL-W	https://doi.org/10.17605/OSF.IO/PYJCH
fetbox_complete	CAD (F3D); CAD (STEP)	CERN-OHL-W	https://doi.org/10.17605/OSF.IO/CRJVB

(continued on next page)

(continued)

Design file name	File type	Open source license	Location
fetbox_enclosure_base	STL	CERN-OHL-W	https://doi.org/10.17605/OSF.IO/CRJVB
fetbox_enclosure_lid	STL	CERN-OHL-W	https://doi.org/10.17605/OSF.IO/CRJVB
FETbox_rev0_Gerber_JLCPCB	Gerber CAM (ZIP folder)	CERN-OHL-W	https://doi.org/10.17605/OSF.IO/CRJVB
FETbox_rev0_PCB	EAGLE design file (SCH); EAGLE design file (BRD)	CERN-OHL-W	https://doi.org/10.17605/OSF.IO/CRJVB
Firmware_FETbox.ino	Firmware (INO)	CERN-OHL-W	https://doi.org/10.17605/OSF.IO/CRJVB
plateflo Online Documentation	Python package ReadTheDocs; Sphinx HTML	GNU-GPL3+ CC BY-SA 4.0	PyPI; Source ReadTheDocs; https://osf.io/hev2z/
Supplementary Data	Folder	GNU-GPL3+	https://doi.org/10.17605/OSF.IO/PYJCH

- skimmer_clamp_M3 – Print-in-place skimmer nozzle clamping mechanism. Fixed atop a drilled Nunc OmniTray lid to allow precise positioning of the skimmer nozzle tip height. CAD files include modelled M3 fastener hardware as assembled.
- perfusion_lid_drill_jig – A guide for marking hole locations on Nunc OmniTray lids for drilling. Slides over top of the lid with holes for a fine-tipped marker.
- petri_drill_jig_<size>_<inlet/outlet> – As above, but for alternative petri dish culture chambers. Two pieces, inlet and outlet sides, that slide together to accommodate variability in petri dish dimension between manufacturers.
- valve_clip_base – Simple stand for the BOM pinch valve clip. Holds the valve horizontal for use on e.g. an incubator shelf.
- skimmer_height_block_<##>mm – Blocks of defined heights, <##>: 1.2, 1.4, 1.6, and 1.8 mm. Placed under the skimmer nozzle before tightening the skimmer clamp for repeatable height setting. Navigate to desired height model using left-side panel at listed OSF link.
- fetbox_complete – CAD model of the FETbox hardware controller with PCB and key electronic components modelled as assembled.
- fetbox_enclosure_base – the bottom half of the FETbox enclosure, into the which the PCB, power inlet, and MOSFET output jacks are mounted. adequate
- fetbox_enclosure_lid – the top cover of the FETbox enclosure. Has ventilation for the output MOSFETs and Arduino. It snap-fits onto the fetbox_enclosure_base.
- FETbox_rev0_Gerber_JLCPCB – Compressed (.zip) manufacturing Gerber (CAM) files. Ready for upload to the JLCPCB website for PCB ordering.
- FETbox_rev0_PCB – Autodesk EAGLE PCB source files for the FETbox_rev0_PCB. SCH and BRD files are co-dependent and must be downloaded together in order to open/modify the design.
- Firmware_FETbox – Arduino “sketch”/firmware for the Arduino Nano development board used in the FETbox hardware controller. Opened with Arduino IDE software.
- plateflo – A Python package containing modules to simplify coding serial control of the FETbox and Ismatec Reglo peristaltic pumps. See <https://plateflo.readthedocs.io>. for more details and usage.
- Online Documentation – searchable, mobile-friendly, companion documentation with sourcing guide, build guide, operating instructions, and programming examples.

Bill of materials

The tabulated bill of materials is available at <https://plateflo.readthedocs.io/en/latest/hardware/bom.html> as well as in [Supplementary Data](#).

Required tools:

FDM 3D printer (e.g. Prusa MK3S) or 3D printing services
 Small drill press, hand drill, or rotary tool (e.g. Dremel)
 Cyanoacrylate (super) glue

Soldering iron (e.g. TS100)
 Flux-core solder (e.g. Stannol Kristall 611)
 Side cutters or similar (e.g. Knipex 78 61 125)
 Hex wrench, 2.5 mm

Optional tools/components:

Isopropanol, 90%+ – for cleaning residual flux from PCB
 Heat-shrink tubing – for DC input jack joint insulation
 Self-adhesive silicone feet - for hardware controller and pinch valve stand

Build instructions

The PlateFlo system build is broken down into four distinct sections: 1) 3D printing & PCB ordering 2) FETbox assembly 3) perfusion plate modification/build. Detailed step-by-step instructions can be found in the project's online documentation (https://plateflo.readthedocs.io/en/latest/hardware/build_guide.html). See [Supplementary Data](#) “plateflo-readthedocs-v1.1.0.zip” for a downloadable copy of the online documentation.

Operating instructions

Operating instructions including setup guidelines, example configurations, skimmer pump operation, as well as plateflo package tutorials and API documentation can be found in the online documentation (<https://plateflo.readthedocs.io/en/latest/hardware/operation.html>). See [Supplementary Data](#) “plateflo-readthedocs-v1.1.0.zip” for a downloadable copy of the online documentation.

Validation and characterization

FETbox benchmarking & performance

Serial communication

Fidelity and maximum throughput of the serial communication protocol implemented in the FETbox firmware and plateflo serial input/output backend were verified using a stress test program. Arduino pin D3 was jumpered to pin D11. D3 was rapidly toggled HIGH/LOW with the state of D11 read after each D3 write command. The round-trip time of each write and read command, that is the elapsed time between starting to send the command and receiving the full response, was also measured for each cycle. This was repeated 10,000 times and logged to a data file ([Supplementary Data](#), `fetbox_serial_stresstest.csv`). Failure to toggle the output state of D3 would result in an erroneous reading as the it would remain unchanged from the previous state, e.g. a low state when a high was commanded. Write commands were executed at 100% fidelity with zero discrepancies observed between the theoretical output of D3 and the read state of pin D11. Write and read commands were executed with round-trip times of 15.3 ± 1.3 ms and 16.0 ± 0.8 ms (mean \pm St.Dev), respectively. For the digital write and read serial commands used here, a sustained command rate of 60–65 Hz can be expected. To validate these timing results, and to benchmark the round-trip time of other FETbox serial commands, a similar test was carried out without the overhead of input data collection. Using the `timeit` Python module, the time to successfully execute each command 50 consecutive times was measured. All commands measured 15.9 ms round-trip times with the exception of hit-and-hold which has an additional 100 ms delay built-in to allow time for the solenoid valve to engage ([Supplementary Table 1](#)). Utilizing a higher baud rate (115200 bps is the default) may enable slightly faster command rates at the risk of decreased reliability, especially when using longer cables.

PWM output

To characterize the MOSFET PWM output waveform, a Rigol DS1102Z-E oscilloscope was connected to FETbox output channel two at the MOSFET gate to measure the output from the Arduino as well as to the negative terminal of the flyback diode to measure the low-side output voltage to the connected device as in [Fig. 3A,B](#). 10X probes limited to 20 MHz were used on both channels. The BOM pinch valve was connected to the FETbox output to serve as an inductive load. A PWM output value of 128 (~50% duty cycle) was set via serial command and the oscilloscope set to trigger on the rising edge of the Arduino PWM output at + 2.5 V ([Fig. 3C](#)). Rise time and fall time at the MOSFET gate were both determined to be ~ 250 ns ([Fig S1A](#)). This allows for PWM values from 5 (2% duty cycle) to 250 (98% duty cycle) to be used before static on or off states may occur ([Fig S2](#)). Flyback voltage spikes, which occur when an inductive load is disconnected during the off phase of the PWM signal, did not exceed 21 V at the highest PWM duty cycle ([Fig S2](#)), which is well within the 60 V drain-source voltage specification of the FQP30N06L MOSFET [[22](#)].

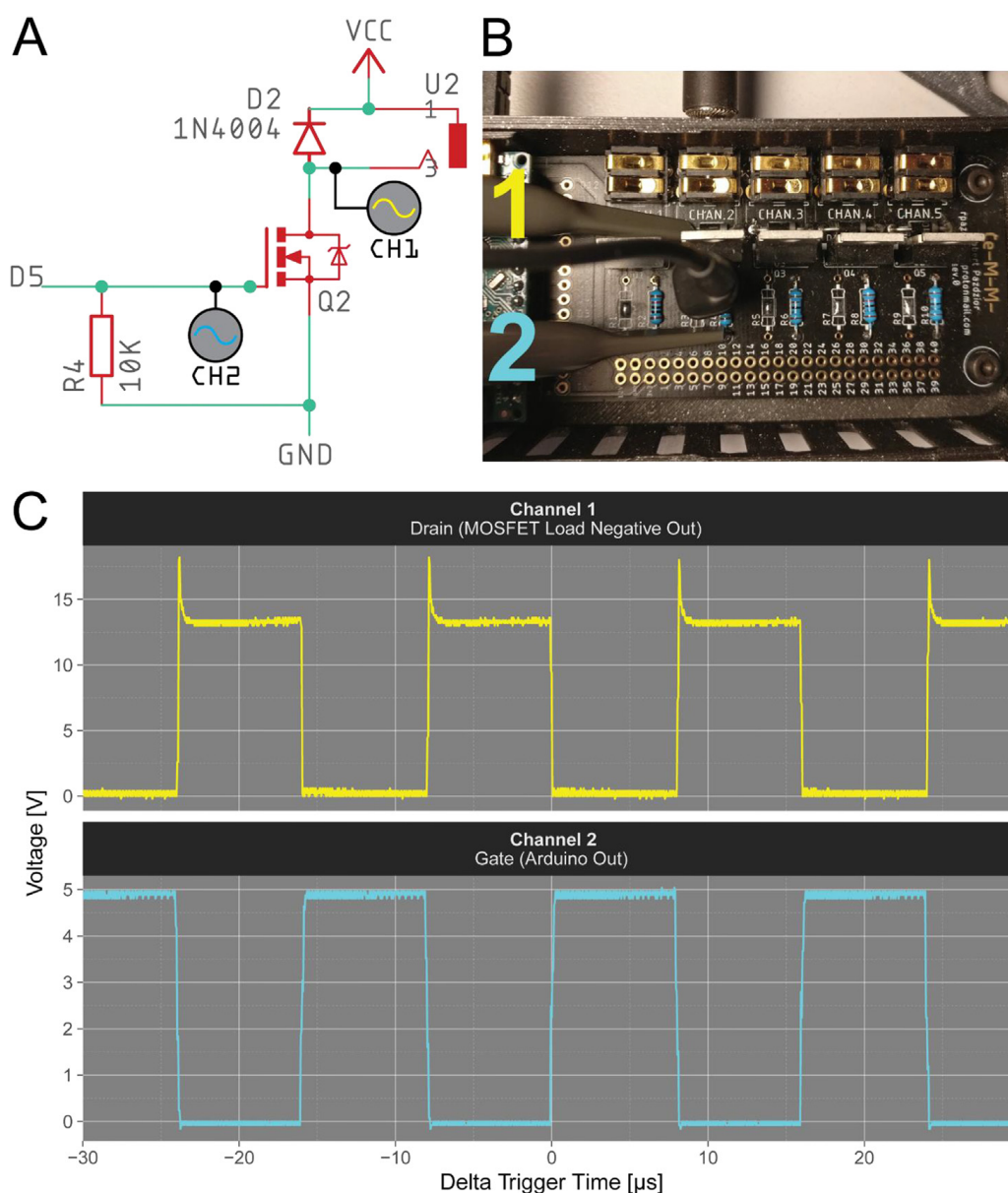


Fig. 3. FETbox Output Channel #2 PWM Waveform and Flyback Voltage Measurement. A) Schematic diagram of output channel #2 with oscilloscope probing points indicated by gray circles with colored waveform inside corresponding with oscilloscope channels 1 (yellow) and channel 2 (cyan) B) Image of probing setup. Grounding clip (black, middle) connected to ground side of the 10 K pull-down resistor, scope channel 1 to the MOSFET output low side, and scope channel 2 to the MOSFET gate to probe the Arduino PWM output. A pinch valve was plugged into the output to provide an inductive load. C) Oscilloscope traces during a 50% duty cycle PWM output. Note the carrier frequency period of $16 \mu\text{s}$ (62.5 kHz), and the freewheeling/flyback voltage spikes on the MOSFET output (yellow) less than 20 V. (For interpretation of the references to colour in this figure legend, the reader is referred to the web version of this article.)

Pinch valve mixing capability

With the exception of much more sophisticated proportional pinch valves, most pinch valves are binary devices, either fully engaged or fully disengaged. Arbitrary mixing ratios can, however, be achieved using the same principle that PWM uses to reduce effective output voltage from digital devices. Toggling the valve position for a fraction of a fixed time window will produce a mixture of the two inputs proportionally (Fig. 4B), provide that there is sufficient post-valve mixing. To validate mixing performance and assess the feasibility of programmable mixing profiles we used solutions of two different concentrations of glucose as a model (Fig. 4A). Two reservoirs of PBS solution, one containing 115 mg/dL (1 g/L nominal) and the other 210 mg/dL (2 g/L nominal) glucose (Fig. 4A) as measured using a Contour Next (Ascensia Diabetes Care) blood glucose meter and test strips, were connected to a pinch valve with a Y fitting. The pinch valve was set to mix the two channels according to the profile in Fig. 4D by varying the on/off duty cycle proportionally to the mixing ratio in two second windows, as illustrated in Fig. 4B. Pumping was handled by a Ismatec Reglo ICC 8-roller peristaltic pump (Cole-Parmer GmbH) at a calibrated flow rate of $250 \mu\text{L}/\text{min}$. The flow was split after the peristaltic pump with another Y-piece and sampled at the

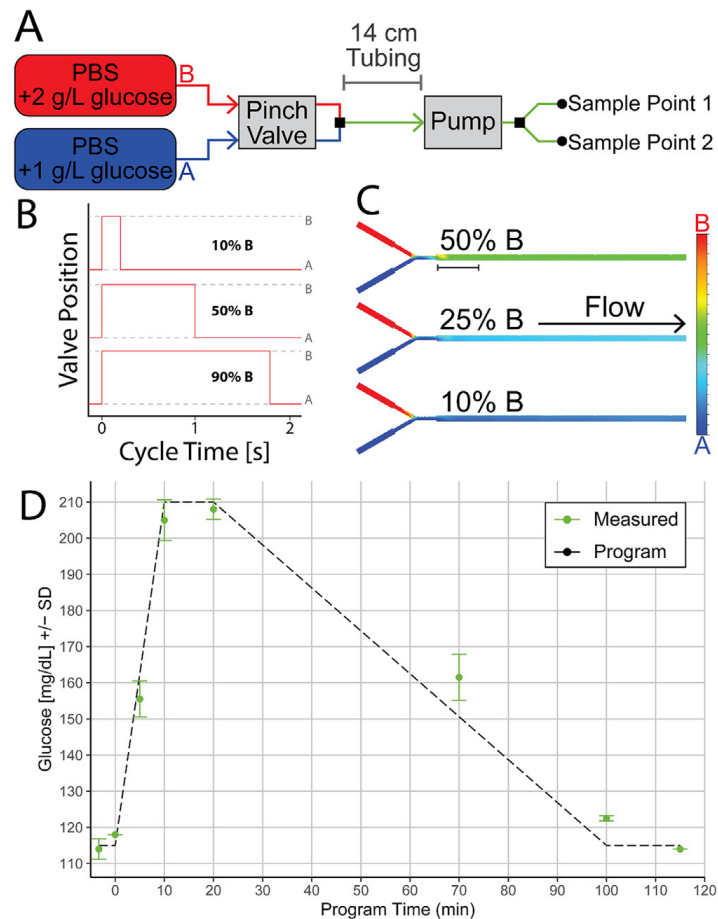


Fig. 4. Reservoir mixing performance evaluation. A) Experimental setup for mixing profile validation. Reservoirs of PBS containing 1–2 g/L were mixed programmatically via pinch valve into a Y-piece and quantified downstream simultaneously at two outlets. B) Illustrated pinch valve input mixing strategy, allows continuous mixing ratio output from discrete valve states. Mixing cycles loop continuously. C) CFD model cross-section of the discrete pinch valve mixing performance around the Y-piece fitting, approximating the region of (A) between the valve and pump. Colored by composition. Scale bar represents 10 mm. D) Programmed blood glucose concentration (dashed line) profile, emulating a post-prandial blood glucose spike in healthy adult human. Experimentally measured points are in green. (For interpretation of the references to colour in this figure legend, the reader is referred to the web version of this article.)

two outlets simultaneously using Contour Next (Ascensia Diabetes Care) blood glucose test strips. Total dead volume from valve to outlets (825 μL , ~ 3 min 20 s) was taken into consideration and sampling timing offset accordingly. The measured glucose profile followed the programmed profile closely, within the 10 mg/dL specified accuracy of the glucose meter (Fig. 4D).

A transient CFD simulation (Autodesk CFD 2019) was also constructed to study the mixing behavior in the pinch valve Y-piece fitting and downstream tubing. The fluid path of the junction was modeled using the measured 1 mm inner diameter and 60° angle of the Y-piece employed in the experimental setup and specified 1.52 mm inner diameter of the peristaltic tubing. A 10 mm segment of tubing was modelled for each input from the pinch valve and a single 140 mm segment of tubing for the output. A mean velocity of 2.296 mm/s in the tubing was calculated based on the 250 $\mu\text{L}/\text{min}$ volumetric flow rate and tubing inner diameter used.

Static boundary conditions of 0 Pa pressure and 2.296 mm/s were applied to the outlet of the 140 mm tubing. Dynamic piecewise-linear boundary conditions for velocity were set at inlet tubing segments to mimic the discrete mixing behavior of the pinch valve in three different mixing ratio scenarios: 10%, 25%, and 50% B, where “B” indicates the 2 g/L glucose solution. E.g. at a 25% B mixing ratio, inlet B had a boundary condition of 2.296 mm/s for 0.5 s while A was at 0.0 mm/s, and then vis-a-versa for the remaining 1.5 s, repeating for the duration of the simulation. Scalar values of 0.0 (solution A) and 1.0 (solution B) were used to define the two glucose solutions with densities of 1.007 g/cm^3 and 1.0013 g/cm^3 , respectively, with a scalar diffusion coefficient of $5.16\text{e-}06$ mm^2/s and dynamic viscosity of 0.001100855 $\text{kg}/\text{m}\cdot\text{s}$ [23]. Initial conditions of scalar value 0.0 and 1.0 were defined in each of the inlet tubing volumes and scalar boundary conditions at the inlets were set accordingly. Turbulent incompressible flow physics were used, but similar results were obtained using laminar flow physics. Mesh sizing was done automatically, and no surface refinement was utilized. All other settings were kept at their default values.

Transient simulations were run for 120 s with 100 ms time-steps to fully capture the 10% mixing valve state duration (200 ms) and qualitative convergence was achieved before 70 s in all models. See [Supplementary Video 1](#) for a real-time

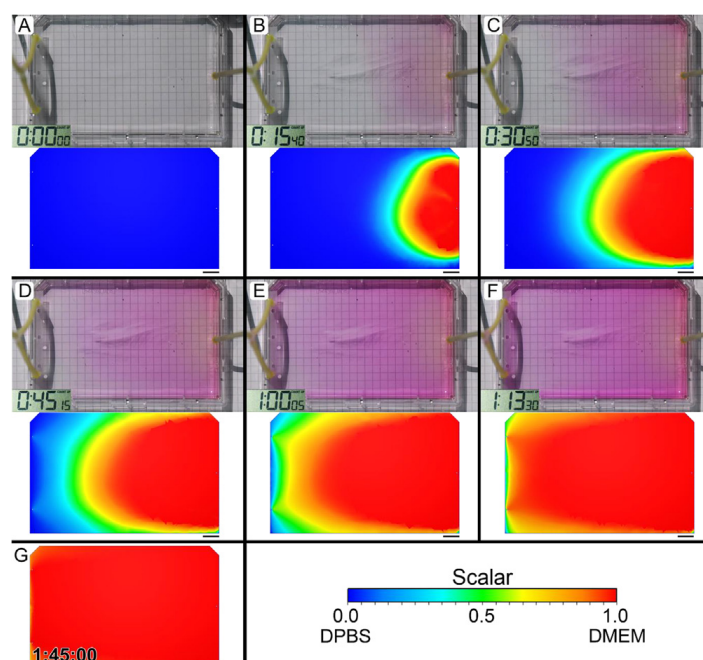


Fig. 5. Visualizing the flow profile of a PlateFlo culture plate. A-F) A plate preloaded with 10 mL of DPBS (colorless) was perfused with DMEM culture medium (pink) at 170 $\mu\text{L}/\text{min}$ while a time lapse was recorded. Stopwatch inset in bottom left of each frame, h:mm:ss time format. A transient scalar mixing CFD model of plate flow at similar time intervals is also visualized below each time-lapse frame as an XY cross section the middle of the medium model. Black scale bar (bottom right, each panel) is 10 mm long. G) Transient model, as above, at 1 h 45 min. (For interpretation of the references to colour in this figure legend, the reader is referred to the web version of this article.)

visualization of the mixing behavior in the Y-piece for all ratios modelled, and [Supplementary Video 2](#) with velocity vectors overlaid for the 50% mixing model. All components necessary to regenerate these data, including CAD model, mesh, and setup conditions can be found in the Autodesk CFD archive share file, [y-piece_mixing_cfd.cfz](#), in [Supplementary Data](#).

Scalar homogeneity near the target mixing ratio was achieved nearly immediately (less than 10 mm) past the Y-piece fitting for all tested mixing ratios ([Fig. 4C](#)), indicating no need for additional mixing devices or tubing length.

Perfusion plate flow profiling

Part of the rationale for selecting OmniTray plates for the perfusion chamber was their rectangular aspect ratio. In order to keep fresh media flowing into the plate and spent media flowing out of it vortices and dead spots should be avoided.

We visualized the profile of flow across the plate by first loading a plate with 10 mL of colorless phosphate buffered saline (PBS) solution. The plate was then perfused with Dulbecco's Modified Eagle Medium (DMEM), a pink-colored solution of similar density, at 170 $\mu\text{L}/\text{min}$. A skimmer pump was not required for the short timescale of this experiment. A tripod mounted camera was used to photograph the plate from above at regular intervals and a lab timer was kept in the frame (lower left, photographs) for timekeeping purposes ([Fig. 5A-F](#), upper). See [Supplementary Video 3](#) for the full time-lapse video.

We also simulated this scenario using transient scalar mixing CFD modeling ([Fig. 5A-F](#), lower; [Fig. 5G](#)), similar to as was conducted in 7.2. Fluid was modeled based on the dimensions of the plate and set to a height corresponding to 10 mL of volume. The P200 nozzles were modelled as 0.6 mm \varnothing cylindrical depressions from the top surface of the fluid extending down until 0.55 mm above the fluid bottom. Inlet and outlet boundary conditions were set at the lower surface of these depressions. Inlet boundary conditions included a developed volumetric flow rate of 170 $\mu\text{L}/\text{min}$ and a scalar value of 0.0 until 1800 sec, then 1.0 for the remainder of the simulation. Outlet boundary conditions were 85 $\mu\text{L}/\text{min}$ volumetric flow rate and 0 Pa pressure. Fluid properties were defined identically to that in section 7.2, approximating culture medium. A steady-state solution was first solved for the velocity (~100 iterations), then a transient solution was found for scalar mixing to visualize the flow profile across the plate up until 8600 s. Simulation results are illustrated using a cross sections along the XY plane, through the middle of the media model and colored according to the scalar mixing ratio of 0.0–1.0 (PBS-DMEM) in [Fig. 5A-F](#), lower and [Fig. 5G](#). See [Supplementary Video 4](#) for the complete simulation animation, and [Supplementary Data](#) for the Autodesk CFD archive share file, [plateflo_perfufion_plate_CFD.cfz](#), to reproduce the model results.

The time required for the DMEM front to traverse the plate was approximately 73 min. Experimental and simulation flow profiles appeared similar. Both showed mixing of the DMEM front as it progressed across the plate, becoming more diffuse towards the outlet side. The chamfered corners of the OmniTray plate (upper left, upper right) appear to improve flow linearity when compared with the orthogonal opposing corners (lower left, lower right) which show some flow stagnation as indicated by the lower scalar value towards the end of the time series. Although not entirely homogenous, the vast majority

of cells seeded onto a perfusion plate are subject to similar microenvironmental conditions as culture medium moves consistently across the plate's surface, with negligible dead spots.

Discussion

Areas for Improvement

Perfusion plate skimmer system

The skimming approach we've taken to plate volume regulation, though relatively simple and cost-effective, is negatively influenced by surface tension and capillary action. Fluid cannot be aspirated unless it contacts the skimmer nozzle. Once the fluid comes into contact with the skimmer nozzle it is drawn up into the bore. As material is removed the fluid level drops. Surface tension, however, maintains an unbroken column of fluid stretched between the nozzle and the bulk fluid, bridging the fluid surface and the nozzle, and permitting continued removal of material from the plate despite the fluid level dropping below the level of the nozzle. The stretches as the level drops until it eventually breaks, at which point the fluid surface is below the level of the skimmer nozzle. Fluid then slowly accumulates until it contacts the skimmer nozzle and the cycle continues. In this way an approximately saw tooth shaped oscillation in fluid volume is created in the plate, the frequency of which is dependent on the inlet/outlet flow rate delta, i.e. faster accumulation results in a higher oscillation rate. For this reason, it is recommended that the flow rate delta be kept as small as possible. Nozzle geometry could potentially be better optimized to minimize this phenomenon [24]. Optimized skimmer geometry would, however, likely come at the expense of additional cost and build/sourcing complexity.

FETbox hardware controller

In the interest of minimizing BOM component count and PCB assembly complexity, a dedicated DC-DC conversion circuit was not implemented on the FETbox board. Instead, the 12 V supply voltage is converted to 5 V and 3.3 V through the Arduino Nano's onboard regulators. Though 12 V is within specification for the input voltage, it is on the upper end of the acceptable range. As such the Nano's linear voltage regulators generate a lot of heat. Drawing additional current from the 5 V line for additional components (status LCD, or LEDs for example) further increases heat output. This could be addressed with a buck converter module such as a Würth Elektronik 173950578 [25], or a suitable dedicated daughter board for higher-current 5 V applications. This would supply the Nano via the 5 V pin, rather than the Vin pin due to the dropout voltage across the Vin regulator circuitry.

If the FETbox is connected by USB and not powered from the 12 V input (e.g. by accidental disconnection) and the MOSFET outputs are engaged, the connected output devices will draw from the Vin pin which in this instance will be connected directly to the USB port 5 V bus. To avoid this, an additional 1 N4004 power diode can be placed between the power input and Vin pin, preventing current from flowing out from the Arduino and keeping the MOSFET output unpowered. Placing a diode in front of the Nano Vin pin has the added benefit of dropping the input voltage by 1 V, reducing the heat output from the Nano's onboard regulators.

Potential applications

The programmability of the PlateFlo system lends itself to dynamic culture protocols where culture conditions are regimented, vary over time in a controlled manner. Certain embryonic stem cell expansion and differentiation protocols, for example, involve a series of culture media changes and/or compound doses to affect developmental progress [26]. In addition to specific molecular cues, numerous studies have demonstrated osteogenic differentiation of mesenchymal stem cells also benefits from biophysical cues in the form of shear stress [27,28]. For example, the perfusion system presented by Pasini et al, which is similar in principle to that of the PlateFlo system, demonstrates improved induction of osteogenic gene expression under flow when compared with induction in static culture [20]. Even very low flow, such as that experienced in interstitial fluid can induce osteogenic differentiation [29,30]. Oscillating fluid shear has also been shown to benefit osteoblast differentiation to a greater extent than continuous perfusion alone [31], and could easily be implemented in the perfusion plate using computer controlled peristaltic pumps such as with the ismatec sub-package in the plateFlo Python library. These protocols could potentially benefit from partial or complete integration into the PlateFlo system but require validation on a case-by-case basis. Flow rate and plate volume can be adjusted to increase or decrease shear stress across the culture surface. For a given volumetric flow rate, a greater plate volume will result in lower linear velocity and therefore lower shear forces. This will result in a lower rate of exchange and therefore greater accumulation of secreted factors and potential for local or even global nutrient depletion. Skimmer height can be set using the various printed skimmer height blocks. See "Operating Instructions" for more details.

In order to maintain pluripotency and stimulate growth, embryonic stem cells (ESCs) are often co-cultured on a layer of "feeder" cells, mouse embryonic fibroblasts [32] or human embryonic stem cells [33], that supply a complex mixture of factors to the ESC. Although strides have been made towards feeder-free expansion and differentiation [34–36], not all ESC lines or differentiation protocols may be amenable to this approach. By adapting the PlateFlo setup showcased in the graphical abstract, for example, it may be possible to co-culture feeder and some ESC lines in physically isolated plates. This has

the potential to simplify downstream processing while benefiting from a constant flow of fresh medium. When expanding embryonic stem cells, waste products such as lactic acid and ammonia can accumulate and limit cell viability in non-perfused systems [37]. Recirculating media however, either partially or fully, may be more economical in certain scenarios given the high cost of ESC culture medium and supplements. This application has not been validated but we believe it to be an interesting avenue for future exploration. Many other biological applications that rely on the use of conditioned media should also benefit from the PlateFlo setup. In all cases, flow rate and plate volume would be the main parameters to adjust. This could be done for each plate individually to e.g. concentrate the secreted factors using a lower plate volume upstream while maintaining the downstream plate at a higher volume for slower exchange.

Alternative culture chambers

The OmniTray was selected early on in the conceptualization of the PlateFlo system for its rectangular shape. Theoretically this yields the most consistent flow across the plate as it minimizes the difference between the longest and shortest path media could take from inlet to outlet. The OmniTray also has a standard footprint that is directly compatible with e.g. plate holders in automated microscopes and is available with a treated culture surface at a price of ca. 10EUR/plate, making it a relatively affordable option. It is, however, a single-source item and therefore susceptible to discontinuation, supply chain disruption, and price hikes.

Nunc offers a four well plate in the same footprint with rectangular wells that each fit a 75 × 25 mm glass slide (ThermoFisher Scientific, cat# 267061). This plate format could be of use when lower flow rates and media consumption are desirable, or material is limited as with e.g. primary tissues. Reducing the volume while maintaining a similar flow rate would also increase the media exchange rate and linear velocity of the fluid. The lack of a treated surface version creates additional preparation steps for use with adherent cells, however. One potential work around would be to use treated slides (e.g. ThermoScientific, cat# 960004) as drop-in culture surfaces. For some applications, non-treated surfaces might be preferred, as in the case of primary pancreatic islet culture. We successfully carried out a pilot experiment with primary pancreatic islets in one of these untreated wells, without noticeable movement of the islets with flow. This format is interesting as a smaller alternative with similar geometry but requires further validation and unfortunately is also a single-source item.

Petri dishes are ubiquitous and available in a range of sizes from many suppliers and manufacturers. The general linear flow characteristics of circular dishes are not as favorable as those of rectangular form factor plates such as the OmniTray (Supplementary Fig. 3). A CFD simulation of particles (representing paths of flow) moving across a 10 cm petri dish (similar in culture area to an OmniTray plate) showed a wider distribution of residence times when compared with the OmniTray (standard deviation 660 s vs 530 s) (Supplementary Fig. 3D). However, their availability, low cost, and range of sizes make them an attractive future-proof alternative to the Nunc OmniTray. As such, we've included design files for 3D printing nozzle hole marking jigs for 6 cm, 10 cm, and 15 cm petri dish lids. These jigs feature a two-part sliding design that allows the jig to adapt to small dimensional variation in petri dish lids between the various manufacturers. We have not validated the use of petri dishes for perfusion experimentally, however, CFD simulations suggest an acceptable flow profile in 10 cm plates.

Integration with open source tools

A commercial multi-channel peristaltic pump is listed in the PlateFlo BOM, the Ismatec Reglo ICC. This is primarily for its flexibility, having individually controllable channels enabling two-plate multiplexing while being able to run with the inlet/outlet flow rate delta required, all in a single unit. Though well-suited to the PlateFlo system, and easily re-configured for different setups, the cost of a single 4-channel unit is extremely high (list price 3600EUR at time of writing). A viable open source alternative could quite easily, for example, make use of a pair of FAST [38] 3D-printed peristaltic pumps, each of which could be controlled via USB from the same computer that interfaces with the FETbox hardware controller. This would also allow a larger number of perfusion plates to be run in parallel than e.g. a single Reglo ICC pump.

A potentially interesting addition to the PlateFlo system which may be of interest in the study of e.g. endocrine culture models, is a downstream sampler for automated supernatant sample collection. The recent BioSamplr [39] system could, for example, be integrated downstream of the PlateFlo system with some minor modifications. An additional dual-channel pinch valve (as in e.g. the BOM) can be placed in the PlateFlo outlet tubing path and used to create sample loop (as in HPLC injectors, for example), allowing the BioSamplr's peristaltic pump to pull supernatant from this section of tubing when engaged, and bypassing it when disengaged (Supplementary Fig. 4). The PlateFlo outlet peristaltic pump should be temporarily disabled during sampling, as the outlet will be blocked by the pinch valve when engaged. Integration of the PlateFlo and BioSamplr Python software would permit complete automated control of both systems from the BioSamplr's Raspberry Pi computer, removing the need for an additional control computer for the FETbox.

Declaration of Competing Interest

The authors declare no conflicts of interest. R.P. gratefully acknowledges support by a DOC PhD Fellowship of the Austrian Academy of Sciences. Research in the Kubicek lab is supported by the Austrian Federal Ministry for Digital and Economic Affairs and the National Foundation for Research, Technology, and Development, the Austrian Science Fund (FWF) F4701

and the European Research Council (ERC) under the European Union's Horizon 2020 research and innovation programme (ERC-CoG-772437).

Appendix A. Supplementary data

Supplementary data to this article can be found online at <https://doi.org/10.1016/j.ohx.2021.e00222>.

References

- [1] J.R. Masters, G.N. Stacey, Changing medium and passaging cell lines, *Nat. Protoc.* 2 (9) (2007) 2276–2284, <https://doi.org/10.1038/nprot.2007.319>.
- [2] Anton G. Kutikhin, Maxim Yu. Sinitsky, Arseniy E. Yuzhalin, Elena A. Velikanova, Shear stress: An essential driver of endothelial progenitor cells, *Journal of Molecular and Cellular Cardiology* 118 (2018) 46–69, <https://doi.org/10.1016/j.yjmcc.2018.03.007>.
- [3] Q. Ma, Z. Ma, M. Liang, F. Luo, J. Xu, C.e. Dou, S. Dong, The role of physical forces in osteoclastogenesis, *J. Cell. Physiol.* 234 (8) (2019) 12498–12507, <https://doi.org/10.1002/jcp.28108>.
- [4] Z. Li, Z. Cui, Three-dimensional perfused cell culture, *Biotechnol. Adv.* 32 (2) (2014) 243–254, <https://doi.org/10.1016/j.biotechadv.2013.10.006>.
- [5] V. Starokozhko, M. Hemmingsen, L. Larsen, S. Mohanty, M. Merema, R.C. Pimentel, A. Wolff, J. Emnéus, A. Aspegren, G. Groothuis, M. Dufva, Differentiation of human-induced pluripotent stem cell under flow conditions to mature hepatocytes for liver tissue engineering, *J. Tissue Eng. Regen. Med.* 12 (5) (2018) 1273–1284.
- [6] D. Bulnes-Abundis, L.M. Carrillo-Cocom, D. Aráiz-Hernández, A. García-Ulloa, M. Granados-Pastor, P.B. Sánchez-Arreola, G. Murugappan, M.M. Alvarez, A simple eccentric stirred tank mini-bioreactor: Mixing characterization and mammalian cell culture experiments, *Biotechnol. Bioeng.* 110 (4) (2013) 1106–1118.
- [7] D.E. Discher, Tissue Cells Feel and Respond to the Stiffness of Their Substrate, *Science* 310 (5751) (2005) 1139–1143.
- [8] A.L. Van Wezel, Growth of Cell-strains and Primary Cells on Micro-carriers in Homogeneous Culture, *Nature* 216 (5110) (1967) 64–65, <https://doi.org/10.1038/216064a0>.
- [9] B. Nankervis, M. Jones, B. Vang, R. Brent Rice Jr, C. Coeshott, J. Beltzer, Optimizing T Cell Expansion in a Hollow-Fiber Bioreactor, *Curr. Stem Cell Rep.* 4 (1) (2018) 46–51, <https://doi.org/10.1007/s40778-018-0116-x>.
- [10] R.A. Knazek, P.M. Gullino, P.O. Kohler, R.L. Dedrick, Cell Culture on Artificial Capillaries: An Approach to Tissue Growth in vitro, *Science* 178 (4056) (1972) 65–67.
- [11] J.B. Dahl, J.-M. Lin, S.J. Muller, S. Kumar, Microfluidic Strategies for Understanding the Mechanics of Cells and Cell-Mimetic Systems, *Annu. Rev. Chem. Biomol. Eng.* 6 (1) (2015) 293–317.
- [12] A. Essaouiba, T. Okitsu, R. Jellali, M. Shinohara, M. Danoy, Y. Tauran, C. Legallais, Y. Sakai, E. Leclerc, Microwell-based pancreas-on-chip model enhances genes expression and functionality of rat islets of Langerhans, *Mol. Cell. Endocrinol.* 514 (2020) 110892, <https://doi.org/10.1016/j.mce.2020.110892>.
- [13] E. Behroodi, H. Latifi, Z. Bagheri, E. Ermis, S. Roshani, M. Salehi Moghaddam, A combined 3D printing/CNC micro-milling method to fabricate a large-scale microfluidic device with the small size 3D architectures: an application for tumor spheroid production, *Sci. Rep.* 10 (1) (2020), <https://doi.org/10.1038/s41598-020-79015-5>.
- [14] T. Schulze et al, A Parallel Perfusion Slide From Glass for the Functional and Morphological Analysis of Pancreatic Islets, *Front. Bioeng. Biotechnol.* 9 (2021), <https://doi.org/10.3389/fbioe.2021.615639>.
- [15] M. G. Moretti, L. E. Freed, and R. S. Langer, 'Oscillating cell culture bioreactor', US20100297233A1, Nov. 25, 2010 Accessed: Jul. 19, 2021. [Online]. Available: <https://patents.google.com/patent/US20100297233A1/en>
- [16] M. G. Moretti, L. E. Freed, and R. S. Langer, 'Oscillating cell culture bioreactor', US9217129B2, Dec. 22, 2015 Accessed: Jul. 19, 2021. [Online]. Available: <https://patents.google.com/patent/US9217129B2/en>
- [17] R. Visone, G. Talò, S. Lopa, M. Rasponi, M. Moretti, Enhancing all-in-one bioreactors by combining interstitial perfusion, electrical stimulation, on-line monitoring and testing within a single chamber for cardiac constructs, *Sci. Rep.* 8 (1) (Nov. 2018) 16944, <https://doi.org/10.1038/s41598-018-35019-w>.
- [18] Y. Abe et al, Improved phosphoproteomic analysis for phosphosignaling and active-kinome profiling in Matrigel-embedded spheroids and patient-derived organoids, *Sci. Rep.* 8 (1) (Jul. 2018) 11401, <https://doi.org/10.1038/s41598-018-29837-1>.
- [19] K. Domansky, W. Inman, J. Serdy, A. Dash, M.H.M. Lim, L.G. Griffith, Perfused multiwell plate for 3D liver tissue engineering, *Lab. Chip* 10 (1) (Jan. 2010) 51–58, <https://doi.org/10.1039/B913221J>.
- [20] A. Pasini, J. Lovecchio, G. Ferretti, E. Giordano, Medium Perfusion Flow Improves Osteogenic Commitment of Human Stromal Cells, *Stem Cells Int.* 2019 (2019), <https://doi.org/10.1155/2019/1304194> e1304194.
- [21] 'EAGLE | PCB Design And Electrical Schematic Software | Autodesk'. <https://www.autodesk.com/products/eagle/overview>, (accessed Dec. 16, 2020).
- [22] Fairchild Semiconductor, 'FQP30N06L - N-Channel QFET MOSFET Datasheet'. Mouser, Nov. 01, 2013, Accessed: Mar. 10, 2021. [Online]. Available: <https://eu.mouser.com/datasheet/2/308/FQP30N06L-D-1809681.pdf>.
- [23] H. Suhaimi, S. Wang, D.B. Das, Glucose diffusivity in cell culture medium, *Chem. Eng. J.* 269 (2015) 323–327, <https://doi.org/10.1016/j.cej.2015.01.130>.
- [24] J. Molenaar, W.G.N. van Heugten, C.J.M. van Rijn, Viscous Liquid Threads with Inner Fluid Flow Inside Microchannels, *ACS Omega* 4 (6) (2019) 9800–9806.
- [25] Würth Elektronik, 'Mag13C Power Module Datasheet'. Digikey, May 01, 2019, Accessed: Mar. 11, 2021. [Online]. Available: https://media.digikey.com/pdf/Data%20Sheets/Wurth%20Electronics%20PDFs/173950378_173950578.pdf.
- [26] Y. Shi, P. Kirwan, F.J. Livesey, Directed differentiation of human pluripotent stem cells to cerebral cortex neurons and neural networks, *Nat. Protoc.* 7 (10) (2012) 1836–1846, <https://doi.org/10.1038/nprot.2012.116>.
- [27] M.D. Aisha, M.N.K. Nor-Ashikin, A.B.R. Sharaniza, H. Nawawi, G.R.A. Froemming, Orbital fluid shear stress promotes osteoblast metabolism, proliferation and alkaline phosphates activity in vitro, *Exp. Cell Res.* 337 (1) (2015) 87–93, <https://doi.org/10.1016/j.yexcr.2015.07.002>.
- [28] Z. Bo, G. Bin, W. Jing, W. Cuifang, A.n. Liping, M.a. Jinglin, J. Jin, T. Xiaoyi, C. Cong, D. Ning, X. Yayi, Fluid shear stress promotes osteoblast proliferation via the α_q -ERK5 signaling pathway, *Connect. Tissue Res.* 57 (4) (2016) 299–306.
- [29] K.M. Kim et al, Shear stress induced by an interstitial level of slow flow increases the osteogenic differentiation of mesenchymal stem cells through TAZ activation, *PLoS One* 9 (3) (2014) e92427, <https://doi.org/10.1371/journal.pone.0092427>.
- [30] U.M. Liegibel et al, Fluid shear of low magnitude increases growth and expression of TGFbeta1 and adhesion molecules in human bone cells in vitro', *Exp. Clin. Endocrinol. Diabetes Off. J. Ger. Soc. Endocrinol. Ger. Diabetes Assoc.* 112 (7) (2004) 356–363, <https://doi.org/10.1055/s-2004-821014>.
- [31] P. Li, Y.-C. Ma, X.-Y. Sheng, H.-T. Dong, H. Han, J. Wang, Y.-y. Xia, Cyclic fluid shear stress promotes osteoblastic cells proliferation through ERK5 signaling pathway, *Mol. Cell. Biochem.* 364 (1-2) (2012) 321–327, <https://doi.org/10.1007/s11010-012-1233-y>.
- [32] J.A. Thomson et al, Embryonic Stem Cell Lines Derived from Human Blastocysts, *Science* 282 (5391) (Nov. 1998) 1145–1147, <https://doi.org/10.1126/science.282.5391.1145>.
- [33] M. Richards, C.-Y. Fong, W.-K. Chan, P.-C. Wong, A. Bongso, Human feeders support prolonged undifferentiated growth of human inner cell masses and embryonic stem cells, *Nat. Biotechnol.* 20 (9) (2002) 933–936, <https://doi.org/10.1038/nbt726>.
- [34] I. Chatterjee, F. Li, E.E. Kohler, J. Rehman, A.B. Malik, K.K. Wary, Induced Pluripotent Stem (iPS) Cell Culture Methods and Induction of Differentiation into Endothelial Cells, *Methods Mol. Biol. Clifton NJ* 1357 (2016) 311–327, https://doi.org/10.1007/7651_2015_203.

- [35] H. Zhu, D.S. Kaufman, An Improved Method to Produce Clinical-Scale Natural Killer Cells from Human Pluripotent Stem Cells, *Methods Mol. Biol.* Clifton NJ 2048 (2019) 107–119, https://doi.org/10.1007/978-1-4939-9728-2_12.
- [36] J. Dahlmann et al, Generation of functional cardiomyocytes from rat embryonic and induced pluripotent stem cells using feeder-free expansion and differentiation in suspension culture, *PLoS One* 13 (3) (2018) e0192652, <https://doi.org/10.1371/journal.pone.0192652>.
- [37] J.T. Cormier, N.I.Z. Nieden, D.E. Rancourt, M.S. Kallos, *Expansion of Undifferentiated Murine Embryonic Stem Cells as Aggregates in Suspension Culture Bioreactors*, *Tissue Eng.* 12 (11) (2006) 3233–3245.
- [38] A. Jönsson, A. Toppi, M. Dufva, The FAST Pump, a low-cost, easy to fabricate, SLA-3D-printed peristaltic pump for multi-channel systems in any lab, *HardwareX* 8 (2020) e00115, <https://doi.org/10.1016/j.ohx.2020.e00115>.
- [39] J.P. Efromson, S. Li, M.D. Lynch, BioSamplr: An open source, low cost automated sampling system for bioreactors, *HardwareX* 9 (2021) e00177, <https://doi.org/10.1016/j.ohx.2021.e00177>.
- [40] G. Talò et al, Industrialization of a perfusion bioreactor: Prime example of a non-straightforward process, *J. Tissue Eng. Regen. Med.* 12 (2) (2018) 405–415, <https://doi.org/10.1002/term.2480>.
- [41] B.F.L. Lai et al, A well plate-based multiplexed platform for incorporation of organoids into an organ-on-a-chip system with a perfusable vasculature, *Nat. Protoc.* 16 (4) (Apr. 2021) 2158–2189, <https://doi.org/10.1038/s41596-020-00490-1>.
- [42] M.S. Mousavi, G. Amoabediny, S.H. Mahfouzi, S.H. Safiabadi Tali, Enhanced articular cartilage decellularization using a novel perfusion-based bioreactor method, *J. Mech. Behav. Biomed. Mater.* 119 (Jul. 2021) 104511, <https://doi.org/10.1016/j.jmbbm.2021.104511>.
- [43] C. Manfredonia et al, Maintenance of Primary Human Colorectal Cancer Microenvironment Using a Perfusion Bioreactor-Based 3D Culture System, *Adv. Biosyst.* 3 (4) (2019) 1800300, <https://doi.org/10.1002/adbi.201800300>.
- [44] C. Hirt et al, Bioreactor-engineered cancer tissue-like structures mimic phenotypes, gene expression profiles and drug resistance patterns observed in vivo, *Biomaterials* 62 (2015) 138–146, <https://doi.org/10.1016/j.biomaterials.2015.05.037>.
- [45] M. Bartnikowski, T.J. Klein, F.P.W. Melchels, M.A. Woodruff, Effects of scaffold architecture on mechanical characteristics and osteoblast response to static and perfusion bioreactor cultures, *Biotechnol. Bioeng.* 111 (7) (2014) 1440–1451, <https://doi.org/10.1002/bit.25200>.
- [46] I.E. Chesnick, F.A. Avallone, R.D. Leapman, W.J. Landis, N. Eidelman, K. Potter, Evaluation of bioreactor-cultivated bone by magnetic resonance microscopy and FTIR microspectroscopy, *Bone* 40 (4) (Apr. 2007) 904–912, <https://doi.org/10.1016/j.bone.2006.10.020>.
- [47] I.J. Jayaprakash, N.S. Jayaprakash, Trends in Monoclonal Antibody Production Using Various Bioreactor Systems 31 (3) (Mar. 2021) 349–357, <https://doi.org/10.4014/jmb.1911.11066>.
- [48] H. Morschett et al, Robotic integration enables autonomous operation of laboratory scale stirred tank bioreactors with model-driven process analysis, *Biotechnol. Bioeng.* 118 (7) (2021) 2759–2769, <https://doi.org/10.1002/bit.27795>.
- [49] Isidro I. A., et al., Online monitoring of hiPSC expansion and hepatic differentiation in 3D culture by dielectric spectroscopy, *Biotechnol. Bioeng.*, doi:10.1002/bit.27751.



Robert Pazdzior is a Canadian citizen born 1993 in Canada. He began studies in Biochemistry & Molecular at Trent University (Peterborough, ON, Canada) in 2011, where he first gained research experience and an interest in research under the supervision of Steven Rafferty through three Natural Sciences and Engineering Research Council of Canada (NSERC) Undergraduate Research awards. He graduated from Trent on the President's Honour Roll in 2015. Following entry into the CeMM PhD program in Vienna, Austria, he then joined the Kubicek lab where he was awarded the Austrian Academy of Sciences DOC PhD fellowship and developed a keen interest in 3D printing, 3D design, mechatronics, and programming during his PhD thesis work on pancreatic α - and β -cell biology and tissue culture models.



Stefan Kubicek, PhD, is an Austrian citizen born 1978 in Vienna. He studied synthetic organic chemistry at the Vienna University of Technology and the Swiss Federal Institute of Technology (with François Diederich, ETH Zürich). For his PhD in Molecular Biology he developed the first specific histone methyltransferase inhibitor at the Institute of Molecular Pathology IMP Vienna (advisor Thomas Jenuwein). He then spent 3 years as a postdoctoral fellow at the Broad Institute of Harvard and MIT in Cambridge, MA, USA (Chemical Biology Program, Stuart Schreiber laboratory). Since 2010 he heads the Platform Austria for Chemical Biology PLACEBO at CeMM. Since 2013 he headed the Christian Doppler laboratory for Chemical Epigenetics and Antiinfectives, a public-private partnership between CeMM, Boehringer Ingelheim, and Haplogen. Since 2017 he heads the Proteomics and Metabolomics Facility at CeMM. Research in the Kubicek lab is funded by the Austrian Academy of Sciences, the European Research Council ERC, the Juvenile Diabetes Research Foundation JDRF, the Austrian Federal Ministry of Science, Research and Economy and the National Foundation for Research, Technology, and Development, and the Austrian Science Fund FWF. Stefan Kubicek studies chromatin, epigenetics and small molecules that change cell fates in oncology and diabetes with a particular focus on metabolism in the cell's nucleus.

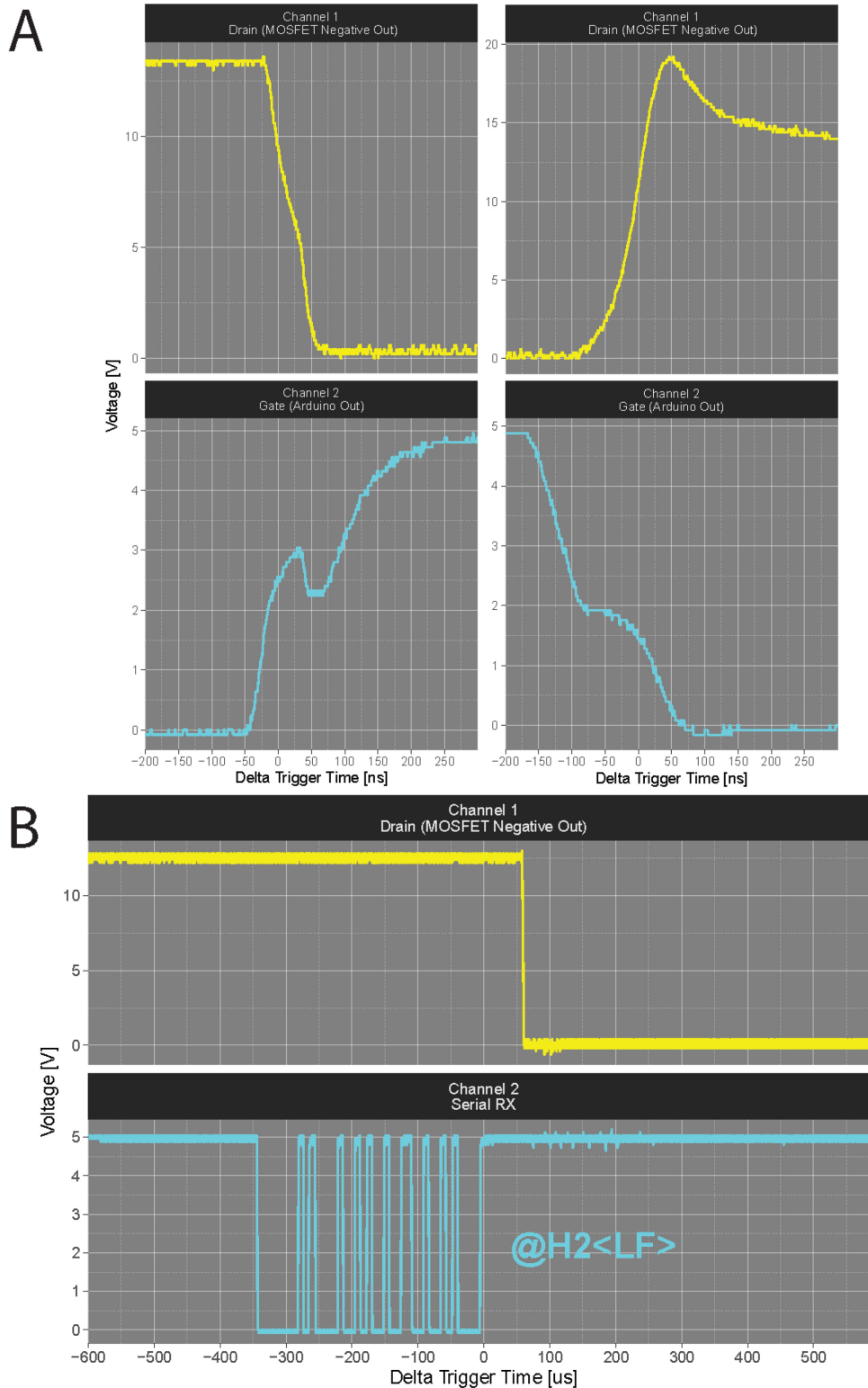
Supplementary Table 1

FETbox serial command timing benchmarks (115200 bps baud rate).

Serial Command (fetbox method)	Transmit (Tx)	Receive (Rx)	Mean Total Time (s) (n = 50)
enable_chan	@H1\n	*\n	0.015944
analog_read	@A15\n	705\n	0.015984
analog_write	@B1553\n	*\n	0.015983
hit_hold_chan	@V155\n	*\n	0.111951
pwm_chan	@S1551\n	*\n	0.015983
disable_chan	@I1\n	*\n	0.015985
query_ID	@#\n	fetbox0\n	0.015987
digital_write	@E04\n	*\n	0.015979
digital_read	@D04\n	0\n	0.015983

Supplementary Figure 1

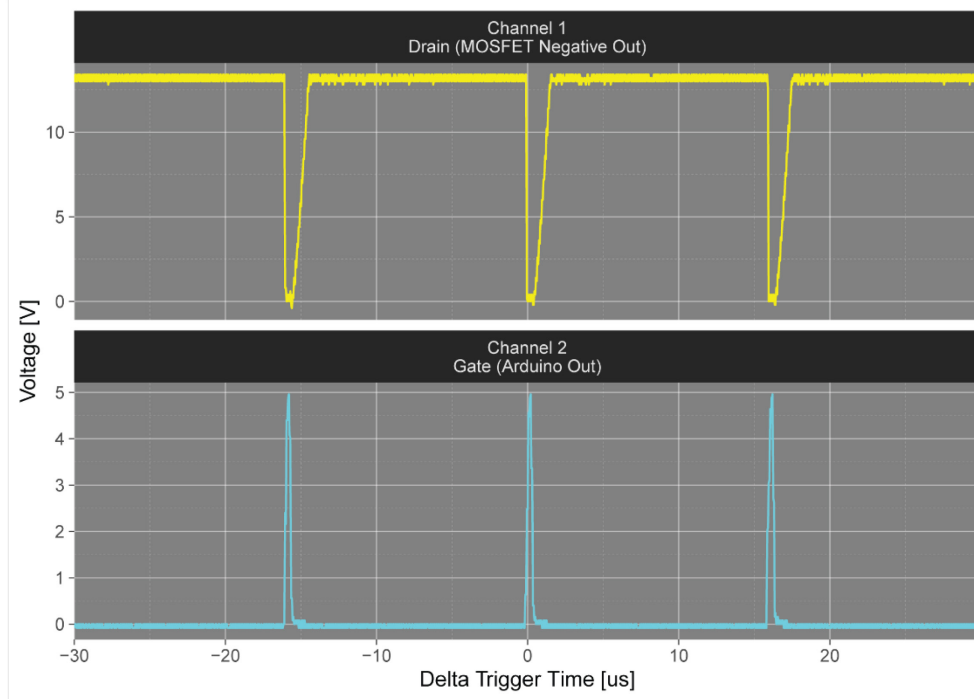
FETbox output channel 2 output characterization. A) PWM output rising (left) and falling (right) edges. Measured as in Figure 3. B) RS232 command reception and execution visualized by scoping the MOSFET output as in Figure 3 and the Arduino Rx pin while sending the “channel enable” command via serial.



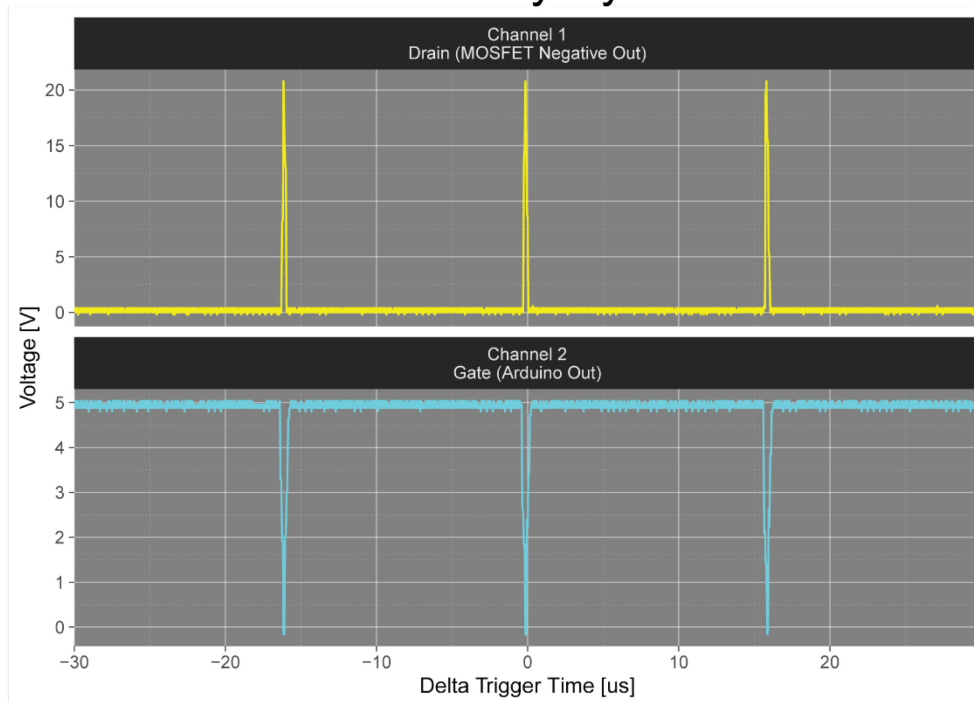
Supplementary Figure 2

FETbox output channel 2 waveform visualization at A) 2% duty cycle, and B) 98% duty cycle. Measured as in Figure 3.

A 2% Duty Cycle

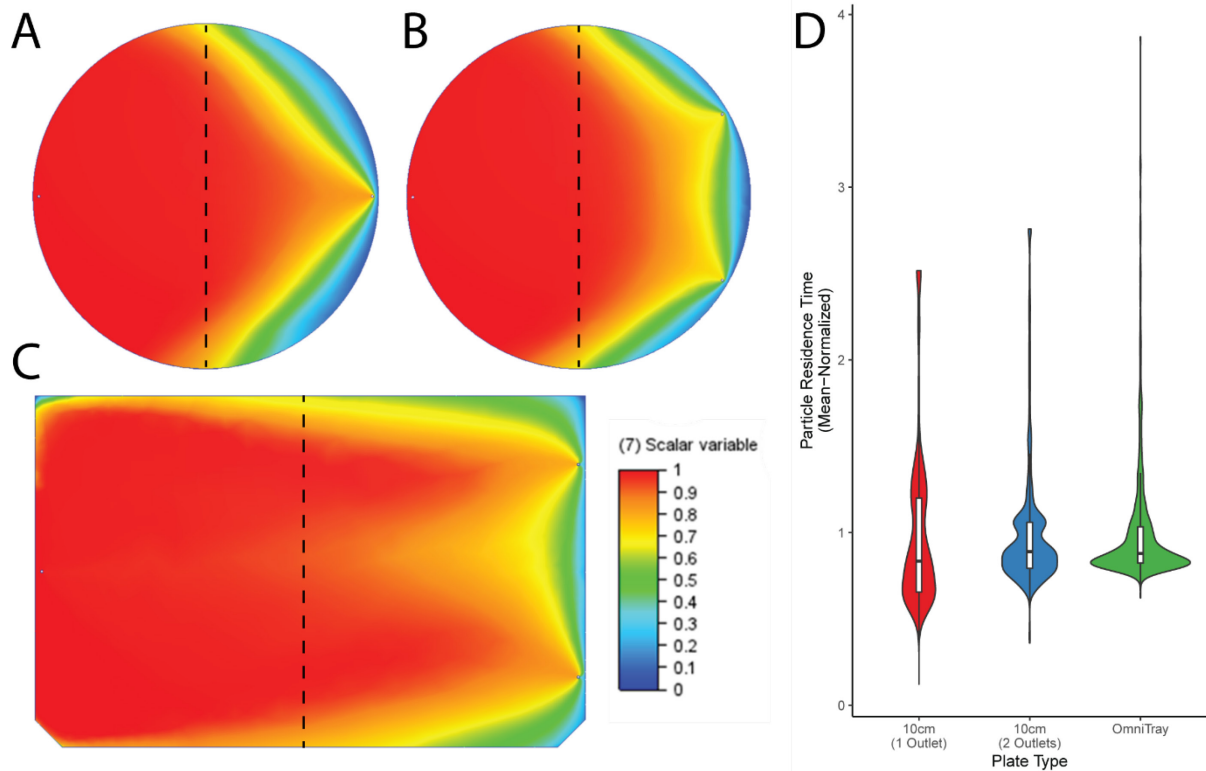


B 98% Duty Cycle



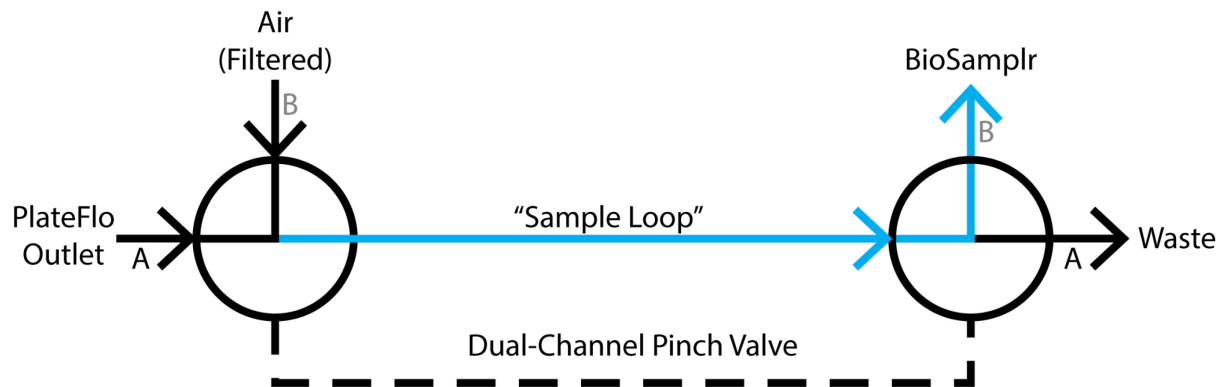
Supplementary Figure 3

Petri dishes as an alternative culture chamber. A-C) Flow profiling using scalar displacement to visualise overall media exchange patterns, as in Figure 5. All snapshots are at 1 h for comparison. A) A 10 cm petri dish with a single inlet nozzle inline with a single outlet. B) A 10 cm petri dish with a single inlet nozzle and dual outlet nozzles. C) Reference PlateFlo OmniTray plate. D) Residence time distribution of particles ($1\ \mu\text{m}$, neutral buoyancy, 1.0 coefficient of restitution) seeded uniformly across the midline of each setup perpendicular to the direction of flow (dashed lines, A-C). $n=1415$ for petri dishes and $n=1078$ for the OmniTray. Standard deviations were 907, 660, and 532 s for the 10 cm single, 10 cm dual, and OmniTray plates.



Supplementary Figure 4

Integration of the BioSamplr automated bioreactor sampler downstream of the PlateFlo system using an additional dual channel pinch valve. Letters denote simultaneous valve positions, e.g. when engaged, path B is enabled and the BioSamplr can pump supernatant from the sample loop, when disengaged path A is permitted and the outlet bypasses the sampler.



PlateFlo

Release 1.1.0

Robert Pazdzior

Oct 05, 2021

HARDWARE

1	Bill of Materials (BOM)	3
1.1	BOM Tables	3
1.2	Required Tools	4
1.3	Optional Tools/Components	5
2	Design Files	7
3	Build Guide	9
3.1	1. 3D Printing Guidelines	9
3.2	1. FETbox Hardware Controller	11
3.3	3. Perfusion Plate	19
4	Operating Instructions	29
4.1	1. System Setup	29
4.2	2. Inlet/Outlet Flow Rate Delta	30
4.3	3. Skimmer Pump Operation	32
4.4	4. Example Perfusion Setups	33
4.5	5. Appendix	36
5	FETbox Serial Control	39
5.1	1. Key Features	39
5.2	2. Quick Start	39
5.3	3. Usage	41
5.4	4. Expanding Functionality	43
6	Perfusion Event Scheduler	45
6.1	1. Key Features	45
6.2	2. Quick Start	45
6.3	3. Usage	46
6.4	4. Working Examples	49
7	PlateFlo API Index	51
7.1	fetbox	51
7.2	scheduler	54
7.3	ismatec	56
7.4	serial_io	65
8	License	67
8.1	Hardware	67
8.2	Software	67

9 Disclaimer	69
10 Indices and Tables	71
Python Module Index	73
Index	75

A modular system for programmable, plate-scale perfusion of adherent cell lines.

File Repository: [OSF \(Open Science Foundation\)](#)

This documentation is written to accompany [PlateFlo – A software-controllable plate-scale perfusion system for culture of adherent cells](#), published in [HardwareX](#) (Oct 2021). See the peer-reviewed article for a detailed description and contextualization of the hardware.

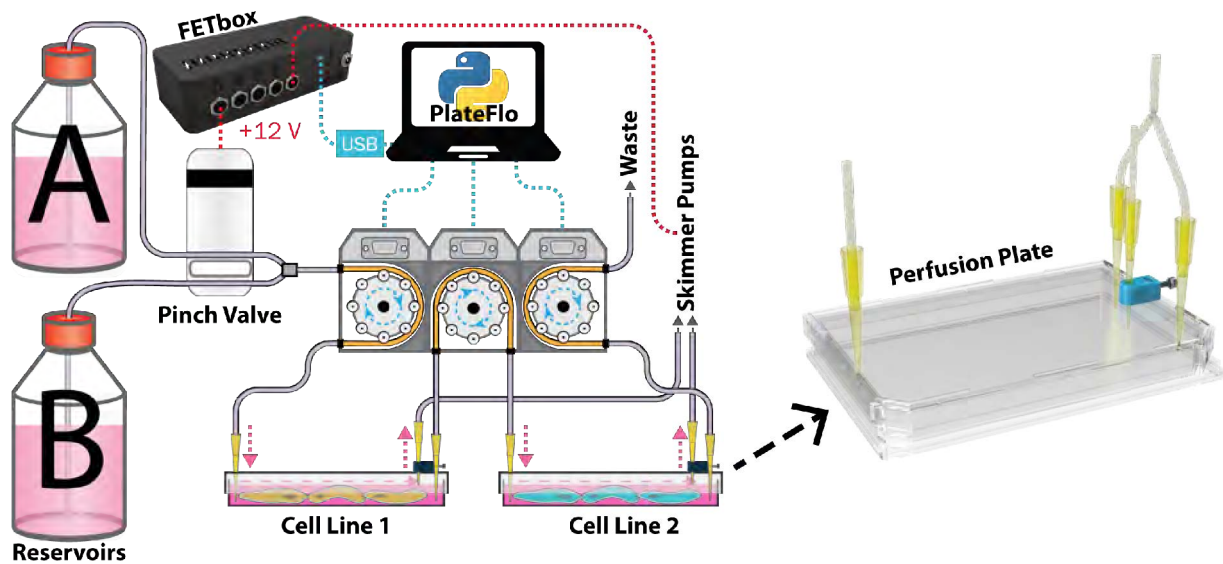


Fig. 1: **Left** Schematic overview of a multi-plate multi-reservoir perfusion setup controlled programmatically using the PlateFlo python package. **Right** PlateFlo perfusion plate. A modified Nunc® OmniTray® culture plate.

BILL OF MATERIALS (BOM)

1.1 BOM Tables

FETbox

Perfusion Plate

Fluidics

Component	Number	Cost per unit (EUR)	Total cost (EUR)	Source of materials	Material
Hardware Controller PCB	1	3.8	3.8	JLCPCB	FR4
Arduino Nano, rev3 (A000005) - development board	1	19.18	19.18	RS Components	
Single-row female header, 36-pin, 2.54mm pitch	2	1.1	2.2	RS Components	
CL13845G - 3.5mm jack, mono, female, w/nut	5	2.61	13.04	RS Components	
3.5mm jack, mono, male	5	2.77	13.85	RS Components	
5.5x2.1mm DC barrel jack, panel mount	1	1.16	1.16	Conrad	
12V DC power supply, 5A (60W)	1	29.99	29.99	Conrad	
FQP30N06L - N-channel MOSFET, TO220 package	5	0.82	4.1	RS Components	
1N4004 - rectifier diode, axial package	5	0.14	0.7	RS Components	
10kOhm resistor, 1/4W, axial package	5	0.13	0.65	RS Components	
100uF electrolytic capacitor, 35V, 2.5mm leg pitch, radial package	1	0.08	0.08	Conrad	
Screw, M3x8mm, DIN912	10	0.03	3.49 ¹	Conrad	Stainless steel

¹ Pack of 100

Component	Number	Cost per unit (EUR)	Total cost (EUR)	Source of materials	Material
Screw, M3x8mm, DIN912	10	0.03	3.49 ²	Conrad	Stainless steel
Hex nut, M3, DIN934	1	0.04	3.58 ²	Conrad	Stainless steel
Nunc OmniTray, one-well treated plates w/lids - 60/case	1	4.82	289.00	Thermo-Fischer Scientific	PS
P200 pipette tips, non-filtered	4			Any	
PCB milling set, 2-3 mm	1	9.31	9.31	Amazon (DE)	

Component	Number	Cost per unit (EUR)	Total cost (EUR)	Source of materials	Material
Bio-Chem Valve 100P Pinch Valve, 12V, 3-way, 1/8"; 100PD3MP12-02B	1	160.71	160.71	msscien-tific	
Spring steel mounting clip for 100P pinch valves; MC-100	1	2.91	2.52	msscien-tific	
Ismatec Reglo ICC, 4 independent-channel, 8-roller peristaltic pump ²	2	2234.83	4469.66	Cole-Parmer	
USB-A to USB-Mini-B cable	3 ³	1.84	5.52	Amazon (DE)	
PharMed BPT Tubing, 1.52mm ID, 3.22mm OD - 100ft	1	176.72	176.72	Cole-Parmer	Ismaprene
ParMed BPT 3-stop tubing, 1.52mm ID (yellow/blue) - 12/pk	1	98.56	98.56	Cole-Parmer	Ismaprene
Assorted 1/16" fittings				Cole-Parmer	PTFE or PVDF

Download Full BOM

BOM Notes

1.2 Required Tools

- FDM 3D printer
- Small drill press, hand drill, or rotary tool (e.g. Dremel)
- Cyanoacrylate (super) glue
- Soldering iron
- Flux-core solder
- Side cutters or similar (e.g. Knipex 78 61 125)
- 2.5 mm hex wrench

² Open-source alternatives are possible

³ One per Reglo ICC, one per FETbox

1.3 Optional Tools/Components

- Isopropanol – for cleaning residual flux from PCB
- Heat-shrink tubing – for DC input jack wire joint protection
- Self-adhesive silicone feet - for hardware controller and valve stand

DESIGN FILES

Design file name	File type	Open source license	Location
skimmer_clamp_M3	STL & CAD (F3Z; STEP)	CERN-OHL-W	https://doi.org/10.17605/OSF.IO/PYJCH
skimmer_height_block_<height>	STL mm.stl	CERN-OHL-W	https://doi.org/10.17605/OSF.IO/PYJCH
perfusion_lid_drill_jig	STL & CAD (STEP)	CERN-OHL-W	https://doi.org/10.17605/OSF.IO/PYJCH
petri_drill_jig_<size>_<inlet/outlet>	STL & CAD (STEP)	CERN-OHL-W	https://doi.org/10.17605/OSF.IO/PYJCH
valve_clip_base	STL & CAD (STEP)	CERN-OHL-W	https://doi.org/10.17605/OSF.IO/PYJCH
fetbox_complete	CAD (F3D, STEP)	CERN-OHL-W	https://doi.org/10.17605/OSF.IO/CRJVB
fetbox_enclosure_base	STL	CERN-OHL-W	https://doi.org/10.17605/OSF.IO/CRJVB
fetbox_enclosure_lid	STL	CERN-OHL-W	https://doi.org/10.17605/OSF.IO/CRJVB
FET-box_rev0_Gerber_JLPCB	Gerber CAM (ZIP'ed folder)	CERN-OHL-W	https://doi.org/10.17605/OSF.IO/CRJVB
FETbox_rev0_PCB	EAGLE design files (SCH + BRD)	CERN-OHL-W	https://doi.org/10.17605/OSF.IO/CRJVB
Firmware_FETbox.ino	Firmware (INO)	CERN-OHL-W	https://doi.org/10.17605/OSF.IO/CRJVB
plateflo	Python package	GNU-GPL3+	PyPI; Source

skimmer_clamp_M3 Print-in-place skimmer nozzle clamping mechanism. Fixed atop a drilled Nunc OmniTray lid to allow precise positioning of the skimmer nozzle tip height. CAD files include modelled M3 fastener hardware as assembled.

perfusion_lid_drill_jig A guide for marking hole locations on Nunc® OmniTray® lids for drilling. Slides over top of the lid with holes for a fine-tipped marker.

petri_drill_jig_<size>_<inlet/outlet> As above, but for alternative petri dish culture chambers. Two pieces, inlet and outlet sides, that slide together to accommodate variability in petri dish dimension between manufacturers.

valve_clip_base Simple stand for the BOM pinch valve clip. Holds the valve horizontal for use on e.g. an incubator shelf.

skimmer_height_block_<##>mm Blocks of defined heights, <##>: 1.2, 1.4, 1.6, and 1.8 mm. Placed under the skimmer nozzle before tightening the skimmer clamp for repeatable height setting.

fetbox_complete CAD model of the FETbox hardware controller with PCB and key electronic components modelled as assembled.

fetbox_enclosure_base Bottom half of the FETbox enclosure, into the which the PCB, power inlet, and MOSFET output jacks are mounted.

fetbox_enclosure_lid the top cover of the FETbox enclosure. Has ventilation for the output MOSFETs and Arduino. It snap-fits onto the fetbox_enclosure_base.

FETbox_rev0_Gerber_JLPCB Compressed (.zip) manufacturing Gerber (CAM)files. Ready for upload to the JL-CPCB website for PCB ordering.

FETbox_rev0_PCB Autodesk EAGLE PCB source files for the FETbox_rev0_PCB. SCH and BRD files are co-dependant and must be downloaded together in order to open/modify the design.

Firmware_FETbox Arduino “sketch”/firmware for the Arduino Nano developmentboard used in the FETbox hardware controller. Opened with Arduino IDE software

plateflo A Python package containing modules to simplify coding serial control of the FETbox and Ismatec Reglo peristaltic pumps.

See *FETbox Serial Control*, *Perfusion Event Scheduler*, and more generally *PlateFlo API Index* for more tutorials and usage usage.

BUILD GUIDE

3.1 1. 3D Printing Guidelines

Parts are designed and oriented optimally for fused deposition modeling (FDM) 3D printing. Parts pictured in proceeding sections were printed on a Prusa i3 MK3S 3D printer in “Galaxy Black” or “Azure Blue” Prusament PLA.

If a 3D printer is not available there are many 3D printing services available, e.g. ShapeWays in the US, or Xometry in the EU, that will ship parts directly to you and offer online quotes after uploading the STLs. If ordering through a service, it’s recommended to order as many of the consumable skimmer clamps as possible to avoid re-ordering later on.

For 3D printing services we recommend:

- Type/technology: FDM/FFF
- Material: PLA
- Layer height (sometimes called resolution): 0.1-0.2 mm
- No support material

Print Settings

Unless otherwise noted, the following print settings can be used as a general guideline when slicing the included design files for printing:

- 0.4 mm extrusion width
- 0.2 mm layer height
- 3 perimeters; 5 top/bottom layers
- 20% infill
- No supports

Parts that warrant special print considerations are discussed in the following sections.

3.1.1 FETbox Enclosure

Depending on several printer-specific conditions including parting cooling, print speed, and material properties, it may be necessary to clean up the overhangs and bridge areas:



Fig. 1: Areas that may require post-print clean-up to remove hanging material.

3.1.2 Skimmer Clamp

This part was modelled with a print-in-place sliding mechanism for securely clamping the P200 tip in place without potentially damaging it with bolt.

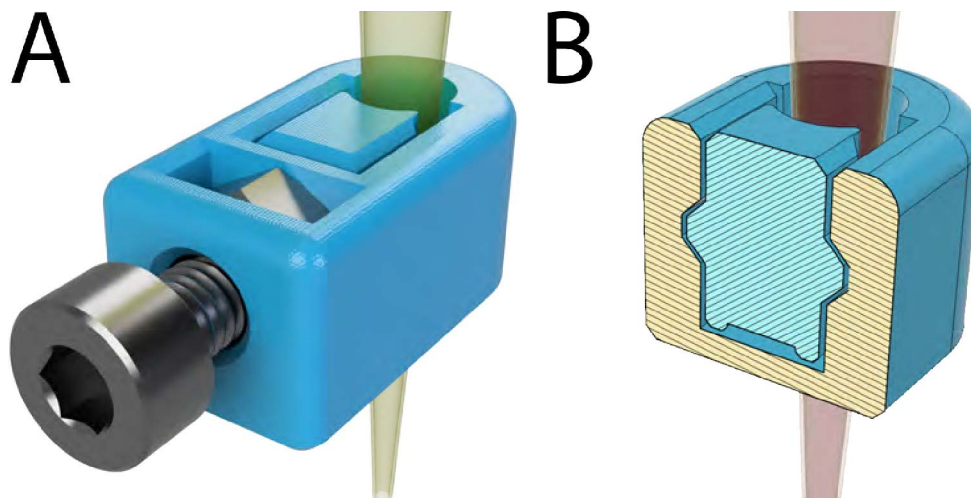


Fig. 2: A) Skimmer clamp, assembled. B) Print-in-place clamping mechanism. Note how the slide does not contact the surrounding clamp body at any point but is fully contained.

The clamp slide should break free with minimal effort and then slide freely after using the method described [here](#). Because of the small size of this part, printing just one at a time can lead to overheating artifacts. Print at least two or three at once while optimizing print settings.

Tip: Most popular slicing software have the option to reduce the material flowrate on un-supported extrusions. The first layers of the underside of the clamp benefit from this feature.

Using PrusaSlicer 2.2.0¹ we had success with a bridge flow ratio of 0.7, for example.

¹ 'PrusaSlicer - Prusa3d.com - 3D printers by Josef Prusa', Prusa3D - 3D Printers from Josef Průša. <https://www.prusa3d.com/prusaslicer/> (accessed Dec. 18, 2020).

Tip: It may also be advantageous to use a 0.1 mm layer height for this part as less material is deposited at once and is less likely to adhere irreversibly unintended layers below.

3.1.3 Skimmer Nozzle Height Blocks

The thickness of the nozzle height setting blocks (and consequently the skimmer nozzle height) is particularly sensitive to first layer height calibration and it is recommended that the printed height be validated with a micrometer, high quality calipers, or more empirically by measuring the residual plate volume.

3.2 1. FETbox Hardware Controller

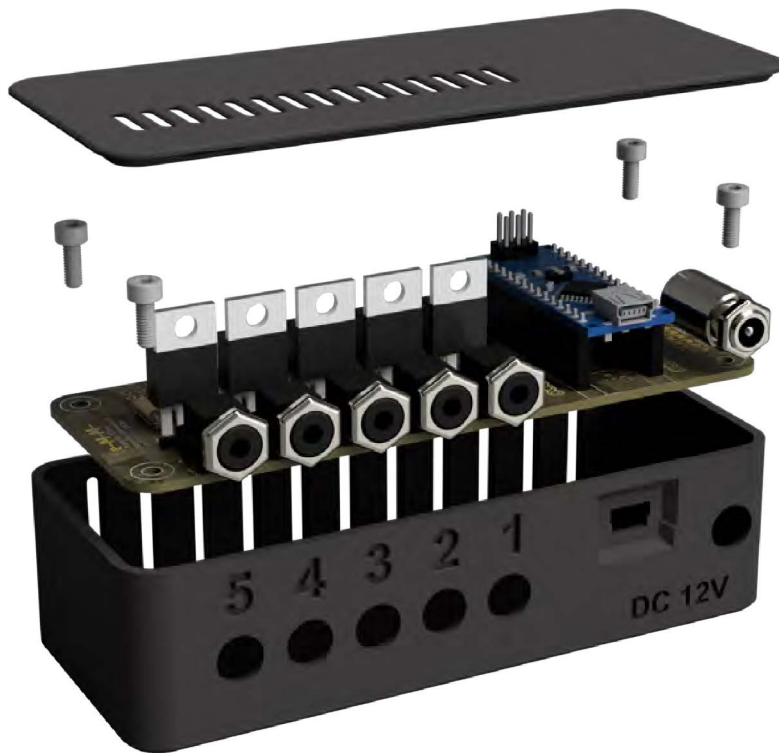


Fig. 3: Exploded FETbox hardware controller.

3.2.1 PCB Ordering

The FETbox printed circuit board (PCB) was designed with professional manufacture in mind and is not necessarily optimized for e.g. DIY milling/etching. There are many services available for small-run prototype PCB production, making it feasible to order several bare PCBs at an affordable rate.

At the time of writing, JLCPCB (China)² offers such a service and provided the boards pictured herein. We opted for a black PCB and ENIG-RoHS surface finish; however, these are optional and primarily cosmetic features in this case.

² 'JLCPCB': <https://jlcpcb.com/> (accessed Dec. 15, 2020).

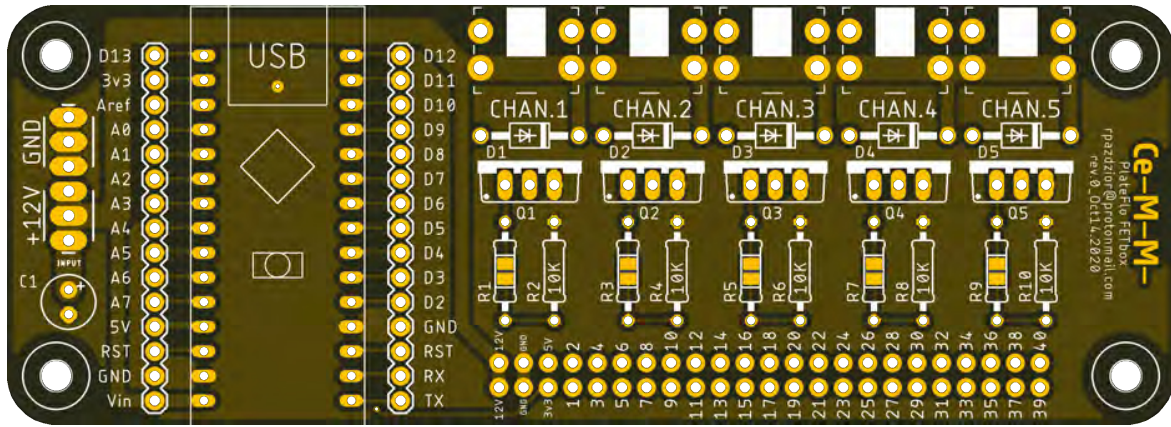


Fig. 4: FETbox PCB render (top).

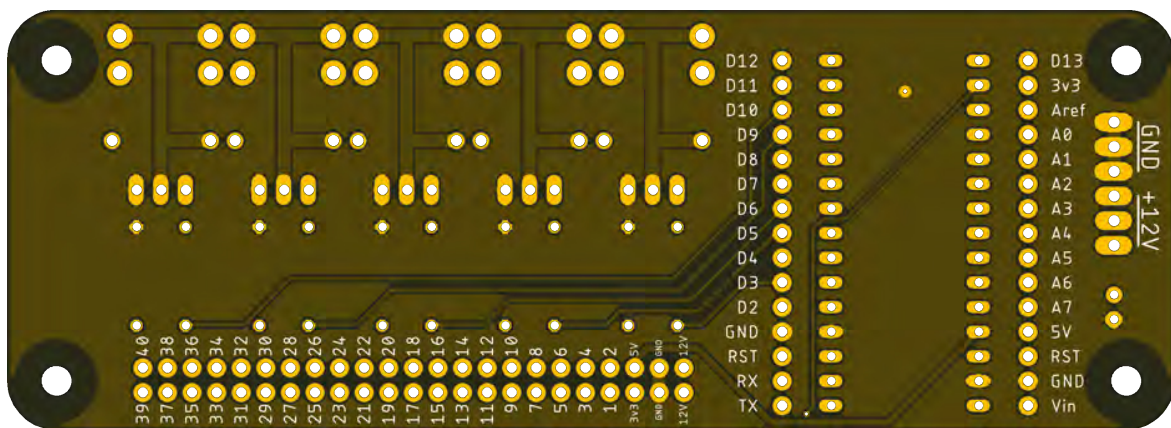


Fig. 5: FETbox PCB render (bottom).

The included Gerber computer aided manufacturing (CAM) files were generated according to JLCPCB's capabilities³ via Autodesk EAGLE⁴ using oxullo's helper files^{5, 6}. Similarly, FETbox_rev0_PCB.brd can be used to generate CAM files for other PCB manufacturers using appropriate specifications and EAGLE design software.

To [place an order with JLCPCB](#), upload FETbox_rev0_Gerber_JLCPCB.zip and select the PCB colour and surface finish as desired. The board dimensions will be derived automatically from the Gerber files.

Other options can be left in their default state:

- 2 layers
- 1 design
- single PCB delivery format
- 1.6mm thickness
- 1 oz copper weight
- no gold fingers, no production file confirmation
- fully tested flying probe
- no castellated holes
- no order number removal.

3.2.2 PCB Assembly

Tip: For ease of assembly, it is recommended to solder diodes and resistors to the PCB prior to the output jacks and MOSFETS as the shorter components are more difficult to access once the taller MOSFETs and output jacks are mounted.

Tip: Axial component leads need to be bent 90° prior to soldering, this can be done with any pair of pliers, however a 3D-printed jig such as <https://www.thingiverse.com/thing:26025> can make the task less finicky. Hole spacing on all diodes and resistors on the PCB are 0.4"/10.16 mm.

Instructions

1. Solder the fly-back diodes (D1-D5) to the board. Ensure the polarity (white stripe) matches that on the PCB silkscreen.



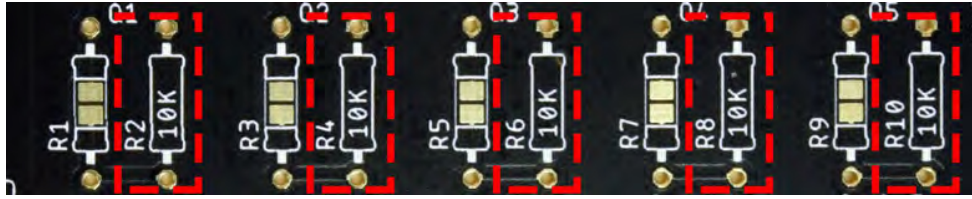
2. Solder the 10kΩ pull-down resistors (R2, R4, R6, R8, R10) to the board.

³ 'JLCPCB Capabilities'. <https://jlcpcb.com/capabilities/Capabilities> (accessed Dec. 15, 2020).

⁴ 'EAGLE | PCB Design And Electrical Schematic Software | Autodesk'. <https://www.autodesk.com/products/eagle/overview> (accessed Dec. 16, 2020).

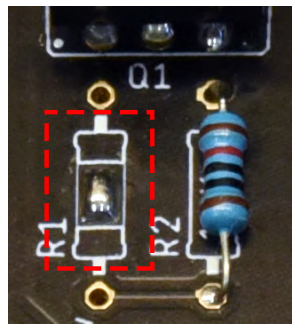
⁵ oxullo, 'oxullo/jlcpcb-eagle', jlcpcb-eagle, Dec. 11, 2020. <https://github.com/oxullo/jlcpcb-eagle> (accessed Dec. 15, 2020).

⁶ JLCPCB, 'JLCPCBofficial/jlcpcb-eagle', Dec. 13, 2020. <https://github.com/JLCPCBofficial/jlcpcb-eagle> (accessed Dec. 15, 2020).

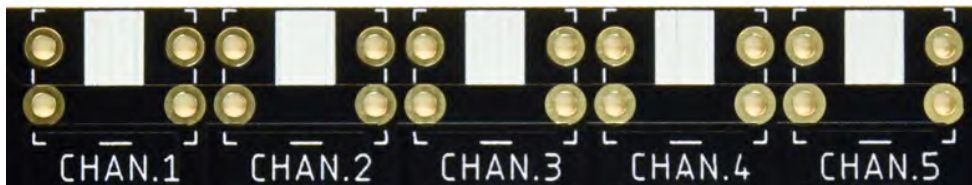


3. *Optional:* Current-limiting gate resistors can be added in the odd-numbered resistor positions (R1, R3, R5, etc.). Though they are not absolutely necessary in the author's opinion.

Caution: If a gate resistor is not used, the central pads at these positions must be bridged with solder as below.



4. Solder the 3.5mm output jacks to the PCB. Note that due to the mass of copper around these solder pads conducting heat away, it may be necessary to increase the soldering iron temperature to make a proper joint here.

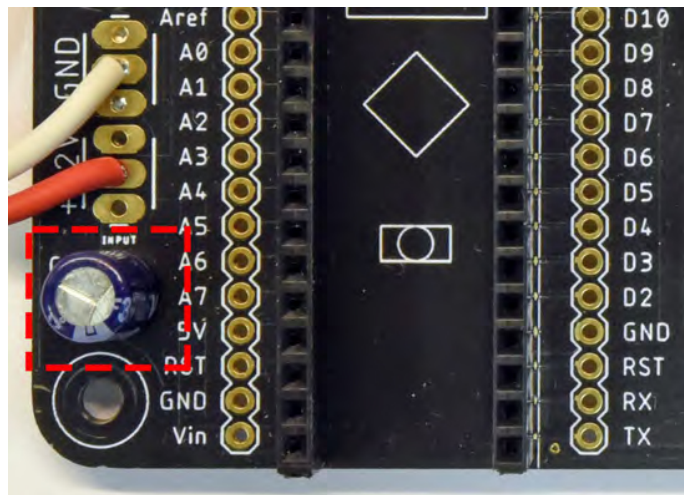
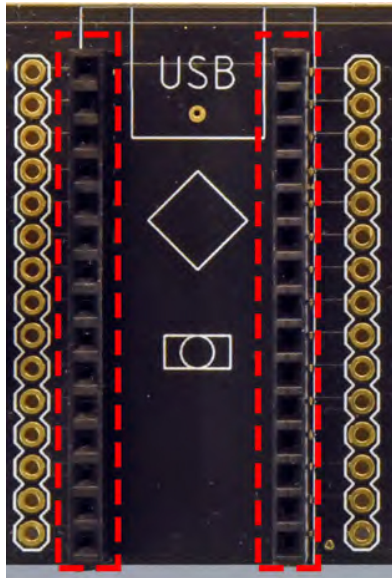


5. Solder the MOSFETs (Q1-Q5) to the PCB. As in the previous step, some of the MOSFETs pads will require more heat to make a proper joint here.



6. Trim two 30-pin strips from the female headers using side cutters.
7. Socket the Arduino Nano pins into the trimmed header strips before soldering the female headers to the board. This will ensure proper alignment and is easier to solder.
8. Solder the decoupling capacitor (C1) to the power input of board.

Warning: Take care with the polarity of the capacitor! The negative terminal will usually have a white stripe and/or shorter lead.



Reversing the polarity may cause the capacitor to explode.

- Cut 2× 2-3 cm of 0.5mm² (20 AWG) wire for the 12V DC input jack and strip a few millimeters from each end.
- Solder one end of each wire to the barrel and center pin tabs of the DC jack, apply heat shrink tubing to the tabs if available.
- Solder the DC jack center pin wire to one of the +12V solder pads at the power input. Likewise, for the barrel wire to one of the GND pads.

Tip: Additional pads, connected in parallel, are provided in case one wishes to power additional devices from the board input.

- Bend the wires into a gentle loop away from the top edge of the board.

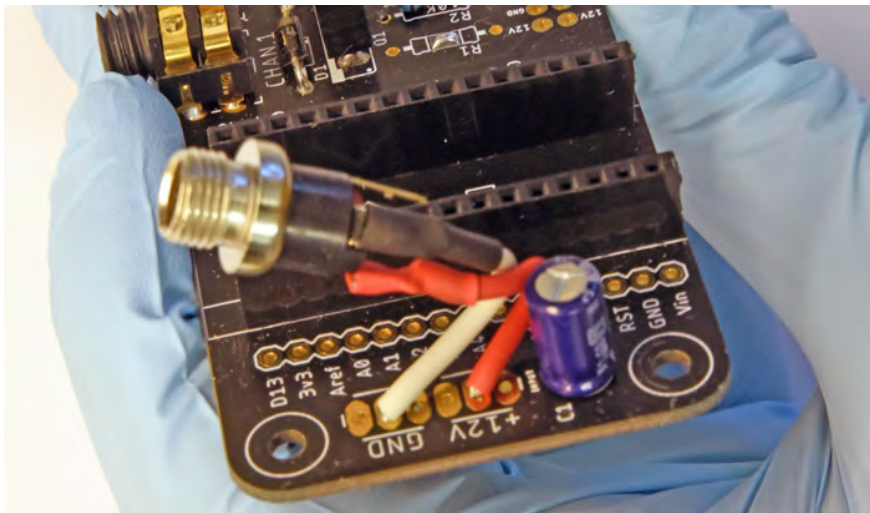


Fig. 6: DC jack wired and soldered.

- Trim excess leads from the bottom of the board using the side cutters if you have not done so already.

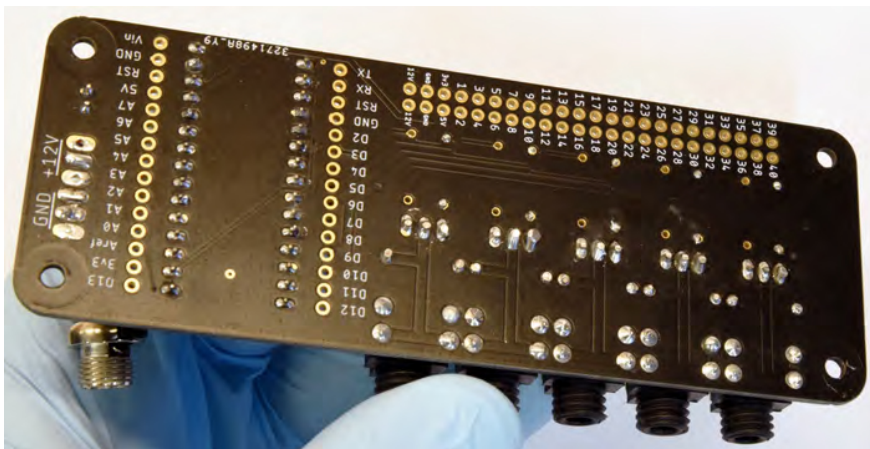


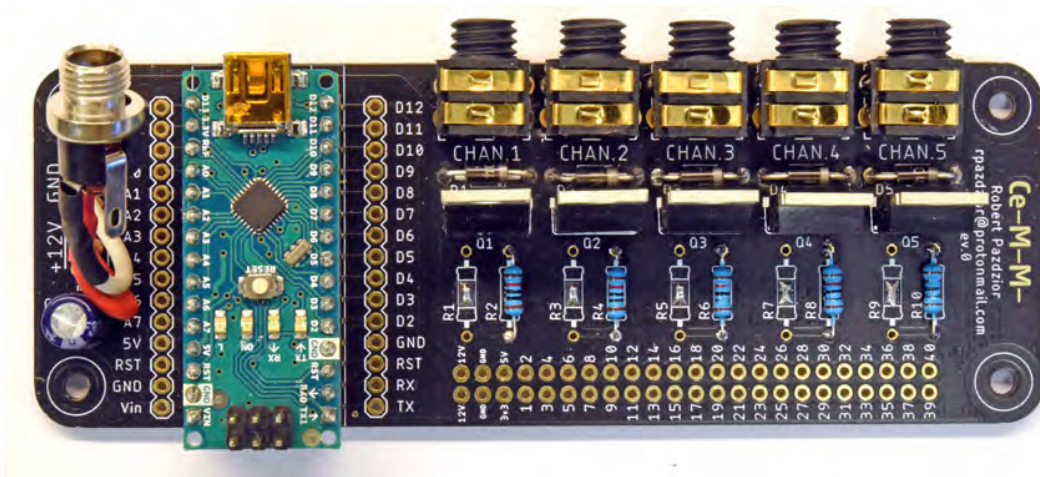
Fig. 7: Soldered and trimmed leads.

3.2.3 Final Assembly

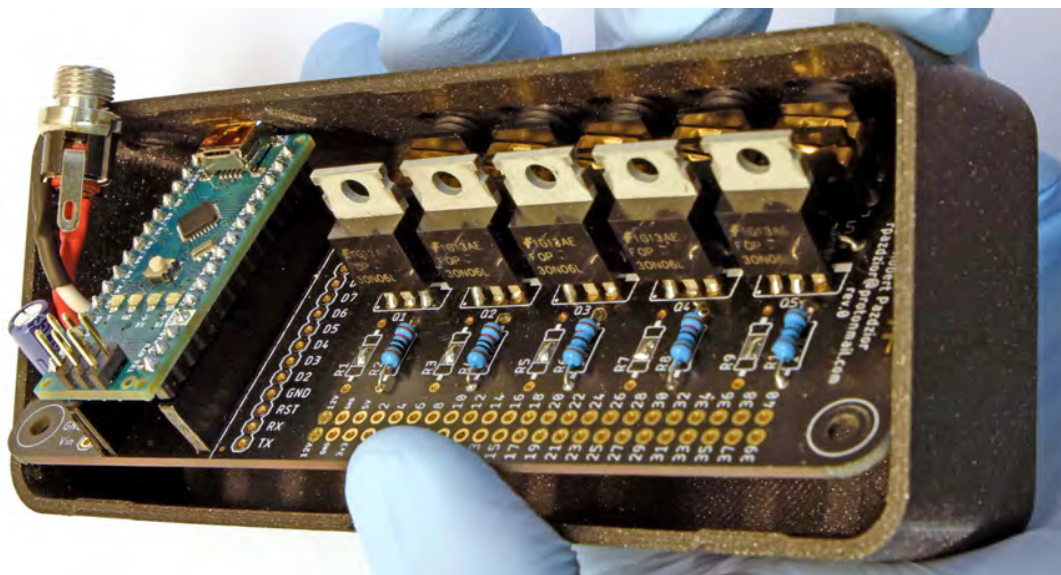
- Using an M3×8 bolt, thread all four standoffs on the inside of the bottom half of the enclosure by driving the bolt in then out, one at a time. There will be significant resistance as the bolt cuts a thread into the printed plastic.

Warning: Do not overtighten! Plastic threads can be easily stripped.

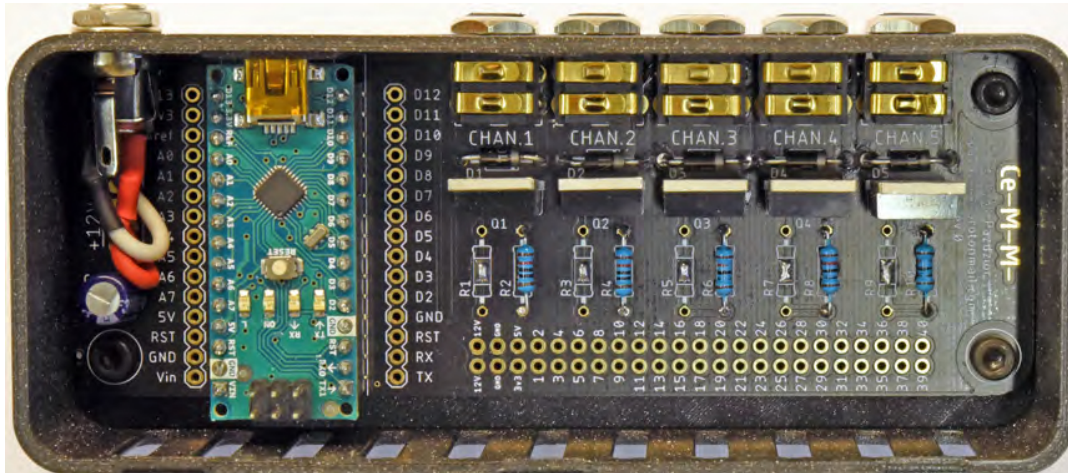
- Ensure there is adequate clearance for the M3 bolt to pass through the PCB mounting holes of the PCB.
PCB machining tolerance varies with manufacturer and a quick pass with a 3 mm drill bit or with the M3 bolt itself might be necessary.
- Remove all nuts and washers from the DC jack and controller output jacks.
- Socket the Arduino Nano into the controller board with its USB port oriented as printed on the PCB silkscreen.



- Insert the board at an angle into the mounting holes of the enclosure. The board will sit flat with the base of the enclosure once these are through.



- Secure the PCB to the enclosure bottom using four M3×8 bolts.
- Re-install the washers and nuts for the DC input jack and controller output jacks. Do not overtighten the nuts on the output jacks.



- Snap the enclosure lid in place with the convective cooling slots over the MOSFET array and Arduino.

3.2.4 Firmware Upload

The FETbox controller firmware is supplied as an Arduino ‘sketch’ for upload via the **Arduino IDE** software.

- Install the **Arduino IDE** software and USB drivers per the [instructions](#) for your system.
- Connect the hardware controller using a USB mini-B cable.
- Open the hardware controller sketch, [Firmware_FETbox.ino](#), with **Arduino IDE**.
- Set the target board, processor and serial port:

Tools -> Board -> Arduino Nano,

Tools -> Processor -> ATmega328P,

Tools -> Port -> <Port>

Note: *Tools -> Get Board Info* can sometimes set these automatically.

- Upload the sketch to the hardware controller Arduino:

Sketch -> Upload

- Once uploaded, verify that the upload was successful:
 - Open the serial monitor: *Tools -> Serial Monitor*
 - Set the line ending to `NewLine` and the baud rate to `115200`.
 - Type `@#` into the serial monitor and press Send or hit the Return key.

If the sketch was successfully uploaded, the board will respond with `fetbox0` in the serial monitor.

3.3 3. Perfusion Plate

3.3.1 Skimmer Nozzle Clamp



Fig. 8: Parts, from left to right: printed skimmer_clamp_M3.stl, M3 hex nut, M3 bolt.

1. Insert the M3 hex nut and thread in the M3 bolt until finger tight.



2. Using a 2.5 mm hex wrench, tighten sharply until the slide breaks free, then continue until the clamp slide has moved through its entire range of motion (below, right).
3. Back off the bolt until it is clear of the slide travel.
4. Using a small flat screwdriver or a P200 tip, push the slide back to its starting position.

3.3.2 Perfusion Plate Lid

See *Petri Dish Perfusion Lid* for notes on building the perfusion plate using a petri dish, rather than the recommended OmniTray.

1. Using the perfusion_lid_drill_jig and a fine-tipped marker, transfer the four nozzle hole locations to the Nunc OmniTray lid.
2. Using a 2.2mm^{*0} PCB milling bit/tool, drill all four marked holes.

Tip: Use a peck drilling technique to limit plastic melt and improve hole dimensional accuracy and consistency.

3. Clean all plastic debris from the lid and wipe with 70% EtOH.

⁰ Drill size will depend on P200 manufacturer and drilling technique. Some experimentation may be necessary here. See *above*.

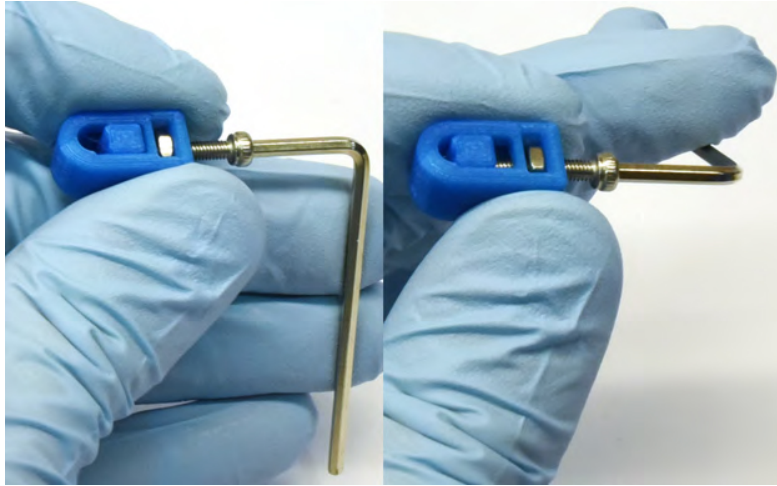


Fig. 9: **Left:** Twist sharply to break the weak connection on the slide underside. **Right** Continue until the end of the slide travel range.

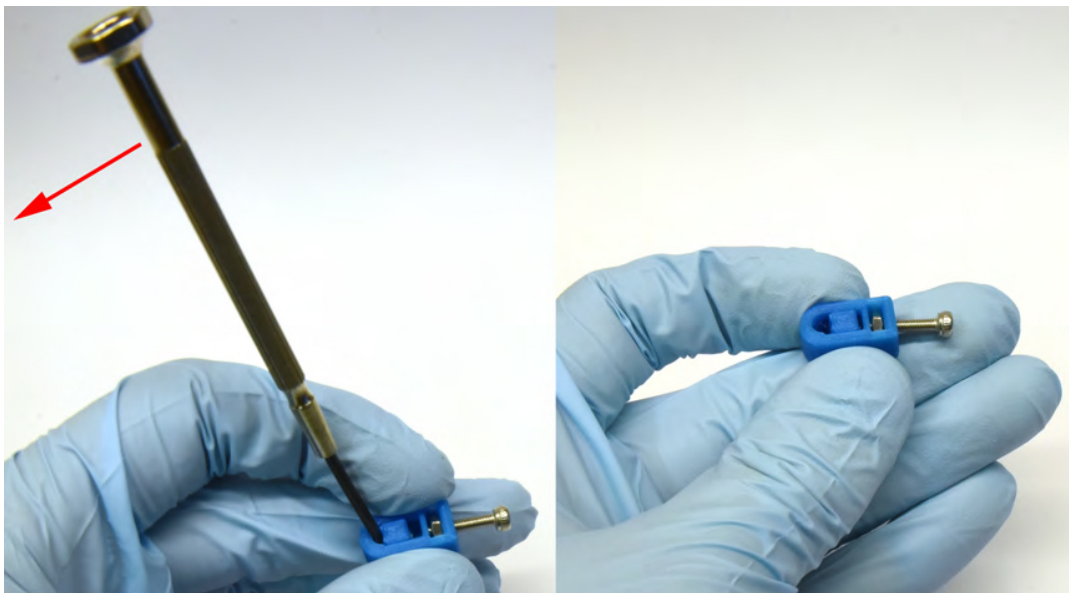
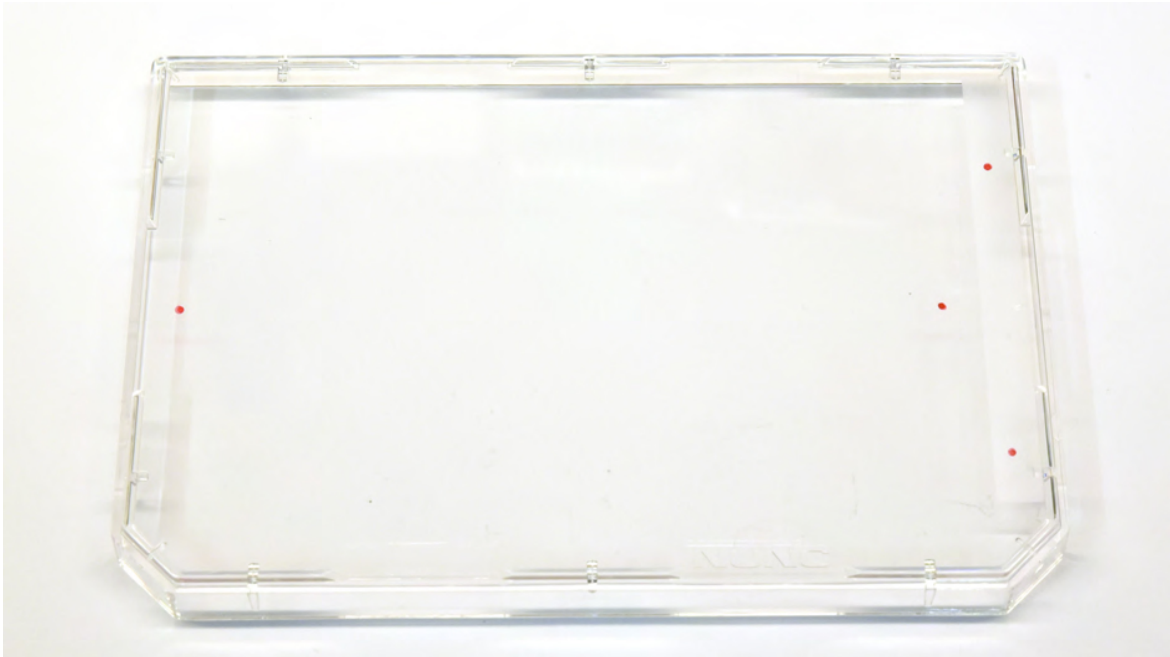
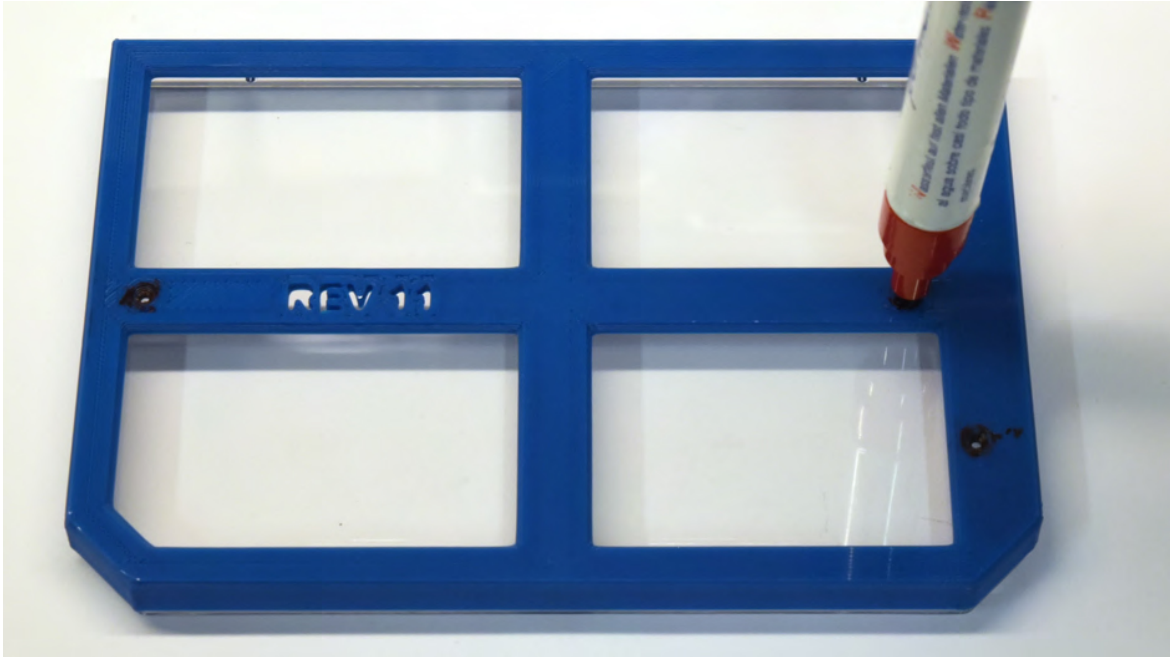
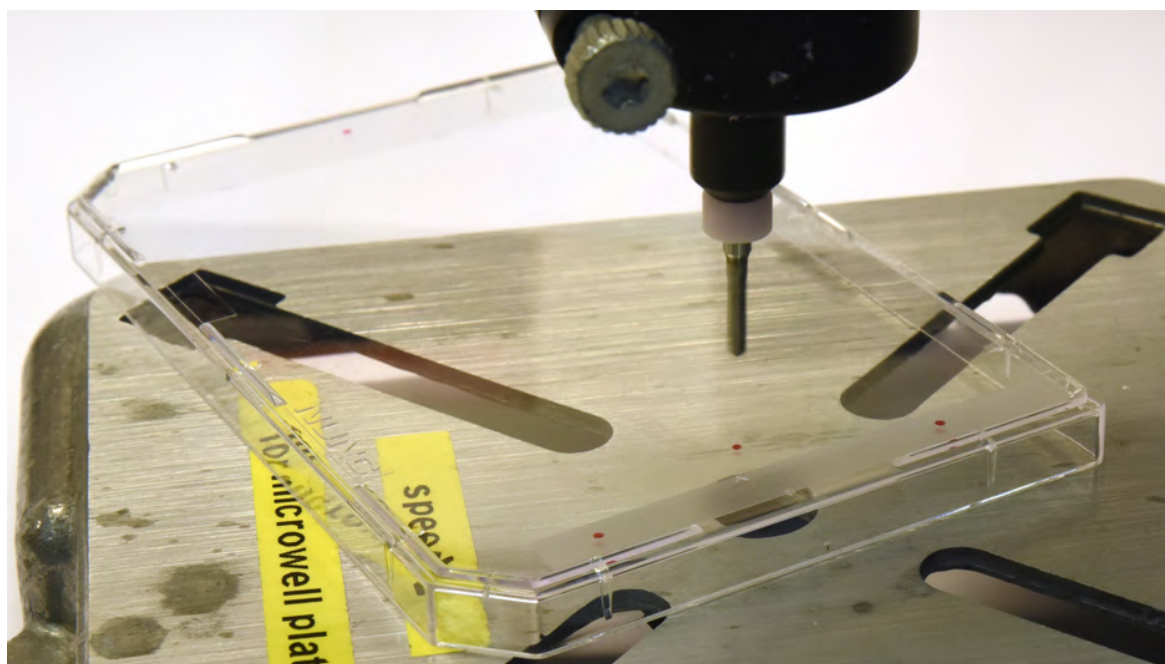


Fig. 10: **Left:** use the screwdriver as a lever to push the slide back, there may be resistance the first time the slide moves. **Right:** The slide back in its starting position, ready for use.







4. Apply a small amount of cyanoacrylate glue to the bottom of a skimmer nozzle clamp.
5. Align the clamp with the drilled skimmer hole as below, press firmly, then allow to cure.

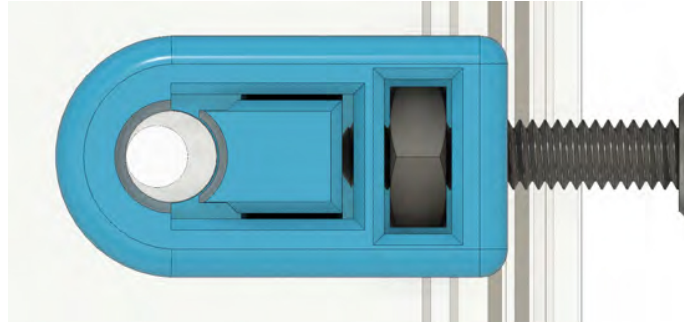


Fig. 11: Align the drilled hole with the edge of the clamp hole farthest from the slide and bolt. This will prevent pinching if the hole sizes differ significantly.

6. Place the lid on an OmniTray base.
7. If necessary, trim P200 to length^{†0}.
8. Insert the inlet and outlet P200 tips firmly into place.

It may be necessary to twist the P200s into final position. With a proper fit, a P200 will sit securely in the drilled hole, with the tip just above the culture surface, but below the expected fluid height (<1 mm, typically).

Note: Small cracks may form around the holes during this step, they can be safely disregarded.

9. Set the skimmer nozzle height:
 - a. Insert a P200 into the nozzle clamp.
 - b. Select the appropriate `skimmer_height_block` thickness for the desired plate volume. See *Selecting Skimmer Height* for more.
 - c. Place the height block in the plate base, underneath the skimmer nozzle.

Note: Keep a spare OmniTray base handy and reuse it for this step, as it's not advisable to use it for cell culture after this.

- d. Ensure the P200 tip touches the height block and the plate lid sits flat on the base when no force is applied to the skimmer P200, as in the figure above.
 - e. While holding the P200 in position, tighten the nozzle clamp bolt using a 2.5 mm hex wrench until the P200 barrel deforms *slightly*.
 - f. Verify the skimmer nozzle position has not changed during clamp tightening
10. Cut two segments of tubing, 6cm in length, join one end with a Y-piece fitting.
11. Press fit the open ends of the tubing into the outlet nozzles.
12. Cut a ~2cm segment of tubing, place it over the remaining Y-piece barb.

⁰ Tip trimming is necessary if a hole diameter is not found that results in a tight fit *and* adequate clearance from the plate bottom, as described above.

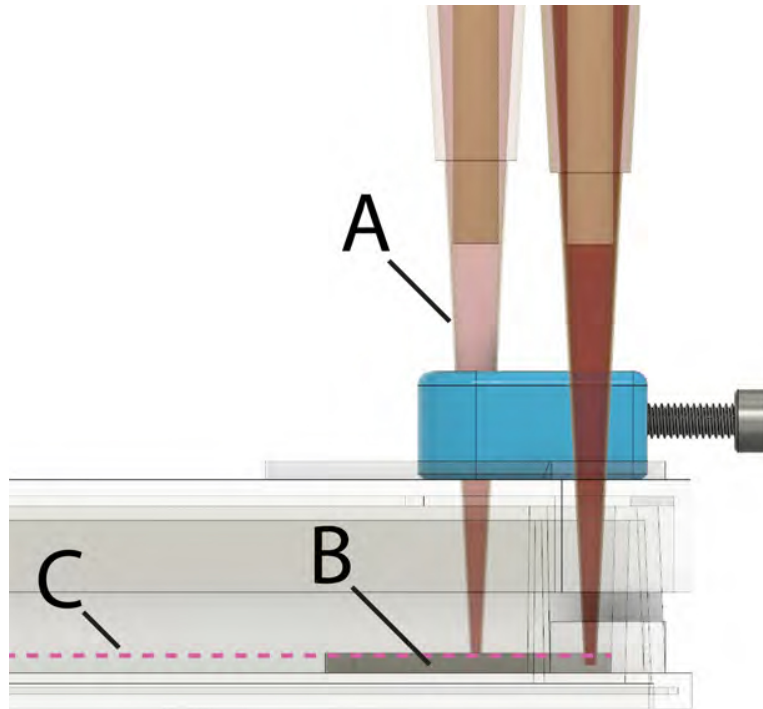


Fig. 12: A: Skimmer nozzle P200. B: Skimmer height block. C: Theoretical media level.

- UV-sterilize the plate lid prior to use. This can be done, for example, with a standard tissue culture cabinet UV cycle by placing the lid(s) bottom-side-up as close to the UV lamp as possible.

3.3.3 Petri Dish Perfusion Lid

6, 10, and 15 cm petri dishes are likely a viable alternative to the rectangular OmniTray, having poorer overall flow characteristics but better availability and variety of size. See the Discussion section in the text, as well as Supplementary Figure 3 for details.

Select the appropriate lid marking jig for the desired petri dish size: `petri_drill_jig_<size>_inlet` and `petri_drill_jig_<size>_outlet`.

- Petri dish marking jigs consist of two parts that slide into one another after printing. This provides some adjustment range to accommodate dimensional variability between manufacturers.

Assemble the printed jig.

- Place the jig atop the plate lid, and while gently holding the two halves together for proper alignment, transfer all four hole locations with a marker.
- With the hole locations marked, remove the lid from the dish and carry on with the build instructions from step 2 in *Perfusion Plate Lid* above.

Important: As petri dishes are generally deeper/taller than the OmniTray, **larger diameter holes** will likely be necessary to fully insert the nozzles.

Similarly, the **skimmer nozzle height** will need to be set higher than in the OmniTray to achieve an equivalent media volume.

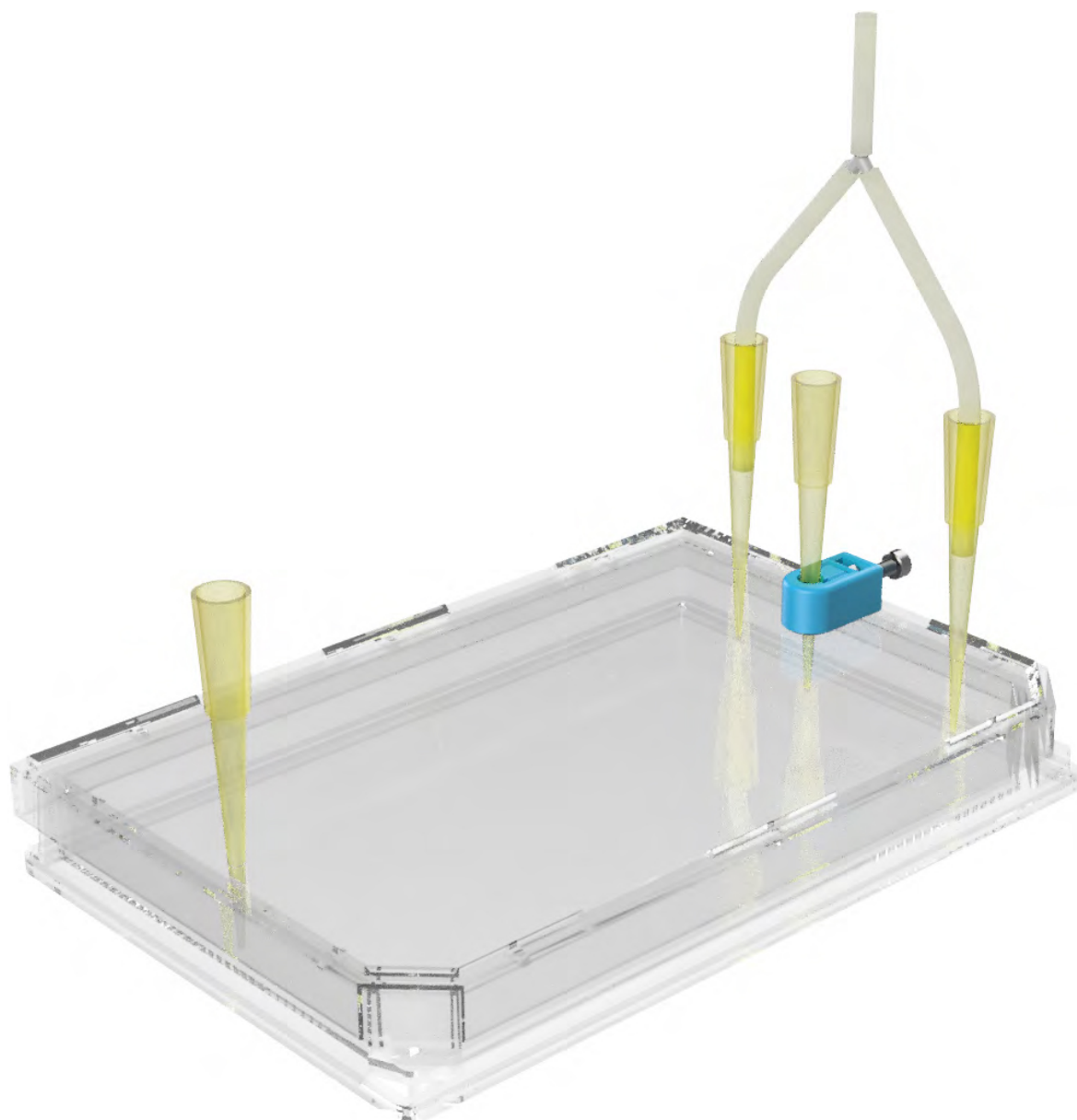


Fig. 13: Outlet tubing assembled.



Fig. 14: Assembled 10 cm petri lid marking jig.



Fig. 15: Transferring hole locations to a 10 cm petri lid.



Fig. 16: All four nozzle hole locations marked in black ink.

References

OPERATING INSTRUCTIONS

4.1 1. System Setup

Instructions here are generalized as much as possible. Several schematic *example setups* illustrate the tubing connections and some potentially interesting experimental configurations.

4.1.1 General Guidelines

- The inlet/outlet pumps, media reservoirs, and fluidic tubing upstream of culture plates should be kept in the culture incubator with the perfusion plates to avoid degassing in the tubing.
- Skimmer pumps, FETbox(es), and the waste reservoir can be placed exterior to the incubator.

Note: Minimize fluid head for the outlet and skimmer pumps as much as possible for maximum performance.

- Preheat the inlet/outlet peristaltic pumps in a dry incubator/oven several degrees higher than the final target temperature. This will minimize formation of potentially damaging condensation on the electronics and mechanical components.

4.1.2 Sterilization & Priming

Sterilization is done *in-place*, without plates connected. Use a straight barbed fitting at the point in the tubing where the plate will eventually be connected. This joint can be easily split and connected directly to the tubing already connected to the plate.

1. Connect a 70% EtOH bottle to all reservoir connections.
2. Disengage the outlet pump tubing from the pump rollers, such that the inlet pumps can pump freely all the way to the waste.
3. Run the inlet pump at full speed until at least several volumes have passed through all of the tubing.

Important: If using pinch valves in the circuit, cycle their positions regularly to ensure full EtOH contact.

4. Disconnect EtOH reservoir, and connect the inlet tubing to all culture media reservoirs.
5. Repeat (3) with media to purge EtOH from the system and prime the tubing with culture medium.

Note: If multiple reservoirs are utilized, take care that the line downstream of the valves contains the correct medium for the start of the experiment.

6. Engage all peristaltic pump head to prevent backflow and avoid spillage when connecting the perfusion plates later.
7. Sterilize the skimmer tubing by pumping 70% EtOH through, then run dry to clear. Wrap exposed tubing ends in sterilized aluminum foil until ready to connect to the perfusion plate.

4.1.3 Perfusion Plate Connection

1. Seed an Nunc OmniTray plate with the desired tissue culture model. Allow cells sufficient time to adhere prior to initiating flow.
2. In the tissue culture cabinet, place the *assembled and sterilized* perfusion lid onto the seeded plate base. Verify that the inlet/outlet nozzles sit below the media surface and do not ride on the culture surface.
3. Transfer the assembled perfusion plate to the incubator.
4. Split the tubing at the joint described in *Sterilization & Priming*. The barbed fitting should remain on the outlet side.
5. Connect the outlet pump tubing to the plate outlet tube, and press fit the bare inlet tubing into inlet P200 nozzle.
6. Connect the skimmer tubing by pressing it entirely into the clamped skimmer P200 nozzle.
7. The system is now ready for operation.

4.2 2. Inlet/Outlet Flow Rate Delta

The “skimming” approach we’ve taken to plate volume regulation requires a slightly higher inlet flow rate than outlet flow rate, with the excess removed in a controlled way by the skimmer system. The inlet/outlet flow rate delta should be kept as small as possible to minimize volume fluctuation.

To determine a safe operating flow rate delta, variability of the inlet/outlet pump flow rates between pumps and/or channels is measured. This can be done in parallel with calibration. The exact method for calibration is model/manufacture specific, but generally a flow rate in the intended operating range is set, run for a fixed period of time, weighed, and the theoretical vs. measured dispensed volume is used to set the calibrated flow rate. A safe flow rate delta takes into account variability between pumps, tubing, and channels. **A safe margin is ~1.5-2x the measured flow rate range.**

If re-calibration between pump tubing replacement is undesirable, variability in different stoppered tubing can also be considered and accounted for in the flow rate delta. For example, below, four different pump tubes were tested randomly across the four channels of two different Ismatec Reglo Digital pumps. In this case high variability is observed and an inlet/outlet flow delta of ~10% would be considered a safe operating margin.

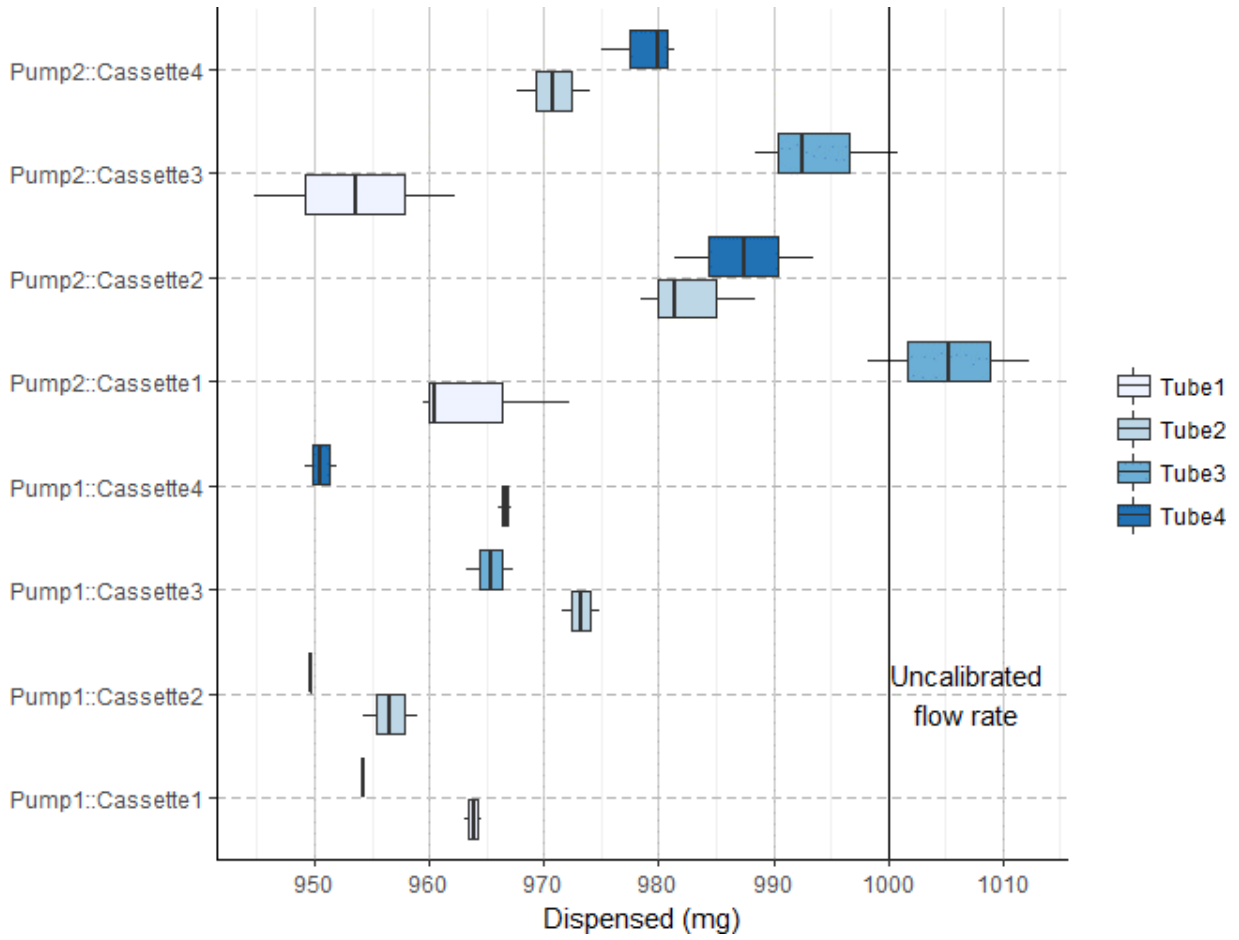


Fig. 1: Measured dispensed volume of random combination of two pumps and four sets of stoppered tubing. Cassettes (spring arm for clamping stoppered tubing down against the rollers) were kept with their original pumps. n = 3 for each data point.

4.3 3. Skimmer Pump Operation

Skimmer pumps do not need to be run continuously. Excess medium accumulates slowly (hours to days) and can therefore be removed intermittently to reduce power consumption and wear on the skimmer pumps/tubing.

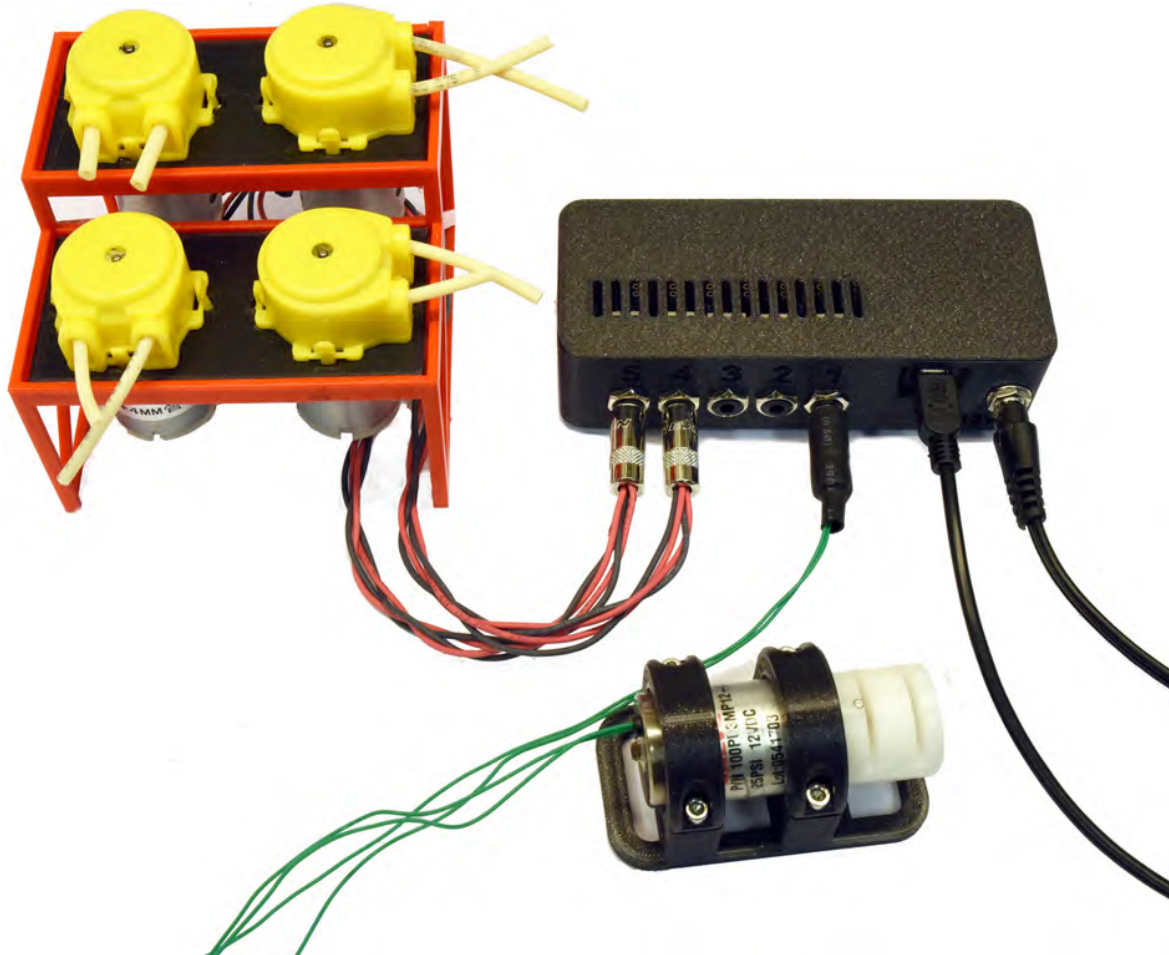


Fig. 2: DC peristaltic pumps (wired in 2x banks of two) connected to a FETbox for use as skimmer pumps (upper left). Pinch valve also pictured (lower right).

When using DC peristaltic pumps controlled by the *FETbox*, as above, the *PlateFlo scheduler module* can be used to run the pumps at regular intervals as below, for example:

```
>>> from plateflo import fetbox, scheduler
>>> from datetime import datetime, timedelta
>>> from time import sleep

>>> # autoconnect to FETbox
>>> fet = auto_connect_fetbox()[0]

>>> # create scheduler
>>> sched = scheduler.Scheduler()
```

(continues on next page)

(continued from previous page)

```
>>> # define skimmer start/stop functions. e.g. skimmers on channels 4 & 5
>>> def run_skimmers():
>>>     fet.enable_chan(4)
>>>     fet.enable_chan(5)

>>> def stop_skimmers():
>>>     fet.disable_chan(4)
>>>     fet.disable_chan(5)

>>> # schedule recurring skimmer events, run for 1 minute every 3 hours
>>> interval = timedelta(hours = 3)
>>> runtime = timedelta(minutes = 1)
>>> event_skim_start = scheduler.RecurringEvent(interval = interval,
>>>                                             task = run_skimmers)
>>> event_skim_stop = scheduler.RecurringEvent(interval = interval,
>>>                                             task = stop_skimmers,
>>>                                             delay = runtime)
>>> sched.add_event(event_skim_start)
>>> sched.add_event(event_skim_stop)

>>> def main():
>>>     sched.monitor()
>>>     sleep(1E-6)

>>> if __name__ == "__main__":
>>>     try:
>>>         while(1):
>>>             main()
>>>     finally:
>>>         fet.kill()
```

4.4 4. Example Perfusion Setups

4.4.1 Single Plate, Single Reservoir Culture

The most fundamental PlateFlo perfusion setup. A single plate is perfused from a single reservoir with a *FETbox* controlled skimmer pump for plate volume control.

Tip: Inlet/outlet **pumps can be run continuously, or intermittently** (to reduce culture medium usage, for example) depending on the requirements of the system under study.

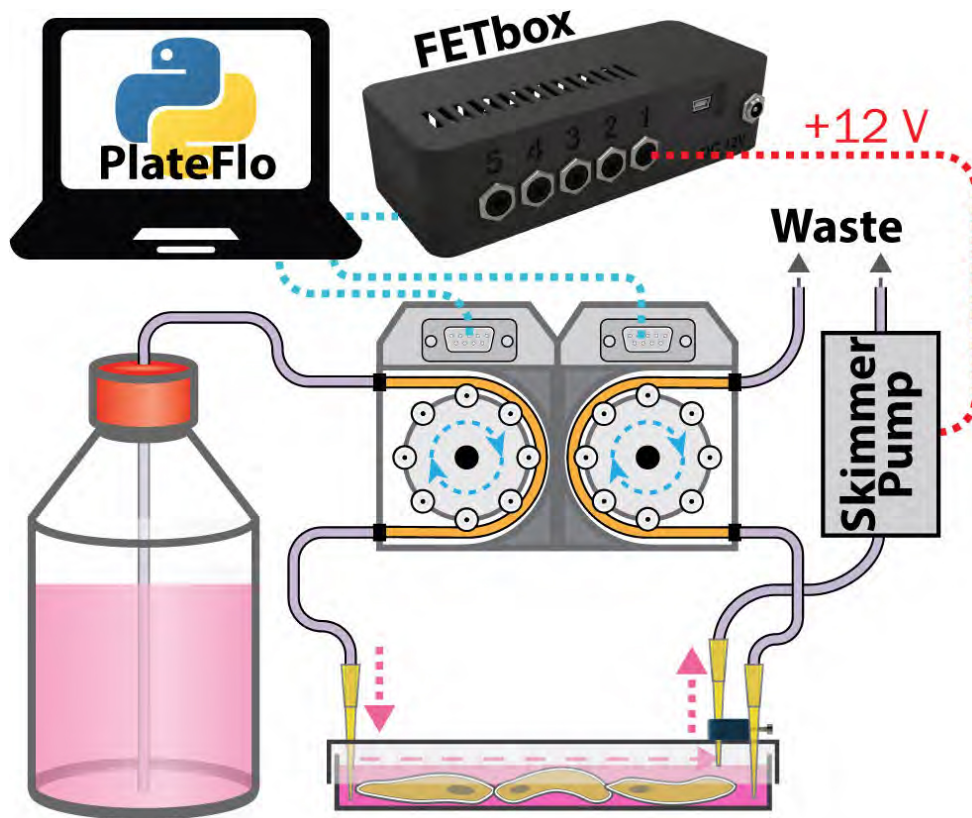


Fig. 3: Single plate, single reservoir perfusion setup.

4.4.2 Dual Reservoir Sequential Flow Culture

Two media reservoirs are selected by a pinch valve (for e.g. glucose stimulation) programmatically using a *FETbox* and *PlateFlo* Python package. In addition to the standard inlet & outlet pumps, a third shared pump channel acts as the outlet pump for plate 1, pumping directly into plate two.

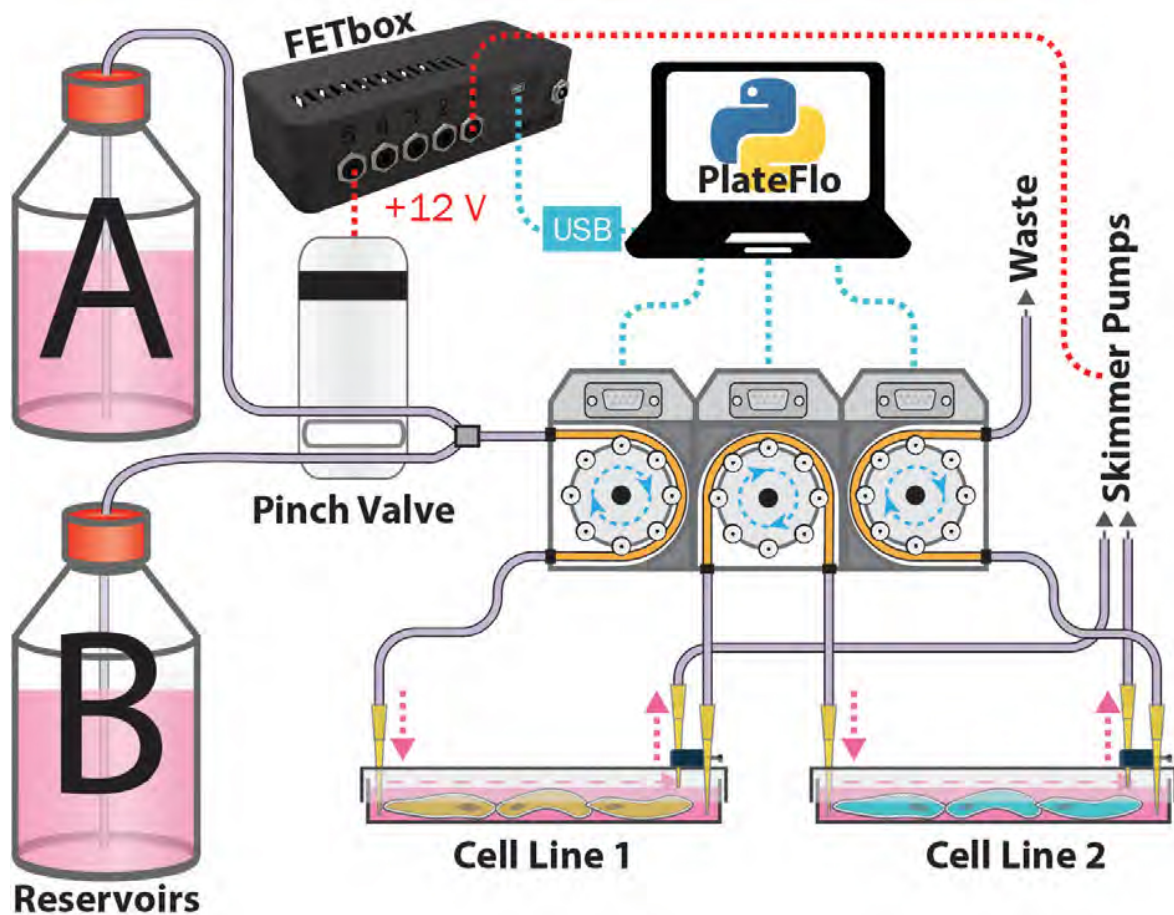


Fig. 4: Dual reservoir, dual sequential culture plate perfusion system.

Note: In this configuration, the *inlet/outlet flow rate delta* is maintained across **all three pumps**. I.e. flow rate 1 > 2 > 3, from left to right.

This setup could be of use, for example, when studying the effect of subjecting *cell line 2* to secreted factors from *cell line 1* upon stimulation with small molecules from *reservoir B*. Similarly, it may be used for development of co-culture differentiation protocols.

4.5 5. Appendix

4.5.1 Selecting Skimmer Height

The following standard curve can be used to as a guide select a height block for the desired plate volume. 1.6 mm is a good starting point at ~10 mL media in the plate.

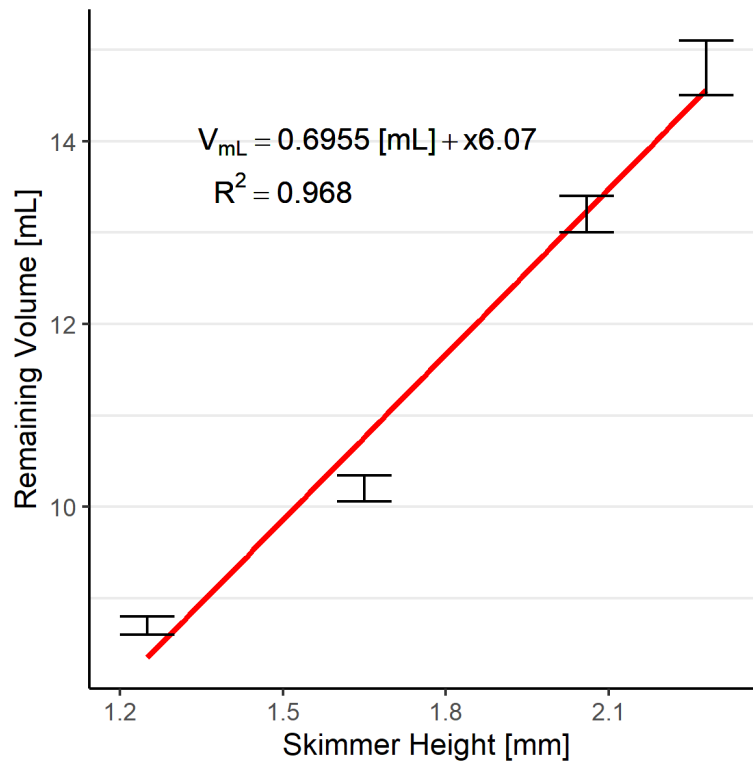


Fig. 5: Plate volume vs. skimmer nozzle height standard curve. Determined by weight. Mean +/- standard deviation, $n = 3$.

1.2, 1.4, 1.6, and 1.8 mm height blocks are provided in the design files as `skimmer_height_block_<height>mm.stl`. See the [build guide](#) for instructions on setting the skimmer nozzle height.

4.5.2 FETbox Serial Commands

If integration with other software, manual control, or otherwise use of the *FETbox Serial Control* Python module is not suitable, the serial command structure is outlined here.

FETbox serial commands have the following structure:

```
@<CMD><BODY>\n
| | | |
| | | | Line feed (LF)
| | | |
| | | Command body, arbitrary length/contents
| | Command code, single ASCII character
Command start
```


	Serial Command	Response
Get Device ID	@#\n	fetbox<id>\n E.g: fetbox0\n
Heartbeat	@?\n	*\n
Enable Channel	@H<chan[1-5]>\n	@H3\n
	E.g. Chan 2 on: @H2\n	
Disable Channel	@I<chan[1-5]>\n	*\n
	E.g. Chan 4 off: @I4\n	
PWM Channel	@S<chan[1-5]><pwm[0-255]>\n	*\n
	E.g. Chan 3 to 80: @S3080\n	
Hit-and-Hold	@V<chan[1-5]><pwm[0-255]>\n	*\n
	E.g. Chan 5 hold 55: V5055\n	
Digital Read	@D<pin[0-21]>\n	<[0 1]>\n
Analog Read	@A<pin[14-21]>\n	<[0-1023]>\n
	E.g. read pin 'A0'(aka 14): @A14\n	E.g. 323\n
Digital Write	@E<pin[0-20]><val[0 1]>\n	*\n
	E.g. Pin D4 HIGH: E041\n	
Analog Write	@B<pin[3,5,6,9,10,11]><pwm[0-255]>\n	*\n
	E.g. Pin D5 to 155: @B05155\n	

FETBOX SERIAL CONTROL

Convenience functions for serial control of the *PlateFlo FETbox*

5.1 1. Key Features

- Simple, high-level hardware control through USB serial communication
- Hit-and-hold capability for power-efficient solenoid operation
- Full Arduino output pin control, including PWM functionality
- Full Arduino digital and analog pin reading functionality
- Asynchronous serial I/O for non-blocking operation via the *serial_io* module
- Logging via the base Python logging module

5.2 2. Quick Start

5.2.1 Installation

The `plateflo` package is hosted on [PyPI](#) and can be installed using `pip`:

```
pip install plateflo
```

or

```
python -m pip install plateflo
```

More detailed instructions on installing Python modules can be found [here](#).

5.2.2 Setup

Instantiate a *FETbox* object:

```
>>> from plateflo import fetbox
>>>
>>> # Connects to a FETbox on serial port 'COM3'
>>> my_fetbox = FETbox(port = "COM3")
```

This creates a *FETbox* object and opens a serial connection with the device.

Note: Device must be connected when the FETbox object is instantiated.

You can automatically instantiate all connected FETboxes with *auto_connect_fetbox()*:

```
>>> # returns a dictionary of FETbox devices, keyed by their IDs
>>> my_fetboxes = auto_connect_fetbox()

>>> # run a motor on MOSFET output channel 1 of device ID 1
>>> my_fetboxes[1].enable_chan(1)
```

Tip: When exiting from your program, call *my_fetbox.kill()* to close the serial port and end all FETbox-associated threads running in the background.

Alternatively, discover connected devices using the *scan_for_fetbox()* function,

```
>>> # Scan systems serial ports for FETbox(es)
>>> fetboxes = scan_for_fetbox()

>>> # One device found:
>>> print(fetboxes)
>>> [{'port':'COM3', 'id':0}, {'port':'COM4', 'id':1}]
>>>

>>> # Multiple devices found:
>>> print(fetboxes)
>>> [{'port':'COM3', 'id':0}, {'port':'COM4', 'id':1}]

>>> # No devices found:
>>> print(fetboxes)
>>> []
```

then instantiate using the result:

```
>>> my_fetbox = FETbox(port = fetboxes[0]['port'])
```

5.3 3. Usage

5.3.1 MOSFET Output Channel Control

There are four built-in methods for control of the FETbox's five MOSFET output channels:

Enable `enable_chan(chan)`

Disable `disable_chan(chan)`

PWM `pwm_chan(chan, pwm)`

Hit-and-Hold `hit_hold_chan(chan, duty)`

`enable_chan()` and `disable_chan()` simply set the specified channel's (chan, 1-5) output either high (+12 V) or low (0 V).

`pwm_chan()` sets a PWM (pulse width modulation) output on the specified channel(chan, 1-5). This can be used to effectively set the channel's output voltage between 0 V (pwm=0) and +12 V (pwm=255).

`hit_hold_chan()` was implemented with solenoid control in mind. Full +12 V is output on the specified channel (chan) briefly, then reduced to the specified PWM duty cycle (duty=0.0-1.0). This reduces power consumption and heat generated when operating solenoid valves.

Technical Note

The PWM carrier wave frequencies differ between output channels:

Channels	Arduino Pins	PWM Frequency (default)
1, 4, 5	D3, D9, D10, D11	31372.55 (490.20) Hz
2, 3	D5, D6	62500.00 (976.56) Hz

These have been increased from the Arduino defaults, so as to move out of the audible range (you/your labmates are welcome).

5.3.2 Arduino Pin Control

All of the Arduino Nano's microcontroller pins are broken out on the FETbox PCB, along with 40 unconnected solder pads and power for development. This allows the end user to connect additional inputs/outputs to customize the FETbox their application.

The `fetbox` module includes basic functionality for serial control of these additional pins.

See the official Arduino website for more details about digital and analog pins:

- <https://arduino.cc/en/Tutorial/DigitalPins>
- <https://arduino.cc/en/Tutorial/AnalogInputPins>

Setting Output Pins

Digital Write `digital_write(pin, val)`

PWM `analog_write(pin, pwm)`

Digital pins (D0-D13) and analog input pins (A0-A5^{*0}) can be both be set to output simple LOW (0V) or HIGH (+5V) signals.

```
>>> # set D7 output to HIGH
>>> my_fetbox.digital_write(7, 1)
>>> # pin D7 now reads +5V
```

The Arduino Nano is only capable of ‘analog’ (PWM) output on pins D3, D5, D6, D9, D10, and D11 - of which, the first five are connected to MOSFET output channels. All of these can still be controlled with the `analog_write()` method, however, only D11 is completely unused. PWM values are 8-bit (0-255).

```
>>> # set D11 to 50% PWM duty cycle
>>> my_fetbox.analog_write(11, 128)
>>> # pin D11 now outputs a +2.5V signal
```

```
>>> # set D10 to 20% PWM duty cycle
>>> my_fetbox.analog_write(10, 51)
>>> # pin D10 now outputs +1V, however MOSFET channel #5 also outputs +2.4V
```

Reading Input Pins

Digital Pins `digital_read(pin)`

Analog Pins `analog_read(pin)`

Arduino input pins can also be queried over the serial interface. Digital pin names are supplied as an `int` (e.g. 1), analog pins names as `str` (e.g. “A3”).

Digital readings return 1 for a HIGH state, or 0 for a LOW state.

```
>>> # Read digital pin 7 (5V signal connected)
>>> reading = my_fetbox.digital_read(7)
>>> print(reading)
>>> 1
```

Analog readings return a 10-bit value (0-1023) which corresponds to a signal voltage approximately 0-5V.

```
>>> # Read analog pin 3 (3.3V signal connected)
>>> reading = my_fetbox.analog_read('A3')
>>> print(reading)
>>> 700
```

Digitally reading an analog pin will return the nearest state (HIGH or LOW) corresponding to the input signal.

```
>>> # Digital read analog pin 3 (3.3V signal connected)
>>> reading my_fetbox.digital_read('A3')
>>> print(reading)
>>> 1
```

⁰ Analog input pins A0-A5 can be read/written digitally, however, A6 and A7 are strictly analog-readable only.

5.3.3 Misc. Methods

- `heartbeat()` - Pings the *FETbox*, returns TRUE if responsive.
- `query_ID()` - Retrieves the *FETbox*'s programmed ID.

5.4 4. Expanding Functionality

5.4.1 Custom Serial Commands

The `plateflo.fetbox` module has two methods for direct serial communication, `send_cmd()` and `send_query()`. These can both send a arbitrary command to the FETbox Arduino, however expect different responses; `send_cmd()` expects a simple pass/fail response, while `send_query()` expects an arbitrary LF-terminated string response terminated.

The FETbox firmware can be easily modified to expand the recognized commands and execute more complex code internally (e.g. reading SPI- or I2C-connected sensors) before sending an informed response string.

Note: If a custom command requires more than 200ms to execute, increase the serial timeout from the default in the pyserial backend:

```
>>> my_fetbox.mod_ser.ser.timeout = 1.0 # 1 second timeout
```

The following serial commands are already defined in `fetbox.CMD`: **CMDS**

```
CMDS = {
    'get_id':      '@#\n',          # FETbox ID inquiry
    'heartbeat':  '@?\n',          # Always returns '*\r'
    'enable':     '@H%i\n',        # Enable channel i
    'disable':    '@I%i\n',        # Disable channel i
    'pwm':        '@S%i%s\n',      # PWM output channel i
    'hithold':    '@V%i%s\n',      # Hit and hold channel i
    'digread':    '@D%02i\n',      # Digital read pin i
    'digwrite':   '@E%02i%i\n',    # digitalWrite pin i
    'anaread':    '@A%02i\n',      # Analog read pin i
    'anawrite':   '@B%02i%03i\n'  # analogWrite pin i
}
```

Firmware Modification

FETbox serial commands have the following structure:

```
@<CMD><BODY>\n
| | | |
| | | | Line feed (LF)
| | | |
| | | | Command body, arbitrary contents
| | | | Command code, single ASCII character
Command start
```

@ is the start of command character, present at the beginning of every FETbox serial command.

The CMD character directs `cmd_interpret(char* cmd)` to execute user-defined code through conditional statements therein.

The BODY of the command is parsed by user code and is command-specific.

```
// Existing commands are defined as macros at the top of the .ino program:
#define CMD_ID      '#' // query device ID
#define CMD_YOURCMD '1' // your custom command

void cmd_interpret(char* cmd) {
    /* Module ID query */
    if(cmd[0] == CMD_ID) {
        Serial.print("fetbox");
        Serial.print(ID);
        Serial.write("\n");
    }

    /* some other commands */
    else if(cmd[0] == CMD_SOMEOTHERCMD) {
        // does other stuff
    }

    /* your amazing command */
    else if(cmd[0] == CMD_YOURCMD) {
        // do something, no <BODY> parameters
        do_something();

        // or parse <BODY> for parameters, then execute a function
        int _chan = (cmd[1]-'0'); // parse channel #
        disco_time(_chan);      // execute disco on provided channel
        ack();                   // command success response
    }

    // ... etc.
}
```


PERFUSION EVENT SCHEDULER

Event scheduler, monitor, and executor.

6.1 1. Key Features

- Simplifies the creation of complex perfusion programs
- Create 'events' - tasks to be carried out at a specific time
- Recurring events - schedule events that repeat at arbitrary intervals
- Monitors scheduled events and executes tasks automatically
- Tasks can be any function - positional and keyword arguments are passed

6.2 2. Quick Start

Event execution times in *scheduler* are defined using `datetime` objects, therefore require the Python `datetime` module to create. `timedelta` is also used when defining relative times.

```
>>> from plateflo import scheduler
>>> from datetime import datetime, timedelta

>>> # instantiate the scheduler object
>>> sched = scheduler.Scheduler()
```

Create a one-time event, *SingleEvent()*, scheduled for 5s after the script starts, and add it to the *Scheduler()*:

```
>>> # define the time
>>> event_time = datetime.now() + timedelta(seconds=5)

>>> # create the event
>>> dinger_event = scheduler.SingleEvent(event_time, print, args=['Ding!'])

>>> # add the event to the scheduler
>>> sched.add_event(dinger_event)
```

Call *monitor()* in the main loop of your script to execute the scheduled event at the defined time.

```
>>> while sched.events:
>>>     sched.monitor()
>>> # five seconds later...
Ding!
```

Tip: Repeatedly calling `monitor()` (or anything else, for that matter) in the main loop will needlessly consume CPU cycles. Depending on what else your main loop is doing and the granularity of your event scheduling, adding a simple `time.sleep(0.05)` 50ms delay can dramatically reduce CPU usage.

6.3 3. Usage

6.3.1 i. Functional Overview

Events

The functional core of the `scheduler` module is its Event objects. Events contain all of the information required to schedule, execute, and reschedule tasks - function calls.

There are two classes of Event object:

One-Time Events `SingleEvent()`

Recurring Events `RecurringEvent()`, `DailyEvent()`

As their names imply, a `SingleEvent()` is executed at a specific time, a `datetime` object, while a `RecurringEvent()` executes repeatedly at a given interval, a `timedelta` object.

Both events execute the supplied task when due - a callable object. Both positional and keyword arguments are passed to the task's function pointer on execution.

Scheduling

The `Scheduler()` keeps track of all Events in an `events` list, each with its own `eventID`, generated and returned when adding events to the scheduler.

Event objects are added `Scheduler()` with the `add_event()` method, and removed using the `remove_event()` method. Events are automatically sorted in the `events` list based on their scheduled execution time, therefore the `events` list can be considered a queue.

The `monitor()` method compares the current system time with that of the first Event in the queue and calls the task function when due. The Event is then popped from the queue and transferred to the `event_history` list.

6.3.2 ii. Creating Event Objects

One-Time Events

Tasks that need only be executed once are created using `SingleEvent()` objects.

The event is executed at the absolute time specified by a `datetime` object. See the section below on defining event tasks.

class `plateflo.scheduler.SingleEvent`(*dateTime*, *task*, *_eventID=None*, *args=[]*, ***kwargs*)
Simple event object, executes once at the specified time.

Parameters

- **dateTime** (*datetime*) – Scheduled execution start time
- **task** (*function pointer*) – Function to execute at scheduled time
- **args** (*list*) – positional arguments, passed to task
- ****kwargs** – keyword arguments passed to task

Recurring Events

Events that take place at regular intervals are created using `RecurringEvent()` objects, which can take several parameters to fine tune define their behaviour:

class `plateflo.scheduler.RecurringEvent`(*interval*, *task*, *start_time=None*, *stop_time=None*, *delay=None*, *_eventID=None*, *_resched=False*, *args=[]*, ***kwargs*)

Event triggered at the specified interval w/ optional start time OR delay.

Parameters

- **interval** (*timedelta*) – Recurrence interval
- **task** (*function pointer*) – Function to execute at scheduled interval
- **start_time** (*datetime*, *optional*) – First occurrence at specified time. Excludes *delay*
- **stop_time** (*datetime*, *optional*) – Terminate recurrence after this time
- **delay** (*timedelta*, *optional*) – Delay first occurrence by this amount. Excludes *start_time*
- **args** (*list*) – Positional arguments, passed to task
- ****kwargs** – Keyword arguments, passed to task

Raises

- **ValueError** – both *start_time* and *delay* parameters are provided.
task function not provided
- **TypeError** – interval not of type *timedelta*

To simplify the definition of daily events that take place at a specific clock time, the `DailyEvent()` class can be used.

class `plateflo.scheduler.DailyEvent`(*task*, *hh=0*, *mm=0*, *s=0*, *args=[]*, ***kwargs*)
Wrapper around `RecurringEvent` for convenient daily task execution.

Parameters

- **hh** (*int*) – Time of day, hour [0-23]

- `mm` (*int*, *default = 0*) – Time of day, minute [0-59]
- `s` (*int*, *default = 0*) – Time of day, seconds [0-59]
- `task` (*function pointer*) – Function executed at scheduled time
- `args` (*list*) – Add positional arguments passed to task
- `kwargs` – Additional keyword arguments passed to task

Returns Daily recurring event.

Return type *RecurringEvent*

Passing Functions to Event Objects

Tasks are passed into Events passed in as callable objects, basically a function's name without the round brackets that usually follow. Positional arguments, `args`, are passed in as a list and keyword arguments passed after all other arguments.

For example, to toggle a valve using a *FETbox* using `hit_hold_chan()` after 3 seconds and then `disable_chan()` 3 seconds after that.

```
>>> # FETbox object
>>> fet = auto_connect_fetbox()[0]

>>> now = datetime.now()

>>> # Using positional arguments
>>> valve_on = scheduler.SingleEvent(dateTime = now + timedelta(seconds=3),
>>>                                  task = fet.hit_hold_chan,
>>>                                  args=[1, 0.8])

>>> # Using a keyword argument
>>> valve_off = scheduler.SingleEvent(dateTime = now + timedelta(seconds=6),
>>>                                   task = fet.disable_chan,
>>>                                   chan = 1)
```

A lambda function can be used to define a callable object whose arguments are undetermined until the time of execution.

```
>>> print_time = lambda : print(datetime.now())
>>> ticker = scheduler.RecurringEvent(interval = timedelta(seconds=1),
>>>                                   task = print_time)
```

6.3.3 iii. Adding/Removing Events

Events are added to the *Scheduler()* using the `add_event()` method, which returns the unique serialized eventID for that event.

```
>>> my_event # any Event type
>>> my_event_id = sched.add_event(my_event)
>>> print(my_event_id)
1
```

The eventID can be used to remove the event from the scheduler e.g. to cancel a *RecurringEvent()*:

```

>>> print(sched.events)
[{'eventID': 1,
  'dateTime': datetime.datetime(2021, 2, 11, 16, 22, 37, 196192),
  'event': <plateflo.scheduler.RecurringEvent object at 0x0000001F2946FBA90>}]
>>> sched.remove_event(my_event_id)
>>> print(sched.events)
[]

```

6.4 4. Working Examples

Toggle a *FETbox*-attached valve at regular intervals for a few cycles:

```

1  >>> from plateflo import scheduler, fetbox, serial_io
2  >>> from datetime import datetime, date, timedelta
3  >>> from time import sleep
4  >>> import logging
5
6  >>> # enable logging to see info in the terminal
7  >>> logging.basicConfig(level=logging.INFO)
8
9  >>> sched = scheduler.Scheduler()
10 >>> # auto-connect to FETbox w/ ID 0
11 >>> fet = fetbox.auto_connect_fetbox()[0]
12
13 >>> # Create recurring events
14
15 >>> INTERVAL = 1 # on/off interval
16 >>> CYCLES = 8  # total on/off cycles
17
18 >>> interval = timedelta(seconds = INTERVAL*2)
19 >>> stop_time = datetime.now() + timedelta(seconds = INTERVAL*2*CYCLES)
20
21 >>> valve_on_evt = scheduler.RecurringEvent(interval = interval,
22 >>>                                         stop_time = stop_time,
23 >>>                                         task = fet.enable_chan,
24 >>>                                         chan = 1) # this is a task keyword argument
25 >>> valve_off_evt = scheduler.RecurringEvent(interval = interval,
26 >>>                                         stop_time = stop_time,
27 >>>                                         task = fet.disable_chan,
28 >>>                                         delay = timedelta(seconds=1),
29 >>>                                         chan = 1) # this is a task keyword argument
30
31 >>> sched.add_event(valve_on_evt)
32 >>> sched.add_event(valve_off_evt)
33
34 >>> def main():
35 >>>     while sched.events:
36 >>>         sched.monitor()
37 >>>         sleep(1E-6)
38 >>>     fet.kill()
39

```

(continues on next page)

(continued from previous page)

```
40 >>> if __name__ == "__main__":  
41 >>>     main()
```

```
>>> # program output:  
INFO:FETbox:Scanning for connected FETbox(es)...  
INFO:FETbox:Scanning COM6...  
INFO:FETbox:         FETbox (ID 0) detected.  
INFO:FETbox:COM6 FETbox (ID: 0) initialized  
INFO:FETbox:COM6 Enabled chan. 1  
INFO:FETbox:COM6 Disabled chan. 1  
INFO:FETbox:COM6 Enabled chan. 1  
INFO:FETbox:COM6 Disabled chan. 1  
INFO:FETbox:COM6 Enabled chan. 1  
INFO:FETbox:COM6 Disabled chan. 1  
INFO:FETbox:COM6 FETbox CLOSED
```

PLATEFLO API INDEX

7.1 fetbox

Serial control of PlateFlo FETbox hardware controllers.

class `plateflo.fetbox.FETbox`(*port*: str, *baud*: int = 115200)
FETbox serial control.

Parameters

- **port** (str) – Serial port name (e.g. 'COM3').
- **baud** (int, default=115200) – Serial baud rate (e.g. 9600).

Returns

Return type FETbox object

mod_ser

Backend PySerial *serial* object

Type Serial

port

Serial port name

Type str

id

Module ID number

Type int

pin_table

Analog pin name to pin number mapping.

Type dict

Raises **ValueError** – provided serial port is not connected to a FETbox device.

analog_read(*pin*: str) → int

Read analog pin value directly from Arduino.

Parameters **pin** (str {'A0', 'A1', 'A2', 'A3', 'A4', 'A5', 'A6', 'A7'}) – Arduino analog pin name.

Returns 10-bit analog pin reading (0-1023). None if query error.

Return type int or None

analog_write(*pin: int, pwm: int*) → bool

Arduino analog write function. Sets PWM value of pin. Arduino Nano PWM pins are 3,5,6,9,10,11. NB: only pin 11 is unrouted to MOSFET gates.

Parameters

- **pin** (*int {3, 5, 6, 9, 10, 11}*) – PWM-capable Arduino pin number.
- **pwm** (*int {0-255}*) – 8-bit PWM output value.

Returns Command success/fail

Return type bool

digital_read(*pin*) → int

Read digital pin value directly from Arduino.

Parameters **pin** (*int {0-13}* or *str {'A0', 'A1', 'A2', 'A3', 'A4', 'A5'}*) – Arduino digital pin number (int) OR Arduino analog pin name (str)

Returns Pin reading: 1 == HIGH, 0 == LOW, None if error

Return type int or None

digital_write(*pin, val: int*) → bool

Arduino digitalWrite functionality. Sets pin HIGH (1) or LOW (0).

Parameters

- **pin** (*int {0-13}* or *,*) – str {'A0'-'A5'} Arduino digital pin number [0-13] or analog pin name [A0-A5] A6/A7 cannot are analog read only.
- **val** (*int {0, 1}*) – Output pin state. 1 (digital HIGH) or 0 (digital LOW)

Returns Command success/failure

Return type bool

disable_chan(*chan: int*) → bool

Set channel (int 1-5) output to LOW.

Parameters **chan** (*int*) – MOSFET output channel number [1-5]

Returns Command success/failure

Return type bool

enable_chan(*chan: int*) → bool

Set channel (int 1-5) output to HIGH.

Parameters **chan** (*int {1-5}*) – MOSFET output channel number [1-5]

Returns Command success/failure

Return type bool

heartbeat() → bool

Ping FETbox, used to confirm active/responsive connection.

Returns Heartbeat found / ping acknowledged

Return type bool

hit_hold_chan(*chan: int, duty: float = 0.5*) → bool

Hit-and-hold for efficient solenoid operation. Sets output HIGH for short period then reduces effective output voltage via PWM.

Parameters

- **chan** (*int* {1-5}) – MOSFET output channel number [1-5]
- **duty** (*float* {0.0-1.0}, *default*=0.5) – Fraction of max PWM output after initial ‘hit’ delay.

Returns Command success/failure

Return type bool

kill()

Kill any threads and close the FETbox serial port

pwm_chan(*chan: int, pwm: int*) → bool

Set given FETbox output channel PWM value.

Parameters

- **chan** (*int* {1-5}) – MOSFET output channel number [1-5]
- **pwm** (*int* {0-255}) – 8-bit PWM value.

Returns Command success/failure

Return type bool

query_ID() → int

Get the FETbox’s unique ID, as defined in firmware.

Returns FETbox’s internal ID [0-9]

Return type int

send_cmd(*cmd: str, attempts: int = 3*) → bool

Send arbitrary command strings. Expect pass/fail-type response from FETbox. Will retry a set number of times if the command fails to execute successfully.

Used internally for all *FETbox* commands.

Parameters

- **cmd** (*str*) – Command string, format varies depending on command.
- **attempts** (*int, default=3*) – Maximum number of retry attempts before command failure.

Returns Command success/failure

Return type bool

send_query(*cmd: str, attempts: int = 3*) → str

Send arbitrary query string. Expects a LF-terminated response. Will retry a set number of times if the query fails to yield a parsable response.

Used internally for all *FETbox* queries.

Parameters

- **cmd** (*str*) – Query string
- **attempts** (*int*) – Maximum number of retry attempts before query failure.

Returns Query response string.

Return type str

plateflo.fetbox.auto_connect_fetbox(*baud: int = 115200*) → Dict[int, *plateflo.fetbox.FETbox*]

Automatically connect to FETbox(es).

Parameters `baud` (*int*, *default=115200*) – Serial baud rate.

Returns FETbox objects keyed by respective ID

Return type `dict[int, FETbox]`

Raises **ConnectionError** – No connected FETbox detected

Non-unique FETbox device IDs detected

`plateflo.fetbox.scan_for_fetbox(baud: int = 115200) → List[Dict[str, int]]`

Scans serial ports for any connected PlateFlo FETbox controllers.

Parameters `baud` (*int*, *default=115200*) – Serial baud rate.

Returns One dict per FETbox containing *port* (str) and *id* (int). Empty if none detected.

Return type `list[dict[str, int]]`

7.2 scheduler

Scheduler for and executing PlateFlo perfusion system events.

`plateflo.scheduler.DailyEvent(task, hh=0, mm=0, s=0, args=[], **kwargs)`

Wrapper around [RecurringEvent](#) for convenient daily task execution.

Parameters

- `hh` (*int*) – Time of day, hour [0-23]
- `mm` (*int*, *default = 0*) – Time of day, minute [0-59]
- `s` (*int*, *default = 0*) – Time of day, seconds [0-59]
- `task` (*function pointer*) – Function executed at scheduled time
- `args` (*list*) – Add positional arguments passed to task
- `kwargs` – Additional keyword arguments passed to task

Returns Daily recurring event.

Return type [RecurringEvent](#)

`class plateflo.scheduler.RecurringEvent(interval, task, start_time=None, stop_time=None, delay=None, _eventID=None, _resched=False, args=[], **kwargs)`

Event triggered at the specified interval w/ optional start time OR delay.

Parameters

- `interval` (*timedelta*) – Recurrence interval
- `task` (*function pointer*) – Function to excute at scheduled interval
- `start_time` (*datetime*, *optional*) – First occurance at specified time. Excludes *delay*
- `stop_time` (*datetime*, *optional*) – Terminate recurrence after this time
- `delay` (*timedelta*, *optional*) – Delay first occurance by this amount. Excludes *start_time*
- `args` (*list*) – Positional arguments, passed to task
- `**kwargs` – Keyword arguments, passed to task

Raises

- **ValueError** – both *start_time* and *delay* parameters are provided.
task function not provided
- **TypeError** – interval not of type *timedelta*

class plateflo.scheduler.**Scheduler**

Event schedule handler. Schedules, monitors, and executes events

events

Unexecuted future event objects.

Type list

event_history

Previous triggered event objects.

Type list

add_event(*event*)

Inserts scheduled event into the event queue.

Parameters *event* (*SingleEvent*, *RecurringEvent*) – *SingleEvent* or *RecurringEvent* object

Returns Event identifier. Can be used to remove event with *remove_event()*

Return type int

monitor()

Call frequently from the main script loop!

Checks if events are due to trigger and transfers triggered events to the event history. Reschedules recurring events if necessary.

remove_event(*eventID*)

Removes the selected event from the scheduler queue.

Parameters *eventID* (*int*) – Unique event identifier.

class plateflo.scheduler.**SingleEvent**(*dateTime*, *task*, *_eventID=None*, *args=[]*, ***kwargs*)

Simple event object, executes once at the specified time.

Parameters

- **dateTime** (*datetime*) – Scheduled execution start time
- **task** (*function pointer*) – Function to execute at scheduled time
- **args** (*list*) – positional arguments, passed to task
- ****kwargs** – keyword arguments passed to task

trigger()

Execute the event task.

7.3 ismatec

7.3.1 ismatec_scanner

Scan system serial ports for connected Ismatec Reglo peristaltic pumps.

`plateflo.ismatec.ismatec_scanner.scan_for_pumps()` → list
Scans system serial ports for connected Ismatec Reglo peristaltic pumps.

Returns

list [{**'pump'** – One *dict* per pump detected. [{**'pump'**:str, **'port'**:str, **'addr'**:int}, ...]

pump : str - Pump model, 'ICC' or 'Digital'.

port : str - Serial port name.

addr : int - Pump internal address.

Return type str, **'port'**:str, **'addr'**:int}, ...]

7.3.2 ismatec_icc

Convenience functions for control of common Ismatec Reglo ICC peristaltic pump functions.

class `plateflo.ismatec.ismatec_icc.RegloICC(port, addr, channels=4, timeout=0.5)`
Ismatec Reglo ICC pump object, for serial control of multi-channel pump.

Parameters

- **port** (*str*) – Serial port on which Reglo ICC is connected. E.g. 'COM3'
- **channels** (*int*, *default=4*) – Number of channels on ICC pump.
- **timeout** (*float*, *default=0.5*) – Time (seconds) to allow pump to respond before commands timeout/fail.

pump_ser

Backend PySerial device object

Type Serial

port

Serial port name

Type str

addr

Pump internal address (for e.g. serial daisy-chaining)

Type str

status

state, direction, and flow rate for all channels. Timestamp of last update.

Type dict

max_flow

Pump maximum flow rate (mL/min)

Type float

n_channels

Number of independant channels on Reglo ICC pump.

Type int

display_text(*txt: str*) → int

Show text on the pump LCD. Maximum 15 character.

Parameters **txt** (*str*) – Text to display on pump LCD. Maximum 15 characters.

Returns

- 1 == Pass
- 0 == Fail
- 1 == Other error

Return type int

get_chan_dir(*chan: int*) → int

Query pump channel head direction.

Parameters **chan** (*int*) – Pump channel number

Returns

- 1 == clockwise
- 1 == counter-clockwise
- 0 == error

Return type int

get_chan_flow(*chan: int*) → float

Query channel set flow-rate.

NB: Not supported when daisy-chaining multiple pumps over single serial interface.

Parameters **chan** (*int*) – Pump channel number

Returns

- channel set flow-rate; otherwise,
- 1.0 == error

Return type float

get_chan_run_state(*chan: int*) → int

Query pump channel run state.

Parameters **chan** (*int*) – Pump channel number

Returns

- 1 == running,
- 0 == stopped,
- 1 == error

Return type int

get_dir() → int

Query pump head direction.

Returns

- Pump head direction:

+1 == clockwise
-1 == counter-clockwise
0 == unknown error

Return type int

get_max_flowrate() → float

Query the maximum achievable flow rate in mL/min.

Returns Maximum pump flow rate (mL/min)

Return type float

kill()

Kill all threads and close the pump's serial port

restore_display() → int

Return the LCD to normal display mode. Used to reset the LCD after *display_text*, for example.

Returns

1 == Pass
0 == Fail
-1 == Other error

Return type int

send_cmd_pass_fail(cmd: str) → int

Send command ``cmd``, to pump. Resend if failure up to a total of three attempts.

See Reglo ICC manual (pp. 17-33) for command structure documentation. http://www.ismatec.com/images/pdf/manuals/14-036_E_ISMATEC_REGLO_ICC_ENGLISH_REV.%20C.pdf

Parameters **cmd** (*str*) – Command string, CR-terminated.

Returns

1 == pass
0 == fail
-1 == error

Return type int

send_cmd_string_resp(cmd_string: str, EOL='\n') → str

Command/query the pump with *cmd*. Resend if failure up to a total of three attempts.

See Reglo ICC manual (pp. 17-33) for command structure documentation. http://www.ismatec.com/images/pdf/manuals/14-036_E_ISMATEC_REGLO_ICC_ENGLISH_REV.%20C.pdf

Parameters **cmd** (*str*) – Command string, CR-terminated.

Returns pump response string

Return type str

set_chan_dir(chan: int, direction: int) → int

Set channel direction: clockwise(+1), or counterclockwise(-1).

Parameters

- **chan** (*int*) – Pump channel number

- **direction** (*int* {-1, +1}) – Channel direction: clockwise (+1) or counter-clockwise (-1)

Returns

- 1 == Pass
- 0 == Fail
- 1 == Other error

Return type int**set_chan_flow**(*flow_rate*, *chan*)

Set channel flow rate in mL/min.

Parameters

- **chan** (*int*) – Pump channel number
- **flow_rate** (*float*) – Flow rate in mL/min

Returns 1 == Pass 0 == Fail -1 == Error

Return type int**set_dir**(*direction*: *int*) → int

Set pump head direction: clockwise(+1), or counterclockwise(-1)

Parameters **direction** (*int* {-1, +1}) – Pump head direction: clockwise (+1) or counter-clockwise (-1)

Returns

- 1 == Pass
- 0 == Fail
- 1 == Other error

Return type int**set_flow**(*flow_rate*: *float*) → float

Set pump flow rate (mL/min). If requested flow rate is above pump limit, set to maximum achievable, *max_flow*.

Returns

- 1 == pass
- 0 == fail
- 1 == error

Return type int**set_mode_flowrate**()

Set pump to volumetric flowrate mode.

Returns

- 1 == pass
- 0 == fail
- 1 == error

Return type int

set_per_chan_mode(*mode: int*)

Set mode for command addressing: channel(1), pump-wide(0)

Parameters **mode** (*int* {0, 1}) – Send pump-wide commands (0) or per-channel (1).

Returns

1 == pass

0 == fail

-1 == error

Return type int

start() → int

Start/run pump, includes all channels with a non-zero flow rate.

Returns

1 == pass

0 == fail

-1 == error

Return type int

start_chan(*chan: int*) → int

Start/run pump channel.

Parameters **chan** (*int*) – Pump channel number

Returns

1 == Pass

0 == Fail

-1 == Other error

Return type int

stop() → int

Stop pump. All channels.

Returns

1 == pass

0 == fail

-1 == error

Return type int

stop_chan(*chan: int*) → int

Stop pump channel.

Parameters **chan** (*int*) – Pump channel number

Returns

1 == Pass

0 == Fail

-1 == Other error

Return type int

update_status()

Update the pump *status* attribute. Must be called manually.

7.3.3 ismatec_dig

Convenience functions for control of common Ismatec Reglo Digital peristaltic pump functions

class `plateflo.ismatec.ismatec_dig.RegloDigital`(*port: str, addr: int*)

Ismatec Reglo Digital pump control serial control.

Parameters

- **port** (*str*) – Serial port on which Relgo Digital is connected. E.g. ‘COM3’.
- **timeout** (*float, default=0.5*) – Time (seconds) to allow pump to respond before commands timeout/fail.

pump_ser

Backend PySerial device object

Type Serial

port

Serial port name

Type str

addr

Pump address (for e.g. serial daisy-chaining)

Type int

status

Dictionary of last pump status update values

timestamp - datetime object of last status update

run_state - pump head state ‘Running’, ‘Idle’, or ‘ERROR’

dir - pump head direction. -1 (CCW); +1 (CW); 0 (ERROR)

flow - current set flow rate (mL/min)

Type {‘timestamp’:datetime, ‘run_state’:str, ‘dir’:int, ‘flow’:float}

max_flow

Pump maximum flow rate

Type float

last_dir

Last set pump head direction. CW == +1; CCW == -1; ERROR == 0.

Type int

display_text(txt)

Show text on the pump LCD, 4 characters max.

Parameters **txt** (*str*) – Text to display on pump LCD. Maximum 4 characters.

Returns

1 == Pass

0 == Fail

-1 == Other error

Return type int

get_dir()

Returns the last direction set via control software. Note Reglo Digital lacks ability to query pump head direction. Tracked in software.

Returns

Last set pump direction:

+1 == clockwise

-1 == counter-clockwise

0 == unknown error

Return type int

get_flow() → float

Query current pump flow rate.

Returns Flow rate in mL/min. OR -1 if an error occurred.

Return type float

get_run_state()

Query pump current run status.

Returns

1 == Running

0 == Stopped

-1 == Other error

-2 == Stopped, motor overload

Return type int

kill()

Kill all threads and close pump serial port

restore_display()

Return the LCD to normal display mode. Used to clear text displayed using *display_text*.

Returns

1 == Pass

0 == Fail

-1 == Other error

Return type int

send_cmd_pass_fail(cmd: str) → int

Send command ``cmd``, to pump. Resend if failure up to a total of three attempts.

See Reglo Digital manual (pp. 33-38) for command structure documentation. http://www.ismatec.com/images/pdf/manuals/Reglo_Digital_new.pdf

Parameters `cmd (str)` – Command string, CR-terminated.

Returns

1 == pass
 0 == fail
 -1 == error

Return type int**send_cmd_string_resp**(*cmd*) → strQuery the pump with *cmd*. Resend if failure up to a total of three attempts.See Reglo Digital manual (pp. 33-38) for command structure documentation. http://www.ismatec.com/images/pdf/manuals/Reglo_Digital_new.pdf**Parameters** *cmd* (*str*) – Command string, CR-terminated.**Returns** pump response string**Return type** str**set_cal_flow**(*flow_rate=12.4*)

Set the calibrated volumetric flow rate at maximum pump speed.

Parameters *flow_rate* (*float*, *default = 12.4*) – Volumetric flow rate (mL/min) at maximum pump head speed. Default 12.4 mL/min.**Returns**

1 == Pass
 0 == Fail
 -1 == Other error

Return type int**set_dir**(*direction*)

Set pump head direction clockwise or counterclockwise.

Parameters *direction* (*int* {-1, +1}) – Pump head direction: clockwise (+1) or counterclockwise (-1)**Returns**

1 == Pass
 0 == Fail
 -1 == Other error

Return type int**set_flow**(*flow_rate: float*) → int

Set pump flow rate.

Parameters *flow_rate* (*float*) – Flow rate in mL/min.**Returns**

1 == Pass
 0 == Fail
 -1 == Other error

Return type int

set_mode_flowrate()

Change pump flow rate to mL/min mode

set_mode_rpm()

Change pump flow rate to RPM speed mode

set_tube_diameter(*diam_mm*)

Sets tubing inner diameter. Determines calibrated volumetric flow rate.

0.13, 0.19, 0.25, 0.38, 0.44, 0.51, 0.57, 0.64, 0.76, 0.89, 0.95, 1.02, 1.09, 1.14, 1.22, 1.30, 1.42, 1.52, 1.65, 1.75, 1.85, 2.06, 2.29, 2.54, 2.79, 3.17

Parameters *diam_mm* (*float* {0.13, 0.19, 0.25, 0.38, 0.44, 0.51, 0.57, 0.64, 0.76, 0.89, 0.95, 1.02, 1.09, 1.14, 1.22, 1.30, 1.42, 1.52, 1.65, 1.75, 1.85, 2.06, 2.29, 2.54, 2.79, 3.17}) – Tubing inner diameter in millimeters

Returns

- 1 == Pass
- 0 == Fail
- 1 == Other error

Return type int

start() → int

Start/run the pump.

Returns

- 1 == Pass
- 0 == Fail
- 1 == Other error

Return type int

stop() → int

Stop the pump.

Returns

- 1 == Pass
- 0 == Fail
- 1 == Other error

Return type int

update_status()

Update the pump *status* attribute. Must be called manually.

7.4 serial_io

Basic threaded serial command/response handling, avoids blocking the main thread with I/O operations during operation.

class plateflo.serial_io.**CmdExecThread**(*master*)

Command queue monitoring thread.

Executes commands from queue and queues the response.

Parameters **master** (*SerialDevice*) – The *SerialDevice* instance over which to send/recieve serial commands.

execution_loop()

Sends commands to the *Serial* device and listens for a defined response.

Command queue objects are dicts containing the string command and EITHER a command length or command EOL character.

Examples

```
{cmd: "1H", respLen: 1} # A single character response
```

```
{cmd: "1#", respEOL: 'n'} # Multiple chars, LF-terminated
```

is_running()

execution_loop run state.

Returns Running

Return type bool

run()

Start *execution_loop* thread

stop()

Stop/join the *execution_loop* thread.

class plateflo.serial_io.**SerialDevice**(*port*, *baud=9600*, *timeout=0.2*)

Handles writing of commands and reading back of responses.

Parameters

- **port** (*str*) – Serial device port name. E.g. "COM4".
- **baud** (*int*, *default=9600*) – Serial device baud rate
- **timeout** (*float*, *default=0.2*) – Time (seconds) to allow device to respond before commands timeout/fail.

port

Serial device port name.

Type str

baud

Serial device baud rate.

Type int

timeout

Time (seconds) to allow device to respond before commands timeout/fail.

Type float

isOpen

Serial device connection open.

Type bool

close()

Close the device serial port

open()

Open the device serial port

write_cmd(cmd, rsp_len=None, EOL=None)

Send command to serial device, expect either a defined response length (*rsp_len*) **–OR–** a terminating character (*EOL*).

Parameters

- **cmd** (*str*) – String to send to serial device.
- **rsp_len** (*int*) – Number of characters to expect in response.
- **EOL** (*str*) – Expected response terminating character (E.g. LF or CR)

Returns Device response string. Empty string in case of response timeout.

Return type str

Raises ValueError – if both *rsp_len* and *EOL* parameters are provided, or if neither is provided

plateflo.serial_io.list_ports()

List available system serial ports.

Returns Serial port names

Return type list

LICENSE

This project is copyright (2021) of Robert Pazdzior. You are free to modify and redistribute all or part of it according to the associated license(s) outlined below.

8.1 Hardware

All hardware described herein is licensed under the [CERN Open Hardware Licence - weakly reciprocal \(v2 or later\)](#) . A full copy of the license is included [here](#).

8.2 Software

All software provided herein is licensed under [GNU General Public License \(v3 or later\)](#). A full copy of the license is included [here](#).

DISCLAIMER

In short, the end user bears full responsibility for their own use and abuse of the provided design files and software. Work safely, respect electricity, and mind your fingers!

Adapted from the [MIT License \(2021\)](#):

Although efforts were made to follow best safety practices in the design, documentation and distribution of this project and all of its contents, **all files, software, instructions, information, and otherwise are provided “AS IS”, without warranty of any kind**, express or implied, including but not limited to the warranties of merchantability, fitness for a particular purpose and noninfringement. In no event shall the authors or copyright holders be liable for any claim, damages, or other liability, whether in an action of contract, tort or otherwise, arising from, out of or in connection with the software, hardware design, or the use or other dealings in the software or hardware.`

INDICES AND TABLES

- genindex
- modindex
- search

PYTHON MODULE INDEX

p

plateflo.fetbox, 51
plateflo.ismatec.ismatec_dig, 61
plateflo.ismatec.ismatec_icc, 56
plateflo.ismatec.ismatec_scanner, 56
plateflo.scheduler, 54
plateflo.serial_io, 65

A

add_event() (*plateflo.scheduler.Scheduler* method), 55
 addr (*plateflo.ismatec.ismatec_dig.RegloDigital* attribute), 61
 addr (*plateflo.ismatec.ismatec_icc.RegloICC* attribute), 56
 analog_read() (*plateflo.fetbox.FETbox* method), 51
 analog_write() (*plateflo.fetbox.FETbox* method), 51
 auto_connect_fetbox() (*in module plateflo.fetbox*), 53

B

baud (*plateflo.serial_io.SerialDevice* attribute), 65

C

close() (*plateflo.serial_io.SerialDevice* method), 66
 CmdExecThread (*class in plateflo.serial_io*), 65

D

DailyEvent() (*in module plateflo.scheduler*), 54
 digital_read() (*plateflo.fetbox.FETbox* method), 52
 digital_write() (*plateflo.fetbox.FETbox* method), 52
 disable_chan() (*plateflo.fetbox.FETbox* method), 52
 display_text() (*plateflo.ismatec.ismatec_dig.RegloDigital* method), 61
 display_text() (*plateflo.ismatec.ismatec_icc.RegloICC* method), 57

E

enable_chan() (*plateflo.fetbox.FETbox* method), 52
 event_history (*plateflo.scheduler.Scheduler* attribute), 55
 events (*plateflo.scheduler.Scheduler* attribute), 55
 execution_loop() (*plateflo.serial_io.CmdExecThread* method), 65

F

FETbox (*class in plateflo.fetbox*), 51

G

get_chan_dir() (*plateflo.ismatec.ismatec_icc.RegloICC* method), 57
 get_chan_flow() (*plateflo.ismatec.ismatec_icc.RegloICC* method), 57
 get_chan_run_state() (*plateflo.ismatec.ismatec_icc.RegloICC* method), 57
 get_dir() (*plateflo.ismatec.ismatec_dig.RegloDigital* method), 62
 get_dir() (*plateflo.ismatec.ismatec_icc.RegloICC* method), 57
 get_flow() (*plateflo.ismatec.ismatec_dig.RegloDigital* method), 62
 get_max_flowrate() (*plateflo.ismatec.ismatec_icc.RegloICC* method), 58
 get_run_state() (*plateflo.ismatec.ismatec_dig.RegloDigital* method), 62

H

heartbeat() (*plateflo.fetbox.FETbox* method), 52
 hit_hold_chan() (*plateflo.fetbox.FETbox* method), 52

I

id (*plateflo.fetbox.FETbox* attribute), 51
 is_running() (*plateflo.serial_io.CmdExecThread* method), 65
 isOpen (*plateflo.serial_io.SerialDevice* attribute), 66

K

kill() (*plateflo.fetbox.FETbox* method), 53
 kill() (*plateflo.ismatec.ismatec_dig.RegloDigital* method), 62
 kill() (*plateflo.ismatec.ismatec_icc.RegloICC* method), 58

L

last_dir (*plateflo.ismatec.ismatec_dig.RegloDigital* at-

tribute), 61
list_ports() (in module *plateflo.serial_io*), 66

M

max_flow (*plateflo.ismatec.ismatec_dig.RegloDigital* attribute), 61
max_flow (*plateflo.ismatec.ismatec_icc.RegloICC* attribute), 56
mod_ser (*plateflo.fetbox.FETbox* attribute), 51
module
 plateflo.fetbox, 51
 plateflo.ismatec.ismatec_dig, 61
 plateflo.ismatec.ismatec_icc, 56
 plateflo.ismatec.ismatec_scanner, 56
 plateflo.scheduler, 54
 plateflo.serial_io, 65
monitor() (*plateflo.scheduler.Scheduler* method), 55

N

n_channels (*plateflo.ismatec.ismatec_icc.RegloICC* attribute), 56

O

open() (*plateflo.serial_io.SerialDevice* method), 66

P

pin_table (*plateflo.fetbox.FETbox* attribute), 51
plateflo.fetbox
 module, 51
plateflo.ismatec.ismatec_dig
 module, 61
plateflo.ismatec.ismatec_icc
 module, 56
plateflo.ismatec.ismatec_scanner
 module, 56
plateflo.scheduler
 module, 54
plateflo.serial_io
 module, 65
port (*plateflo.fetbox.FETbox* attribute), 51
port (*plateflo.ismatec.ismatec_dig.RegloDigital* attribute), 61
port (*plateflo.ismatec.ismatec_icc.RegloICC* attribute), 56
port (*plateflo.serial_io.SerialDevice* attribute), 65
pump_ser (*plateflo.ismatec.ismatec_dig.RegloDigital* attribute), 61
pump_ser (*plateflo.ismatec.ismatec_icc.RegloICC* attribute), 56
pwm_chan() (*plateflo.fetbox.FETbox* method), 53

Q

query_ID() (*plateflo.fetbox.FETbox* method), 53

R

RecurringEvent (class in *plateflo.scheduler*), 54
RegloDigital (class in *plateflo.ismatec.ismatec_dig*), 61
RegloICC (class in *plateflo.ismatec.ismatec_icc*), 56
remove_event() (*plateflo.scheduler.Scheduler* method), 55
restore_display() (*plateflo.ismatec.ismatec_dig.RegloDigital* method), 62
restore_display() (*plateflo.ismatec.ismatec_icc.RegloICC* method), 58
run() (*plateflo.serial_io.CmdExecThread* method), 65

S

scan_for_fetbox() (in module *plateflo.fetbox*), 54
scan_for_pumps() (in module *plateflo.ismatec.ismatec_scanner*), 56
Scheduler (class in *plateflo.scheduler*), 55
send_cmd() (*plateflo.fetbox.FETbox* method), 53
send_cmd_pass_fail() (*plateflo.ismatec.ismatec_dig.RegloDigital* method), 62
send_cmd_pass_fail() (*plateflo.ismatec.ismatec_icc.RegloICC* method), 58
send_cmd_string_resp() (*plateflo.ismatec.ismatec_dig.RegloDigital* method), 63
send_cmd_string_resp() (*plateflo.ismatec.ismatec_icc.RegloICC* method), 58
send_query() (*plateflo.fetbox.FETbox* method), 53
SerialDevice (class in *plateflo.serial_io*), 65
set_cal_flow() (*plateflo.ismatec.ismatec_dig.RegloDigital* method), 63
set_chan_dir() (*plateflo.ismatec.ismatec_icc.RegloICC* method), 58
set_chan_flow() (*plateflo.ismatec.ismatec_icc.RegloICC* method), 59
set_dir() (*plateflo.ismatec.ismatec_dig.RegloDigital* method), 63
set_dir() (*plateflo.ismatec.ismatec_icc.RegloICC* method), 59
set_flow() (*plateflo.ismatec.ismatec_dig.RegloDigital* method), 63
set_flow() (*plateflo.ismatec.ismatec_icc.RegloICC* method), 59
set_mode_flowrate() (*plateflo.ismatec.ismatec_dig.RegloDigital* method),

63
 set_mode_flowrate() (plateflo.ismatec.ismatec_icc.RegloICC method), 59
 set_mode_rpm() (plateflo.ismatec.ismatec_dig.RegloDigital method), 64
 set_per_chan_mode() (plateflo.ismatec.ismatec_icc.RegloICC method), 59
 set_tube_diameter() (plateflo.ismatec.ismatec_dig.RegloDigital method), 64
 SingleEvent (class in plateflo.scheduler), 55
 start() (plateflo.ismatec.ismatec_dig.RegloDigital method), 64
 start() (plateflo.ismatec.ismatec_icc.RegloICC method), 60
 start_chan() (plateflo.ismatec.ismatec_icc.RegloICC method), 60
 status (plateflo.ismatec.ismatec_dig.RegloDigital attribute), 61
 status (plateflo.ismatec.ismatec_icc.RegloICC attribute), 56
 stop() (plateflo.ismatec.ismatec_dig.RegloDigital method), 64
 stop() (plateflo.ismatec.ismatec_icc.RegloICC method), 60
 stop() (plateflo.serial_io.CmdExecThread method), 65
 stop_chan() (plateflo.ismatec.ismatec_icc.RegloICC method), 60

T

timeout (plateflo.serial_io.SerialDevice attribute), 65
 trigger() (plateflo.scheduler.SingleEvent method), 55

U

update_status() (plateflo.ismatec.ismatec_dig.RegloDigital method), 64
 update_status() (plateflo.ismatec.ismatec_icc.RegloICC method), 60

W

write_cmd() (plateflo.serial_io.SerialDevice method), 66

2.2 Continuous perfusion alters selenoprotein expression and lipid metabolism in pancreatic islet cell lines

2.2.1 Continuous perfusion causes cell type-dependent growth effects

We cultured murine pancreatic endocrine cell lines α TC1-LT and β TC3 in the PlateFlo perfusion system at a flow-rate of 170 μ L/min. (**Figure 4A**). To enable attachment of these adherent cell lines, we seeded cells two days prior to perfusion start on experimental day 0. Once perfusion is started, fresh media enters the PlateFlo perfusion plate through the inlet nozzle and is simultaneously withdrawn from the opposite side of the plate by the outlet and skimmer nozzles (**Figure 4B-C**). Nutrients are delivered and consumed, and waste products, as well as secreted factors, are collected as the media flows across the plate. This directed flow has the potential to create a gradient of nutrient availability and cell secretions across the culture plates, with the effect likely to be compounded as cell density increases. To examine whether such potential gradient has a significant effect on β TC3 cell growth, we measured cell density with an automated microscope over the course of six days of perfusion or static culture. As live-staining dyes can affect cell growth (Purschke *et al*, 2010), we opted to use brightfield cell area as a less intrusive method for approximation of cell density in fifteen quadrants (3W \times 5L) across the plate. This allowed the same cell clusters to be imaged from measurement-to-measurement, and to calculate fold-expansion relative to the cell area at the onset of perfusion (D0) in both static and perfused plates. No significant correlation was observed between position along the axis of flow and cell area fold-expansion in the perfused plate or static plate on day six of perfusion (**Figure 4D**), suggesting such position-dependent effects to be negligible at least for proliferation rate. We then quantified the effect of perfusion on overall cell growth in more detail. In both α TC1-LT and β TC3 we used trypsinization followed by Trypan Blue staining and automated cell counting to measure cell numbers on days three and five (**Figure 4E**). Fold-expansion was calculated relative to a co-seeded plate harvested at day zero for both static and perfused plates. Statistically significant differences in fold-expansion were observed from perfusion day three and perfusion day five for α TC1-LT and β TC3, respectively. α TC1-LT was found to expand to a lesser extent under continuous perfusion relative to static controls (D5 fold-expansion: static=15.84 \pm 0.23, perfused=13.12 \pm 0.19; $n=2$, p -value < 0.05) while the opposite was found to be true for β TC3s which expanded to greater extent under continuous perfusion (D3 fold-expansion: static=2.64 \pm 0.13, perfused=3.78 \pm 0.12, $n=2$, p -value < 0.05; D5 fold-expansion: static=5.79 \pm 0.18, perfused=8.44 \pm 0.13, $n=2$, p -value < 0.05).

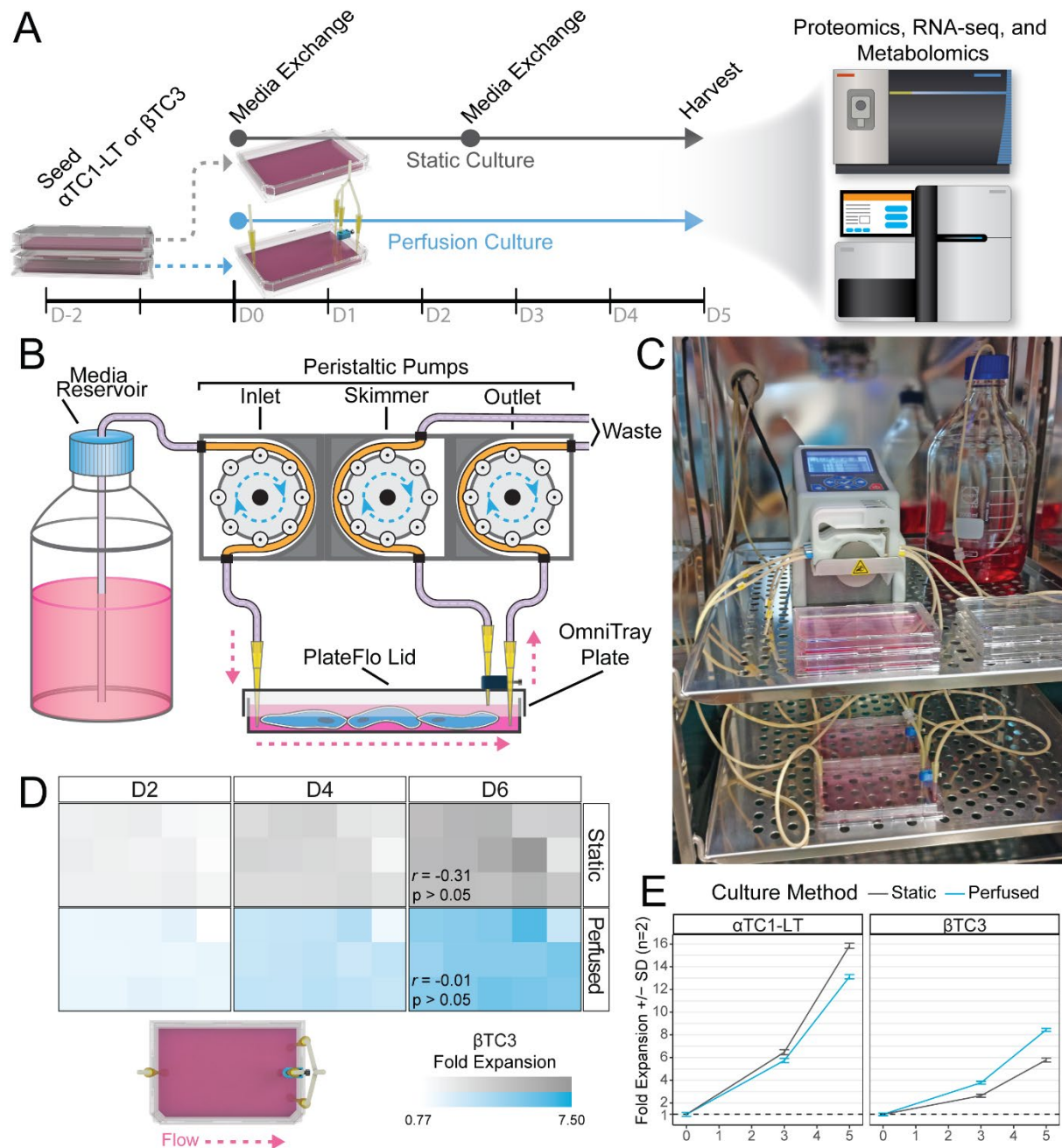


Figure 4: Workflow overview and growth characterization. **A)** General workflow. α TC1-LT or β TC3 cell lines are seeded into a pair of single-well plates and allowed to adhere fully for two days. Media is exchanged in both plates, and the perfusion plate is fitted with a PlateFlo lid and connected to a perfusion system. Media is exchanged in the static plate on day two, as is done in typical static culture. Both plates are harvested on day five for proteomics, RNA-sequencing, or metabolomics analysis. **B)** Schematic overview of the PlateFlo setup used in this experiment. **C)** The PlateFlo perfusion system with two perfusion plates in parallel (lower shelf) and two static control plates (upper shelf, along with pump and reservoir). Skimmer pumps/waste are kept external to the incubator. **D)** Fold-expansion of β TC3 in static and perfusion plates over six days, as estimated using brightfield cell area. Day six statistics indicate the estimated Pearson's correlation (r) between fold-expansion and distance from the inlet along the axis of flow and associated Student's t -test (p -value). **E)** Growth curves (cont'd) as

determined by automated counting of trypsinized cells from individual plates. Normalized to day zero cell counts.

2.2.2 Selenoprotein expression is upregulated by continuous perfusion culture

To explore the effects of continuous perfusion on protein expression in an unbiased fashion we employed quantitative global proteomics through tandem mass tagging (TMT) on α TC1-LT ($n=4$) and β TC3 ($n=3$). In total we quantified 7713 and 6950 protein groups in α TC1-LT and β TC3 datasets, respectively (see **Figure 5A**). We set a fold-change cut-off of 1.5-fold and FDR-corrected p -value cut-off of 0.05 to define significantly changed proteins. Based on these criteria we identified 22 proteins that were upregulated and 16 proteins that were downregulated by perfusion culture in α TC1-LT (**Supplementary Table 1**). Likewise, in β TC3 we identified 11 perfusion-upregulated and 15 perfusion-downregulated proteins (**Supplementary Table 2**).

Immediately apparent in both datasets was the overrepresentation of selenoproteins – proteins containing the rare amino acid, selenocysteine; 15 of the 23 Swiss-Prot-annotated selenoproteins (The UniProt Consortium, 2021) were quantified in each of our proteomic datasets. Of those, seven (α TC1-LT) and five (β TC3) were upregulated on the protein level (see **Figure 5A**). This most notably includes Glutathione Peroxidase 1 (GPX1) and 4 (GPX4) as well as Selenoprotein S (SELENOS) and Selenoprotein K (SELENOK) in both datasets. In **Figure 5B** we examine the differential expression of all quantified selenoproteins and find that in both datasets, all but one selenoprotein trends upwards in both datasets. WikiPathways ontology analysis of the significantly upregulated proteins (**Figure 5C**) confirms this enrichment, with “selenium metabolism/selenoproteins” consistently scoring highest using EnrichR’s combined score metric (Xie *et al*, 2021) after filtering for FDR-corrected p -values less than 0.05 in both datasets.

We then sought to validate the differential expression of selenoproteins under perfusion and to better understand its kinetics. Two additional independent biological replicates were harvested after three and five days of perfusion (along with static control plates) for each cell line. Blotting for GPX1 as a readout for selenoprotein expression, we observed robust increases in GPX1 protein staining from day three in both cell lines (**Figure 5E-F**). In α TC1-LT the band intensity ratio was 7.2 ± 0.85 on D3, and 4.7 ± 2.4 on D5 (perfused/static control, mean \pm StDev, $n=2$). In β TC3 the band intensity ratio was 6.4 ± 0.049 on D3, and 6.9 ± 0.49 on D5 (perfused/static control, mean \pm St.Dev, $n=2$). See **Supplementary Figure S1** for whole membrane staining and Ponceau loading control of both biological replicates in each cell line.

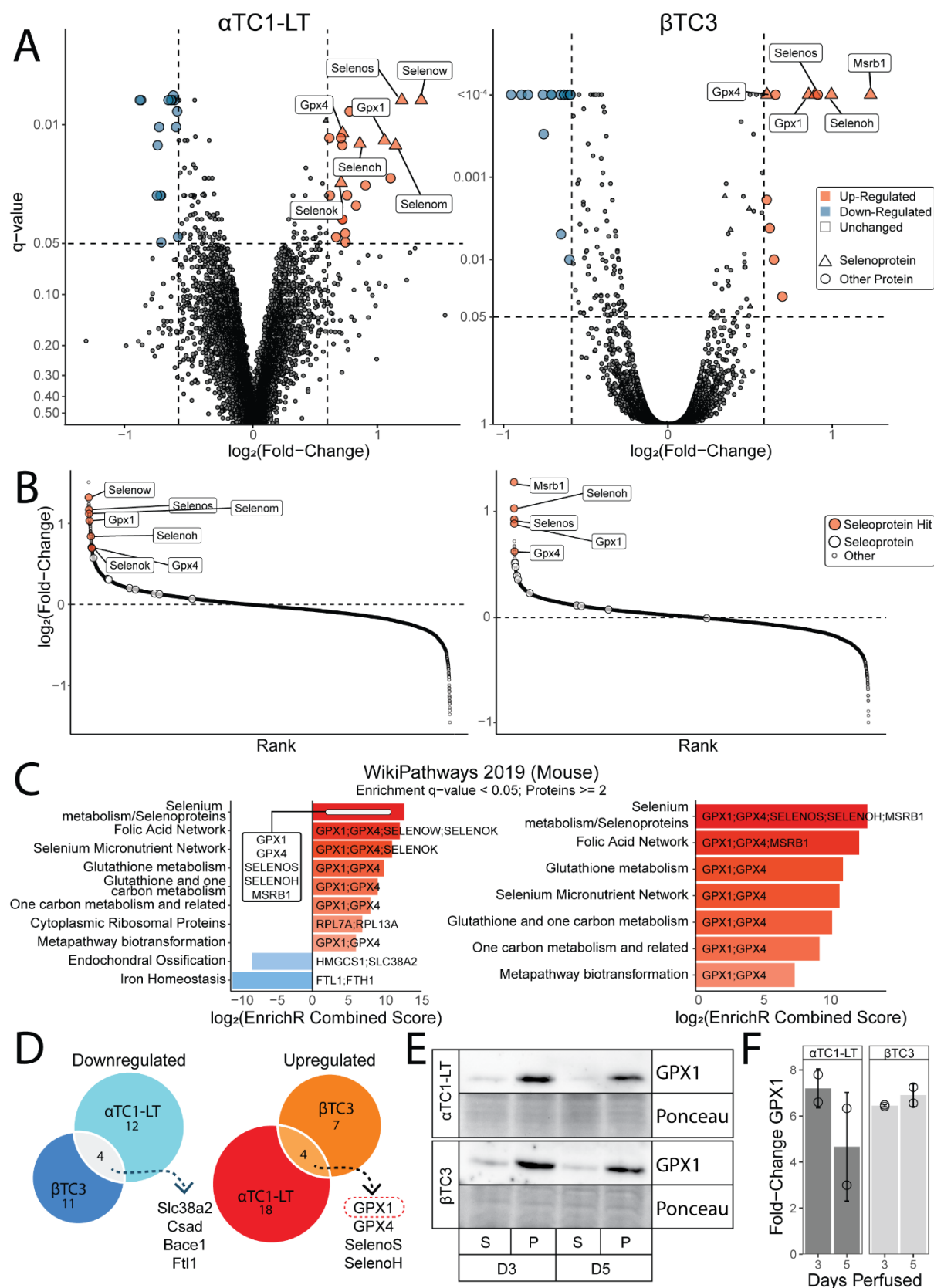


Figure 5: Quantitative global proteomics reveals perfusion culture upregulates numerous selenoproteins in both α TC1-LT and β TC3. A) Volcano plots of quantitative proteomics comparison between 5 d perfused and static conditions, highlighting upregulated selenoproteins. B) Waterfall plot indicating an upward trend in expression of numerous selenoproteins. C) Ontology analysis of (cont'd) significantly up- and down-regulated proteins using the WikiPathways (2019) mouse ontology database.

A negative *EnrichR* score multiplier is enforced for categories enriched with downregulated proteins for illustrative purposes. **D)** Overlapping up- and down-regulated protein hits. **E)** Western blot validation of the commonly upregulated glutathione peroxidase 1 (GPX1) showing significant difference in expression at least as early as day three of perfusion. Ponceau as loading control. **F)** Quantification of GPX1 band intensity in panel E.

2.2.3 Continuous perfusion culture alters the expression of genes involved in lipid metabolism

We next profiled the transcriptome-wide effects of perfusion culture on these two cell lines (**Figure 6A-C**). A fold-change cutoff ≥ 1.5 and FDR-corrected p -value statistical significance of $q < 0.05$ was used to identify differentially regulated transcripts (**Figure 6A**). In α TC1-LT ($n=3$) we identified 50 upregulated and 45 downregulated protein-coding transcripts. In β TC3 ($n=4$) we identified 141 upregulated and 211 downregulated protein-coding gene transcripts with statistical significance.

In both cell lines, downregulated transcripts were significantly enriched in cholesterol metabolic and biosynthetic pathways (**Figure 6B**). Annotated genes in these pathways in α TC1-LT overlap completely with those in β TC3 and include NAD(P)-dependent steroid dehydrogenase-like (*Nsdhl*), lanosterol synthase (*Lss*), methylsterol monooxygenase 1 (*Msmo1*), and stearoyl CoA desaturases 1 (*Scd1*) and 2 (*Scd2*). *Lss* catalyzes the formation of the first four-membered sterol, lanosterol (Huff & Telford, 2005). Notably, all enzyme-encoding genes downstream of *Lss* in cholesterol biosynthesis (WikiPathways WP103) were also significantly downregulated (*Cyp51*, *Msmo1*, *Nsdhl*, *Sc5d*, and *Dhcr7*) in β TC3 and partially in α TC1-LT (*Msmo1* and *Nsdhl*). Further upstream in the cholesterol biosynthetic pathway, we observe down regulation of 3-hydroxy-3-methylglutaryl-CoA synthase 1 (*Hmgsc1*) and mevalonate pyrophosphate decarboxylase (*Mvd*), key enzymes in the mevalonate pathway, along with farnesyl diphosphate synthase (*Fdps*) which is responsible for the synthesis of farnesyl pyrophosphate, a key sterol and intermediate and signaling molecule (Chen *et al*, 2021).

There are four known stearoyl CoA desaturases (*Scd1-4*) in mouse. These enzymes are responsible for catalyzing the rate-limiting step in mono-unsaturated fatty acid (MUFA) synthesis, particularly for 16- and 18-carbon fatty acids. Strikingly, all four were significantly downregulated in β TC3, and in α TC1-LT all except *Scd3* were significantly down (annotated, **Figure 6A**). We then validated this effect in a time course experiment using qPCR to quantify *Scd1* and *Scd4* level in perfused and static α TC1-LT plates in biological duplicate. Plates were harvested after one, two, and three days of perfusion, along with their static control counterparts. *Scd1* mRNA levels decreased significantly ($\log_2FC = -1.45$, $p < 0.05$) and plateaued by perfusion day two, while *Scd4* was only significantly affected by perfusion after

three days ($\log_2FC = -2.4$; $p < 0.05$). The day five datapoints are derived from RNA-seq data and are plotted for illustrative purposes.

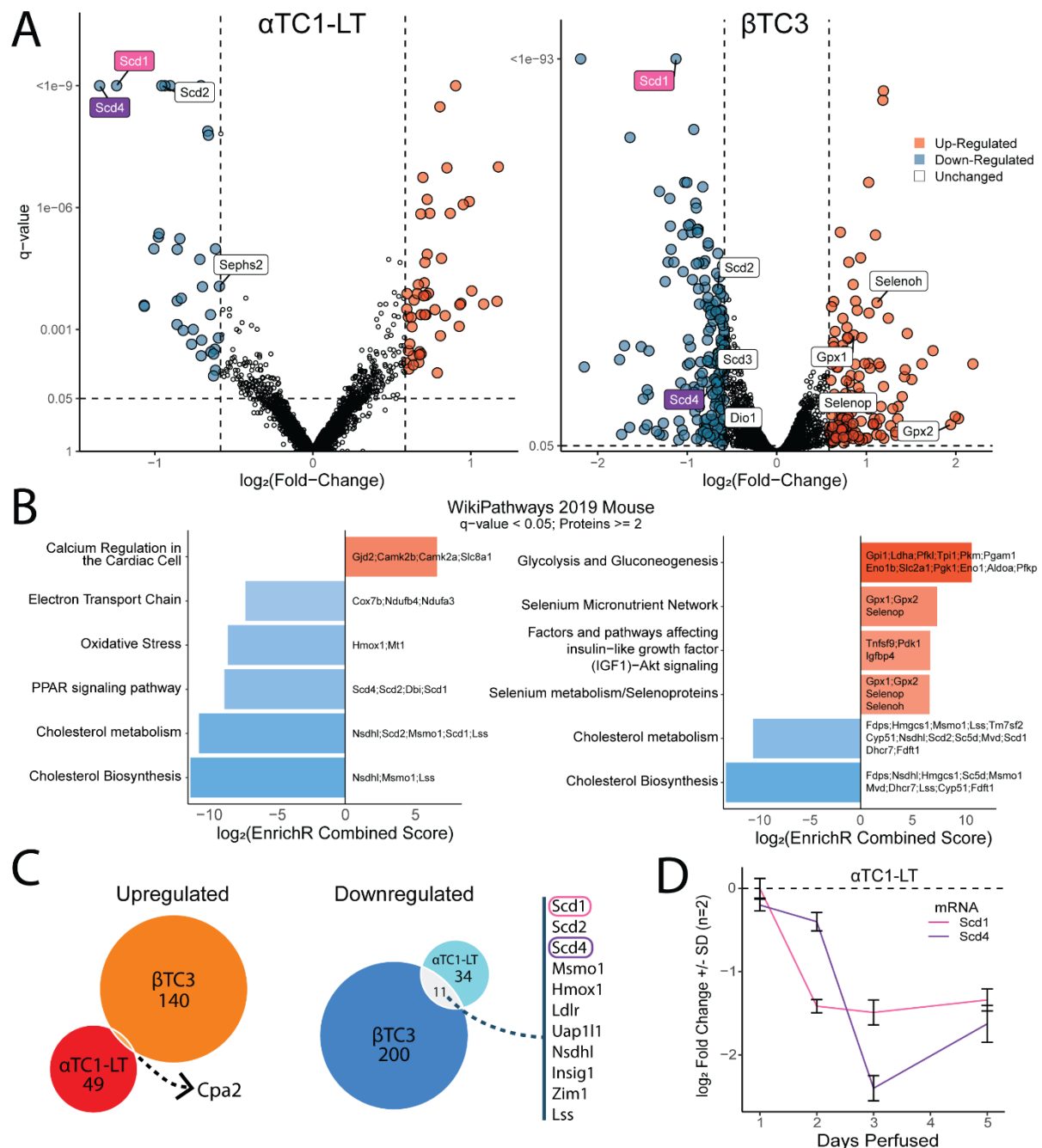


Figure 6: RNA-sequencing reveals differential expression of numerous metabolic enzymes, especially those associated with lipid and cholesterol metabolism. A) RNA-seq volcano plots highlighting mutually downregulated stearoyl Co-A desaturases *Scd1*, *Scd2*, *Scd4* as well as any differentially expressed selenoprotein transcripts. Hit genes are those with greater than 1.5-fold change and an FDR-corrected p-value (q-value) less than 0.05. **B)** Gene ontology enrichment analysis of hit genes. **C)** Venn diagram of α TC1-LT/ β TC3 hit genes. **D)** RT-qPCR validation of *Scd1* and *Scd4* transcript abundance fold-changes of perfused cells relative to static control harvested on each day as indicated. Genes of interest were normalized to the housekeeping gene *Actb*. Day five fold-changes are derived from RNA-seq data and displayed for illustrative purposes.

2.2.4 Selenoprotein upregulation does not correspond with oxidative stress signatures

Given the role that GPX1 and GPX4 play in oxidative stress defense we next sought to assess whether markers of oxidative stress were upregulated by continuous perfusion. To do so we made use of a set of 125 previously published oxidative stress genes by Sharif-Askari et al. consisting of 32 oxidative-responsive genes, 56 antioxidant genes, and 37 pro-oxidant genes (Saheb Sharif-Askari *et al*, 2021). We cross-referenced this gene set with Next-Generation Sequencing α TC1-LT and β TC3 transcriptomes under static and perfusion culture conditions (**Supplementary Figure S2**). A fold-change cut-off of 1.5-fold and FDR-corrected p-value cut-off of 0.05 were used to determine significance. Only *Gpx1*, and *Selenop* (both selenoprotein genes) were found to be significantly upregulated upon perfusion, and only in β TC3. And transcription of the anti-oxidant genes heme oxygenase 1 (*Hmox1*), and NADH:Ubiquinone Oxidoreductase Subunit B4 (*Ndufb4*), and metallothionein (*Mt1*) were found to be significantly down-regulated in both cell lines. Given that only 2 of the 125 oxidative stress markers we assessed were upregulated by perfusion culture, it is unlikely that selenoprotein up-regulation was induced by oxidative stress.

2.2.5 Fatty acid & lipid composition are altered in α TC1-LT.

Given the extent of transcriptional changes induced by continuous perfusion culture, we next sought to evaluate whether these transcription changes also resulted in corresponding changes in fatty acid and lipid composition. We therefore applied a targeted free fatty acid (FFA) panel and untargeted lipidomics to α TC1-LT cells cultured in static conditions or in perfusion culture for three days (**Figure 7**).

Of the free fatty acid species quantified, C3:0 (proprionic acid), and C4:0 (butanoic acid) were both found to increase in abundance with perfusion (**Figure 7C**). More striking however was the depletion of oleic acid (C18:1) following perfusion. C18:1 was reliably quantified in all four static control replicates (mean \pm StDev = 128.5 \pm 33.3 pmol) but below the limit of quantification (LOQ = 2 pmol) in all four perfused samples (**Figure 7D**, indicating at least a 64-fold drop in oleic acid abundance under continuous perfusion conditions. Interestingly, the saturated precursor to oleic acid, steric acid (C18:0), was not found to be significantly altered by continuous perfusion culture.

Untargeted lipidomics analysis showed a number of significantly altered lipid species when using >2 fold-change and FDR-corrected p-value < 0.05 cut-off (**Figure 7A-B**). Upregulated species were predominantly phosphatidylcholines (PC 38:5, 38:4, 40:5, and 34:0) and a phosphatidylethanolamine (PE 38:4). The number of lipid species that were found to decrease following perfusion were far greater and varied, see **Figure 7B** for a complete list of hit species.

Following the results of the FFA panel, we examined lipid species that were most likely to contain at least one oleic acid (C18:1) tail unit, such as 18:1 (as in a cholesterol ester), 36:1 (C18:1/C18:0), and 36:2 (2×C18:1). Of the seven lipid species quantified in our dataset five were found to have significantly altered abundance. In line with our FFA panel results, all five of these potential oleic acid-containing lipid species were depleted following perfusion. The cholesterol ester CE(18:1), which contains an oleic acid linked to cholesterol, was significantly depleted ($\log_2FC = -1.34$, $q = 0.016$). PE(O-36:2) ($\log_2FC = -2.88$, $q = 0.006$), PE(36:2) ($\log_2FC = -2.94$, $q = 0.008$), PC(36:2) ($\log_2FC = -2.06$, $q = 0.004$), and PC(36:1) ($\log_2FC = -1.18$, $q = 0.004$) were also depleted and likely to contain a C18:1 tail.

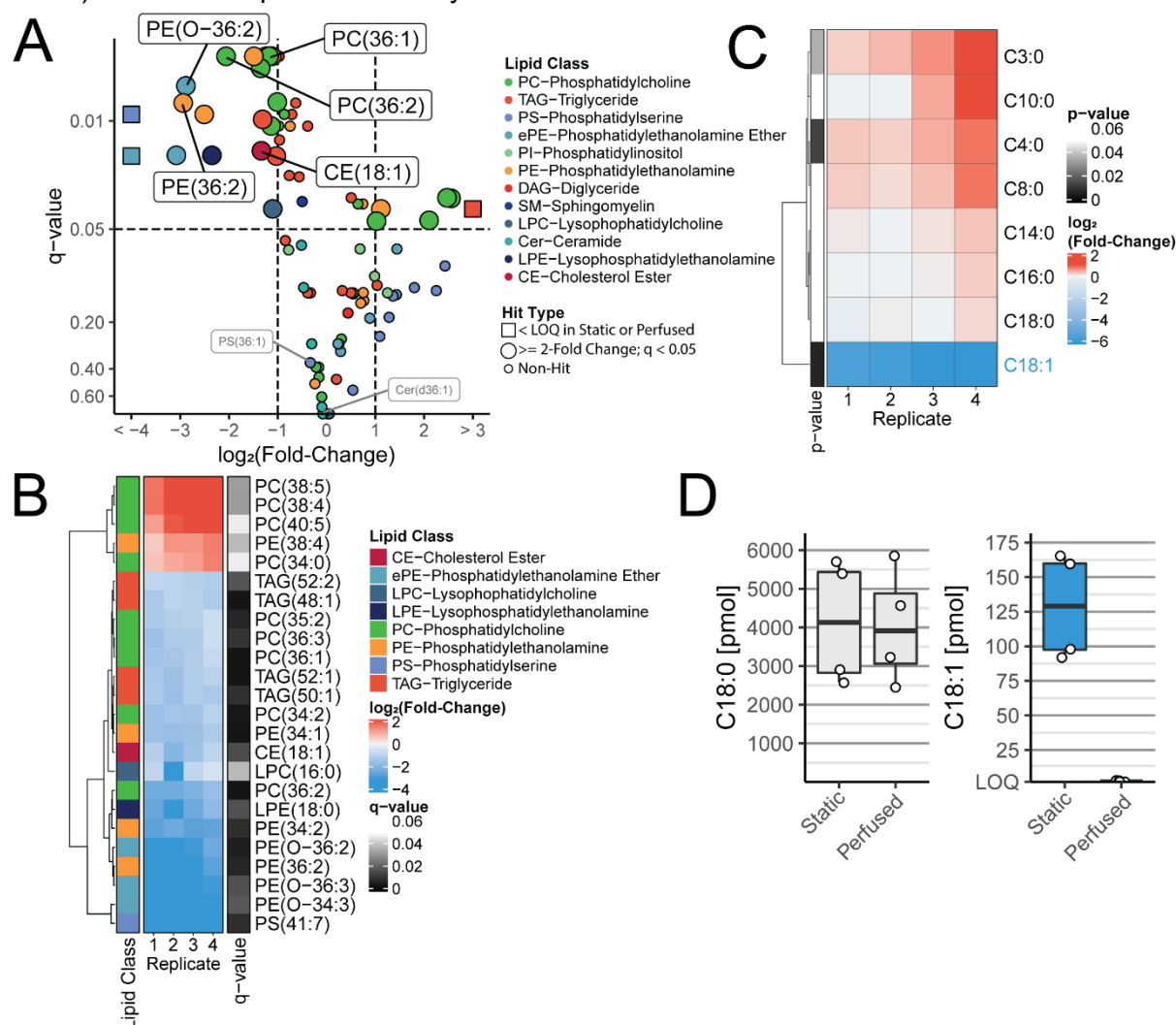


Figure 7: Perfusion culture alters fatty acid and lipid composition of α TC1-LT cells in perfusion culture, particularly oleic acid (C18:1) and oleic-acid derived phospholipids. A) Untargeted lipidomic analysis volcano plot of perfused versus statically cultured α TC1-LT cells ($n=4$). Significantly different lipids are those with greater than 2-fold change and FDR-corrected p -value of less than 0.05. Species that were below the limit-of-quantification in all replicates for either perfused or static conditions are indicated by squares and fold-change was fixed at the maximum observed for each replicate. Lipid species likely derived from oleic acid (C18:1) are labelled. B) Heatmap representation of hits from panel

A. **C)** Heatmap of fold-change for quantified free fatty acids. **D)** Raw replicate quantification of stearic (C18:0) and oleic acid (C18:1) in each condition/replicate.

2.2.6 Supplementary Data

Table 2: Significantly up- and down-regulated proteins in perfused vs. static culture of α TC1-LT.

Uniprot	Gene Name	Description	log ₂ FC	FDR	Uniprot	Gene Name	Description	log ₂ FC	FDR
P63300	Selenow	selenoprotein w	1.32	0.0071	P29391	Ftl1	Ferritin light chain 1	-0.89	0.0071
Q9BCZ4	Selenos	selenoprotein S	1.17	0.0071	P09528	Fth1	Ferritin heavy chain	-0.88	0.0071
Q8VHC3	Selenom	Selenoprotein M	1.12	0.013	Q8JZK9	Hmgcs1	hydroxymethylglutaryl-CoA synthase, cytoplasmic	-0.75	0.026
P12970	Rpl7a	60S ribosomal protein L7a	1.08	0.020	Q8CFE6	Slc38a2	sodium-coupled neutral amino acid transporter 2	-0.75	0.013
P11352	Gpx1	Glutathione peroxidase 1	1.03	0.012	P15105	Glul	Glutamine synthetase	-0.74	0.010
Q9QXM0	Abhd2	Monoacylglycerol lipase ABHD2	0.88	0.023	P07091	S100a4	Protein S100-A4	-0.73	0.026
Q3UQA7	Selenoh	Selenoprotein H	0.84	0.013	Q4V9W2	Srek1ip1	protein SREK1IP1	-0.72	0.026
Q504N0	Cpa2	Carboxypeptidase A2	0.81	0.030	P54763	Ephb2	Ephrin type-B receptor 2	-0.72	0.049
Q9QZ49	Ubxn8	UBX domain-containing protein 8	0.76	0.0083	P56818	Bace1	Beta-secretase 1	-0.66	0.0071
Q8BLK3	Lsamp	Limbic system-associated membrane protein	0.74	0.026	Q08890	Ids	iduronate 2-sulfatase	-0.64	0.0071
Q9CRB6	Tppp3	Tubulin polymerization-promoting protein family member 3	0.73	0.049	Q80X71	Tmem106b	Transmembrane protein 106B	-0.64	0.0071
P19253	Rpl13a	60S ribosomal protein L13a	0.73	0.044	P35951	Ldlr	Low-density lipoprotein receptor	-0.63	0.0067
O70325-1	Gpx4	Phospholipid hydroperoxide glutathione peroxidase, mitochondrial	0.70	0.011	P97798-1	Neo1	neogenin	-0.61	0.0071
P84244	H3-3a	histone H3.3	0.70	0.036	Q9DBE0	Csad	Cysteine sulfinic acid decarboxylase	-0.60	0.010
P84244	H3-3b	histone H3.3	0.70	0.036	POCL69	Znf703	Zinc finger protein 703	-0.60	0.0083
P26339	Chga	Chromogranin-A	0.70	0.013	Q9WUZ9	Entpd5	Ectonucleoside triphosphate diphosphohydrolase 5	-0.59	0.046
Q9JLJ1	Selenok	selenoprotein K	0.69	0.022					
Q80TL0	Ppm1e	Protein phosphatase 1E	0.69	0.012					
Q62011	Pdpm	Podoplanin	0.65	0.046					
Q8BTY1	Kyat1	Kynurenine--oxoglutarate transaminase 1	0.60	0.026					
P70232-2	Chl1	Isoform 2 of Neural cell adhesion molecule L1-like protein	0.60	0.030					
A6H6A9-3	Rabgap1l	Isoform 3 of Rab GTPase-activating protein 1-like	0.60	0.012					

RESULTS

Table 3: Significantly up- and down-regulated proteins in perfused vs. static culture of β TC3.

Uniprot	Gene Name	Description	log ₂ FC	FDR	Uniprot	Gene Name	Description	log ₂ FC	FDR
Q9JLC3	Msrb1	Methionine-R-sulfoxide reductase B1	1.23	8.62E-15	Q8CFE6	Slc38a2	sodium-coupled neutral amino acid transporter 2	-0.95	3.45E-12
Q3UQA7	Selenoh	Selenoprotein H	0.99	8.62E-15	P28798	Grn	Granulins	-0.89	8.62E-15
Q6KAU8-1	Atg16l2	Autophagy-related protein 16-2	0.91	5.57E-06	P07309	Ttr	Transthyretin	-0.85	8.62E-15
Q9BCZ4	Selenos	selenoprotein S	0.90	4.19E-06	P18581-1	Slc7a2	cationic amino acid transporter 2	-0.76	7.37E-08
P11352	Gpx1	Glutathione peroxidase 1	0.86	8.62E-15	Q9QY73	Tmem59	Transmembrane protein 59	-0.76	0.00030
Q6GQX2	Nckap5l	Nck-associated protein 5-like	0.70	0.028	Q61207	Psap	Prosaposin	-0.71	8.62E-15
Q8C3R1-1	Brat1	BRCA1-associated ATM activator 1	0.66	1.73E-05	P29391	Ftl1	Ferritin light chain 1	-0.71	5.65E-06
Q7TPB0	Plppr3	Phospholipid phosphatase-related protein type 3	0.65	0.010	P56818	Bace1	Beta-secretase 1	-0.65	1.27E-05
Q61398	Pcolce	Procollagen C-endopeptidase enhancer 1	0.62	0.0042	Q9CRG1	Tm7sf3	Transmembrane 7 superfamily member 3	-0.65	0.0050
O70325-1	Gpx4	Phospholipid hydroperoxide glutathione peroxidase, mitochondrial	0.60	2.54E-08	P60041	Sst	Somatostatin	-0.63	3.60E-09
O08677-2	Kng1	Isoform LMW of Kininogen-1	0.60	0.0019	Q920Q8-1	Ivns1abp	Influenza virus NS1A-binding protein homolog	-0.63	3.73E-05
					Q61703	Itih2	Inter-alpha-trypsin inhibitor heavy chain H2	-0.61	6.15E-06
					Q99J21-1	Mcoln1	Mucolipin-1	-0.60	0.010
					Q31125	Slc39a7	Zinc transporter SLC39A7	-0.60	4.00E-06
					Q9DBE0	Csad	Cysteine sulfinic acid decarboxylase	-0.59	3.49E-08

Table 4: Top 25 differentially expressed protein-coding transcripts in perfused vs. static culture of α TC1-LT

Gene Name	Description	log ₂ FC	FDR	Gene Name	Description	log ₂ FC	FDR
Gucy2c	guanylate cyclase 2c	1.18	9.96E-08	Scd4	stearoyl-coenzyme A desaturase 4	-1.35	1.00E-09
Srpk3	serine/arginine-rich protein specific kinase 3	1.17	2.02E-04	Scd1	stearoyl-Coenzyme A desaturase 1	-1.24	1.00E-09
Nobox	NOBOX oogenesis homeobox	1.08	2.38E-04	Ins2	insulin II	-1.07	2.52E-04
Vnn3	vanin 3	1.01	1.12E-04	Fcor	Foxo1 corepressor	-1.07	2.69E-04
Cpa2	carboxypeptidase A2, pancreatic	0.99	7.07E-07	Gm4356	NA	-1.01	1.03E-05
Eno3	enolase 3, beta muscle	0.95	8.41E-07	S100a4	S100 calcium binding protein A4	-0.98	5.32E-06
Fam129a	family with sequence similarity 129, member A	0.94	2.28E-04	Gng5	guanine nucleotide binding protein (G protein), gamma 5	-0.97	4.34E-06
Rassf4	Ras association (RalGDS/AF-6) domain family member 4	0.93	2.46E-04	Scd2	stearoyl-Coenzyme A desaturase 2	-0.96	1.00E-09
2810459M11Rik	RIKEN cDNA 2810459M11 gene	0.93	8.40E-04	Hmox1	heme oxygenase 1	-0.94	1.00E-09
Ift57	intraflagellar transport 57	0.90	1.00E-09	Lss	lanosterol synthase	-0.90	1.00E-09
Camk2b	calcium/calmodulin-dependent protein kinase II, beta	0.87	1.39E-06	Dok7	docking protein 7	-0.86	7.56E-04
Dpp6	dipeptidylpeptidase 6	0.85	1.05E-07	Zim1	zinc finger, imprinted 1	-0.86	1.07E-05
Ppp1r3c	protein phosphatase 1, regulatory subunit 3C	0.84	4.58E-04	Nop10	NOP10 ribonucleoprotein	-0.86	1.98E-04
Tmem117	transmembrane protein 117	0.81	1.78E-05	Cox7b	cytochrome c oxidase subunit 7B	-0.84	5.82E-06
H2aw	H2A.W histone	0.81	1.43E-03	Ndufa3	NADH:ubiquinone oxidoreductase subunit A3	-0.83	1.70E-04
Rsph1	radial spoke head 1 homolog (Chlamydomonas)	0.80	3.30E-09	1190007107Rik	RIKEN cDNA 1190007107 gene	-0.82	1.06E-03
Neb	nebulin	0.79	1.17E-02	Mt1	metallothionein 1	-0.77	2.30E-03
Nsg2	neuron specific gene family member 2	0.77	3.25E-04	Mgst3	microsomal glutathione S-transferase 3	-0.76	1.00E-03
Cuedc1	RIKEN cDNA 2210416O15 gene	0.74	1.39E-06	Dbi	diazepam binding inhibitor	-0.72	1.88E-05
Chl1	cell adhesion molecule L1-like	0.73	1.29E-04	Insig1	insulin induced gene 1	-0.71	1.00E-09
Clu	clusterin	0.72	1.41E-05	Atp5md	ATP synthase membrane subunit DAPIT	-0.71	4.45E-03
Pam	peptidylglycine alpha-amidating monooxygenase	0.72	6.29E-07	Rbis	ribosomal biogenesis factor	-0.70	1.83E-03
Thbs3	thrombospondin 3	0.72	4.33E-04	Uap111	UDP-N-acteylglucosamine pyrophosphorylase 1-like 1	-0.70	8.89E-05
Akap7	A kinase (PRKA) anchor protein 7	0.72	1.45E-04	Msmo1	methylsterol monooxygenase 1	-0.67	1.31E-08
Myo10	myosin X	0.71	2.25E-05	Ldlr	low density lipoprotein receptor	-0.66	1.65E-08

Table 5: Top 25 differentially expressed protein-coding transcripts in perfused vs. static culture of β TC3

Gene Name	Description	log ₂ FC	FDR	Gene Name	Description	log ₂ FC	FDR
Slc16a3	solute carrier family 16 (monocarboxylic acid transporters), member 3	2.19	2.08E-21	Uap11l	UDP-N-acetylglucosamine pyrophosphorylase 1-like 1	-2.19	1.00E-93
ccdc198	coiled-coil domain containing 198	2.03	1.78E-08	Drc1	dynein regulatory complex subunit 1	-2.15	1.06E-20
Col17a1	collagen, type XVII, alpha 1	1.99	5.97E-09	Tcn2	transcobalamin 2	-1.76	1.98E-22
Gpx2	glutathione peroxidase 2	1.94	4.89E-07	Dmbt1	deleted in malignant brain tumors 1	-1.73	1.04E-04
Bnip3	BCL2/adenovirus E1B interacting protein 3	1.74	1.46E-24	1700016C15Rik	RIKEN cDNA 1700016C15 gene	-1.70	1.01E-25
Il6ra	interleukin 6 receptor, alpha	1.62	2.05E-21	Grid2ip	glutamate receptor, ionotropic, delta 2 (Grid2) interacting protein 1	-1.64	2.24E-06
Neb1	nebulette	1.51	9.93E-18	Dpp7	dipeptidylpeptidase 7	-1.64	4.22E-75
Colgalt2	collagen beta(1-O)galactosyltransferase 2	1.49	4.59E-06	Blnk	B cell linker	-1.51	1.70E-25
Fhad1	forkhead-associated (FHA) phosphopeptide binding domain 1	1.46	1.26E-28	Pgm5	phosphoglucomutase 5	-1.49	4.15E-13
Slc2a1	solute carrier family 2 (facilitated glucose transporter), member 1	1.43	4.49E-20	Hpgds	hematopoietic prostaglandin D synthase	-1.48	5.95E-06
Pdk1	pyruvate dehydrogenase kinase, isoenzyme 1	1.43	2.23E-18	Parp3	poly (ADP-ribose) polymerase family, member 3	-1.45	6.11E-07
Smtnl2	smoothelin-like 2	1.41	2.00E-05	Fn3k	fructosamine 3 kinase	-1.45	2.78E-15
Stc1	stanniocalcin 1	1.40	1.15E-13	Tmem144	transmembrane protein 144	-1.44	3.62E-14
Mcub	mitochondrial calcium uniporter dominant negative beta subunit	1.35	2.59E-11	Cnm1	cyclin M1	-1.43	1.59E-24
Preli2	PRELI domain containing 2	1.35	2.08E-08	Aloxe3	arachidonate lipoxygenase 3	-1.34	1.80E-05
Gucy1a1	guanylate cyclase 1, soluble, alpha 1	1.33	1.79E-04	Hsd17b14	hydroxysteroid (17-beta) dehydrogenase 14	-1.31	1.01E-04
Fat3	FAT atypical cadherin 3	1.33	2.70E-05	Gnpda1	glucosamine-6-phosphate deaminase 1	-1.31	2.57E-62
Sid1	SID1 transmembrane family, member 1	1.30	8.49E-11	Aldh11l1	aldehyde dehydrogenase 1 family, member L1	-1.27	1.55E-04
Ak4	adenylate kinase 4	1.27	8.98E-07	Rbp3	retinol binding protein 3, interstitial	-1.27	2.31E-07
Ankrd37	ankyrin repeat domain 37	1.25	2.98E-32	Rragd	Ras-related GTP binding D	-1.25	6.15E-41
Zscan4c	zinc finger and SCAN domain containing 4C	1.20	8.60E-04	Il18rap	interleukin 18 receptor accessory protein	-1.21	1.50E-45
Fam162a	family with sequence similarity 162, member A	1.19	4.58E-16	Amdhd2	amidohydrolase domain containing 2	-1.19	1.20E-60
Tpi1	triosephosphate isomerase 1	1.19	3.71E-86	Flcn	folliculin	-1.19	4.43E-54
Aldoa	aldolase A, fructose-bisphosphate	1.19	6.23E-84	Oasl1	2'-5' oligoadenylate synthetase-like 1	-1.18	1.41E-48
Lcp2	lymphocyte cytosolic protein 2	1.16	2.58E-11	Slc23a4	solute carrier family 23 member 4	-1.15	2.43E-13

Table 6: Mouse primer sequences used in RT-qPCR analyses.

Gene	Orientation	Sequence
<i>Actb</i>	fwd	GGTGGGAATGGGTCAGAAGGAC
<i>Actb</i>	rev	GGCCACACGCAGCTCATTGT
<i>Scd1</i>	fwd	TTCTTGGGATACACTCTGGTGC
<i>Scd1</i>	rev	CGGGATTGAATGTTCTTGTCGT
<i>Scd4</i>	fwd	GCCCACTTGCCACAAGAGAT
<i>Scd4</i>	rev	GTAGCTGGGGTCATACAGATCA

Figure S1: Whole membrane Ponceau and GPX1 immunostaining time-course. Lanes are annotated as [time-point][condition][biological replicate] where S=static culture and P=perfusion culture. A-B) α TC1-LT membrane A) Ponceau staining loading control B) GPX1 immunostaining. C-D) β TC3 membrane C) Ponceau staining loading control D) GPX1 immunostaining. Note that in B and D that the membrane was cut between 25-35 kDa and another unrelated antibody was blotted in the top membrane. A non-specific band is present in the GPX1-blotted membranes is present at 15 kDa.

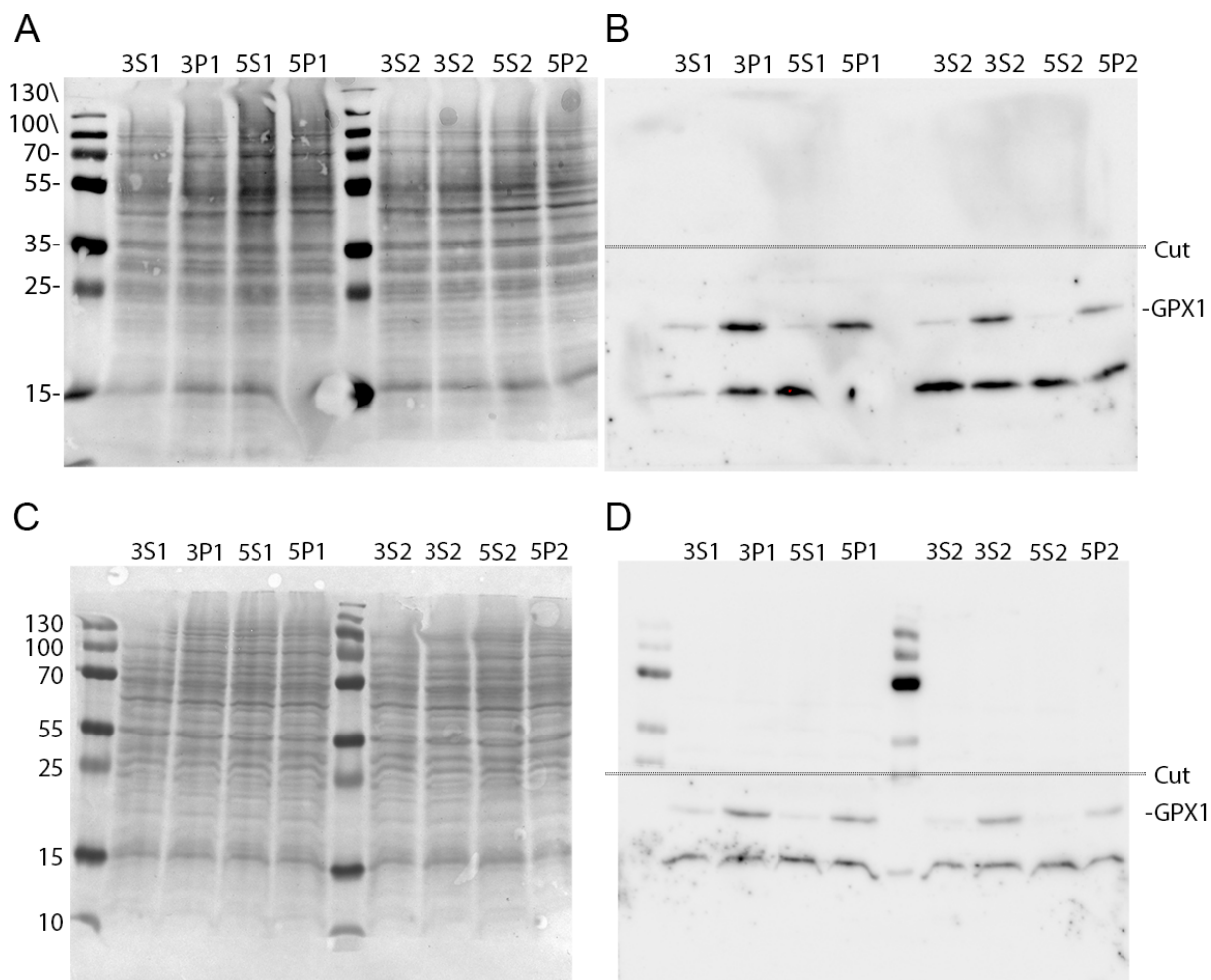


Figure S2: Bulk RNA-seq \log_2 fold-changes (perfused/static) of curated oxidative stress marker genes in A) α TC1-LT and B) β TC3. 1.5-fold change cut-offs are indicated by dashed vertical lines.

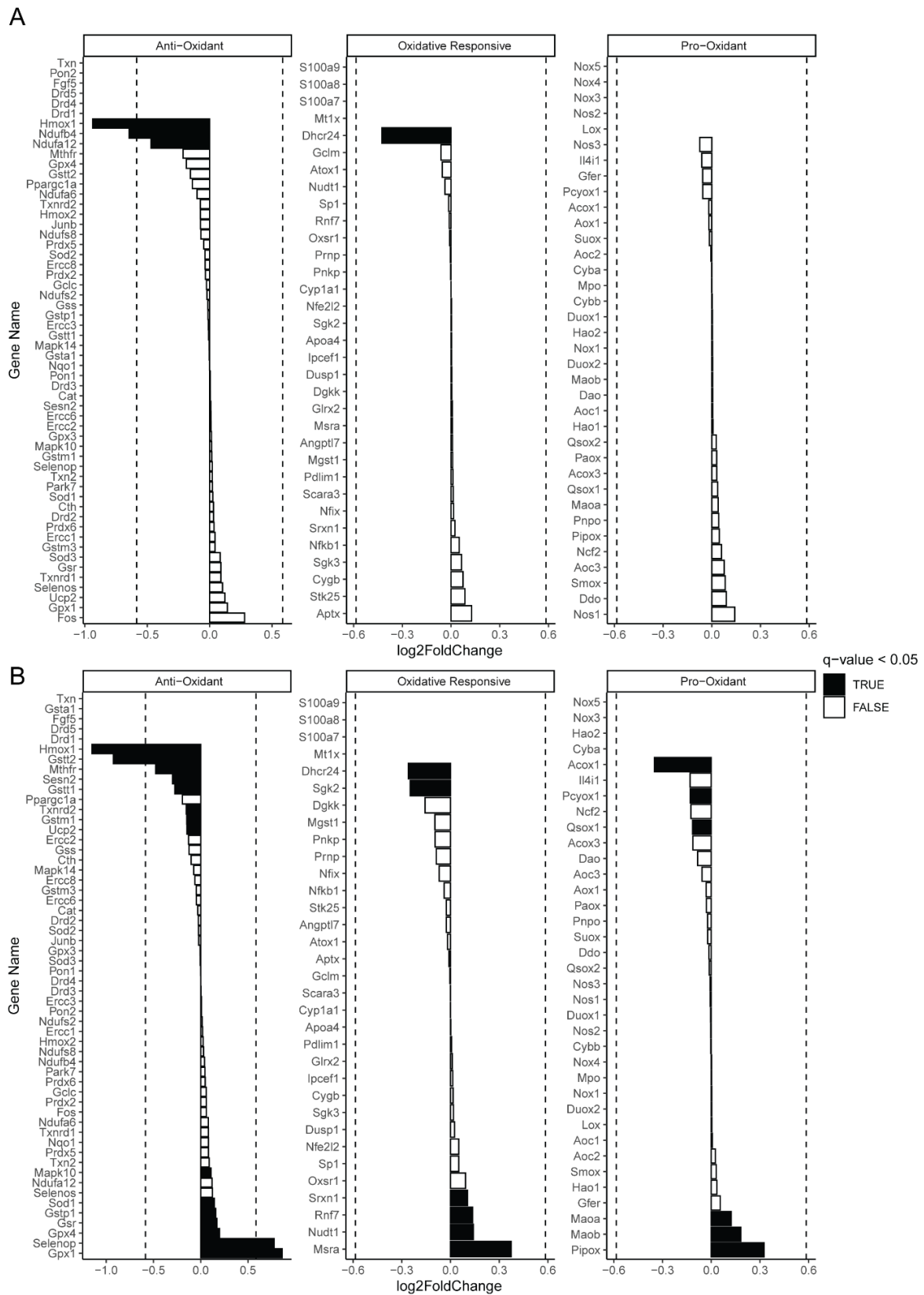
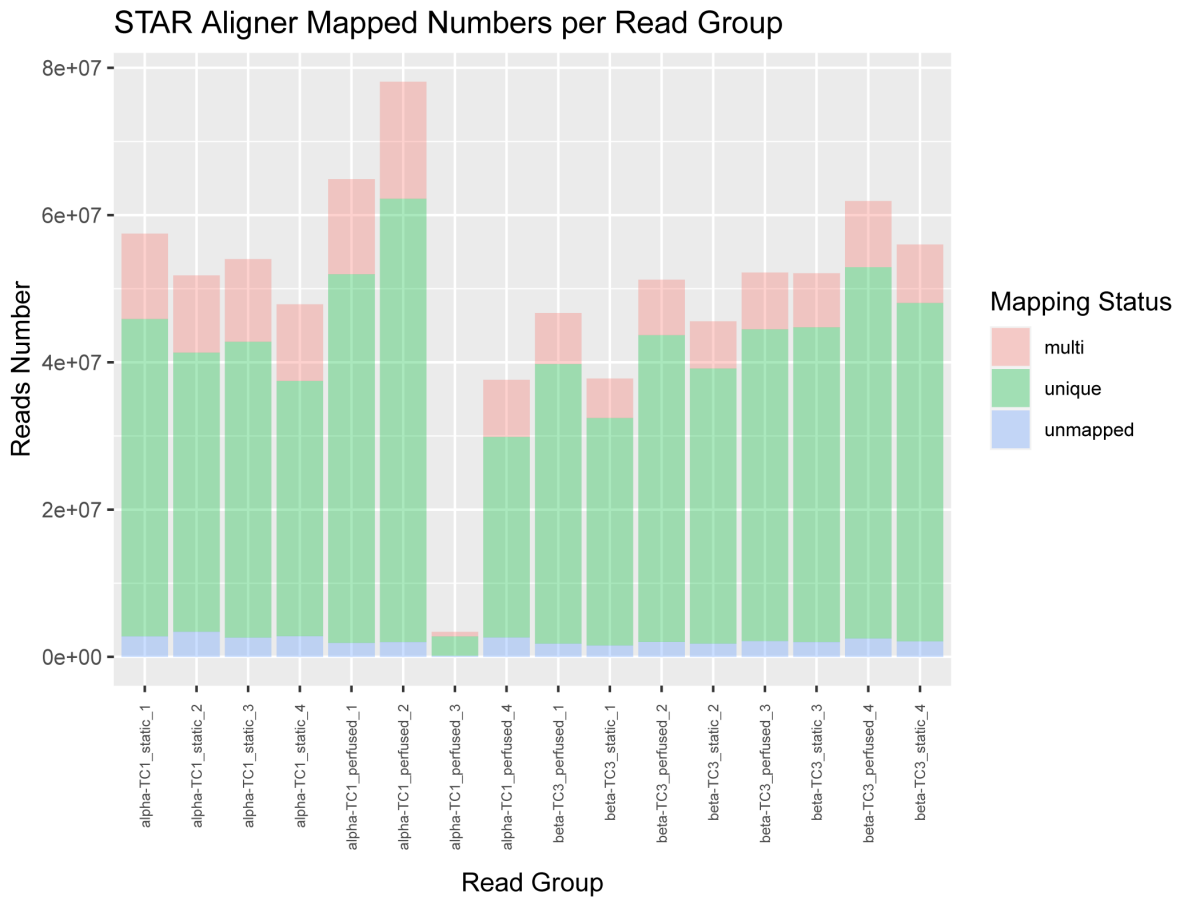


Figure S3: RNA-sequencing STAR Aligner mapped read counts for each sample sequenced. Note the unusually low read count of alpha-TC1_perfused_3. For this reason, this biological replicate was excluded from our analyses.



3. DISCUSSION

3.1 General Discussion

We demonstrate clearly that continuous perfusion culture has an effect on murine pancreatic islet cell lines α TC1-LT and β TC3 from as early as 48-72 h. Wide-spread selenoprotein upregulation and lipid metabolic pathway suppression were seen in both cell lines, and untargeted lipidomics and free fatty acid analysis in α TC1-LT revealed significantly altered lipid composition following continuous perfusion culture.

The selenoprotein family of proteins is defined by the presence of the selenium-containing amino acid, selenocysteine (Sec) in their primary structure (Kryukov *et al*, 2003). Structurally Sec is nearly identical to cysteine, with the sulfur atom of its side chain substituted by selenium. Sec is incorporated through translational recoding of the UGA stop codon, which requires binding of a specialized tRNA complex to one or more 3' UTR selenocysteine insert sequences (SECIS). This is an energetically expensive and inefficient process and selenoprotein synthesis is well-regulated (Zhang *et al*, 2021; Hatfield *et al*, 2014). There are only 25 known selenoproteins in human, and 24 in mouse (Hariharan & Dharmaraj, 2020). It is therefore quite striking to observe so many selenoproteins upregulated in the relatively small proteomics hit sets: 7 of the 22 up-regulated proteins in α TC1-LT and 5 of 11 in β TC3 (**Figure 5A**). Globally we also observe a qualitative upward trend in nearly every quantified selenoprotein in our proteomics datasets (**Figure 5B**).

In both our proteomics datasets, we identified GPX1, GPX4, SELENOS, and SELENOH as significantly upregulated (**Figure 5D**). Though most selenoproteins are functional redox enzymes, their specific biological functions vary, and to a large extent are unknown (Kryukov *et al*, 2003; Touat-Hamici *et al*, 2014). GPX1 and GPX4 are ubiquitously expressed in mammalian tissues and catalyze the reduction of hydrogen peroxide, organic peroxides, and lipid peroxides to combat oxidative stress which could otherwise lead to lipid peroxidation and subsequent ferroptosis. SELENOS is a transmembrane protein primarily localized to the ER and functions in misfolded protein removal, ER-stress induced apoptosis, and more generally oxidative stress mitigation through its own glutathione peroxidase activity (Ye *et al*, 2004; Gao *et al*, 2004). Meanwhile SELENOH is a nucleolar oxidoreductase that has been shown to regulate p53 (Cox *et al*, 2016). Of these, GPX1, GPX4, and SELENOS have been shown up-regulation in response to oxidative stress induction in HEK293 (Touat-Hamici *et al*, 2014). Given that we do not find any evidence of oxidative stress in our RNA-seq data (**Supplementary Figure S2**), it is likely that the reason for global selenoprotein upregulation may lie in another commonality – regulation by selenium availability.

In routinely used cell culture medium, such as that utilized in this study, selenium is supplied by the serum used to supplement minimal nutrient medium – it is not, for example, a standard component of DMEM. Selenoprotein P (SELENOP), which contains ten selenocysteine residues, is the primary source of serum selenium and constitutes more than 50% of the total selenium content of human serum (Saito & Takahashi, 2002). Selenium deficiency has been shown to have a global effect on selenoprotein expression, primarily at the translational level (Howard *et al*, 2013); for example, Jurkat cells cultured in medium with serum depleted of SELENOP showed significant reduction in GPX1 and GPX4 activity (Saito & Takahashi, 2002). And even in culture medium supplemented with 10% serum, selenium availability has been found to be limiting (Baker *et al*, 1998). In continuous perfusion culture fresh medium is constantly introduced into the tissue culture plate, thus the availability of nutrients such as selenium are greater than that in static culture. Therefore, we believe that the global selenoprotein upregulation observed on the protein level is consistent with increased selenium availability, and that in static culture selenium is a limiting factor in selenoprotein expression. The primarily translational regulation of selenoprotein expression in response to selenium supply may also explain why selenoprotein differential expression was not quite as striking in our RNA-seq datasets. The amino acid serine has also been found to have a synergistic effect with selenium on the expression of selenoproteins (Long *et al*, 2020). Although, given the relatively high concentration of serine in the DMEM used here (see Table 1), it is unlikely that serine is a limiting factor in static culture.

RNA-sequencing revealed a widespread suppression of lipid metabolic gene transcription following continuous perfusion culture in both cell lines (overview in **Figure 8**). In particular, cells cultured under perfusion culture showed significant perturbation of the cholesterol biosynthetic pathway. Cholesterol plays a major role in regulating plasma membrane organization, fluidity, and stability and is an essential component of animal cell membranes (Yeagle, 1991; Wüstner & Solanko, 2015). Cholesterol is either imported from the extracellular environment, mostly as low-density lipoproteins (LDL), or produced intracellularly by *de novo* synthesis from acetyl CoA (Das *et al*, 2014). Regulation of cholesterol homeostasis is complex and takes place on several levels (Bhattarai *et al*, 2021; Das *et al*, 2014; Ikonen, 2008), one of which is the sterol response element binding protein (SREBP) system which regulates the expression of most genes in the cholesterol biosynthetic pathway. SREBPs SREBP-1a, SREBP-1c, and SREBP-2 are transmembrane transcription factors found in the ER membrane, where when intracellular sterol levels are high they form a complex with SREBP-cleavage activating protein (SCAP) and insulin-induced gene (INSIG) that is extremely sensitive to changes in intracellular cholesterol concentration (Radhakrishnan *et al*, 2008). In complex with INSIG, SCAP/SREBPs are retained in the ER membrane, however when

intracellular sterol levels decline, SCAP/SREBPs dissociate from INSIG and are transported to the Golgi (Esquejo *et al*, 2021). There, proteolytic cleavage by site-1 and site-2 proteases liberates SREBP's cytosolic N-terminal domain which travels to the nucleus and promotes SREBP target gene transcription (Horton *et al*, 2002).

Culture medium supplemented with 10% FBS contains only about 2-3% of the cholesterol and lipid concentration of human plasma (Hayavi & Halbert, 2005). Many cell lines used in routine tissue culture contain unnaturally high cholesterol concentrations, which can possibly be attributed to their cancerous origins (Else, 2020). The α TC1-LT and β TC3 cell lines used in this study are also tumor-derived, originating from transgenic mouse adenoma (Fletcher, 1981) and insulinoma (Efrat *et al*, 1988), respectively. It may be that LDL becomes limiting in static culture as cells proliferate, upregulating cholesterol biosynthesis to compensate. Excess cholesterol is sequestered as cholesteryl esters in order to prevent accumulation of free cholesterol in cellular membranes (Das *et al*, 2014). Interestingly, we did not see an increase in cholesteryl esters (CE) (**Figure 7AB**), but rather a downregulation, though we were only able to quantify one species - CE(18:1). LDL is taken up through the LDL receptor (LDLR), the abundance of which is regulated in order to control LDL uptake and cholesterol homeostasis via proprotein convertase subtilisin/kexin type 9 (PCSK9) (Maxwell *et al*, 2005). Excess sterol promotes PCSK9 transcription via SREBPs, which in turn increases LDLR degradation and therefore decreases LDL uptake (Jeong *et al*, 2008). LDLR protein abundance was found to be significantly reduced upon perfusion culture in α TC1-LT (\log_2 FC = -0.61, $q < 0.05$) despite negligible changes in *Pcsk9* transcription in RNA-seq. These results suggest that the cellular cholesterol needs of α TC1-LT and β TC3 are better met by perfusion, as biosynthesis and uptake are reduced while no evidence of cholesterol excess is present in the form of cholesteryl esters.

Cell lines in routine cell culture conditions also tend to contain more than double the mono-unsaturated fatty acid proportion compared to their primary tissue equivalents, primarily as oleic acid (C18:1), while saturated fatty acids are relatively unchanged (Else, 2020). In line with our other observations the fatty acid profile of perfused cells appears to move in a more physiological direction; C18:1 abundance was dramatically reduced following perfusion while the most abundant saturated fatty acids, C16:0 and C18:0 were relatively unaffected. Unfortunately we were unable to quantify poly-unsaturated fatty acids which should increase following perfusion if the trend towards a more physiological lipid profile is robust (Else, 2020). The marked decrease in C18:1 upon perfusion is in line with the down regulation of stearoyl CoA desaturase 1,2, and 4 (*Scd1/2/4*) transcripts observed in RNA-sequencing in both cell lines. SCDs introduce a double bond between the 9th and 10th carbons of 16- and 18-carbon fatty acids (palmitic acid and stearic acid) (Paton & Ntambi, 2009). As *Scds* are also regulated

by SREBPs this may also be driven by sterol supply. Nearly every lipid species likely to contain at least one C18:1 tail quantified in our lipidomics assay was downregulated upon perfusion as well (annotated **Figure 7A**).

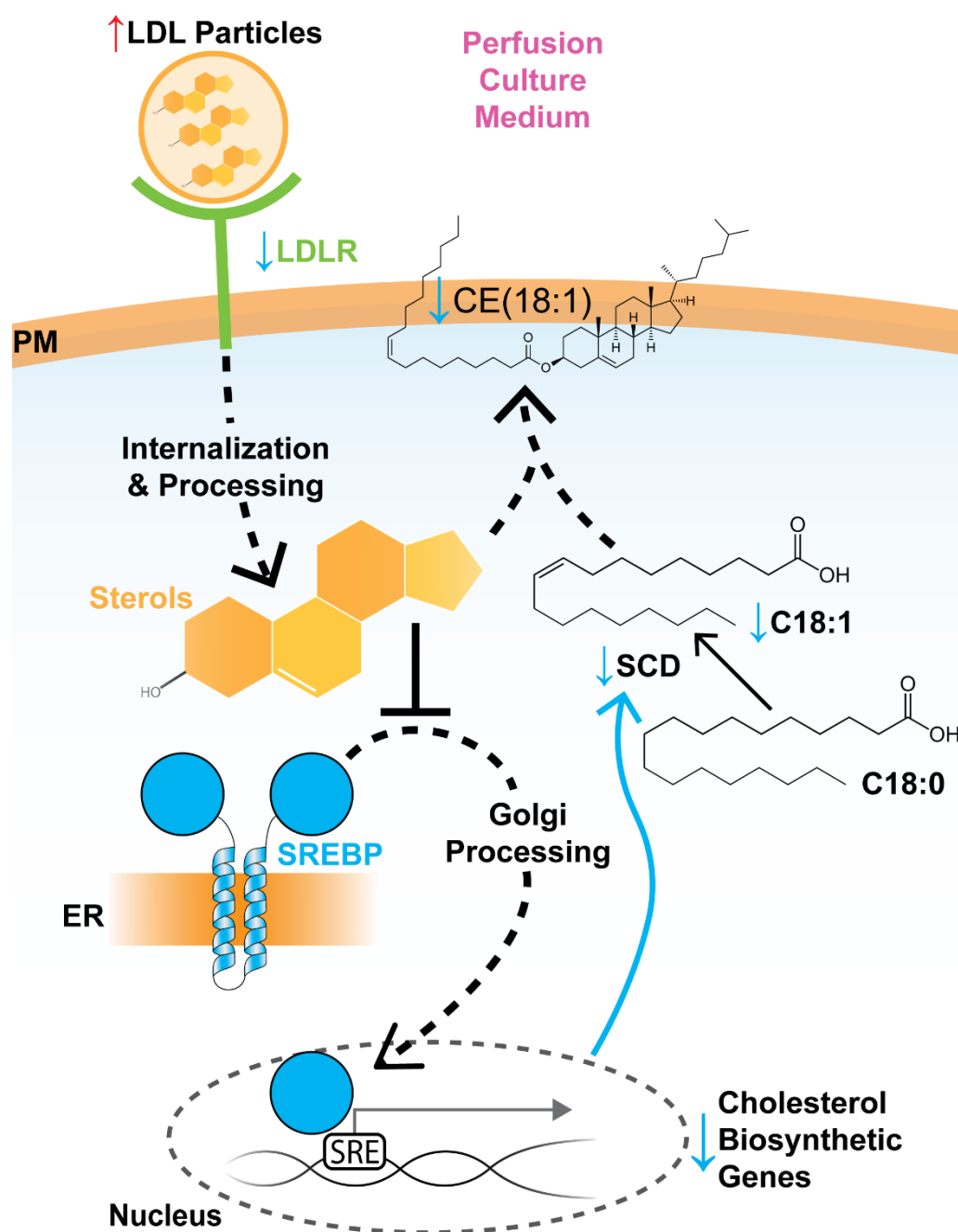


Figure 8: Overview of the effects of perfusion culture on lipid metabolic pathways revolving around cholesterol sensing. Abbreviations: PM (plasma membrane), ER (endoplasmic reticulum), LDLR (low-density lipoprotein receptor), SRE (sterol response element), SCD (stearoyl CoA desaturase), CE (cholesteryl ester).

One complex cellular process at the interface of lipids and selenoprotein function is ferroptosis. This is a relatively newly discovered form of programmed cell death which gets its name from its dependence on iron (Dixon *et al*, 2012). During ferroptosis, liberated ferrous (Fe^{2+}) iron

generates reactive lipid peroxides that can propagate in the presence of oxygen, particularly through PUFAs, leading to the accumulation of membrane damage and cell death (Conrad & Pratt, 2019). GPX4 was one of the first key regulators of ferroptosis to be discovered (Yang *et al*, 2014; Friedmann Angeli *et al*, 2014). It actively suppresses the accumulation of lipid peroxides by catalyzing their reduction using glutathione and its active-site selenocysteine (Ingold *et al*, 2018). Interestingly, subunits of the iron storage protein, ferritin light and heavy chains (FTL1 and FTH1, respectively), were downregulated in both cell lines' proteomics datasets (**Table 2 & 3**). Increased ferritin expression has been shown to increase resistance to ferroptosis (Yang & Stockwell, 2008). Autolytic digestion of ferritin, dependant on *Atg5*, *Atg7*, and *Ncoa4*, can liberate iron and decrease ferritin abundance (Hou *et al*, 2016), although none of these genes were found to be differentially expressed upon perfusion. Ferritin gene *Fth1* and *Ftl1* gene transcripts, were unchanged by perfusion, along with iron responsive protein 1 (*Irp1*), a transcription factor that regulates gene expression in response to iron concentration by binding iron responsive elements (IREs). Expression of several other canonical IRE-containing genes (*Alas2*, *Aco2*, *Hao1*, *Slc11a2*, *Ndufs1*, and *Slc40a1*, for example) were also unchanged following perfusion. Overall, this hints towards protein-level regulation of ferritin, though it's not immediately clear how. We attempted to quantify intracellular iron to see if this correlates with observed changes in ferritin protein expression, but iron levels in both cell lines and conditions were below the detection limit for the method we utilized (Sigma-Aldrich #MAK025) even in exceptionally concentrated lysates. The mechanism and implications of protein-level ferritin down-regulation by perfusion warrant further investigation. The susceptibility of perfused cells to lipid peroxidation would be of particular interest, given the competing results with respect to GPX4 and ferritin expression.

Interestingly, in β TC3 specifically, glycolytic pathway genes were significantly upregulated upon perfusion (**Figure 6B**) including the facilitative glucose transporter *Slc2a1* (also known as GLUT1). Dietary selenium supplementation has been shown to suppress glycolytic gene transcription in white blood cells (Jablonska *et al*, 2016), however, we do not observe differential regulation of *Insr*, *Adipor2*, *Myc*, or *Hif1a* as they did, and rather see a more robust upregulation. Glycolysis can also be induced by hypoxia (Kierans & Taylor, 2021) – and if the nutrient medium were oxygen-deficient due to poor gas diffusion into the media reservoir and tubing, for example, this could create hypoxic conditions in the perfusion plates. However, we would expect poor cell growth and the induction of hypoxia inducible factor 1 α (HIF-1 α), neither of which we observe in our data. Given that perfusion induced increased growth rate in β TC3 specifically, the upregulation of glycolytic pathway genes may be associated with supporting increased proliferation.

We have demonstrated that simply introducing flow into an otherwise identical tissue culture method can have a substantial effect on the metabolic state and composition of cells in culture. This can lead to increased or decreased proliferation as seen here in β TC3 and α TC1-LT, respectively. Increased nutrient availability of perfusion culture increases the translation of selenium-limited selenoproteins and decreases cholesterol biosynthesis, apparently moving cellular lipid composition closer to that of primary tissue. Our data provide evidence that routine culture medium, such as DMEM supplemented with 10% FBS as used in this study, is likely deficient in sources of selenium, lipids, and sterols. Further investigation is required to quantify this, however 48-72h in static culture appears to be long enough to deplete the medium sufficiently to cause differential protein and gene regulation when compared with perfusion culture. We believe the proteomics, RNA-sequencing, and lipid profiling data presented here demonstrates the need for more careful consideration of culture conditions in both static and perfusion culture system and can serve as a valuable resource in tissue engineering works moving forward.

3.2 Conclusions and Outlook

We have successfully developed a novel perfusion culture system and characterized its effects on the adherent endocrine cell lines α TC1-LT and β TC3. The most striking effects of perfusion culture on α TC1-LT and β TC3 were a marked downregulation of lipid metabolic pathways revolving around sterol sensing (**Figure 6**), and a global upregulation of selenoprotein expression (**Figure 5**). Both effects are become apparent within 72 h, which on the same timescale as the interval between media changes in static culture. We attribute these primarily to limited lipid and selenium availability under static culture conditions that is alleviated by the continuous renewal of culture medium in the perfused condition.

In order to test this hypothesis, however, further experiments are required. Direct quantification of medium sterol and selenium content over the course of a typical static culture experiment would be necessary to confirm depletion. Based on our results, we would expect a rapid depletion of low-density lipoprotein and selenoprotein P, primary sources of cholesterol and selenium in sera, respectively, within 72 h of culture under static conditions. Given the diffusive limitation of nutrients in static culture, however, it may be that bulk measurements are insufficient, rather that the local concentrations of these nutrients around the cells in culture are more depleted than the bulk medium. To assess this case, a defined volume of culture medium could be recirculated using the PlateFlo system, rather than continuously introducing fresh media, and sampled regularly for quantification.

It would also be of interest to assess whether recirculation alone is sufficient to induce the effects observed with continuous media renewal, using *Scd1/4* transcripts and GPX1 protein as markers of improved lipid and selenium nutritional status in culture. Utilizing a dual-channel pinch valve controlled with the FETbox system described in 2.1.2, it would also be possible to partially recirculate media while introducing fresh media at a defined proportion. Such a setup could be used to assess the minimum proportion of fresh culture media required for improved feeding of the cells in culture. This would be of particulate benefit in reducing FBS and media consumption, one of the costliest aspects of utilizing the perfusion setup as described in this work. Further optimization of FBS concentration could also prove beneficial in reducing the cost and ecological impact of perfusion culture experiments.

Genetic screening utilizing CRISPR-Cas9 has been used to identify genes as conditionally essential depending on medium composition (Rossiter *et al*, 2021) as well as in hypoxic conditions (Jain *et al*, 2020). We are currently applying genetic screening methods to identify conditionally essential genes in perfusion culture utilizing a targeted library of ~450 guides. 87 of the proteins and genes found to be differentially expressed in perfusion culture, including all of those found to be in common between both cell lines and the top fifteen by fold-change

magnitude in each dataset, were included in the library with four guides each. Thirteen curated genes involved in sterol metabolism and fatty acid biosynthesis were also included in the library with four guides each. Most genes were present in the well established Brie mouse library, and so guides for genes were used directly in this screen (Doench *et al*, 2016) while the remaining guides were designed using the GUIDES tool (Meier *et al*, 2017). Guides for known essential genes and non-targeting control guides were also incorporated in the guide pool. We carried out the screen using the CROP-seq system (Datlinger *et al*, 2017) in α TC1-LT and β TC3 using the conditions outlined in section 4.2. We are currently awaiting sequencing results and hope that they will shed more light on the importance of these genes in perfusion culture.

Overall, we've shown that the dynamic perfusion culture system we've developed is directly compatible with adherent cell lines routinely cultured under static conditions. The range of potential applications for this system, several of which are discussed in the publication in Section 2.1.2, remains to be fully explored. We hope that the tools provided here inspire new and exciting experiments in culture moving forward.

4. MATERIALS & METHODS

All relevant materials and methods pertaining to the published work in section 2.1 are contained therein. Materials and methods pertaining to the unpublished results in section 2.2 are described below.

4.1 Cell Culture

α TC1-LT and β TC3 cell lines were kindly provided by Novo Nordisk. All cells were cultured in low-glucose (1 g/L) Dulbecco's modified Eagle's medium containing stable glutamine and sodium pyruvate (Biowest L0066) supplemented with 10% fetal bovine serum (Gibco 10500064), 50 U/mL penicillin, and 50 μ g/mL streptomycin.

All biological replicates were conducted with cells thawed from common liquid nitrogen aliquot batches in order to avoid passage number variability and allowed to recover for 7-14 days prior to seeding. Following recovery from thawing, cells were trypsinized and live cells were counted using Trypan Blue (0.4%) and an Introgen Countess II (Thermo-Fisher) automated cell counter before seeding onto Nunclon Delta treated Nunc OmniTray single-well plates (Thermo-Fisher 165218). α TC1-LT were seeded at a live cell density of $7.5E5$ cells per plate, and β TC3 were seeded at $1.5E6$ cells per plate to accommodate growth rate differences between the two cell lines.

4.2 Continuous Perfusion Cell Culture

Static control plates and perfusion plates were seeded 48 h prior to starting each perfusion experiment to allow for cells to attach fully as described in the previous section before media was exchanged in both plates at a volume of 10 mL. PlateFlo perfusion plate lids were built as described in Section 2.1.2 with skimmer nozzles set to maintain 10 mL of medium in the plate, then sterilized using 70% EtOH followed by one hour of UV exposure in a tissue culture cabinet. Pump tubing (PharMed BPT, 1.52mm ID; Cole-Parmer 9580936s) was sterilized by autoclaving, connected to the peristaltic pump (4-channel, 8-roller, Ismatec Reglo ICC; Cole-Parmer 7800180) washed with 70% EtOH, then purged and primed with culture medium before connecting to the PlateFlo perfusion plates as in **Figure 4B-C**.

Plates were perfused at a rate of 145 $\mu\text{L}/\text{min}$ on the inlet channel, 120 $\mu\text{L}/\text{min}$ on the outlet channel, and skimmer pumps run at maximum speed for 60 s every 5 min. See Section 2.1.2, sub-section “Hardware Description”, for an explanation of fluid level maintenance using the “skimmer” system.

For five-day experiments, culture media in static control plates was exchanged once after 48-72 h (**Figure 4A**) using media aliquoted from the perfusion reservoir during preparation. Media aliquots for the static culture plates were stored in the incubator along with the perfusion culture plate media reservoir.

$\alpha\text{TC1-LT}$ cells were harvested for proteomics, RNA-seq and lipidomics in parallel using an AllPrep RNA/Protein extraction kit (QIAGEN 80404). The manufacturers protocol was modified for in-plate lysis by increasing the volume of lysis buffer to 600 $\mu\text{L}/\text{plate}$, incubating in the plate for 5 min at room temperature, then scraping using a cell lifter to maximize collection efficiency. 100 μL of this lysate was then processed for lipidomics and FFA analysis. Lysates were split between two RNeasy spin-columns so as not to overload them. The purified RNA and protein fractions were then quantified and submitted for proteomics and RNA-sequencing.

βTC3 cells were initially harvested identically to $\alpha\text{TC1-LT}$, however, despite being processed in parallel with the $\alpha\text{TC1-LT}$ samples, the quality of RNA extracted from all βTC3 samples was too low to warrant submission for sequencing. The protein fraction was however used for proteomics. βTC3 samples harvested for RNA-sequencing were instead lysed directly in the plate using an RNeasy Mini kit (QIAGEN 74106) and four additional biological replicates.

4.3 Automated Cell Imaging and Area Analysis

Cells in Nunc OmniTray plates were imaged using the bright field of an Operetta (Perkin Elmer) automated microscope with a 20x objective. A custom plate profile was defined in the Operetta's Harmony software in order to image the OmniTray plates. The plates were defined using three 'rows' and five 'columns', allowing automated imaging of 15 quadrants across the one-well plates surface. These were inset several millimeters from the edges of the plate. Five fields of view (in an "X" arrangement) and two planes were imaged for each 'well' in order to avoid excessive handling time and cell stress.

Images were processed using CellProfiler 3.0 image processing software (McQuin *et al*, 2018). Briefly, illumination correction was performed on each field-of-view, followed by edge enhancement, and finally primary object identification and subsequent area quantification. The total cell area of each 'well' was used to approximate cell density in that quadrant of the plate, and fold-expansion was calculated for each quadrant relative to images taken just prior to starting the perfusion experiment.

4.4 Western Blotting

α TC1-LT and β TC3 cells were harvested by trypsinization, followed by washing in PBS before being flash frozen in liquid N₂. Thawed pellets were suspended and lysed in RIPA buffer with protease inhibitor cocktail (Roche) for 30 min at 4°C with regular vortexing. The resultant lysate was clarified by centrifugation at 15000 RCF for 10 min at 4°C. The supernatant protein concentrations were determined using Pierce BCA Protein Assay Kit (Thermo-Fisher 23225). Protein concentrations were normalized by dilution with lysis buffer and loaded onto a 12% SDS-polyacrylamide gel after denaturing at 95°C for 5 min in Laemmli buffer. Gels were transfer by electrophoresis to a nitrocellulose membrane (General Electric Healthcare Life Science). Membranes were stained with Ponceau as a loading control and imaged with a ChemiDoc MP imaging system (Bio-Rad). Membranes were blocked using 5% skim milk powder (w/w) in TBS-T for 45 min at room temperature. Membranes were probed using rabbit polyclonal anti-GPX1 (abcam ab22604) diluted 1:1000 in TBS-T (0.2%) with 5% BSA overnight at 4°C. HRP-labelled secondary (Jackson ImmunoResearch) was diluted 1:15000 with TBS-T for 1 h at room temperature. Membranes were then imaged using Clarity ECL Western Blotting Substrate (Bio-Rad) on the ChemiDoc MP (Bio-Rad) imaging system. Bands were quantified using ImageJ software gel analysis tool (Schneider *et al*, 2012).

4.5 RT-qPCR

RNA for RT-qPCR was isolated using the RNeasy Mini kit (QIAGEN 74106) and quantified using a NanoDrop 1000 Spectrophotometer (Thermo-Fisher Scientific). RNA purity was

assessed using A_{260}/A_{280} ratio, with $A_{260}/A_{280} \geq 2$ deemed acceptable. Sample RNA concentrations were normalized by dilution and reverse transcribed using the LunaScript RT SuperMix kit (NEB E3010). Quantitative real-time PCR was performed using a Luna Universal qPCR Master Mix (NEB M3003) on a LightCycler 480 real-time PCR system (Roche). Results were normalized to the β -actin (*Actb*) housekeeping gene and relative expression quantified using the $2^{-\Delta\Delta C_t}$ method. Primer sequences are detailed in **Section 2.2.6 Supplementary Table 6**.

4.6 Proteomics

4.6.1 Sample Preparation

Samples were processed using an adapted single-pot solid-phase-enhanced sample preparation (SP3) methodology published by Hughes et. al. (Hughes *et al*, 2019). In short, equal volumes (125 μ L/ 6250 μ g) of two different kind of paramagnetic carboxylate modified particles (SpeedBeads 45152105050250 and 65152105050250, GE Healthcare, UK) were mixed, washed three times with 250 μ L water and reconstituted to a final concentration of 50 μ g/ μ L with LC-MS grade water (LiChrosolv, MERCK KgaA, Germany). SDS-containing samples from the immunoprecipitation step were reduced with a final concentration of 50 mM DTT and incubated at 60°C for 1 hour. After cooling down to room temperature, reduced cysteines were alkylated with iodoacetamide at a final concentration of 55 mM for 30 min in the dark. For tryptic digestion, 400 μ g of mixed beads were added to reduced and alkylated samples, vortexed gently and incubated for 5 minutes at room temperature. The formed particles-protein complexes were precipitated by addition of acetonitrile to a final concentration of 70% [V/V], mixed briefly before incubating for 18 minutes at room temperature. Particles were then immobilized using a magnetic rack (DynaMag™-2 Magnet, Thermo Scientific, USA) and supernatant discarded. SDS was removed by washing two times with 200 μ L 70% ethanol and one time with 180 μ L 100% acetonitrile. After removal of organic solvent, particles were resuspended in 100 μ L of 50 mM NH_4HCO_3 and samples digested by incubating with 1 μ g of Trypsin overnight at 37°C. Peptides were cleaned up by acidifying the samples to a final concentration of 1% TFA prior to immobilizing the beads on the magnetic rack to perform solid phase extraction of the recovered supernatant using C18 solid phase extraction (SPE) columns (SUM SS18V, NEST group, USA) according to the manufacturer. Peptides were eluted using two times 50 μ L 90% acetonitrile, 100 mM TEAB buffer pH 8.0 and labeled with TMT 6/10-plex™ reagents according to the manufacturer (Pierce, Rockford, IL). After quenching of the labeling reaction, labeled peptides were pooled, organic solvent removed in vacuum concentrator and labelled peptides cleaned via C18 SPE.

4.6.2 Offline Fractionation via RP-HPLC at High pH

Tryptic peptides were re-buffered in 20 mM ammonium formate buffer pH 10, shortly before separation by reversed phase liquid chromatography at pH 10. Peptides were separated into 96 time-based fractions on a Phenomenex column (150 × 2.0 mm Gemini-NX 3 μm C18 110Å, Phenomenex, Torrance, CA, USA) using an Agilent 1200 series HPLC system fitted with a binary pump delivering solvent at 100 μL/min. Acidified fractions were consolidated into 36 fractions via a concatenated strategy described by Wang *et al.* (Wang *et al.*, 2011). After solvent removal in a vacuum concentrator, samples were reconstituted in 5% formic acid for LC-MS/MS analysis and kept at -80°C until analysis.

4.6.3 2D-RP/RP Liquid Chromatography Mass Spectrometry

Mass spectrometry was performed on an Orbitrap Fusion Lumos mass spectrometer (ThermoFisher Scientific, San Jose, CA) coupled to an Dionex Ultimate 3000RSLC nano system (ThermoFisher Scientific, San Jose, CA) via Nanoflex source interface. Tryptic peptides were loaded onto a trap column (Pepmap 100 5μm, 5 × 0.3 mm, ThermoFisher Scientific, San Jose, CA) at a flow rate of 10 μL/min using 2% ACN and 0.1% TFA as loading buffer. After loading, the trap column was switched in-line with a 50 cm, 75 μm inner diameter analytical column (packed in-house with ReproSil-Pur 120 C18-AQ, 3 μm, Dr. Maisch, Ammerbuch-Entringen, Germany). Mobile-phase A consisted of 0.4% formic acid in water and mobile-phase B of 0.4% formic acid in a mix of 90% acetonitrile and 10% water. The flow rate was set to 230 nL/min and a 90 min gradient used (6 to 30% solvent B within 81 min, 30 to 65% solvent B within 8 min and, 65 to 100% solvent B within 1 min, 100% solvent B for 6 min before equilibrating at 6% solvent B for 18 min). Analysis was performed in a data-dependent acquisition mode. Full MS scans were acquired with a scan range of 375 - 1650 m/z in the orbitrap at a resolution of 120,000 (at 200Th). Automatic gain control (AGC) was set to a target of 2×10^5 and a maximum injection time of 50 ms. Precursor ions for MS² analysis were selected using a TopN dependant scan approach with a max cycle time of 3 seconds. MS² spectra were acquired in the orbitrap (FT) at a resolution of 50,000 (at 200 Th). Precursor isolation in the quadrupole was set to 0.5 Da. Higher energy collision induced dissociation (HCD) was used with a normalized collision energy (NCE) of 38%. AGC was set to 1×10^5 with a maximum injection time of 105 ms. Dynamic exclusion for selected ions was 60 s. A single lock mass at *m/z* 445.120024 for recalibration was employed (Olsen *et al.*, 2005). Xcalibur version 4.0.0 and Tune 2.1 were used to operate the instrument.

4.6.4 Data Analysis

Acquired raw data files were processed using the Proteome Discoverer 2.4.1.15 platform, utilizing the Sequest HT database search engine and Percolator validation software node (V3.04) to remove false positives with a false discovery rate (FDR) of 1% on PSM, peptide and protein level under strict conditions. Searches were performed with full tryptic digestion against the mouse SwissProt database v2017.10.25 (25097 sequences plus 298 common contaminants) with up to two miscleavage sites. Oxidation (+15.9949 Da) of methionine and phosphorylation (+79.9660 Da) of serin, threonine and tyrosine were set as variable modification, whilst carbamidomethylation (+57.0214 Da) of cysteine residues and TMT 6-plex labelling of peptide N-termini and lysine residues were set as fixed modifications. For phosphopeptides phosphorylation (+79.9663 Da) of serine, threonine and tyrosine was additionally included as a variable modification. Data was searched with mass tolerances of ± 10 ppm and 0.02 Da on the precursor and fragment ions (HCD), respectively. Results were filtered to include peptide spectrum matches (PSMs) with Sequest HT cross-correlation factor (Xcorr) scores of ≥ 1 and 1% FDR peptide confidence. The ptmRS algorithm was additionally used to validate phosphopeptides with a set score cutoff of 75. PSMs with precursor isolation interference values of $\geq 50\%$ or average TMT-reporter ion signal-to-noise values (S/N) ≤ 10 were excluded from quantitation. Isotopic impurity correction and TMT channel-normalization based on total peptide amount were applied. TMT channel assignment was as follows (C=static control, P=perfused, #=biological replicate): α TC1-LT (126=C1, 127N=P1, 127C=C2, 128N=P2, 128C=C3, 129N=P3, 129C=C4, 130N=P4), β TC3 (126=C1, 127N=P1, 128C=C2, 129N=P2, 130C=C3, 131N=P3). Reporter channel abundances were normalized to equal total peptide signal in each TMT channel.

Normalized protein abundances from the α TC1-LT dataset were fit to a linear model, and empirical Bayes moderated t-statistics used to calculate p-values using Bioconductor limma (3.44.3) (Ritchie *et al*, 2015). p-values were then corrected for false discovery rate using the qvalue R package (2.20.0) (Storey *et al*, 2020). For the β TC3 dataset, protein abundance ratios were calculated directly from grouped protein TMT abundance values and \log_2 transformed. For statistical analysis, p-value calculation, and FDR-corrected p-value calculation, the integrated ANOVA hypothesis test in Proteome Discoverer was used.

For ontology enrichment analysis, the Bioconductor EnrichR package (3.0) (Jawaid, 2021) was used to query multiple databases for exploratory data analysis, including the WikiPathways 2019 mouse database (Martens *et al*, 2021). Significantly enriched pathways were selected as those containing at least two genes and an FDR-corrected p-value of < 0.05 .

The Enrichr combined score was used for plotting purposes only, and a negative factor applied to pathways enriched for in down-regulated hits.

4.7 RNA-Sequencing

4.7.1 NGS Library Preparation.

The amount of total RNA was quantified using the Qubit 2.0 Fluorometric Quantitation system (Thermo Fisher Scientific, Waltham, MA, USA) and the RNA integrity number (RIN) was determined using the Experion Automated Electrophoresis System (Bio-Rad, Hercules, CA, USA). RNA-seq libraries were prepared with the TruSeq Stranded mRNA LT sample preparation kit (Illumina, San Diego, CA, USA) using Sciclone and Zephyr liquid handling workstations (PerkinElmer, Waltham, MA, USA) for pre- and post-PCR steps, respectively. Library concentrations were quantified with the Qubit 2.0 Fluorometric Quantitation system (Life Technologies, Carlsbad, CA, USA) and the size distribution was assessed using the Experion Automated Electrophoresis System (Bio-Rad, Hercules, CA, USA). For sequencing, samples were diluted and pooled into NGS libraries in equimolar amounts.

4.7.2 Next-Generation Sequencing and Raw Data Acquisition.

Expression profiling libraries were sequenced on HiSeq 3000/4000 instruments (Illumina, San Diego, CA, USA) following a 50-base-pair, single-end recipe. Raw data acquisition (HiSeq Control Software, HCS, HD 3.4.0.38) and base calling (Real-Time Analysis Software, RTA, 2.7.7) was performed on-instrument, while the subsequent raw data processing off the instruments involved two custom programs based on Picard tools (2.19.2) (epigen/picard, 2021). In a first step, base calls were converted into lane-specific, multiplexed, unaligned BAM files suitable for long-term archival (IlluminaBasecallsToMultiplexSam, 2.19.2-CeMM). In a second step, archive BAM files were demultiplexed into sample-specific, unaligned BAM files (IlluminaSamDemux, 2.19.2-CeMM).

4.7.3 Data Analysis

NGS reads were mapped to the Genome Reference Consortium GRCm38 assembly via “Spliced Transcripts Alignment to a Reference” (STAR) (Dobin *et al*, 2013) utilising the “basic” Ensembl transcript annotation from version e100 (April 2020) as reference transcriptome. Since the mm10 assembly flavour of the UCSC Genome Browser was preferred for downstream data processing with Bioconductor packages for entirely technical reasons, Ensembl transcript annotation had to be adjusted to UCSC Genome Browser sequence region names. STAR was run with options recommended by the ENCODE project. Aligned NGS reads overlapping Ensembl transcript features were counted with the

Bioconductor (3.11) GenomicAlignments (1.24.0) package via the summarizeOverlaps function in Union mode, taking into account that the Illumina TruSeq stranded mRNA protocol leads to sequencing of the first strand so that all reads needed inverting before counting. Transcript-level counts were aggregated to gene-level counts and the Bioconductor DESeq2 (1.28.1) package (Love *et al*, 2014) was used to test for differential expression based on a model using the negative binomial distribution.

An initial exploratory analysis included principal component analysis (PCA), multi-dimensional scaling (MDS), sample distance and expression heatmap plots, all annotated with variables used in the expression modelling (ggplot2, 3.3.2, and Bioconductor ComplexHeatmap, 2.4.3) (Wickham, 2016; Gu *et al*, 2016), as well as volcano plots (Bioconductor EnhancedVolcano, 1.6.0)(Blighe, 2021). Biologically meaningful results were extracted from the model, log₂-fold values were shrunk with the CRAN ashR (2.2.-47) package (Stephens, 2017), while two-tailed p-values obtained from Wald testing were adjusted with the Bioconductor Independent Hypothesis Weighting (IHW, 1.16.0) package(Ignatiadis *et al*, 2016). The resulting gene lists were annotated, filtered for significantly differentially up- and down-regulated genes and independently subjected to gene set enrichment analysis (Enrichr)(Xie *et al*, 2021).

One biological replicate in αTC1-LT was omitted from analysis on the grounds of having an exceptionally low read count in the perfused condition (**Supplementary Figure S3**).

4.8 Free Fatty Acid Quantification

A derivatization procedure followed by LC-MS analysis was employed for the absolute quantification of free fatty acids in cell extracts. 10 µL of cell lysate was mixed with 20 µL of isotopically labelled internal standard mixture and 20 µL of acetonitrile were added. The derivatization was performed by adding 20 µL of 5 mM 2-hyrazinoquinoline, 20 µL of 5 mM triphenylphosphine and 20 µL of 5mM 2,2'-dipyridyldisulfide. Samples were incubated at 60 °C for 2 hours. The derivatization was stopped by putting the samples on ice and adding 100 µL water. After centrifugation the supernatant was used for LC-MS analysis. A Vanquish™ UHPLC system (Thermo Fisher Scientific) coupled to an Orbitrap Fusion™ Lumos™ Tribrid™ mass spectrometer (Thermo Fisher Scientific) was used for LC-MS analysis. The chromatographic system was equipped with an Accucore C18 column, 2.6 µm, 150 x 2.1 mm inclusive a precolumn (Thermo Fisher Scientific) maintained at 50 °C. The separation was carried out using 0.15 % formic acid (v/v) with 10 mM ammonium formate in water as mobile phase A and 88 % (v/v) isopropanol 10 % (v/v) acetonitrile, 0.10 % (v/v) formic acid with 10 mM ammonium formate as mobile phase B at a flow rate of 0.4 mL/min. For elution of analytes the gradient of mobile phase B was applied with the total analysis time of 20 min. Sample

injection volume was set to 2 μL . The mass spectrometer was operated in a positive electrospray ionization mode: spray voltage 3.5 kV; sheath gas flow rate 60 arb; auxiliary gas flow rate 20 arb; capillary temperature 285 $^{\circ}\text{C}$. For the analysis a full MS scan mode with a scan range m/z 150 to 520, resolution 120000, AGC target $2e5$ and a maximum injection time 50 ms was applied. A ten-point linear calibration curve with internal standardization and $1/x$ weighing was constructed for the quantification of the metabolites. The data processing was performed using the TraceFinder™ 4.1 software (Thermo Fisher Scientific). Fatty acids detected in all samples of one condition but in none of the other were considered specially – the abundance of the non-detected samples in this set were set to the limit of quantification for that species in order to calculate fold-changes. Statistical significance was calculated using pairwise two-tailed Student's t-test. A fold change cut-off of 1.5 fold and p -value of less than 0.05 were used to determine significance.

4.9 Semi-Quantitative Untargeted Lipidomics

4.9.1 Sample Preparation

50 μL of cell lysate was transferred into a glass vial, 10 μL internal standard solution (SPLASH® Lipidomix®, Avanti Polar Lipids) and 140 μL methanol were added. After vortexing, 500 μL MTBE were added and the mixture was incubated in a shaker for 10 min at room temperature. Phase separation was induced by adding 100 μL MS-grade water. After 10 min of incubation at room temperature, the samples were centrifuged at 1000 $\times g$ for 10min. An aliquot of 450 μL of the upper phase (organic) was collected and dried under nitrogen using a MiniVap™ (Porvair Sciences). The samples were reconstituted in 200 μL methanol and used for LCMS analysis.

4.9.2 LC-MS

The LC-MS analysis was performed using a Vanquish™ UHPLC system (Thermo Fisher Scientific) combined with an Orbitrap Fusion™ Lumos™ Tribrid™ mass spectrometer (Thermo Fisher Scientific). Lipid separation was performed by reversed phase chromatography employing an Accucore C18, 2.6 μm , 150 \times 2 mm (Thermo Fisher Scientific) analytical column at a column temperature of 35 $^{\circ}\text{C}$. As mobile phase A an acetonitrile/water (50/50, v/v) solution containing 10 mM ammonium formate and 0.1 % formic acid was used. Mobile phase B consisted of acetonitrile/isopropanol/water (10/88/2, v/v/v) containing 10 mM ammonium formate and 0.1% formic acid. The flow rate was set to 400 $\mu\text{L}/\text{min}$. A gradient of mobile phase B was applied to ensure optimal separation of the analysed lipid species. The mass spectrometer was operated in ESI-positive and -negative mode, capillary voltage 3500 V (positive) and 3000 V (negative), vaporize temperature 320 $^{\circ}\text{C}$, ion transfer tube temperature

285 °C, sheath gas 60 arbitrary units, aux gas 20 arbitrary units and sweep gas 1 arbitrary unit. Orbitrap MS scan mode at 120000 mass resolution was employed for lipid detection. The scan range was set to 250-1200 m/z for both positive and negative ionization mode, the AGC target was set to 2.0e5 and the intensity threshold to 5.0e3. The data analysis was performed using the TraceFinder™ 4.1 software (Thermo Fisher Scientific).

4.9.3 Data Analysis

Lipid species abundances were normalized to the sample mean. Lipids quantified in all samples of one condition but in none of the other were considered specially – the abundance of the non-detected samples in this set were set to the estimated limit of quantification for that species. Statistical significance was calculated using pairwise two-tailed Student's t-test. t-test *p*-values were adjusted using Benjamini-Hochberg (aka FDR) correction for multiple testing. A 1.5-fold change in normalized mean abundance and a *q*-value of less than 0.05 were used set as criteria for significance of hits. Lipid species were labelled according to the LIPID MAPS classification system (Liebisch *et al*, 2020). Heatmaps were generated using ComplexHeatmaps for R (Gu *et al*, 2016).

5. REFERENCES

- Arda HE, Li L, Tsai J, Torre EA, Rosli Y, Peiris H, Spitale RC, Dai C, Gu X, Qu K, *et al* (2016) Age-Dependent Pancreatic Gene Regulation Reveals Mechanisms Governing Human β Cell Function. *Cell Metab* 23: 909–920
- Asfari M, Janjic D, Meda P, Li G, Halban PA & Wollheim CB (1992) Establishment of 2-mercaptoethanol-dependent differentiated insulin-secreting cell lines. *Endocrinology* 130: 167–178
- Baker LE (1929) The Chemical Nature of the Substances Required for Cell Multiplication. *J Exp Med* 49: 163–182
- Baker LE (1936) Artificial Media for the Cultivation of Fibroblasts, Epithelial Cells and Monocytes. *Science* 83: 605–606
- Baker LE & Carrel A (1926a) Effect of the Amino Acids and Dialyzable Constituents of Embryonic Tissue Juice on the Growth of Fibroblasts. *J Exp Med* 44: 397–407
- Baker LE & Carrel A (1926b) Action on Fibroblasts of the Protein Fraction of Embryonic Tissue Extract. *J Exp Med* 44: 387–395
- Baker LE & Carrel A (1928) The Effect of Digests of Pure Proteins on Cell Proliferation. *J Exp Med* 47: 353–370
- Baker RDJ, Baker SS & Rao R (1998) Selenium Deficiency in Tissue Culture: Implications for Oxidative Metabolism. *J Pediatr Gastroenterol Nutr* 27: 387–392
- Bakhti M, Böttcher A & Lickert H (2019) Modelling the endocrine pancreas in health and disease. *Nat Rev Endocrinol* 15: 155–171
- Barati G, Nadri S, Hajian R, Rahmani A, Mostafavi H, Mortazavi Y & Taramchi AH (2019) Differentiation of microfluidic-encapsulated trabecular meshwork mesenchymal stem cells into insulin producing cells and their impact on diabetic rats. *J Cell Physiol* 234: 6801–6809
- Bernard AB, Lin C-C & Anseth KS (2012) A Microwell Cell Culture Platform for the Aggregation of Pancreatic β -Cells. *Tissue Eng Part C Methods* 18: 583–592
- Bertram R & Pernarowski M (1998) Glucose Diffusion in Pancreatic Islets of Langerhans. *Biophys J* 74: 1722–1731
- Bevacqua RJ, Dai X, Lam JY, Gu X, Friedlander MSH, Tellez K, Miguel-Escalada I, Bonàs-Guarch S, Atla G, Zhao W, *et al* (2021) CRISPR-based genome editing in primary human pancreatic islet cells. *Nat Commun* 12: 2397
- Bhattarai A, Likos EM, Weyman CM & Shukla GC (2021) Regulation of cholesterol biosynthesis and lipid metabolism: A microRNA management perspective. *Steroids* 173: 108878
- Blighe K (2021) EnhancedVolcano: publication-ready volcano plots with enhanced colouring and labeling

- Bottino R, Balamurugan AN, Tse H, Thirunavukkarasu C, Ge X, Profozich J, Milton M, Ziegenfuss A, Trucco M & Piganelli JD (2004) Response of Human Islets to Isolation Stress and the Effect of Antioxidant Treatment. *Diabetes* 53: 2559–2568
- Bou-Ghannam S, Kim K, Grainger DW & Okano T (2021) 3D cell sheet structure augments mesenchymal stem cell cytokine production. *Sci Rep* 11: 8170
- Brindley DA, Davie NL, Culme-Seymour EJ, Mason C, Smith DW & Rowley JA (2012) Peak serum: implications of serum supply for cell therapy manufacturing. *Regen Med* 7: 7–13
- Brissova M, Fowler MJ, Nicholson WE, Chu A, Hirshberg B, Harlan DM & Powers AC (2005) Assessment of Human Pancreatic Islet Architecture and Composition by Laser Scanning Confocal Microscopy. *J Histochem Cytochem* 53: 1087–1097
- Burrows MT (1910) The Cultivation of Tissues of the Chick-Embryo Outside the Body. *J Am Med Assoc* 55: 2057–2058
- Campbell JE & Newgard CB (2021) Mechanisms controlling pancreatic islet cell function in insulin secretion. *Nat Rev Mol Cell Biol*: 1–17
- Carrel A (1912) On the Permanent Life of Tissues Outside of the Organism. *J Exp Med* 15: 516–528
- Carrel A (1913a) Artificial Activation of the Growth in Vitro of Connective Tissue. *J Exp Med* 17: 14–19
- Carrel A (1913b) Contributions to the Study of the Mechanism of the Growth of Connective Tissue. *J Exp Med* 18: 287–298
- Carrel A (1923) A Method for the Physiological Study of Tissues in Vitro. *J Exp Med* 38: 407–418
- Carrel A & Burrows MT (1910) Cultivation of Sarcoma Outside of the Body: A Second Note. *J Am Med Assoc* 55: 1554–1554
- Carrel A & Burrows MT (1911a) Cultivation of Tissues in Vitro and Its Technique. *J Exp Med* 13: 387–396
- Carrel A & Burrows MT (1911b) An Addition to the Technique of the Cultivation of Tissues in Vitro. *J Exp Med* 14: 244–247
- Carrel A & Ebeling A (1924) Indice de croissance du serum sanguin. *Compt Rend Soc Biol* 90: 170
- Carrel A & Lindbergh CA (1935) The Culture of Whole Organs. *Science* 81: 621–623
- Chen J, Zhang X, Li L, Ma X, Yang C, Liu Z, Li C, Fernandez-Cabezudo MJ, al-Ramadi BK, Wu C, *et al* (2021) Farnesyl pyrophosphate is a new danger signal inducing acute cell death. *PLOS Biol* 19: e3001134
- Cheng HW, Yuan MT, Li CW & Chan BP (2020) Cell-derived matrices (CDM)—Methods, challenges and applications. In *Methods in Cell Biology* pp 235–258. Elsevier

- Cheng K, Delghingaro-Augusto V, Nolan CJ, Turner N, Hallahan N, Andrikopoulos S & Gunton JE (2012) High Passage MIN6 Cells Have Impaired Insulin Secretion with Impaired Glucose and Lipid Oxidation. *PLOS ONE* 7: e40868
- Choi YY, Chung BG, Lee DH, Khademhosseini A, Kim J-H & Lee S-H (2010) Controlled-size embryoid body formation in concave microwell arrays. *Biomaterials* 31: 4296–4303
- Coecke S, Balls M, Bowe G, Davis J, Gstraunthaler G, Hartung T, Hay R, Merten O-W, Price A, Schechtman L, *et al* (2005) Guidance on Good Cell Culture Practice: A Report of the Second ECVAM Task Force on Good Cell Culture Practice. *Altern Lab Anim* 33: 261–287
- Conrad M & Pratt DA (2019) The chemical basis of ferroptosis. *Nat Chem Biol* 15: 1137–1147
- Cox AG, Tsomides A, Kim AJ, Saunders D, Hwang KL, Evason KJ, Heidel J, Brown KK, Yuan M, Lien EC, *et al* (2016) Selenoprotein H is an essential regulator of redox homeostasis that cooperates with p53 in development and tumorigenesis. *Proc Natl Acad Sci* 113: E5562–E5571
- Das A, Brown MS, Anderson DD, Goldstein JL & Radhakrishnan A (2014) Three pools of plasma membrane cholesterol and their relation to cholesterol homeostasis. *eLife* 3: e02882
- Datlinger P, Rendeiro AF, Schmidl C, Krausgruber T, Traxler P, Klughammer J, Schuster LC, Kuchler A, Alpar D & Bock C (2017) Pooled CRISPR screening with single-cell transcriptome readout. *Nat Methods* 14: 297–301
- Davis JC, Alves TC, Helman A, Chen JC, Kenty JH, Cardone RL, Liu DR, Kibbey RG & Melton DA (2020) Glucose Response by Stem Cell-Derived β Cells In Vitro Is Inhibited by a Bottleneck in Glycolysis. *Cell Rep* 31: 107623
- Delplanque B & Jacotot B (1987) Influence of environmental medium on fatty acid composition of human cells: Leukocytes and fibroblasts. *Lipids* 22: 241–249
- Discher DE (2005) Tissue Cells Feel and Respond to the Stiffness of Their Substrate. *Science* 310: 1139–1143
- Dixon SJ, Lemberg KM, Lamprecht MR, Skouta R, Zaitsev EM, Gleason CE, Patel DN, Bauer AJ, Cantley AM, Yang WS, *et al* (2012) Ferroptosis: An Iron-Dependent Form of Nonapoptotic Cell Death. *Cell* 149: 1060–1072
- Dobin A, Davis CA, Schlesinger F, Drenkow J, Zaleski C, Jha S, Batut P, Chaisson M & Gingeras TR (2013) STAR: ultrafast universal RNA-seq aligner. *Bioinforma Oxf Engl* 29: 15–21
- Doench JG, Fusi N, Sullender M, Hegde M, Vaimberg EW, Donovan KF, Smith I, Tothova Z, Wilen C, Orchard R, *et al* (2016) Optimized sgRNA design to maximize activity and minimize off-target effects of CRISPR-Cas9. *Nat Biotechnol* 34: 184–191
- Drew JE, Farquharson AJ, Vase H, Carey FA, Steele RJC, Ross RA & Bunton DC (2015) Molecular Profiling of Multiplexed Gene Markers to Assess Viability of *Ex Vivo* Human Colon Explant Cultures. *BioResearch Open Access* 4: 425–430
- Dulbecco R & Freeman G (1959) Plaque production by the polyoma virus. *Virology* 8: 396–397

- Eagle H (1955a) The Specific Amino Acid Requirements of a Human Carcinoma Cell (strain Hela) in Tissue Culture. *J Exp Med* 102: 37–48
- Eagle H (1955b) The Specific Amino Acid Requirements of a Mammalian Cell (strain L) in Tissue Culture. *J Biol Chem* 214: 839–852
- Eagle H (1959) Amino Acid Metabolism in Mammalian Cell Cultures. *Sci New Ser* 130: 432–437
- Earle W (1943) Production of malignancy in vitro. IV. The mouse fibroblast cultures and changes seen in the living cells. *J Natl Cancer Inst* 4: 165–212
- Eaton WJ & Roper MG (2021) A microfluidic system for monitoring glucagon secretion from human pancreatic islets of Langerhans. *Anal Methods Adv Methods Appl* 13: 3614–3619
- Ebeling AH (1922) A Ten Year Old Strain of Fibroblasts. *J Exp Med* 35: 755–759
- Efrat S (2004) Regulation of Insulin Secretion: Insights from Engineered β -cell Lines. *Ann N Y Acad Sci* 1014: 88–96
- Efrat S, Linde S, Kofod H, Spector D, Delannoy M, Grant S, Hanahan D & Baekkeskov S (1988) Beta-cell lines derived from transgenic mice expressing a hybrid insulin gene- oncogene. *Proc Natl Acad Sci* 85: 9037–9041
- Efrat S, Surana M & Fleischer N (1991) Glucose induces insulin gene transcription in a murine pancreatic beta-cell line. *J Biol Chem* 266: 11141–11143
- Else PL (2020) The highly unnatural fatty acid profile of cells in culture. *Prog Lipid Res* 77: 101017
- epigen/picard (2021) Computational Epigenetics
- Erickson P, Houwayek T, Burr A, Teryek M & Parekkadan B (2021) A continuous flow cell culture system for precision cell stimulation and time-resolved profiling of cell secretion. *Anal Biochem* 625: 114213
- Esquejo RM, Roqueta-Rivera M, Shao W, Phelan PE, Seneviratne U, am Ende CW, Hershberger PM, Machamer CE, Espenshade PJ & Osborne TF (2021) Dipyrindamole Inhibits Lipogenic Gene Expression by Retaining SCAP-SREBP in the Endoplasmic Reticulum. *Cell Chem Biol* 28: 169-179.e7
- Essaouiba A, Jellali R, Shinohara M, Scheidecker B, Legallais C, Sakai Y & Leclerc E (2021) Analysis of the behavior of 2D monolayers and 3D spheroid human pancreatic beta cells derived from induced pluripotent stem cells in a microfluidic environment. *J Biotechnol* 330: 45–56
- Fischer A (1941) The Nature of the Growth-Promoting Substances in the Embryonic Tissue Juice. *Acta Physiol Scand* 3: 54–70
- Fischer A (1948) Amino-acid metabolism of tissue cells in vitro. *Biochem J* 43: 491–497
- Fletcher DJ (1981) Characterization of proinsulin- and proglucagon-converting activities in isolated islet secretory granules. *J Cell Biol* 90: 312–322

- Fomina-Yadlin D, Kubicek S, Walpita D, Dančik V, Hecksher-Sørensen J, Bittker JA, Sharifnia T, Shamji A, Clemons PA, Wagner BK, *et al* (2010) Small-molecule inducers of insulin expression in pancreatic α -cells. *Proc Natl Acad Sci* 107: 15099–15104
- Fraczek J, Bolleyn J, Vanhaecke T, Rogiers V & Vinken M (2013) Primary hepatocyte cultures for pharmaco-toxicological studies: at the busy crossroad of various anti-dedifferentiation strategies. *Arch Toxicol* 87: 577–610
- Friedlander MSH, Nguyen VM, Kim SK & Bevacqua RJ (2021) Pancreatic Pseudoislets: An Organoid Archetype for Metabolism Research. *Diabetes* 70: 1051–1060
- Friedmann Angeli JP, Schneider M, Proneth B, Tyurina YY, Tyurin VA, Hammond VJ, Herbach N, Aichler M, Walch A, Eggenhofer E, *et al* (2014) Inactivation of the ferroptosis regulator Gpx4 triggers acute renal failure in mice. *Nat Cell Biol* 16: 1180–1191
- Gao Y, Feng HC, Walder K, Bolton K, Sunderland T, Bishara N, Quick M, Kantham L & Collier GR (2004) Regulation of the selenoprotein Sels by glucose deprivation and endoplasmic reticulum stress - Sels is a novel glucose-regulated protein. *FEBS Lett* 563: 185–190
- Gartler SM (1968) Apparent HeLa Cell Contamination of Human Heteroploid Cell Lines. *Nature* 217: 750–751
- Gerlach JC, Hout M, Edsbagge J, Björquist P, Lübberstedt M, Miki T, Stachelscheid H, Schmelzer E, Schatten G & Zeilinger K (2010) Dynamic 3D Culture Promotes Spontaneous Embryonic Stem Cell Differentiation *In Vitro*. *Tissue Eng Part C Methods* 16: 115–121
- Gey G, Coffman, WD, & Kubicek, MT (1952) Tissue culture studies of the proliferative capacity of cervical carcinoma and normal epithelium. *Cancer Res* 12: 264–265
- Giuliani M, Moritz W, Bodmer E, Dindo D, Kugelmeier P, Lehmann R, Gassmann M, Groscurth P & Weber M (2005) Central Necrosis in Isolated Hypoxic Human Pancreatic Islets: Evidence for Postisolation Ischemia. *Cell Transplant* 14: 67–76
- Glieberman AL, Pope BD, Zimmerman JF, Liu Q, Ferrier JP, Kenty JHR, Schrell AM, Mukhitov N, Shores KL, Tepole AB, *et al* (2019) Synchronized stimulation and continuous insulin sensing in a microfluidic human Islet on a Chip designed for scalable manufacturing. *Lab Chip* 19: 2993–3010
- Green AD, Vasu S & Flatt PR (2018) Cellular models for beta-cell function and diabetes gene therapy. *Acta Physiol* 222: e13012
- Gu Z, Eils R & Schlesner M (2016) Complex heatmaps reveal patterns and correlations in multidimensional genomic data. *Bioinformatics* 32: 2847–2849
- Halban PA, Powers SL, George KL & Bonner-Weir S (1987) Spontaneous Reassociation of Dispersed Adult Rat Pancreatic Islet Cells Into Aggregates With Three-Dimensional Architecture Typical of Native Islets. 36: 8
- Halldorsson S, Lucumi E, Gómez-Sjöberg R & Fleming RMT (2015) Advantages and challenges of microfluidic cell culture in polydimethylsiloxane devices. *Biosens Bioelectron* 63: 218–231

- Hamaguchi K, Gaskins HR & Leiter EH (1991) NIT-1, a pancreatic beta-cell line established from a transgenic NOD/Lt mouse. *Diabetes* 40: 842–849
- Hamaguchi K & Leiter EH (1990) Comparison of cytokine effects on mouse pancreatic alpha-cell and beta-cell lines. Viability, secretory function, and MHC antigen expression. *Diabetes* 39: 415–425
- Hanahan D & Weinberg RA (2000) The hallmarks of cancer. *cell* 100: 57–70
- Hanahan D & Weinberg RA (2011) Hallmarks of Cancer: The Next Generation. *Cell* 144: 646–674
- Hariharan S & Dharmaraj S (2020) Selenium and selenoproteins: it's role in regulation of inflammation. *Inflammopharmacology*: 1–29
- Harrison RG, Greenman MJ, Mall FP & Jackson CM (1907) Observations of the living developing nerve fiber. *Anat Rec* 1: 116–128
- Hatfield DL, Tsuji PA, Carlson BA & Gladyshev VN (2014) Selenium and selenocysteine: roles in cancer, health, and development. *Trends Biochem Sci* 39: 112–120
- Hayavi S & Halbert GW (2005) Synthetic Low-Density Lipoprotein, a Novel Biomimetic Lipid Supplement for Serum-Free Tissue Culture. *Biotechnol Prog* 21: 1262–1268
- Hayflick L (1998) A Brief History of the Mortality and Immortality of Cultured Cells. *Keio J Med* 47: 174–182
- Hayflick L & Moorhead PS (1961) The serial cultivation of human diploid cell strains. *Exp Cell Res* 25: 585–621
- Hilderink J, Spijker S, Carlotti F, Lange L, Engelse M, van Blitterswijk C, de Koning E, Karperien M & van Apeldoorn A (2015) Controlled aggregation of primary human pancreatic islet cells leads to glucose-responsive pseudoislets comparable to native islets. *J Cell Mol Med* 19: 1836–1846
- Holman RT (1998) The Slow Discovery of the Importance of ω 3 Essential Fatty Acids in Human Health. *J Nutr* 128: 427S–433S
- Holmes FL (1993) The old martyr of science: The frog in experimental physiology. *J Hist Biol* 26: 311–328
- Horton JD, Goldstein JL & Brown MS (2002) SREBPs: activators of the complete program of cholesterol and fatty acid synthesis in the liver. *J Clin Invest* 109: 1125–1131
- Hou W, Xie Y, Song X, Sun X, Lotze MT, Zeh HJ, Kang R & Tang D (2016) Autophagy promotes ferroptosis by degradation of ferritin. *Autophagy* 12: 1425–1428
- Howard MT, Carlson BA, Anderson CB & Hatfield DL (2013) Translational redefinition of UGA codons is regulated by selenium availability. *J Biol Chem* 288: 19401–19413
- Huff M & Telford D (2005) Lord of the rings – the mechanism for oxidosqualene:lanosterol cyclase becomes crystal clear. *Trends Pharmacol Sci* 26: 335–340
- Hughes CS, Moggridge S, Müller T, Sorensen PH, Morin GB & Krijgsveld J (2019) Single-pot, solid-phase-enhanced sample preparation for proteomics experiments. *Nat Protoc* 14: 68–85

- Hughes DL, Hughes A, Soonawalla Z, Mukherjee S & O'Neill E (2021) Dynamic Physiological Culture of Ex Vivo Human Tissue: A Systematic Review. *Cancers* 13: 2870
- Hwang JW, Lee BR, Jung MJ, Jung HS, Hwang YH, Kim MJ, Lee SH & Lee DY (2011) Functional clustering of pancreatic islet cells using concave microwell array. *Macromol Res* 19: 1320–1326
- Ichihara Y, Utoh R, Yamada M, Shimizu T & Uchigata Y (2016) Size effect of engineered islets prepared using microfabricated wells on islet cell function and arrangement. *Heliyon* 2: e00129
- Ignatiadis N, Klaus B, Zaugg JB & Huber W (2016) Data-driven hypothesis weighting increases detection power in genome-scale multiple testing. *Nat Methods* 13: 577–580
- Ikonen E (2008) Cellular cholesterol trafficking and compartmentalization. *Nat Rev Mol Cell Biol* 9: 125–138
- Ingold I, Berndt C, Schmitt S, Doll S, Poschmann G, Buday K, Roveri A, Peng X, Porto Freitas F, Seibt T, *et al* (2018) Selenium Utilization by GPX4 Is Required to Prevent Hydroperoxide-Induced Ferroptosis. *Cell* 172: 409-422.e21
- In't Veld P & Marichal M (2010) Microscopic Anatomy of the Human Islet of Langerhans. In *The Islets of Langerhans*, Islam MdS (ed) pp 1–19. Dordrecht: Springer Netherlands
- Jablonska E, Reszka E, Gromadzinska J, Wieczorek E, Krol MB, Raimondi S, Socha K, Borawska MH & Wasowicz W (2016) The Effect of Selenium Supplementation on Glucose Homeostasis and the Expression of Genes Related to Glucose Metabolism. *Nutrients* 8: 772
- Jacoby F & Darke SJ (1948) Animal Tissue Culture with a Synthetic Medium. *Nature* 161: 768–769
- Jain IH, Calvo SE, Markhard AL, Skinner OS, To T-L, Ast T & Mootha VK (2020) Genetic Screen for Cell Fitness in High or Low Oxygen Highlights Mitochondrial and Lipid Metabolism. *Cell* 181: 716-727.e11
- Jawaid W (2021) enrichR: Provides an R Interface to 'Enrichr'
- Jayaprakash IJ and NS (2021) Trends in Monoclonal Antibody Production Using Various Bioreactor Systems. 31: 349–357
- Jensen AB (1948) Animal Tissue Cells in Protein-Free Media. *Nature* 161: 273–273
- Jeong HJ, Lee H-S, Kim K-S, Kim Y-K, Yoon D & Park SW (2008) Sterol-dependent regulation of proprotein convertase subtilisin/kexin type 9 expression by sterol-regulatory element binding protein-2 β . *J Lipid Res* 49: 399–409
- Jochems CEA, van der Valk JBF, Stafleu FR & Baumans V (2002) The Use of Fetal Bovine Serum: Ethical or Scientific Problem? *Altern Lab Anim* 30: 219–227
- Jun Y, Lee J, Choi S, Yang JH, Sander M, Chung S & Lee S-H (2019) In vivo–mimicking microfluidic perfusion culture of pancreatic islet spheroids. *Sci Adv* 5: eaax4520
- Katakura Y, Alam S & Shirahata S Immortalization by Gene Transfection. 23

- Kierans SJ & Taylor CT (2021) Regulation of glycolysis by the hypoxia-inducible factor (HIF): implications for cellular physiology. *J Physiol* 599: 23–37
- Kim Y-S, Asif A, Chethikkattuveli Salih AR, Lee J-W, Hyun K-N & Choi K-H (2021) Gravity-Based Flow Efficient Perfusion Culture System for Spheroids Mimicking Liver Inflammation. *Biomedicines* 9: 1369
- Kimmel J, Hayden L & Pollock H (1975) Isolation and characterization of a new pancreatic polypeptide hormone. *J Biol Chem* 250: 9369–9376
- Kryukov GV, Castellano S, Novoselov SV, Lobanov AV, Zehtab O, Guigó R & Gladyshev VN (2003) Characterization of Mammalian Selenoproteomes. *Science* 300: 1439–1443
- Lambert RA & Hanes FM (1911) The Cultivation of Tissue in Plasma from Alien Species. *J Exp Med* 14: 129–138
- Lawlor N, Youn A, Kursawe R, Ucar D & Stitzel ML (2017) Alpha TC1 and Beta-TC-6 genomic profiling uncovers both shared and distinct transcriptional regulatory features with their primary islet counterparts. *Sci Rep* 7: 11959
- Lee PJ, Hung PJ, Rao VM & Lee LP (2006) Nanoliter scale microreactor array for quantitative cell biology. *Biotechnol Bioeng* 94: 5–14
- Lee YN, Yi HJ, Goh H, Park JY, Ferber S, Shim IK & Kim SC (2020) Spheroid Fabrication Using Concave Microwells Enhances the Differentiation Efficacy and Function of Insulin-Producing Cells via Cytoskeletal Changes. *Cells* 9: 2551
- Lewis MR (1922) The Importance of Dextrose in the Medium of Tissue Cultures. *J Exp Med* 35: 317–322
- Lewis MR & Lewis WH (1911) The cultivation of tissues from chick embryos in solutions of NaCl, CaCl₂, KC1 and NaHCO₃. *Anat Rec* 5: 277–293
- Lewis WH & Lewis MR (1912) The cultivation of chick tissues in media of known chemical constitution. *Anat Rec* 6: 207–211
- Li J, Casteels T, Frogne T, Ingvorsen C, Honoré C, Courtney M, Huber KVM, Schmitner N, Kimmel RA, Romanov RA, *et al* (2017a) Artemisinin Target GABA A Receptor Signaling and Impair α Cell Identity. *Cell* 168: 86-100.e15
- Li M, Zheng D-J, Field LL & Bonnevie-Nielsen V (2009) Murine Pancreatic Beta TC3 Cells Show Greater 2', 5'-Oligoadenylate Synthetase (2'5'AS) Antiviral Enzyme Activity and Apoptosis Following IFN- α or Poly(I:C) Treatment than Pancreatic Alpha TC3 Cells. *Exp Diabetes Res* 2009: 631026
- Li X, Brooks JC, Hu J, Ford KI & Easley CJ (2017b) 3D-templated, fully automated microfluidic input/output multiplexer for endocrine tissue culture and secretion sampling. *Lab Chip* 17: 341–349
- Liebisch G, Fahy E, Aoki J, Dennis EA, Durand T, Ejsing CS, Fedorova M, Feussner I, Griffiths WJ, Köfeler H, *et al* (2020) Update on LIPID MAPS classification, nomenclature, and shorthand notation for MS-derived lipid structures. *J Lipid Res* 61: 1539–1555

- Lim UM, Yap MGS, Lim YP, Goh L-T & Ng SK (2013) Identification of Autocrine Growth Factors Secreted by CHO Cells for Applications in Single-Cell Cloning Media. *J Proteome Res* 12: 3496–3510
- Lin C-C & Anseth KS (2011) Cell-cell communication mimicry with poly(ethylene glycol) hydrogels for enhancing beta-cell function. *Proc Natl Acad Sci U S A* 108: 6380–6385
- Liu S, Harata M, Promes JA, Burand AJ, Ankrum JA & Imai Y (2019) Lentiviral Mediated Gene Silencing in Human Pseudoislet Prepared in Low Attachment Plates. *J Vis Exp JoVE*: 10.3791/59578
- Locke FS (1895) On a Supposed Action of Distilled Water as such on certain Animal Organisms. *J Physiol* 18: 319–331
- Loeb L (1897) Über die entstehung von bindegewebe, leucocyten und roten blutkörperchen aus epithel und über eine methode. *Isol Gewebsteile Zu Zücht Chic Druck Von Max Stern Co*: 1–56
- Long J, Liu Y, Zhou X & He L (2020) Dietary Serine Supplementation Regulates Selenoprotein Transcription and Selenoenzyme Activity in Pigs. *Biol Trace Elem Res*
- Love MI, Huber W & Anders S (2014) Moderated estimation of fold change and dispersion for RNA-seq data with DESeq2. *Genome Biol* 15: 550
- Manfredonia C, Muraro MG, Hirt C, Mele V, Governa V, Papadimitropoulos A, Däster S, Soysal SD, Droeser RA, Mechera R, *et al* (2019) Maintenance of Primary Human Colorectal Cancer Microenvironment Using a Perfusion Bioreactor-Based 3D Culture System. *Adv Biosyst* 3: 1800300
- Marquina-Sanchez B, Fortelny N, Farlik M, Vieira A, Collombat P, Bock C & Kubicek S (2020) Single-cell RNA-seq with spike-in cells enables accurate quantification of cell-specific drug effects in pancreatic islets. *Genome Biol* 21: 106
- Martens M, Ammar A, Riutta A, Waagmeester A, Slenter DN, Hanspers K, A. Miller R, Digles D, Lopes EN, Ehrhart F, *et al* (2021) WikiPathways: connecting communities. *Nucleic Acids Res* 49: D613–D621
- Masters JR (2002) HeLa cells 50 years on: the good, the bad and the ugly. *Nat Rev Cancer* 2: 315–319
- Masters JR & Stacey GN (2007) Changing medium and passaging cell lines. *Nat Protoc* 2: 2276–2284
- Maxwell KN, Fisher EA & Breslow JL (2005) Overexpression of PCSK9 accelerates the degradation of the LDLR in a post-endoplasmic reticulum compartment. *Proc Natl Acad Sci U S A* 102: 2069–2074
- McCluskey JT, Hamid M, Guo-Parke H, McClenaghan NH, Gomis R & Flatt PR (2011) Development and Functional Characterization of Insulin-releasing Human Pancreatic Beta Cell Lines Produced by Electrofusion *. *J Biol Chem* 286: 21982–21992
- McCoy TA, Maxwell M & Kruse PF (1959) The Amino Acid Requirements of the Jensen Sarcoma in Vitro. *Cancer Res* 19: 6

- McKee TJ & Komarova SV (2017) Is it time to reinvent basic cell culture medium? *Am J Physiol-Cell Physiol* 312: C624–C626
- McLimans WF, Crouse EJ, Tunnah KV & Moore GE (1968) Kinetics of gas diffusion in mammalian cell culture systems. I. Experimental. *Biotechnol Bioeng* 10: 725–740
- McQuin C, Goodman A, Chernyshev V, Kametsky L, Cimini BA, Karhohs KW, Doan M, Ding L, Rafelski SM, Thirstrup D, *et al* (2018) CellProfiler 3.0: Next-generation image processing for biology. *PLOS Biol* 16: e2005970
- Meier JA, Zhang F & Sanjana NE (2017) GUIDES: sgRNA design for loss-of-function screens. *Nat Methods* 14: 831–832
- Miyazaki J, Araki K, Yamato E, Ikegami H, Asano T, Shibasaki Y, Oka Y & Yamamura K (1990) Establishment of a pancreatic beta cell line that retains glucose-inducible insulin secretion: special reference to expression of glucose transporter isoforms. *Endocrinology* 127: 126–132
- Mohr JC, de Pablo JJ & Palecek SP (2006) 3-D microwell culture of human embryonic stem cells. *Biomaterials* 27: 6032–6042
- Moore GE, Gerner RE & Franklin HA (1967) Culture of Normal Human Leukocytes. *JAMA* 199: 519–524
- Moore GE, Ito E, Ulrich K & Sandberg AA (1966) Culture of human leukemia cells. *Cancer* 19: 713–723
- Morgan JF, Morton HJ & Parker RC (1950) Nutrition of Animal Cells in Tissue Culture. I. Initial Studies on a Synthetic Medium.,. *Proc Soc Exp Biol Med* 73: 1–8
- Myasnikova D, Osaki T, Onishi K, Kageyama T, Zhang Molino B & Fukuda J (2019) Synergic effects of oxygen supply and antioxidants on pancreatic β -cell spheroids. *Sci Rep* 9: 1802
- Nelson CD, Powell JL, Price DM, Hersom MJ, Yelich JV, Drewnoski ME, Bird SL & Bridges GA (2016) Assessment of serum 25-hydroxyvitamin D concentrations of beef cows and calves across seasons and geographical locations¹. *J Anim Sci* 94: 3958–3965
- Neuman RE & McCoy TA (1958) Growth-promoting properties of pyruvate oxal-acetate, and alpha-ketoglutarate for isolated Walker carcinosarcoma 256 cells. *Proc Soc Exp Biol Med Soc Exp Biol Med N Y N* 98: 303–306
- Newland B, Ehret F, Hoppe F, Eigel D, Pette D, Newland H, Welzel PB, Kempermann G & Werner C (2020) Static and dynamic 3D culture of neural precursor cells on macroporous cryogel microcarriers. *MethodsX* 7: 100805
- Noda M, Komatsu M & Sharp GW (1996) The betaHC-9 pancreatic beta-cell line preserves the characteristics of progenitor mouse islets. *Diabetes* 45: 1766–1773
- Olsen JV, de Godoy LMF, Li G, Macek B, Mortensen P, Pesch R, Makarov A, Lange O, Horning S & Mann M (2005) Parts per million mass accuracy on an Orbitrap mass spectrometer via lock mass injection into a C-trap. *Mol Cell Proteomics MCP* 4: 2010–2021

- Pagliuca FW, Millman JR, Gürtler M, Segel M, Van Dervort A, Ryu JH, Peterson QP, Greiner D & Melton DA (2014) Generation of Functional Human Pancreatic β Cells In Vitro. *Cell* 159: 428–439
- Paraskevas S, Maysinger D, Wang R, Duguid WP & Rosenberg L (2000) Cell Loss in Isolated Human Islets Occurs by Apoptosis. *Pancreas* 20: 270–276
- Paton CM & Ntambi JM (2009) Biochemical and physiological function of stearyl-CoA desaturase. *Am J Physiol Endocrinol Metab* 297: E28–37
- Paw BH & Zon LI (1998) Chapter 4 Primary Fibroblast Cell Culture. In *Methods in Cell Biology*, Detrich HW, Westerfield M & Zon LI (eds) pp 39–43. Academic Press
- Pellegrino E & Gutierrez MG (2021) Human stem cell-based models for studying host-pathogen interactions. *Cell Microbiol* 23: e13335
- Place TL, Domann FE & Case AJ (2017) Limitations of oxygen delivery to cells in culture: An underappreciated problem in basic and translational research. *Free Radic Biol Med* 113: 311–322
- Poitout V, Olson LK & Robertson RP (1996) Insulin-secreting cell lines: classification, characteristics and potential applications. *Diabetes Metab* 22: 7–14
- Poitout V, Stout LE, Armstrong MB, Walseth TF, Sorenson RL & Robertson RP (1995) Morphological and Functional Characterization of β TC-6 Cells—an Insulin-Secreting Cell Line Derived From Transgenic Mice. *Diabetes* 44: 306–313
- Potter SW & Morris JE (1985) Development of mouse embryos in hanging drop culture. *Anat Rec* 211: 48–56
- Powers AC, Efrat S, Mojsov S, Spector D, Habener JF & Hanahan D (1990a) Proglucagon processing similar to normal islets in pancreatic alpha-like cell line derived from transgenic mouse tumor. *Diabetes* 39: 406–414
- Powers AC, Efrat S, Mojsov S, Spector D, Habener JF & Hanahan D (1990b) Proglucagon Processing Similar to Normal Islets in Pancreatic α -Like Cell Line Derived From Transgenic Mouse Tumor. *Diabetes* 39: 406–414
- Price PJ & Gregory EA (1982) Relationship between in vitro growth promotion and biophysical and biochemical properties of the serum supplement. *In Vitro* 18: 576–584
- Puck TT, Cieciura SJ & Robinson A (1958) Genetics of Somatic Mammalian Cells. *J Exp Med* 108: 945–956
- Purschke M, Rubio N, Held KD & Redmond RW (2010) Phototoxicity of Hoechst 33342 in time-lapse fluorescence microscopy. *Photochem Photobiol Sci* 9: 1634
- Radhakrishnan A, Goldstein JL, McDonald JG & Brown MS (2008) Switch-like Control of SREBP-2 Transport Triggered by Small Changes in ER Cholesterol: A Delicate Balance. *Cell Metab* 8: 512–521
- Radvanyi F, Christgau S, Baekkeskov S, Jolicoeur C & Hanahan D (1993) Pancreatic beta cells cultured from individual preneoplastic foci in a multistage tumorigenesis pathway: a potentially general technique for isolating physiologically representative cell lines. *Mol Cell Biol* 13: 4223–4232

- Rajkov J, Weber AA, Salzburger W & Egger B (2018) Adaptive phenotypic plasticity contributes to divergence between lake and river populations of an East African cichlid fish. *Ecol Evol* 8: 7323–7333
- Ramachandran K, Huang H-H & Stehno-Bittel L (2015) A Simple Method to Replace Islet Equivalents for Volume Quantification of Human Islets. *Cell Transplant* 24: 1183–1194
- Ravassard P, Hazhouz Y, Pechberty S, Bricout-Neveu E, Armanet M, Czernichow P & Scharfmann R (2011) A genetically engineered human pancreatic β cell line exhibiting glucose-inducible insulin secretion. *J Clin Invest* 121
- Reid YA (2011) Characterization and Authentication of Cancer Cell Lines: An Overview. In *Cancer Cell Culture: Methods and Protocols*, Cree IA (ed) pp 35–43. Totowa, NJ: Humana Press
- Ribeiro D, Kvist AJ, Wittung-Stafshede P, Hicks R & Forsl w A (2018) 3D-Models of Insulin-Producing β -Cells: from Primary Islet Cells to Stem Cell-Derived Islets. *Stem Cell Rev Rep* 14: 177–188
- Ricordi C, Gray DWR, Hering BJ, Kaufman DB, Warnock GL, Kneteman NM, Lake SP, London NJM, Socci C, Alejandro R, *et al* (1990) Islet isolation assessment in man and large animals. *Acta Diabetol Lat* 27: 185–195
- Ringer S (1882) Concerning the Influence exerted by each of the Constituents of the Blood on the Contraction of the Ventricle. *J Physiol* 3: 380–393
- Ringer S (1883) A further Contribution regarding the influence of the different Constituents of the Blood on the Contraction of the Heart. *J Physiol* 4: 29–42
- Ritacco FV, Wu Y & Khetan A (2018) Cell culture media for recombinant protein expression in Chinese hamster ovary (CHO) cells: History, key components, and optimization strategies. *Biotechnol Prog* 34: 1407–1426
- Ritchie ME, Phipson B, Wu D, Hu Y, Law CW, Shi W & Smyth GK (2015) limma powers differential expression analyses for RNA-sequencing and microarray studies. *Nucleic Acids Res* 43: e47
- Rossiter NJ, Huggler KS, Adelman CH, Keys HR, Soens RW, Sabatini DM & Cantor JR (2021) CRISPR screens in physiologic medium reveal conditionally essential genes in human cells. *Cell Metab* 33: 1248-1263.e9
- Ruoslahti E & Pierschbacher MD (1987) New Perspectives in Cell Adhesion: RGD and Integrins. *Science* 238: 491–497
- Saheb Sharif-Askari N, Saheb Sharif-Askari F, Mdkhana B, Hussain Alsayed HA, Alsafar H, Alrais ZF, Hamid Q & Halwani R (2021) Upregulation of oxidative stress gene markers during SARS-COV-2 viral infection. *Free Radic Biol Med* 172: 688–698
- Saito K, Iwama N & Takahashi T (1978) Morphometrical Analysis on Topographical Difference in Size Distribution, Number and Volume of Islets in the Human Pancreas. *Tohoku J Exp Med* 124: 177–186
- Saito Y & Takahashi K (2002) Characterization of selenoprotein P as a selenium supply protein. *Eur J Biochem* 269: 5746–5751

- Sanford KK, Earle WR & Likely GD (1948) The growth in vitro of single isolated tissue cells. *J Natl Cancer Inst* 9: 229–246
- Sankar KS, Green BJ, Crocker AR, Verity JE, Altamentova SM & Rocheleau JV (2011) Culturing pancreatic islets in microfluidic flow enhances morphology of the associated endothelial cells. *PLoS One* 6: e24904
- Santerre RF, Cook RA, Crisel RM, Sharp JD, Schmidt RJ, Williams DC & Wilson CP (1981) Insulin synthesis in a clonal cell line of simian virus 40-transformed hamster pancreatic beta cells. *Proc Natl Acad Sci U S A* 78: 4339–4343
- Sauvageau G, Iscove NN & Humphries RK (2004) In vitro and in vivo expansion of hematopoietic stem cells. *Oncogene* 23: 7223–7232
- Schaffer WI (1990) Terminology associated with cell, tissue and organ culture, molecular biology and molecular genetics. *In Vitro Cell Dev Biol* 26: 97–101
- Schmied BM, Ulrich A, Matsuzaki H, Batra SK, Pour PM, Ding X, Adrian TE, Ricordi C & Moyer MP (2000) Maintenance of human islets in long term culture. *Differentiation* 66: 173–180
- Schneider CA, Rasband WS & Eliceiri KW (2012) NIH Image to ImageJ: 25 years of image analysis. *Nat Methods* 9: 671–675
- Schulze T, Mattern K, Erfle P, Brüning D, Scherneck S, Dietzel A & Rustenbeck I (2021) A Parallel Perfusion Slide From Glass for the Functional and Morphological Analysis of Pancreatic Islets. *Front Bioeng Biotechnol* 9
- Schulze T, Mattern K, Früh E, Hecht L, Rustenbeck I & Dietzel A (2017) A 3D microfluidic perfusion system made from glass for multiparametric analysis of stimulus-secretion coupling in pancreatic islets. *Biomed Microdevices* 19: 47
- Shaikh Mohammed J, Wang Y, Harvat TA, Oberholzer J & Eddington DT (2009) Microfluidic Device for Multimodal Characterization of Pancreatic Islets. *Lab Chip* 9: 97–106
- Shinohara M, Kimura H, Montagne K, Komori K, Fujii T & Sakai Y (2014) Combination of microwell structures and direct oxygenation enables efficient and size-regulated aggregate formation of an insulin-secreting pancreatic β -cell line. *Biotechnol Prog* 30: 178–187
- Singh V (2002) Disposable Bioreactor for Cell Culture Using Wave-Induced Agitation. In *New Developments and New Applications in Animal Cell Technology*, Merten O-W Perrin P & Griffiths B (eds) pp 399–407. Dordrecht: Kluwer Academic Publishers
- Skelin M (2010) Pancreatic beta cell lines and their applications in diabetes mellitus research. *ALTEX*: 105–113
- Sokolowska P, Zukowski K, Janikiewicz J, Jastrzebska E, Dobrzyn A & Brzozka Z (2021) Islet-on-a-chip: Biomimetic micropillar-based microfluidic system for three-dimensional pancreatic islet cell culture. *Biosens Bioelectron* 183: 113215
- Stephens M (2017) False discovery rates: a new deal. *Biostatistics* 18: 275–294
- Storey JD, Bass AJ, Dabney A & Robinson D (2020) qvalue: Q-value estimation for false discovery rate control

- Tao T, Wang Y, Chen W, Li Z, Su W, Guo Y, Deng P & Qin J (2019) Engineering human islet organoids from iPSCs using an organ-on-chip platform. *Lab Chip* 19: 948–958
- The UniProt Consortium (2021) UniProt: the universal protein knowledgebase in 2021. *Nucleic Acids Res* 49: D480–D489
- ThermoFischer Scientific 11150 - Medium 199.
- ThermoFischer Scientific 21010 - Basal Medium Eagle (BME), no Glutamine.
- ThermoFischer Scientific 31095 - MEM.
- ThermoFischer Scientific 11965 - DMEM, high glucose.
- ThermoFischer Scientific 11875 - RPMI 1640.
- Touat-Hamici Z, Legrain Y, Bulteau A-L & Chavatte L (2014) Selective Up-regulation of Human Selenoproteins in Response to Oxidative Stress. *J Biol Chem* 289: 14750–14761
- Tsai A-C, Liu Y, Yuan X, Chella R & Ma T (2017) Aggregation kinetics of human mesenchymal stem cells under wave motion. *Biotechnol J* 12: 1600448
- Tsonkova VG, Sand FW, Wolf XA, Grunnet LG, Kirstine Ringgaard A, Ingvorsen C, Winkel L, Kalisz M, Dalgaard K, Bruun C, *et al* (2018) The EndoC- β H1 cell line is a valid model of human beta cells and applicable for screenings to identify novel drug target candidates. *Mol Metab* 8: 144–157
- Turkoglu Sasmazel H, Alazzawi M & Kadim Abid Alsaheb N (2021) Atmospheric Pressure Plasma Surface Treatment of Polymers and Influence on Cell Cultivation. *Molecules* 26: 1665
- Tyrode M (1910) The mode of action of some purgative salts. *Arch Int Pharmacodyn* 20: 205–223
- Valk J van der, Bieback K, Buta C, Cochrane B, Dirks WG, Fu J, Hickman JJ, Hohensee C, Kolar R, Liebsch M, *et al* (2018) Fetal bovine serum (FBS): Past – present – future. *ALTEX - Altern Anim Exp* 35: 99–118
- van der Valk J, Brunner D, De Smet K, Fex Svenningsen Å, Honegger P, Knudsen LE, Lindl T, Noraberg J, Price A, Scarino ML, *et al* (2010) Optimization of chemically defined cell culture media – Replacing fetal bovine serum in mammalian in vitro methods. *Toxicol In Vitro* 24: 1053–1063
- Vogelaar JPM & Erlichman E (1933) A Feeding Solution for Cultures of Human Fibroblasts. *Am J Cancer* 18: 28–38
- Walker JT, Haliyur R, Nelson HA, Ishahak M, Poffenberger G, Aramandla R, Reihsmann C, Luchsinger JR, Saunders DC, Wang P, *et al* (2020) Integrated human pseudoislet system and microfluidic platform demonstrate differences in GPCR signaling in islet cells. *JCI Insight* 5: e137017
- Wang Y, Yang F, Gritsenko MA, Wang Y, Clauss T, Liu T, Shen Y, Monroe ME, Lopez-Ferrer D, Reno T, *et al* (2011) Reversed-phase chromatography with multiple fraction concatenation strategy for proteome profiling of human MCF10A cells. *Proteomics* 11: 2019–2026

- Wassmer C-H, Bellofatto K, Perez L, Lavallard V, Cottet-Dumoulin D, Ljubicic S, Parnaud G, Bosco D, Berishvili E & Lebreton F (2020) Engineering of Primary Pancreatic Islet Cell Spheroids for Three-dimensional Culture or Transplantation: A Methodological Comparative Study. *Cell Transplant* 29: 0963689720937292
- White PR (1946) Cultivation of animal tissues in vitro in nutrients of precisely known constitution. *Growth* 10: 231–289
- Wickham H (2016) ggplot2: Elegant Graphics for Data Analysis Springer-Verlag New York
- Wierup N, Svensson H, Mulder H & Sundler F (2002) The ghrelin cell: a novel developmentally regulated islet cell in the human pancreas. *Regul Pept* 107: 63–69
- Williams SJ, Schwasinger-Schmidt T, Zamierowski D & Stehno-Bittel L (2012) Diffusion into human islets is limited to molecules below 10kDa. *Tissue Cell* 44: 332–341
- Witkowski JA (1979) Alexis Carrel and the mysticism of tissue culture. *Med Hist* 23: 279–296
- Witkowski JA (1980) Dr. Carrel's immortal cells. *Med Hist* 24: 129–142
- Wittingen J & Frey CF (1974) Islet Concentration in the Head, Body, Tail and Uncinate Process of the Pancreas: *Ann Surg* 179: 412–414
- Wu X, Wang S, Li M, Li J, Shen J, Zhao Y, Pang J, Wen Q, Chen M, Wei B, *et al* (2020) Conditional reprogramming: next generation cell culture. *Acta Pharm Sin B* 10: 1360–1381
- Wüstner D & Solanko K (2015) How cholesterol interacts with proteins and lipids during its intracellular transport. *Biochim Biophys Acta BBA - Biomembr* 1848: 1908–1926
- Xie Z, Bailey A, Kuleshov MV, Clarke DJB, Evangelista JE, Jenkins SL, Lachmann A, Wojciechowicz ML, Kropiwnicki E, Jagodnik KM, *et al* (2021) Gene Set Knowledge Discovery with Enrichr. *Curr Protoc* 1: e90
- Yang WS, SriRamaratnam R, Welsch ME, Shimada K, Skouta R, Viswanathan VS, Cheah JH, Clemons PA, Shamji AF, Clish CB, *et al* (2014) Regulation of Ferroptotic Cancer Cell Death by GPX4. *Cell* 156: 317–331
- Yang WS & Stockwell BR (2008) Synthetic Lethal Screening Identifies Compounds Activating Iron-Dependent, Nonapoptotic Cell Death in Oncogenic-RAS-Harboring Cancer Cells. *Chem Biol* 15: 234–245
- Yao T & Asayama Y (2017) Animal-cell culture media: History, characteristics, and current issues. *Reprod Med Biol* 16: 99–117
- Ye Y, Shibata Y, Yun C, Ron D & Rapoport TA (2004) A membrane protein complex mediates retro-translocation from the ER lumen into the cytosol. *Nature* 429: 841–847
- Yeagle PL (1991) Modulation of membrane function by cholesterol. *Biochimie* 73: 1303–1310
- Yu Y, Gamble A, Pawlick R, Pepper AR, Salama B, Toms D, Razian G, Ellis C, Bruni A, Gala-Lopez B, *et al* (2018) Bioengineered human pseudoislets form efficiently from donated tissue, compare favourably with native islets in vitro and restore normoglycaemia in mice. *Diabetologia* 61: 2016–2029

- Zaldumbide A, Alkemade G, Carlotti F, Nikolic T, Abreu JR, Engelse MA, Skowera A, de Koning EJ, Peakman M, Roep BO, *et al* (2013) Genetically Engineered Human Islets Protected From CD8-mediated Autoimmune Destruction In Vivo. *Mol Ther* 21: 1592–1601
- Zhang Y, Swanda RV, Nie L, Liu X, Wang C, Lee H, Lei G, Mao C, Koppula P, Cheng W, *et al* (2021) mTORC1 couples cyst(e)ine availability with GPX4 protein synthesis and ferroptosis regulation. *Nat Commun* 12: 1589
- Zuellig RA, Cavallari G, Gerber P, Tschopp O, Spinass GA, Moritz W & Lehmann R (2017) Improved physiological properties of gravity-enforced reassembled rat and human pancreatic pseudo-islets. *J Tissue Eng Regen Med* 11: 109–120

6. CURRICULUM VITAE

Robert Pazdzior

23/07/1993

Canadian

rpazdzior@cemm.at

Vienna, Austria

Education

- Jan 2016 - Present **PhD in Molecular Medicine**
CeMM – Research Center for Molecular Medicine of the Austrian Academy of Sciences
Supervisor: Dr. Stefan Kubicek
Vienna, Austria
- Sept 2015 - Dec 2015 **PhD Introductory Program**
Lectures and lab rotations
CeMM,
Vienna, Austria
- Sept 2014 - Apr 2015 **Honours Thesis**
Supervisor: Dr. Steven Rafferty
Trent University | Peterborough, Canada
Title: “Biophysical Studies of *Giardia intestinalis* Cytochromes *b_s*”
- Sept 2011 – Apr 2015 **Honours Bachelor’s in Biochemistry and Molecular Biology**
Trent University | Peterborough, Canada

Experience

- May - Aug 2013 - 2015 **Undergraduate Student Researcher**
Dr. Steven Rafferty’s lab,
Trent University | Peterborough, Canada
- Sept 2014 - Dec 2014 **Teaching Assistant**
Chemistry Department
Trent University | Peterborough, Canada
- Sept 2014 - Dec 2014 **Assistant Laboratory Technician**
Chemistry Department
Trent University | Peterborough, Canada

Awards

- 2017-2020 **DOC PhD Fellowship**
- 2016 **Austrian Proteomics Association – Travel Stipend**
To attend the EMBO Advanced Proteomics workshop in Brixen, Italy
- Sept 2011 - Apr 2015 **Full-Tuition Scholarship**
For achieving an average grade of higher than 90% each semester at Trent University
- 2015 **Society of Chemistry Industry Student Merit Award;
NSERC Undergraduate Student Research Awards**
- 2014 **Canadian Society for Chemistry Silver Medal;
Robert Annett Scholarship;**

**Makhija Prize in Chemistry;
NSERC Undergraduate Student Research Awards**

2013 **Graham Hartley Prize;
NSERC Undergraduate Student Research Awards**

Scientific Meetings

- 2019 **Young Scientists Association (YSA) PhD Symposium (Poster Presentation)**
- 2018 **Keystone Symposium: Frontiers in Islet Biology and Diabetes (Poster Presentation)**
- 2017 **DOC PhD Fellowship Poster Exhibition**
- 2016 **EMBO Workshop: Advanced Proteomics (Poster Presentation)**

Publications

Pazdzior R, Kubicek S. (2021). *PlateFlo–A software-controllable plate-scale perfusion system for culture of adherent cells*. HardwareX 10. e00222.

<https://doi.org/10.1016/j.ohx.2021.e00222>

Yang ZA, Pazdzior R, Yee J, Rafferty S. (2016). *Reduction potential and heme-pocket polarity in low potential cytochrome b5 of Giardia intestinalis*. J Inorg Biochem 158:110-114.

<https://doi.org/10.1016/j.jinorgbio.2016.02.021>

Pazdzior R, Yang ZA, Mesbahuddin MS, Yee J, van der Est A, Rafferty S. (2015). *Low reduction potential cytochrome b5 isotypes of Giardia intestinalis*. Exp Parasitol 157:197-201.

<https://doi.org/10.1016/j.exppara.2015.08.004>